

**Some pages of this thesis may have been removed for copyright restrictions.**

If you have discovered material in AURA which is unlawful e.g. breaches copyright, (either yours or that of a third party) or any other law, including but not limited to those relating to patent, trademark, confidentiality, data protection, obscenity, defamation, libel, then please read our [Takedown Policy](#) and [contact the service](#) immediately

CRYSTALLOGRAPHIC STUDIES OF MAGNETITE AND TITANOMAGHEMITE

BY

STEPHEN COLLYER

Thesis submitted for the degree of

Doctor of Philosophy

at the

University of Aston in Birmingham

March 1986

To my Mother and Father

THE UNIVERSITY OF ASTON IN BIRMINGHAM  
CRYSTALLOGRAPHIC STUDIES OF MAGNETITE AND TITANOMAGHEMITE

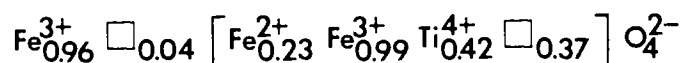
STEPHEN COLLYER

Submitted for the degree of  
Doctor of Philosophy  
March 1986

SUMMARY

The crystal structure of natural magnetite has been investigated on the basis of previously published X-ray intensity data and a newly acquired, more extensive data base. Both investigations show that the structure does not conform to the centrosymmetrical space group  $Fd\bar{3}m$ , as is normally assumed, but the non-centrosymmetrical space group  $F\bar{4}3m$ . The structure refinement provides values for the atom positions, anisotropic thermal parameters and bond lengths. A study of Friedel related pairs of X-ray intensities shows that Friedel's law is violated in magnetite, further confirming that the space group is non-centrosymmetrical. It was found that the octahedral site cations in magnetite do not occupy special positions at the centres of the octahedral interstices as they should under the space group  $Fd\bar{3}m$ , but are displaced along  $\langle 111 \rangle$  directions leading to  $F\bar{4}3m$  symmetry. A mechanism is known for the origin of these displacements and the likelihood of similar displacements occurring in other natural and synthetic spinels is discussed.

The crystal structure of a natural titanomaghemite was determined by a combination of X-ray diffraction and Mössbauer spectroscopy. This was confirmed as possessing a primitive cubic Bravais lattice with the space group  $P4_332$  and the structural formula:



where  $\square$  represents a cation vacancy. As the above formula shows, there are cation vacancies on both tetrahedral and octahedral sites, the majority being restricted to octahedral sites. No tetrahedral site  $\text{Fe}^{2+}$  or  $\text{Ti}^{4+}$  was observed. Values for the atom positions, anisotropic thermal parameters and bond lengths have been determined for this particular specimen.

Key Words

MAGNETITE, TITANOMAGHEMITE, SPINEL STRUCTURE,  
X-RAY DIFFRACTION, MÖSSBAUER SPECTROSCOPY.

## TABLE OF CONTENTS

	<u>Page</u>
Title Page	i
Summary	ii
Contents	iii

### CHAPTER 1

#### INTRODUCTION

1.1 Introduction	1
1.2 Details of the Spinel Structure	4
1.3 The Structure of Magnetite	10
1.4 The Structure of Maghemite	11
1.5 Compositional Variations in Synthetic Spinel	12
1.6 Compositional Variations in Natural Magnetites and Maghemites	14
1.7 Electrical Properties of Magnetite and Substituted Magnetites	20
1.8 Magnetic Properties of Magnetite and Maghemite	24
1.9 Cation Distribution in Spinel and the Crystal Chemistry of Iron-Titanium Oxides	27
1.10 Cation Distribution of Titanomaghemites	31
1.11 Thesis Layout	40

## CHAPTER 2

### REVIEW OF PUBLICATIONS RELATING TO THE SYMMETRY OF THE SPINEL GROUP OF COMPOUNDS

	<u>Page</u>
2.1 Review of Indirect Evidence in Favour of $F\bar{4}3m$ Symmetry for the Spinels	41
2.2 Double Diffraction	47
2.3 Diffraction Evidence	48
2.3.1 Electron Diffraction Evidence	49
2.3.2 Neutron Diffraction Evidence	51
2.3.3 X-Ray Diffraction Evidence	53
2.4 The Spinels Under $F\bar{4}3m$ Symmetry	56

## CHAPTER 3

### A RE-EXAMINATION OF STRUCTURE FACTOR DATA FOR MAGNETITE

3.1 Introduction	58
3.2 Inspection of the Original Structure Factor Data	59
3.3 Crystal Structure Refinement Procedure	61
3.4 Results and Discussion	64
3.5 Conclusions	73

## CHAPTER 4

### REFINEMENT OF THE CRYSTAL STRUCTURE OF MAGNETITE

	<u>Page</u>
4.1 Introduction	76
4.2 Electron Microprobe Analysis	78
4.3 Mössbauer Spectrum of Magnetite Specimen BMDM11 at Room Temperature	78
4.4 X-Ray Data Collection	83
4.5 Treatment of the X-Ray Data	85
4.6 Crystal Structure Refinement	89
4.7 Results and Discussion	91

## CHAPTER 5

### THE USE OF X-RAY ANOMALOUS SCATTERING IN STUDIES OF THE SYMMETRY OF MAGNETITE

5.1 Introduction	116
5.2 Anomalous Scattering	118
5.3 Practical Difficulties Arising When Using Anomalous Scattering	124
5.3.1 Absorption	125
5.3.2 Extinction	125
5.3.3 Double Diffraction	126
5.3.4 Thermal Diffuse Scattering	126

	<u>Page</u>
5.3.5 Counting Statistics	126
5.3.6 Inhomogeneous X-Ray Beam	126
5.4 Data Collection	127
5.5 Results and Discussion	130

## CHAPTER 6

### THE CRYSTAL STRUCTURE OF TITANOMAGHEMITE

#### SPECIMEN BM1929,1687

6.1 Review of Publications Relating to the Symmetry of Maghemite	133
6.2 Mössbauer Spectrum of Maghemite	140
6.3 Mössbauer Spectra of Maghemite Specimens M1 and M2 at Room Temperature	142
6.4 Mössbauer Spectra of Maghemite Specimens M1 and M2 at 4.2 K in a Longitudinal Magnetic Field of 4.2 T	147
6.5 Mössbauer Spectrum of Titanomaghemite Specimen BM1929,1687 at Room Temperature	153
6.6 Mössbauer Spectrum of Titanomaghemite Specimen BM1929,1687 at 4.2 K in a Longitudinal Magnetic Field of 4.2 T	157
6.7 Data Collection	160
6.8 Treatment of the X-Ray Data	162
6.9 Crystal Structure Refinement	163
6.10 Results and Discussion	164

	<u>Page</u>
6.11 Summary of Conclusions	173
 <u>CHAPTER 7</u>	
DISCUSSION AND CONCLUSIONS	
7.1 Summary of Major Conclusions on the Structure and Symmetry of Magnetite	174
7.2 A Proposed Displacement Mechanism giving rise to $F\bar{4}3m$ Symmetry in Magnetite	175
7.3 Physical Properties Exhibited by a Non-Centrosymmetrical Material	183
7.3.1 Ferroelectricity	183
7.3.2 Piezoelectricity	184
7.3.3 Pyroelectricity	184
7.3.4 Frequency Doubling	185
7.4 The Structure and Symmetry of Titanomaghemite: Major conclusions	186
7.5 A Comparison of the Observed Cation Distribution in Titanomaghemite Specimen BM1929,1687 with that Predicted by Theory	188
7.6 Suggestions for Further Work	193

## APPENDICES

Appendix I	Data Reduction Procedures and the Crystallographic Software used in the Structure Refinements	
		<u>Page</u>
I.1	Introduction	197
I.2	Data Reduction	197
I.2.1	Subtraction of Background Counts	198
I.2.2	Standard Deviation of Peak	199
I.2.3	Intensity Control and Orientation	199
I.2.4	Lorentz and Polarization Corrections	200
I.3	X-Ray 74	201
I.3.1	Atomic Scattering Factors	205
I.3.2	Temperature Factors	205
I.3.3	Absorption Correction	206
I.3.4	Extinction Correction	207
I.3.5	Scale Factor	208
I.3.6	Less-Thans	209
Appendix II	Specimen Preparation for Single Crystal X-Ray Studies	210
Appendix III	Electron Microprobe Analysis	213
Appendix IV	Mössbauer Spectroscopy	214
Appendix V	Structure Factors for Magnetite Produced by a Re-Examination of Experimental Data Published by Fleet (1981)	215

	<u>Page</u>
Appendix VI Structure Factors for Magnetite Produced by Fleet (1981)	219
Appendix VII Structure Factors for Magnetite Specimen BMDM11	220
Appendix VIII Structure Factors for Titanomaghemite Specimen BM1929,1687	227
REFERENCES	229
ACKNOWLEDGEMENTS	249

## LIST OF TABLES

	<u>Page</u>
Table 1.1 Atom positions for the spinel structure according to $Fd\bar{3}m$ symmetry.	6
Table 1.2 Cations occurring in tetrahedral and octahedral sites in synthetic spinels.	13
Table 1.3 Compositional parameters used by various authors to characterize titanomaghemites (after Lindsley, 1976).	32
Table 2.1 Atom positions for the spinel structure according to $F\bar{4}3m$ symmetry.	57
Table 3.1 Weak reflexions taken from Fleet (1981).	63
Table 3.2 Final structure parameters.	65
Table 3.3.1 R-factor breakdown for $Fd\bar{3}m$ symmetry.	67
Table 3.3.2 R-factor breakdown for $F\bar{4}3m$ symmetry.	68
Table 3.4 Some sensitive reflexions.	70
Table 3.5 Structure factors for the $Fd\bar{3}m$ forbidden reflexions.	72

	<u>Page</u>	
Table 3.6	Calculated bond lengths.	74
Table 4.1	Electron microprobe data for magnetite specimen BMDM11.	77
Table 4.2	Mössbauer parameters for magnetite specimen BMDM11 at room temperature.	80
Table 4.3	Mössbauer parameters found by previous authors for magnetite at room temperature.	82
Table 4.4	Final structure parameters.	92
Table 4.5.1	R-factor breakdown for $Fd\bar{3}m$ symmetry.	94
Table 4.5.2	R-factor breakdown for $F\bar{4}3m$ symmetry.	95
Table 4.5.3	R-factor breakdown for $F\bar{4}3m$ symmetry with the $Fd\bar{3}m$ forbidden reflexions included in the refinement.	96
Table 4.6	Reflexions produced by oxygen only scattering under $Fd\bar{3}m$ symmetry.	100
Table 4.7	Structure factors for the 76 weakest reflexions.	102

	<u>Page</u>
Table 4.8 Comparison of bond lengths with those found by previous authors.	105
Table 4.9 Calculated bond lengths for $Fd3m$ and $F\bar{4}3m$ symmetry.	107
Table 4.10 The significance of differences in bond lengths between the $Fd3m$ and $F\bar{4}3m$ structure refinements.	108
Table 4.11 Some sensitive reflexions.	109
Table 4.12 Structure factors for the 27 $Fd3m$ forbidden reflexions.	111
Table 5.1 Structure factors for Friedel pairs of reflexions.	131
Table 6.1 Cell parameters and space groups reported for a number of natural and synthetic maghemites.	139
Table 6.2 Mössbauer parameters for maghemite specimen M1 at room temperature and at 4.2 K.	145
Table 6.3 Mössbauer parameters for maghemite specimen M2 at room temperature and at 4.2 K.	146
Table 6.4 Mössbauer parameters found by previous authors for maghemite.	151

	<u>Page</u>	
Table 6.5	Mössbauer parameters for members of the solid solution series $(1-x)\text{FeTiO}_3 \cdot x\text{Fe}_2\text{O}_3$ at room temperature (after Shirane et al. 1962).	155
Table 6.6	Mössbauer parameters for titanomaghemite specimen BM1929,1687 at room temperature and at 4.2 K.	156
Table 6.7	Calculation of the structural formula for titanomaghemite specimen BM1929,1687.	159
Table 6.8	Atom positions for titanomaghemite according to $P4_332$ symmetry.	165
Table 6.9	Final values for atom positions for titanomaghemite specimen BM1929,1687 along with those for $\text{LiFe}_5\text{O}_8$ (Tomas et al. 1983) and $\text{LiAl}_5\text{O}_8$ (Famery et al. 1979).	168
Table 6.10	Final values for anisotropic temperature factors for titanomaghemite specimen BM1929,1687 along with those for $\text{LiFe}_5\text{O}_8$ (Tomas et al. 1983) and $\text{LiAl}_5\text{O}_8$ (Famery et al. 1979).	169

	<u>Page</u>
Table 6.11 Bond lengths for titanomaghemite specimen BM1929,1687 under $P4_332$ symmetry.	171
Table 6.12 R-factor breakdown for $P4_332$ symmetry.	172

## LIST OF FIGURES

	<u>Page</u>
Figure 1.1 A unit cell of the spinel structure (after Gorter, 1954).	5
Figure 1.2 The normal spinel structure.	8
Figure 1.3 The inverse spinel structure.	9
Figure 1.4 Variation of the cell parameter with composition for the solid solution series $(1-x)\text{Fe}_3\text{O}_4 \cdot x\text{Fe}_2\text{TiO}_4$ (after Lindsley, 1965).	15
Figure 1.5 The $\text{FeO}-\text{Fe}_2\text{O}_3-\text{TiO}_2$ ternary diagram.	17
Figure 1.6 Variation of the cell parameter with composition for the solid solution series $\text{Fe}_3\text{O}_4-\text{Fe}_2\text{O}_3$ (after Lindsley, 1976).	18
Figure 1.7 Variation of the electrical conductivity of $\text{Fe}_3\text{O}_4$ with temperature (after Miles et al. 1957).	21
Figure 1.8 Schematic diagram to represent the oxidation of $\text{Fe}^{2+}$ and $\text{Fe}^{3+}$ leading to the production of titanomaghemite from titanomagnetite.	34

	<u>Page</u>
Figure 2.1 An illustration of the difference between the point symmetries $\bar{3}m$ and $3m$ (after Grimes and Collett, 1971a).	43
Figure 2.2 Octahedral ion sublattice of the spinel structure (after Grimes, 1973).	46
Figure 2.3 Atom shifts at an octahedral site in the spinel structure giving rise to $F\bar{4}3m$ symmetry.	55
Figure 4.1 Mössbauer spectrum of magnetite specimen BMDM11 at room temperature.	79
Figure 4.2 The Cad-4 diffractometer.	84
Figure 4.3 Histograms for four groups of equivalent reflexions.	87
Figure 4.4 Histograms for four groups of equivalent reflexions.	88
Figure 4.5 Atom shifts in magnetite giving rise to $F\bar{4}3m$ symmetry in one eighth of the unit cell.	113
Figure 4.6 Atom shifts in magnetite giving rise to $F\bar{4}3m$ symmetry in one eighth of the unit cell.	114

	<u>Page</u>
Figure 4.7 A unit cell of magnetite made up of figures 4.5 and 4.6.	115
Figure 5.1 Variation of the real and imaginary anomalous scattering components for iron with wavelength (after Woolfson, 1979).	119
Figure 5.2 Vector representation of a Friedel pair of reflexions for a centrosymmetrical structure in the presence of anomalous scattering (after Stout and Jensen, 1968).	121
Figure 5.3 Vector representation of a Friedel pair of reflexions for a non-centrosymmetrical structure in the presence of anomalous scattering (after Stout and Jensen, 1968).	122
Figure 5.4 Phase differences arising in a non-centrosymmetrical structure with and without anomalous scattering (after Glusker and Trueblood, 1972).	123
Figure 5.5 Histograms for two Friedel pairs of reflexions.	129
Figure 6.1 Mössbauer spectrum of maghemite specimen M1 at room temperature.	143

	<u>Page</u>
Figure 6.2 Mössbauer spectrum of maghemite specimen M2 at room temperature.	144
Figure 6.3 Mössbauer spectrum of maghemite specimen M1 at 4.2 K.	148
Figure 6.4 Mössbauer spectrum of maghemite specimen M2 at 4.2 K.	149
Figure 6.5 Mössbauer spectrum of titanomaghemite specimen BM1929,1687 at room temperature.	154
Figure 6.6 Mössbauer spectrum of titanomaghemite specimen BM1929,1687 at 4.2 K.	158
Figure 7.1 Potential conditions at an octahedral site.	177
Figure II.1 Air driven sphere grinder.	211

## CHAPTER 1

### INTRODUCTION

#### 1.1 Introduction

Magnetite ( $\text{Fe}_3\text{O}_4$ ) is a compound of considerable scientific importance from the geological and technological point of view as well as being a mineral of economic significance as a source of iron. It occurs in all major rock types (igneous, metamorphic and sedimentary) and is often formed by crystallization from melts but may also form from high and low-temperature aqueous solutions (Elsdon, 1975; Deer, Howie and Zussman, 1962; Rumble, 1976). Magnetite crystallizes with essentially the same structure as that of the mineral spinel ( $\text{MgAl}_2\text{O}_4$ ). The spinel structure is based on that of diamond with one molecule of spinel corresponding to an atom of carbon in the diamond structure. The general chemical formula for spinel oxides tends to conform to  $\text{PQ}_2\text{O}_4$ , where P and Q represent metal cations and O an oxygen anion. One third of the cations occupy tetrahedral sites and the remaining two thirds are in octahedral sites. This atomic arrangement gives rise to a unit cell with a lattice constant double that of the oxygen subcell. There are 8 of these oxygen subcells in the spinel structure, each unit cell therefore contains 32 oxygen anions which form 64 tetrahedral and 32 octahedral sites. Eight of the tetrahedral and 16 octahedral sites are occupied (Muller and Roy, 1974).

In the region of oxidation and weathering at the Earth's surface, magnetite may be oxidized to maghemite ( $\gamma\text{-Fe}_2\text{O}_3$ ) which also possesses,

at least to a first approximation, the spinel structure. The chemical formula for maghemite may be re-written as  $\text{Fe}_{8/3}\square_{1/3}\text{O}_4$ , where  $\square$  represents a cation vacancy. This general formula indicates that 1/9 of the cation sites occupied in stoichiometric magnetite are vacant in maghemite. A complete solid solution series exists between magnetite and maghemite, partial oxidation of magnetite leads to the production of intermediate members of this series.

Magnetite occurs in ore deposits of iron and titanium and when found in conjunction with haematite ( $\alpha\text{-Fe}_2\text{O}_3$ )-ilmenite ( $\text{FeTiO}_3$ ) solid solutions it may be used as an indicator of temperature and oxygen fugacity, leading to a better understanding of formation conditions in the igneous and metamorphic rocks in which it occurs (Buddington and Lindsley, 1964; Spencer and Lindsley, 1981). It is the primary carrier of natural remanent magnetization (NRM) in rocks and as such is the most important mineral as regards the interpretation of rock magnetic and palaeomagnetic data (O'Reilly, 1984).

Extensive use is made of magnetite and the related compounds known as spinel ferrites in the telecommunications industry, mainly because of their extremely high electrical resistivity compared with that of metals. The specific resistivity of spinel ferrites ranges from  $10^2$  to  $10^{10}$   $\Omega\text{cm}$  which is up to fifteen orders of magnitude greater than that of iron. The advantage of this is that in high frequency applications the use of spinel ferrites prevents undesirable losses due to eddy currents, whereas at such frequencies eddy current losses are the main drawback of metals. This intrinsic property makes the spinel ferrites indispensable materials in the telecommunications and electronics industries where frequencies ranging from  $10^3$  to  $10^{11}$  Hz have to be handled.

Magnetic recording uses a transducer which converts variations in current into similar magnetic fields. These energize a moving magnetic tape leaving a record of these currents as remanent magnetization on the tape. For this process to give efficient reproduction it is necessary for the magnetic recording medium to have a high remanent magnetization and a more or less linear relationship between the strength of the magnetic field at the tape and the remanent magnetization remaining after the field has been removed.  $\text{Fe}_3\text{O}_4$  and  $\gamma\text{-Fe}_2\text{O}_3$  are the principal materials used in the manufacture of these magnetic recording tapes. The discovery that some polycrystalline spinel ferrites have an almost rectangular hysteresis loop and can therefore be used as computer memory elements was a find of significant importance for the computer industry. Until 1970, nearly all main-frame computer memories consisted of ferrite cores, so the whole of computer development was closely connected with the development of synthetic magnetite and its related derivatives (Wohlfarth, 1982). The industrial applications of the spinels has been reviewed by Grimes (1975).

The aim of the present study has been to investigate the precise crystal structure and crystal chemistry of magnetite and of maghemite. Although both of these materials are known to possess the 'spinel structure', uncertainties remain as regards the exact symmetry (and hence space group), precise atom positions and the distribution of cations and of vacancies in both of these extremely important materials. The techniques employed in this work have been X-ray diffraction by single crystals of magnetite and maghemite and  $^{57}\text{Fe}$  Mössbauer spectroscopy on powdered samples of these materials. Electron microprobe analysis has also been used to determine the compositions of the materials studied.

The remaining sections in Chapter 1 describe the spinel structure in general, along with information on the structures of magnetite and maghemite available prior to the present work. Compositional variations in natural and synthetic magnetites and maghemites leading to the production of various iron-titanium oxides are also considered. Electrical and magnetic properties of iron-titanium oxides along with the various models proposed to explain the cation distributions in this extensive range of compounds are then discussed because of the close connections between these properties and the crystal structure. The final section in this chapter describes the organization of the thesis.

## 1.2 Details of the Spinel Structure

The unit cell is face centred cubic and contains eight molecules. Each cell contains 32 anions which form a face centred cubic framework, bound together by interstitial cations: as with most oxides the anions are appreciably larger than the cations. One variable parameter exists, the oxygen positional or u-parameter. The anions provide two types of interstitial site: firstly, there are 64 sites with tetrahedral coordination of which 8, the A-sites, are occupied. Secondly, there are 32 sites with octahedral coordination, of which 16, the B-sites, are occupied. Conventionally the overall symmetry is described within the space group  $Fd\bar{3}m$  (International Tables for X-Ray Crystallography Vol. I).

Under  $Fd\bar{3}m$  symmetry two alternative sets of tetrahedral and octahedral coordinates exist depending upon the choice of origin. These are 8(a) (tetrahedral) and 16(d) (octahedral) or alternatively 8(b) and 16(c). During this study both sets of coordinates have been used but the results here are presented in terms of 8(a) and 16(d). Coordinates and

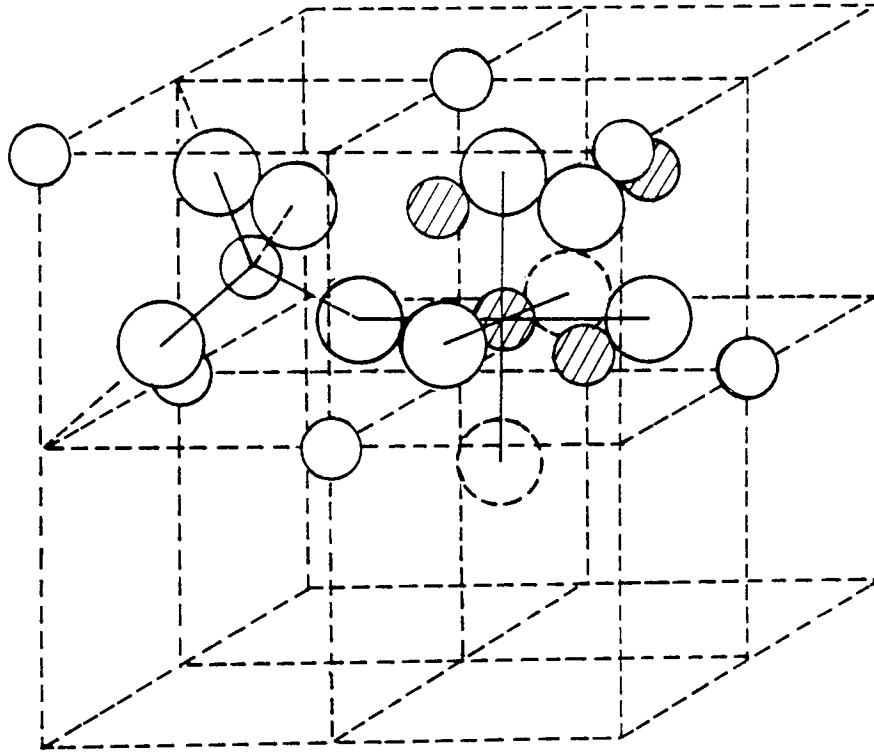


Figure 1.1 A unit cell of the spinel structure (after Gorter, 1954). The positions of ions are shown in two octants. Dashed circles represent ions in other octants. Large circles represent anions, small open circles ions on tetrahedral sites and the small hatched circles ions on octahedral sites.

Table 1.1 Atom positions for the spinel structure according to  $Fd\bar{3}m$  symmetry.

The symbol  $u$  represents the oxygen positional parameter.

Origin at  $\bar{4}3m$

The face centred cubic translations:-

$$(000; 0\frac{1}{2}\frac{1}{2}; \frac{1}{2}0\frac{1}{2}; \frac{1}{2}\frac{1}{2}0; )_+$$

Ion	Position	Point symmetry	Coordinates of equivalent positions
$Fe^{3+}$	8(a)	$\bar{4}3m$	$0,0,0; \frac{1}{4}, \frac{1}{4}, \frac{1}{4}.$
$Fe^{2.5+}$	16(d)	$\bar{3}m$	$\frac{5}{8}, \frac{5}{8}, \frac{5}{8}; \frac{5}{8}, \frac{7}{8}, \frac{7}{8};$ $\frac{7}{8}, \frac{5}{8}, \frac{7}{8}; \frac{7}{8}, \frac{7}{8}, \frac{5}{8}.$
$O^{2-}$	32(e)	$3m$	$u, u, u; \frac{1}{4}-u, \frac{1}{4}-u, \frac{1}{4}-u;$ $u, \bar{u}, \bar{u}; \frac{1}{4}-u, \frac{1}{4}+u, \frac{1}{4}+u;$ $\bar{u}, u, \bar{u}; \frac{1}{4}+u, \frac{1}{4}-u, \frac{1}{4}+u;$ $\bar{u}, \bar{u}, u; \frac{1}{4}+u, \frac{1}{4}+u, \frac{1}{4}-u;$

Origin at centre ( $\bar{3}m$ )

The face centred cubic translations:-

$$(0,0,0; 0\frac{1}{2}\frac{1}{2}; \frac{1}{2}0\frac{1}{2}; \frac{1}{2}\frac{1}{2}0; )_+$$

Ion	Position	Point symmetry	Coordinates of equivalent positions
$Fe^{3+}$	8(b)	$\bar{4}3m$	$\frac{3}{8}, \frac{3}{8}, \frac{3}{8}; \frac{5}{8}, \frac{5}{8}, \frac{5}{8};$
$Fe^{2.5+}$	16(c)	$\bar{3}m$	$0,0,0; 0, \frac{1}{4}, \frac{1}{4};$ $\frac{1}{4}, 0, \frac{1}{4}; \frac{1}{4}, \frac{1}{4}, 0;$
$O^{2-}$	32(e)	$3m$	$u, u, u; u, \frac{1}{4}-u, \frac{1}{4}-u;$ $\frac{1}{4}-u, u, \frac{1}{4}-u; \frac{1}{4}-u, \frac{1}{4}-u, u;$ $\bar{u}, \bar{u}, \bar{u}; \bar{u}, \frac{3}{4}+u, \frac{3}{4}+u;$ $\frac{3}{4}+u, \bar{u}, \frac{3}{4}+u; \frac{3}{4}+u, \frac{3}{4}+u, \bar{u};$

site symmetries for these two sets are given in table 1.1. The oxygen anions occupy the special positions 32(e), the coordinates of which must be found by experiment. Once the u-parameter has been determined the oxygen positional coordinates, in terms of u, can then be derived from the 32(e) symmetry operations given in table 1.1

The u-parameter in the first case is equal to  $3/8+\delta$ ; in an ideal spinel structure  $\delta=0$ . In practice  $\delta$  is often positive but negative values do occur (Muller and Roy, 1974). The relative sizes of tetrahedral and octahedral interstices depend quite sensitively on the value of  $\delta$ . If  $\delta$  is positive, the anions move outwards in  $\langle 111 \rangle$  directions and the tetrahedral interstice is increased in size and the octahedral interstice correspondingly decreases. Point symmetry of the tetrahedral site is cubic ( $\bar{4}3m$ ) and is maintained irrespective of the value of  $\delta$ , but the octahedral site distorts to trigonal ( $\bar{3}m$ ) point symmetry such that the anions are equidistant from the trivalent cations. The entire oxygen framework can expand or contract to accommodate cations of larger or smaller ionic radii.

Each unit cell of the spinel structure is made up of two different groups of four cubes with edges  $a/2$  and identical atomic positions. These atomic positions are different in two octants sharing a face and identical in two octants sharing only an edge. The structure can be seen more clearly if the positions of atoms are drawn in two adjacent octants only, as shown in figure 1.1 for an ideal spinel. The whole cell can be generated by placing identical contents into octants connected by a cell edge. For simplicity, in the description of the structure so far it has been assumed that 8 divalent cations occupy the 8(a) positions and the 16 trivalent cations the 16(d) positions. Barth and Posnjak (1931) found that this 'normal' structure was correct for many spinels but to account

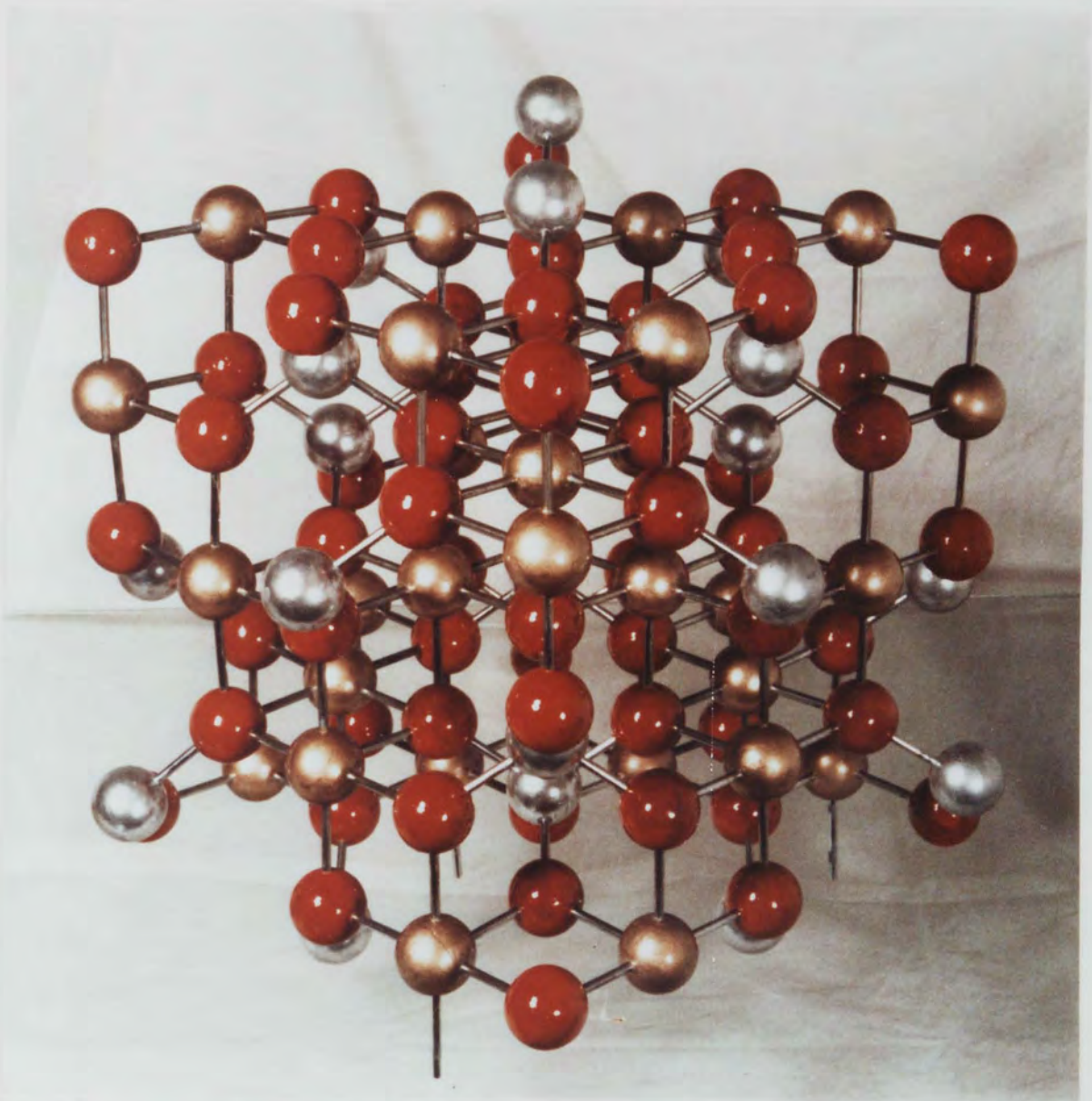


Figure 1.2 The normal spinel structure. Silver spheres represent divalent cations on tetrahedral sites, gold spheres trivalent cations on octahedral sites, and red spheres oxygen anions.

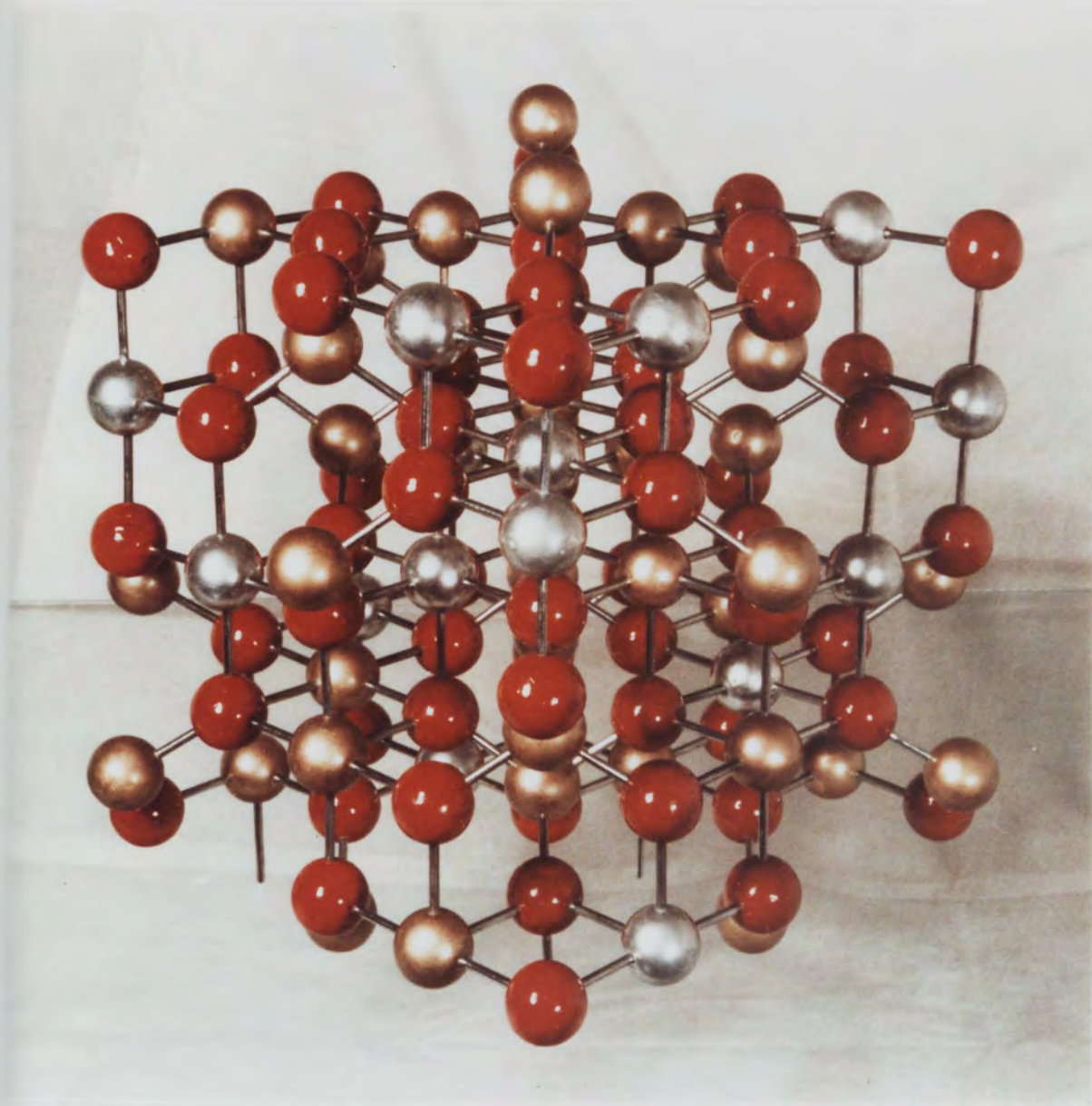


Figure 1.3 The inverse spinel structure. Silver spheres represent divalent cations on octahedral sites, gold spheres trivalent cations on tetrahedral and octahedral sites, and red spheres oxygen anions

for the X-ray intensities produced by others it was necessary to define 'inverse' spinels. Here, half the trivalent cations occupy the tetrahedral sites while the octahedral sites are randomly shared by divalent and the remaining trivalent cations. The normal distribution may be represented by  $P[Q_2]O_4$  and the inverse by  $Q[PQ]O_4$ , where the atoms in square brackets are those on octahedral sites. Spinel with any intermediate composition may be represented by  $(P_{1-x}Q_x)[P_xQ_{2-x}]O_4$ , where  $x$  is the degree of inversion and equal to zero for a normal spinel and unity for an inverse spinel. The normal and inverse spinel structures are shown in figures 1.2 and 1.3 respectively.

Although the above general description of the spinel structure is accepted, there still remain uncertainties regarding the correct space group assignment for members of the spinel family, including the iron/titanium oxides. Grimes et al. (1983) for example, published an X-ray diffraction study of  $MgAl_2O_4$  which showed that the space group for this material was  $F\bar{4}3m$  rather than  $Fd3m$ , as is normally assumed.

### 1.3 The Structure of Magnetite

The room temperature structure of magnetite was originally determined, independently, by Bragg (1915a,b) and by Nishikawa (1915). They found it to crystallize with the same structure as that of the mineral spinel ( $MgAl_2O_4$ ). Because of the similar X-ray scattering factors of  $Fe^{2+}$  and  $Fe^{3+}$  ions it was not possible for early workers to determine the true structural formula for magnetite using X-ray diffraction techniques. Both workers therefore assumed the structural formula to be  $Fe^{2+}[Fe_2^{3+}]O_4^{2-}$  with the oxygen positional parameter ( $u$ ) equal to 0.375. More detailed work carried out by Claassen (1926) gave

$u=0.379(1)$  while Hamilton (1958) found  $u=0.3798(2)$ . Recently Fleet (1981) found  $u=0.3799(1)$ .

Verwey and deBoer (1936) used electrical conductivity measurements to demonstrate that magnetite is an inverse spinel with the structural formula  $\text{Fe}^{3+}[\text{Fe}^{2+}\text{Fe}^{3+}]_4\text{O}_4^{2-}$  (the ions between square brackets are on octahedral sites) and a unit cell content  $\text{Fe}_8^{3+}[\text{Fe}_8^{2+}\text{Fe}_8^{3+}]\text{O}_{32}^{2-}$ . The oxygen ions are in equipoint position 32(e), and form a face centred cubic framework with 8  $\text{Fe}^{3+}$  ions per unit cell in tetrahedral sites, with position 8(a), and 8  $\text{Fe}^{2+}$  ions and the remaining 8  $\text{Fe}^{3+}$  ions randomly distributed over octahedral sites with position 16(d).

An extensive survey of existing literature shows that a number of different values have been reported for the cell parameter of magnetite. This variation seems to have come about because much of the material studied has not been well characterized; these variations are probably due to the presence of impurities in the samples. Careful X-ray analysis of stoichiometric natural and synthetic single crystals has given values for the cell parameter in the range  $8.393 \text{ \AA}$  to  $8.3963 \text{ \AA}$ .

Despite a substantial amount of X-ray work, spectroscopic measurements and studies of the electrical and magnetic properties, uncertainties still remain as to the precise symmetry of magnetite and to the cation distribution of titaniferous magnetites. The solution of these problems forms a major part of this thesis.

#### 1.4 The Structure of Maghemite

It has been proposed, on the basis of a limited amount of X-ray and electron diffraction evidence, that the space group of maghemite is given by the enantiomorphous pair  $P4_132$ - $P4_332$  (Braun, 1952; Smith,

1979). If small changes in atom position and the presence of cation vacancies are ignored this proposed space group would simplify to that normally assumed for the spinel structure (Fd3m). However, no detailed study of the crystal structure of maghemite has been undertaken. Such a study is one of the main aims of the present work.

On the basis of the limited amount of data available previous workers have assumed the cation vacancies to be restricted to octahedral sites and the structural formula to be  $\text{Fe}^{3+}[\text{Fe}_{1.67}^{3+}\square_{0.33}]_4\text{O}_4^{2-}$ , with a unit cell content of  $\text{Fe}_8^{3+}[(\text{Fe}_{1.33}^{3+}\square_{2.67})\text{Fe}_{12}^{3+}]_{32}\text{O}_{32}^{2-}$ , where  $\square$  represents a cation vacancy and the ions between square brackets are on octahedral sites. If the proposed structure is correct, then the atomic arrangement in maghemite is very similar to that of ordered  $\text{LiFe}_5\text{O}_8$  (Tomas et al. 1983), but with the 1.33  $\text{Fe}^{3+}$  ions and 2.67 vacancies in maghemite occupying the positions normally occupied by the 4 lithium ions in  $\text{LiFe}_5\text{O}_8$ .

### 1.5 Compositional Variations in Synthetic Spinel

If we take the general formula for a spinel oxide as  $\text{PQ}_2\text{O}_4$ , there are three basic types of synthetic spinel:  $\text{P}^{2+}\text{Q}_2^{3+}\text{O}_4^{2-}$  (2-3 spinels),  $\text{P}^{4+}\text{Q}_2^{2+}\text{O}_4^{2-}$  (4-2 spinels) and  $\text{P}^{6+}\text{Q}_2^{+}\text{O}_4^{2-}$  (6-1 spinels). Other possible types can be formed from these three by substitution, for example,  $\text{P} \rightarrow 1/2(\text{P}^{++} + \text{Q}^{3+})$  giving  $\text{P}_{0.5}^{++}\text{Q}_{2.5}^{3+}\text{O}_4^{2-}$ , or  $\text{P}^{2+} \rightarrow \square_{0.33} + \text{Q}^{3+}$  giving the  $\gamma\text{-Fe}_2\text{O}_3$  type cation-deficient spinels.

A wide range of cations with radii ranging from 0.4 to 1.0 Å can be incorporated into the spinel structure, most into both tetrahedral and octahedral sites. Table 1.2 gives a list of these cations. The smallest cations, with valencies greater than 4, e.g.  $\text{Mo}^{6+}$  and  $\text{W}^{6+}$ , are only

Table 1.2 Cations occurring in tetrahedral and octahedral sites in the three basic synthetic spinel types.

Type	Tetrahedral ions	Octahedral ions
2-3	Al <sup>3+</sup> , Ga <sup>3+</sup> , Fe <sup>3+</sup> , Ni <sup>2+</sup> , Cu <sup>2+</sup> , Mg <sup>2+</sup> , Co <sup>2+</sup> , Zn <sup>2+</sup> , In <sup>3+</sup> , Fe <sup>2+</sup> , Mn <sup>2+</sup> , Cd <sup>2+</sup> .	Al <sup>3+</sup> , Co <sup>3+</sup> , Cr <sup>3+</sup> , Ga <sup>3+</sup> , V <sup>3+</sup> , Fe <sup>3+</sup> , Mn <sup>3+</sup> , Co <sup>2+</sup> , Mg <sup>2+</sup> , Rh <sup>3+</sup> , Ti <sup>3+</sup> , Ni <sup>2+</sup> , Cu <sup>2+</sup> , Fe <sup>2+</sup> , In <sup>3+</sup> , Mn <sup>2+</sup> .
4-2	Si <sup>4+</sup> , Ge <sup>4+</sup> , Mg <sup>2+</sup> , Co <sup>2+</sup> , Zn <sup>2+</sup> , Fe <sup>2+</sup> , Mn <sup>2+</sup> .	Mn <sup>2+</sup> , Y <sup>4+</sup> , Ti <sup>4+</sup> , Mo <sup>4+</sup> , Co <sup>2+</sup> , Mg <sup>2+</sup> , Ni <sup>2+</sup> , Sn <sup>4+</sup> , Zn <sup>2+</sup> , Fe <sup>2+</sup> , Mn <sup>2+</sup> .
1-6	Mo <sup>6+</sup> , W <sup>6+</sup> .	Li <sup>+</sup> , Na <sup>+</sup> , Ag <sup>+</sup> .

found in tetrahedral sites while the large monovalent cations such as  $\text{Li}^+$ ,  $\text{Na}^+$  and  $\text{Ag}^+$ , occurring mainly in 6-1 spinels, are confined to the octahedral sites. It is this wide range of possible cation substitutions that makes synthetic spinels one of the most extensive range of compounds known, in fact more than 200 different forms exist. A summary of the compositional ranges for some of the most important synthetic spinels, together with structural parameters is given by Blasse (1964), see also Borrelli (1975).

#### 1.6 Compositional Variations in Natural Magnetites and Maghemites

In principle, end-member magnetite should contain 48.24wt%  $\text{Fe}^{3+}$  and 24.12wt%  $\text{Fe}^{2+}$ , but in natural specimens it is possible for large percentages of  $\text{V}^{3+}$  and  $\text{Cr}^{3+}$  to substitute for  $\text{Fe}^{3+}$ , small amounts of  $\text{Al}^{3+}$  replacing  $\text{Fe}^{3+}$  are also found. Major substitutions of  $\text{Ca}^{2+}$ ,  $\text{Mg}^{2+}$  and  $\text{Mn}^{2+}$  for  $\text{Fe}^{2+}$  can occur and in the extreme case it is possible for  $\text{Mg}^{2+}$  to completely replace  $\text{Fe}^{2+}$  leading to the formation of magnesioferrite ( $\text{MgFe}_2\text{O}_4$ ). Minor replacements of  $\text{Fe}^{2+}$  by  $\text{Ni}^{2+}$ ,  $\text{Co}^{2+}$  and  $\text{Zn}^{2+}$  is not uncommon. Small percentages of  $\text{Si}^{2+}$  as an impurity have been reported, some of this is likely to be present in the form of non-opaque mineral impurities but it is possible that some  $\text{Si}^{2+}$  does enter the structure. Many magnetites are found to contain a significant amount of titanium, in fact a complete solid solution series exists between magnetite and ulvöspinel ( $\text{Fe}_2\text{TiO}_4$ ) above  $600^\circ\text{C}$ . Intermediate members of this series are known as titanomagnetites and their oxidation products, the titanomaghemites. The introduction of titanium into the structure leads to an increase in the unit cell parameter from  $8.396 \text{ \AA}$  in magnetite to  $8.53 \text{ \AA}$  for ulvöspinel (see figure 1.4). Naturally occurring

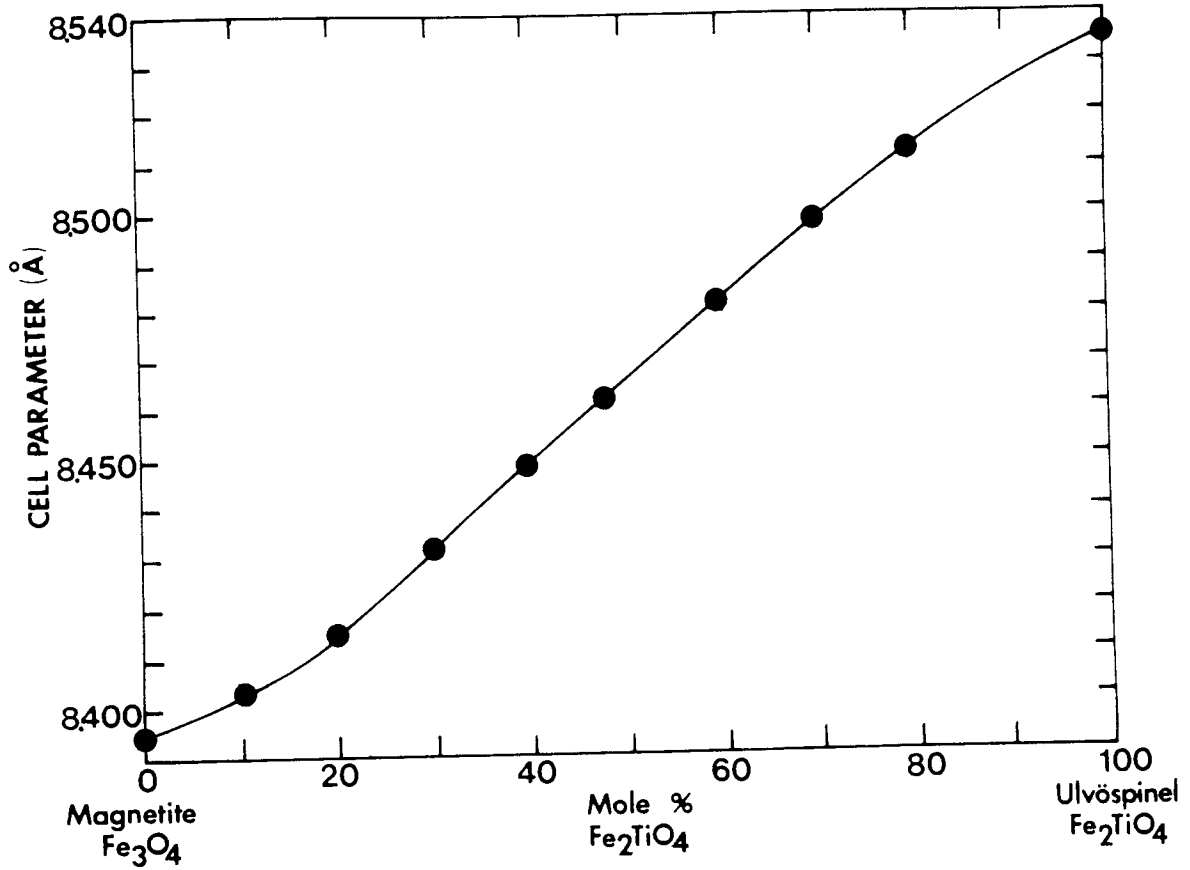


Figure 1.4 Variation of the cell parameter with composition found by previous authors in the  $(1-x)\text{Fe}_3\text{O}_4 \cdot x\text{Fe}_2\text{TiO}_4$  solid solution series (after Lindsley, 1965).

titanomagnetites usually contain divalent and trivalent cation impurities such as Mg, Al, Cr, Mn and Zn which replace a percentage of the iron. The concentrations of these cations can sometimes be appreciable (Creer and Ibbetson, 1970), Al is usually found to be the most abundant (Özdemir and O'Reilly, 1981).

The spinels which are the main concern of this study all lie in the  $\text{Fe}_3\text{O}_4$ - $\text{Fe}_2\text{TiO}_4$ - $\text{Fe}_2\text{TiO}_5$ - $\text{Fe}_2\text{O}_3$  quadrilateral of the  $\text{FeO}$ - $\text{Fe}_2\text{O}_3$ - $\text{TiO}_2$  ternary diagram (figure 1.5). The base of figure 1.5 represents the complete solid solution series between magnetite and maghemite. For intermediate members of this series the number of cations, when recalculated on the basis of 32 oxygens, is less than 24, reaching a value of 21.33 for end-member maghemite; i.e. there is a continuous increase in the number of cation vacancies per unit cell from 0 (in magnetite) to 2.67 (in end-member maghemite) for members of this series. The low temperature oxidation of magnetite to maghemite involves a replacement of three ferrous ions in the octahedral sites of magnetite by two ferric ions. This oxidation process leads to a continuous decrease in the cell parameter from  $8.396 \text{ \AA}$  in magnetite to somewhere between  $8.330 \text{ \AA}$  and  $8.340 \text{ \AA}$  in maghemite (see figure 1.6). Because of the continuous solid solution series, all stages of the oxidation of magnetite to maghemite are found in nature and consequently the optical and other physical properties vary for intermediate members of this series. Natural maghemites, particularly those from the Bushveld igneous complex of South Africa contain significant percentages of  $\text{TiO}_2$  and also quantities of  $\text{FeO}$  (Nicholls, 1955).  $\text{FeO}$  is occasionally found to be present in non-titaniferous maghemites (Basta, 1959).

Maghemite is metastable with respect to haematite ( $\alpha$ - $\text{Fe}_2\text{O}_3$ ) and cannot be formed directly from it. At suitable pressures and at elevated

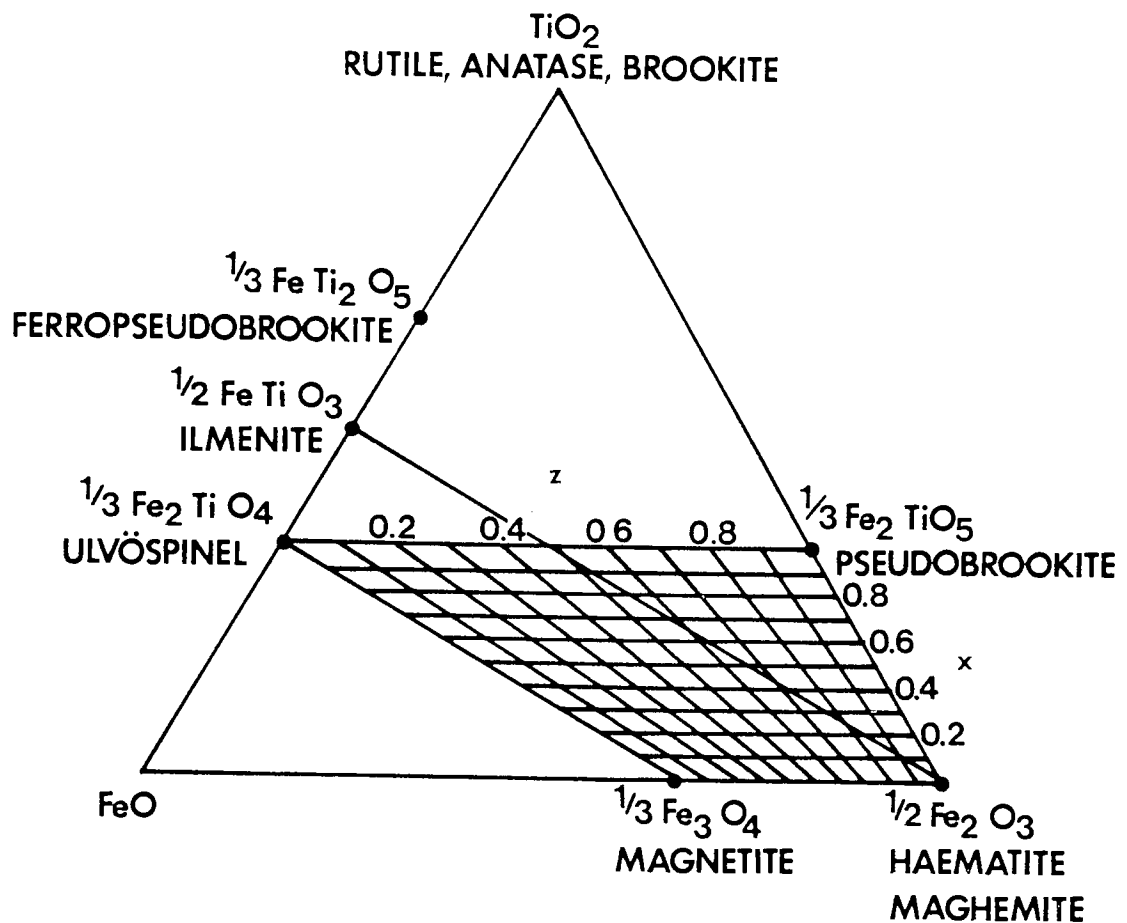


Figure 1.5 The  $\text{FeO}-\text{Fe}_2\text{O}_3-\text{TiO}_2$  ternary diagram showing the major solid solution series: magnetite-ulvöspinel, magnetite-maghemite, haematite-ilmenite and pseudobrookite-ferropseudobrookite. The  $\text{Fe}_3\text{O}_4-\text{Fe}_2\text{TiO}_4-\text{Fe}_2\text{TiO}_5-\text{Fe}_2\text{O}_3$  quadrilateral represents the titanomaghemites below  $350^\circ\text{C}$ . Any titanomaghemite within this quadrilateral may be described by the parameters  $x$  and  $z$ .

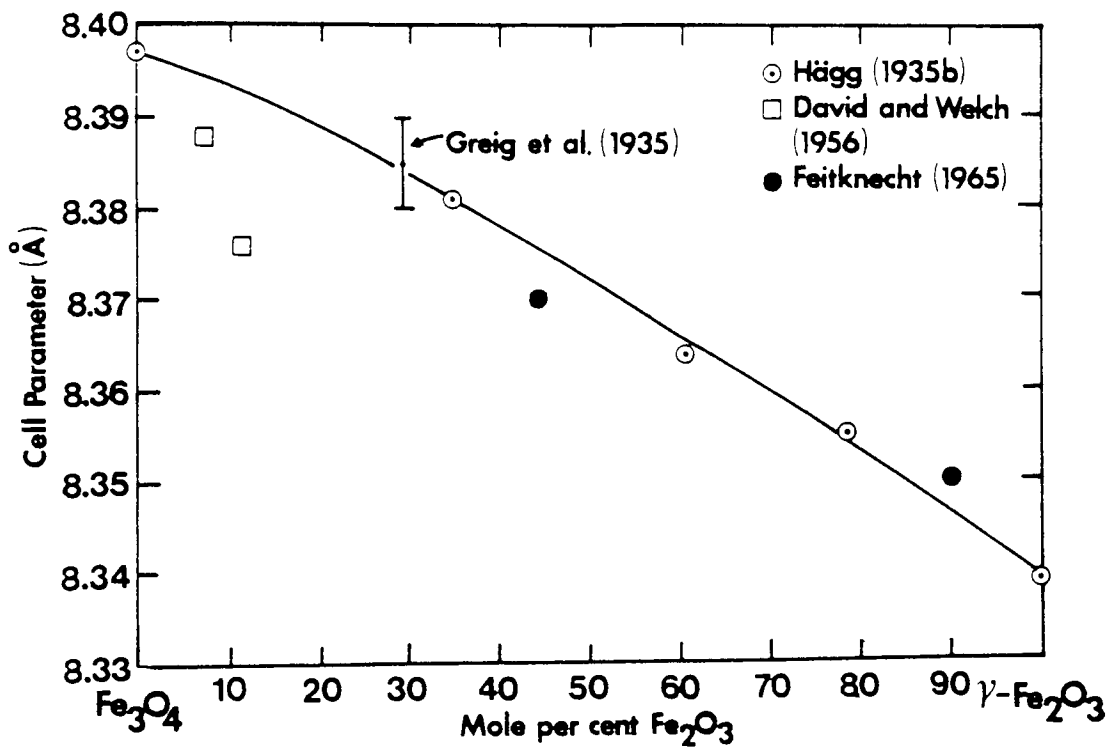
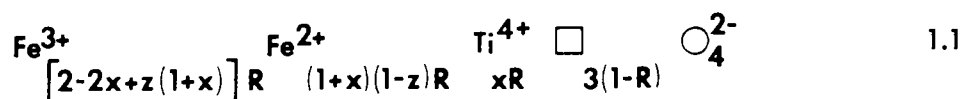


Figure 1.6 Variation of the cell parameter with composition found by previous authors for spinels in the  $\text{Fe}_3\text{O}_4$ - $\text{Fe}_2\text{O}_3$  solid solution series (after Lindsley, 1976).

temperatures maghemite is found to invert to haematite, this means that it is unlikely for maghemite to occur as a primary mineral in intermediate to high-temperature deposits. Values for the transition temperature of maghemite to haematite ranging from 200°C to 800°C have been reported in the literature (see for example Kushiro, 1960; Kachi et al. 1963; Readman and O'Reilly, 1970). The precise temperature seems to vary depending upon the previous history of the sample, the presence of small amounts of impurities and for synthetic specimens, the method of sample preparation.

The left-hand side of the  $\text{Fe}_3\text{O}_4$ - $\text{Fe}_2\text{TiO}_4$ - $\text{Fe}_2\text{TiO}_5$ - $\text{Fe}_2\text{O}_3$  quadrilateral (see figure 1.5) represents the magnetite-ulvöspinel solid solution series, which is continuous at high temperatures, but exsolution occurs below 600°C. The composition of any spinel lying within the quadrilateral may be defined by the parameters x and z, where x is the ratio of iron to titanium and z the oxidation parameter. Spinel such as magnetite and the titanomagnetites with  $z=0$  are stoichiometric and therefore have a cation to anion ratio of 3:4. Maghemite and the titanomaghemites with  $z<1$  are non-stoichiometric and the cation anion ratio is therefore no longer 3:4. The general formula for any spinel lying within the quadrilateral may be expressed by:



where  $z = (\text{number of Fe}^{2+} \text{ ions oxidized}) / (\text{original number of Fe}^{2+} \text{ ions})$ ,  
 $x = \text{Fe}_2\text{TiO}_4 / (\text{Fe}_3\text{O}_4 + \text{Fe}_2\text{TiO}_4)$  and  $R = 3 / [8+z(1+x)]$ . R is often referred to as the spinel stoichiometry parameter, it is equal to the ratio of oxygen ions in the stoichiometric case to that in the non-stoichiometric case.

Titanomaghemites result from the low-temperature oxidation of titanomagnetites, they are non-stoichiometric metastable spinels which invert, without a change of chemical composition, at temperatures above 350°C or at elevated pressure (Kushiro, 1960) to a multiphase mixture of titanomagnetite and ilmenohematite (Nagata, 1961; Readman and O'Reilly, 1970). The products resulting from inversion are found to be very much dependent upon the composition of the parent titanomagnetite. Usually any Fe<sup>2+</sup> in the titanomaghemite goes into an iron-rich spinel phase, Ti<sup>4+</sup> goes to the formation of ilmenite or in highly oxidized samples, anatase (TiO<sub>2</sub>) or pseudobrookite (Fe<sub>2</sub>TiO<sub>5</sub>). Haematite appears as an inversion product of the most highly oxidized specimens.

#### 1.7 Electrical Properties of Magnetite and Substituted Magnetites

At room temperature magnetite has an electrical conductivity ( $\sigma$ ) of the order of 250  $\Omega^{-1} \text{cm}^{-1}$ . A plot of conductivity against the reciprocal of the absolute temperature ( $T^{-1}$ ) covering a broad temperature range, is shown in figure 1.7. Above 150 K magnetite behaves as a semiconductor with thermally activated electrical conductivity. Parker and Tinsley (1976) showed that at temperatures very much greater than the Curie temperature (858 K), the conductivity is given by the formula:

$$\sigma = AT^{-1} \exp(-q/kT) \quad 1.2$$

where  $A=490 \Omega^{-1} \text{cm}^{-1} \text{K}$ ,  $q=99(3) \times 10^{-3} \text{eV}$  and  $k$ =Boltzmann's constant. The above equation is also found to predict the maximum observed in the conductivity versus temperature curve (figure 1.7) at approximately 1100 K. Below the Curie temperature, magnetite behaves as a metal and

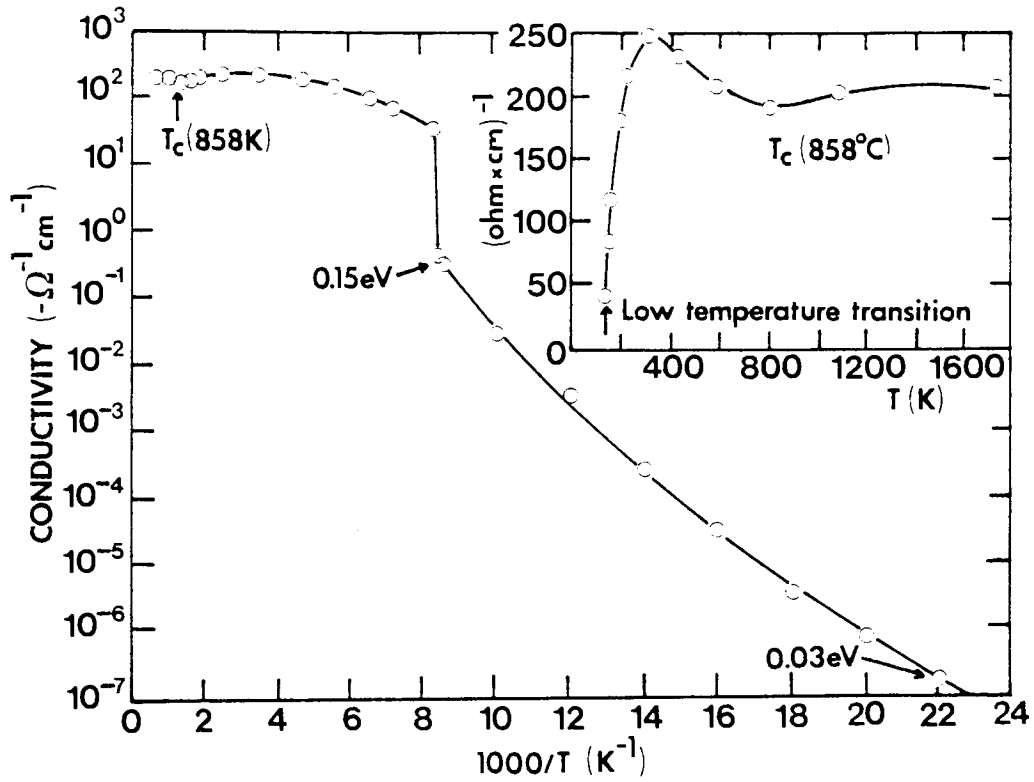


Figure 1.7 Variation of the electrical conductivity of a single crystal of  $\text{Fe}_3\text{O}_4$  with temperature (after Miles et al. 1957)

the conductivity departs from that given by the above equation. In the vicinity of room temperature a second maximum in the electrical conductivity occurs (see figure 1.7).

At low temperatures, magnetite undergoes an ordering transition. Above the transition there are equal numbers of  $\text{Fe}^{2+}$  and  $\text{Fe}^{3+}$  ions distributed at random over the octahedral sites. Verwey, Haayman and Romeijn (1947) suggested that a rapid electron exchange process was taking place between  $\text{Fe}^{2+}$  and  $\text{Fe}^{3+}$  ions on the octahedral sites. This fast electron hopping has since been confirmed (see for example Bauminger et al. 1961; Ito et al. 1963; Sawatzky et al. 1969). Below the transition a reduction in crystal symmetry provides separate sites for  $\text{Fe}^{2+}$  and  $\text{Fe}^{3+}$  ions and the electrons move to satisfy this. This transition is normally referred to as the Verwey transition and occurs at approximately 119 K. The precise temperature is very much dependent upon sample purity. The transition is accompanied by a decrease in the electrical conductivity by a factor of 100, a specific heat anomaly and a decrease in the ease of magnetization. Verwey, Haayman and Romeijn (1947) proposed that the transition to the low-temperature phase, which was originally thought to be orthorhombic, came about because of a discontinuation of the electron hopping process accompanied by an ordering of the  $\text{Fe}^{2+}$  and  $\text{Fe}^{3+}$  ions on octahedral sites. Orthorhombic symmetry for the low-temperature phase was apparently confirmed by Hamilton (1958). Since the work of Hamilton (1958) there has been much controversy as to the structure of the low-temperature phase. Orthorhombic symmetry has been disproved using electron diffraction by Chikazumi et al. (1971); using X-ray diffraction by Iida et al. (1973) and Vieland (1975); using neutron diffraction by Shirane et al. (1975) and Iizumi et al. (1975). The most recent study, carried out using

neutron diffraction by Iizumi et al. (1982) has shown the low-temperature phase to be monoclinic with space group Cc. Below the transition, down to a temperature of around 10 K magnetite behaves as a semiconductor with a temperature dependent activation energy. In this region the conductivity depends upon a formula derived by Mott (1969) given by:

$$\sigma = A \exp(-B/T^{1/4}) \quad 1.3$$

Any model which attempts to explain the electrical conductivity of magnetite must also explain the occurrence of the Verwey transition. The most recent models use the idea of a splitting of the electronic  $3d^6$  levels of octahedral  $Fe^{2+}$  in the low-temperature phase by an energy gap of approximately 0.1 eV. Charge transport is then brought about by carriers, either created by thermal activation across the energy gap or introduced by impurities or by oxygen non-stoichiometry. These separate energy levels form narrow sub-bands which overlap above the transition.

The presence of small amounts of impurity or oxygen non-stoichiometry has two main effects. Firstly, the low-temperature phase becomes imperfect, this lowers the temperature of the Verwey transition and can even lead to its disappearance altogether at certain critical impurity concentrations. Secondly, the ratio of ferrous to ferric ions changes which introduces charge carriers into one of the split sub-bands i.e. positive charge carriers (holes) into the lower filled band or electrons into the higher empty bands, depending upon the impurity present. As the concentration of impurities increases the resultant fluctuations of the electrostatic potential makes the free motion of charge carriers more difficult. These charge carriers may be thermally

activated to 'hop' to other ions and thereby contribute to the electrical transport.

The electrical conductivity of the low-temperature phase is very sensitive to oxygen non-stoichiometry. Conversely, above the transition the influence is small since both sub-bands overlap and the relative change in charge carrier numbers is very small. Impurity ions have similar effects as cation vacancies: cations with valencies 1 or 2 reduce the number of ferrous ions and introduce holes; cations with higher valencies act as donors. In each case the effect is small above the Verwey transition.

In conclusion, over a fairly broad temperature range the electrical conductivity of magnetite can be represented by:

$$\sigma = AT^{-\beta} \exp(-q/kT) \quad \beta = 0.1 \text{ or } 3/2 \quad 1.4$$

The activation energy for the conduction process to occur above the Verwey transition is equal to the sum of the energy  $q_n$  needed to remove an electron from the  $\text{Fe}^{2+}$  ion plus the mobility activation energy  $q_\mu$  required to transfer an electron between  $\text{Fe}^{2+}$  and  $\text{Fe}^{3+}$ .

### 1.8 Magnetic Properties of Magnetite and Maghemite

Magnetite possesses a type of magnetic ordering known as ferrimagnetism. The tetrahedral sites form a magnetic substructure (A) and the octahedral sites a second substructure (B), these two substructures are crystallographically inequivalent. The magnetic moments of the two substructures align antiparallel. Néel (1948) proposed the name ferrimagnetism for this type of magnetic ordering.

The magnetic properties of magnetite and its derivatives arise because of: the presence of unpaired 3d electrons; superexchange interactions between adjacent cations; the unequal numbers of cations on tetrahedral and octahedral sites. The oxygen ions have no net magnetic moment, hence the magnetic properties are due entirely to the unpaired 3d electrons of the iron atoms. The magnetic moment of any atom containing 3d electrons is normally the sum of the electron spin and the orbital moments. In any spinel oxide however, the orbital contribution to the net magnetic moment is quenched by electronic fields produced by the surrounding oxygen anions. The atomic magnetic moment ( $m$ ) then becomes the moment due to the electron spin and is equal to  $\mu_{\beta}n$ , where  $\mu_{\beta}$  equals one Bohr magneton and  $n$  is the number of unpaired electrons (see for example Bleaney and Bleaney, 1978). The magnetic moment of the  $\text{Fe}^{2+}$  ion is then due to the four unpaired electron spins and equals  $4\mu_{\beta}$ . The trivalent ion gives up two 4s and one 3d electron so that  $\text{Fe}^{3+}$  has a net magnetic moment of  $5\mu_{\beta}$ .

The cations are separated by the larger oxygen anions which prevents direct contact between the cation orbitals. This makes direct magnetic exchange interactions very weak indeed. Instead, indirect exchange (superexchange) occurs via the 2p orbitals of the anions. Superexchange involves the temporary transfer of one of the oxygen 2p-electrons to the unfilled d-shell of the neighbouring cation. The oxygen anion now has one unpaired spin and has become temporarily paramagnetic. While in this state it is able to interact with the cation. The effect results in antiparallel alignment of the electron spins of the cations on tetrahedral and octahedral sites. Apart from the electronic structure of cations, the magnetic exchange interactions are very much dependent upon the distance and angles between two interacting cations and the

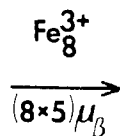
intervening anion. Usually only the interactions between the two cations in contact with the anion are considered important, the remaining interactions are very weak and make only a minor contribution to the magnetic properties.

Superexchange interactions exist between cations on tetrahedral or A-sites, these are referred to as AA interactions, similarly between the octahedral or B-site ions there are BB interactions. A third type of interaction takes place between ions on A and B-sites and is known as the AB interaction. All three interactions are believed to be antiferromagnetic in character. The strength of the interaction depends on the degree of orbital overlap of oxygen 2p-orbitals and the cation 3d-orbitals. The interaction decreases as the distance between the cations increases and as the angle of cation-oxygen-cation decreases from  $180^\circ$  to  $90^\circ$ . According to Néel (1948) the AB interaction is the most important in spinel ferrites since the angle is around  $125^\circ$  while the BB interaction is negligible because the angle equals  $90^\circ$ . The interaction is such that antiparallel alignment of the magnetic moments of the ions on tetrahedral and octahedral sites results (Néel, 1948).

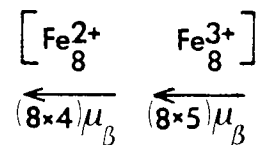
Magnetite possesses the inverse spinel structure (see section 1.3) with 8  $\text{Fe}^{3+}$  ions on tetrahedral sites and 8  $\text{Fe}^{2+}$  and 8  $\text{Fe}^{3+}$  ions on octahedral sites.

The magnetic structure may be represented by:

Tetrahedral sites



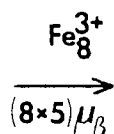
Octahedral sites



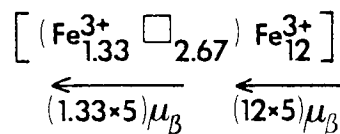
Since the moments of tetrahedral and octahedral sites are opposed the resultant magnetic moment of one molecule of magnetite is just that of the  $\text{Fe}^{2+}$  ions, that is  $32\mu_\beta$  per unit cell or  $4\mu_\beta$  per molecule. Smit and Wijn (1959) found a value of  $4.1\mu_\beta$  by experiment. The discrepancy of  $0.1\mu_\beta$  per molecule is thought to arise because of incomplete quenching of the orbital moment.

For maghemite the magnetic structure may be represented by:

Tetrahedral sites



Octahedral sites



The resultant moment for this structural formula is  $26.67\mu_\beta$  and the moment per molecule of  $\gamma\text{-Fe}_2\text{O}_3$  is  $2.5\mu_\beta$ .

### 1.9 Cation Distribution in Spinel and the Crystal Chemistry of Iron-Titanium Spinel Oxides

Early attempts to explain the cation distribution of spinels used simple electrostatic theory in which the ions were regarded as charged, polarizable, rigid spheres with a definite radius. The lattice energy being represented by the sum of the Madelung potential, the polarization

energy and the Born repulsive forces (Verwey and Heilmann, 1947; Romeijn, 1953). Goodenough and Loeb (1955) realized that these conventional electrostatic energy considerations are a gross oversimplification of the problem. They found tetrahedral and octahedral covalent bonds to have a considerable influence on, not only the cation distribution, but lattice distortion effects and the magnetic exchange mechanisms as well. This led to the proposal of a new magnetic exchange interaction, semicovalent exchange, in an attempt to explain the magnetic properties of the spinels in the presence of these two types of hybrid covalent bond.

Crystal field theory along with experimentally obtained optical absorption data was used by McClure (1957) to calculate octahedral site preference energies for transition metal ions in the spinel structure. The ion with the largest octahedral site preference energy occupies the octahedral sites thereby determining whether the spinel is normal or inverse. Cation distributions predicted by this model were in good agreement with most of those found by experiment. Dunitz and Orgel (1957) also discussed the cation distribution in spinel oxides in terms of crystal field theory. The crystal field stabilization energies predicted varied in such a way as to account for the observed cation distributions reasonably well. Unfortunately, two important factors were not taken into account in this model. Firstly, the variation of Madelung energy as a function of the oxygen positional parameter (Verwey et al. 1948; Gorter, 1954) was not allowed for, and secondly, no account of the variation in crystal field stabilization energy with atomic number for ions in tetrahedral and octahedral sites was made, i.e. as the atomic number increases, and the ionic radius decreases, the tetrahedral site becomes more stable with respect to the octahedral site. Dunitz and

Orgel (1957) were surprised that crystal field theory did give such good agreement between predicted cation distributions and those found by experiment. It seems that this agreement is partially due to the limited amount of experimental data available to them at the time.

The effects of the Madelung energy and the short-range repulsive interaction due to electron orbital overlap between neighbouring ions in addition to the crystal field terms were included by Miller (1959). On this basis a set of site preference energies were calculated. It was found that, with the exception of spinels containing  $V^{3+}$ , the results accounted well for observed cation distributions in spinels containing transition and non-transition metal ions and a number of previously unexplained distributions were resolved.

Navrotsky and Kleppa (1967) studied the cation distribution in spinels using a thermodynamic approach. They equated the entropy change associated with the disordering of an initially normal spinel with the configurational entropy: the molar enthalpy of interchange of ions on tetrahedral sites with those on octahedral sites was then calculated from previously published cation distribution data. The resulting interchange enthalpies were then used to calculate site preference energies for divalent and trivalent cations in spinels. The results indicated that  $Zn^{2+}$ ,  $Cd^{2+}$  and  $In^{3+}$  ions have a strong tetrahedral site preference;  $Cu^{2+}$ ,  $Ni^{2+}$ ,  $Al^{3+}$ ,  $Mn^{3+}$  and  $Cr^{3+}$  have a strong octahedral site preference and  $Fe^{3+}$ ,  $Ga^{3+}$ ,  $Co^{2+}$ ,  $Mn^{2+}$ ,  $Mg^{2+}$  and  $Fe^{2+}$  have a small if not zero tetrahedral site preference. No data were available at that time for  $Ti^{4+}$ , but it was assumed to have a large octahedral site preference.  $Cr^{3+}$  was found to have the largest octahedral site preference of all the first transition metal ions. This particular model predicts that if the difference between the site preference energies for

the two cations in a binary spinel is large then a normal or an inverse spinel results, and if the difference is small, an intermediate distribution with significant temperature dependence is predicted.

Comparison of the site preference energies found by Navrotsky and Kleppa (1967) with those of Dunitz and Orgel (1957), McClure (1957) and Miller (1959) shows that, with the exception of  $\text{Co}^{2+}$ , agreement in all four cases is very good.

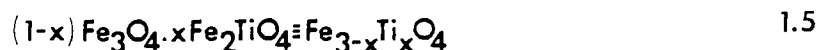
Mendelyevian type models, with scales based on pseudopotential theory were employed by Price, Price and Burdett (1982) to predict the cation distribution in spinels. This completely different approach to the problem is based on the assumption that if a physical property can be found experimentally which has a considerable influence on the distribution of ions between tetrahedral and octahedral sites, then that property must be related in some fundamental way to the parameters which determine the cation distribution. Qualitative rules result which predict the site preferences of the various cations from published data.

Structural sorting diagrams used by Price, Price and Burdett (1982) showed that a plot of the core size of ions on tetrahedral sites against those on octahedral sites, or alternatively a plot of electronegativities of the tetrahedral site ions against those of octahedral sites leads to a sorting of spinels into normal and inverse structures. Of the 172 spinels studied all but four were found to have cation distributions in agreement with that predicted by this approach. It was concluded from these results and from the thermodynamic approach (Navrotsky and Kleppa, 1967; O'Neill and Navrotsky, 1983) that ionic size and electronegativity are major factors in determining the cation distribution in spinels, far more so than the much smaller contribution from crystal field stabilization energies.

A modification to the model describing the thermodynamics of the cation distribution in spinels, originally given by Navrotsky and Kleppa (1967), was presented by O'Neill and Navrotsky (1983). This latter model, based on lattice energy calculations, revealed that the enthalpy change arising when cation disordering occurs is not linearly related to the degree of cation disorder but is related by a quadratic equation. Data available for the variation of cation distribution in spinels with temperature are found to agree well with this quadratic. There are two notable exceptions to this; namely  $\text{Fe}_3\text{O}_4$  and  $\text{MgAl}_2\text{O}_4$ . For  $\text{Fe}_3\text{O}_4$  it is necessary to include an additional term which takes account of the non-configurational entropy. The behaviour of  $\text{MgAl}_2\text{O}_4$  could not be adequately explained by this simple model.

#### 1.10 Cation Distribution of Titanomaghemites

The titanomagnetites are members of the solid solution series between magnetite ( $\text{Fe}_3\text{O}_4$ ) and ulvöspinel ( $\text{Fe}_2\text{TiO}_4$ ). Akimoto, Katsura and Yoshida (1957) showed that this series could be represented by:



where  $0 < x < 1$ . Titanomaghemites are single phase, metastable, non-stoichiometric spinels, resulting from the low temperature oxidation of titanomagnetite. The composition of a titanomaghemite is normally given in terms of two parameters, the first expresses the iron/titanium ratio and the second the degree of oxidation of the specimen. The Fe/Ti ratio is usually given as the atomic or molar fraction of  $\text{Fe}_3\text{O}_4$  or  $\text{Fe}_2\text{TiO}_4$  present in the parent titanomagnetite and has been shown to remain

Table 1.3 Details of the compositional parameters used by various authors to characterize titanomaghemites (after Lindsley, 1976).

Iron/Titanium Ratio		Oxidation Parameter		Reference
Definition	Range	Definition	Range	
$x = \frac{\text{Fe}_3\text{O}_4}{\text{Fe}_3\text{O}_4 + \text{Fe}_2\text{TiO}_4}$	$0 \leq x < 1$	—————	—————	Chevallier, Bolfa and Mathieu (1955).
$x = \frac{\text{Fe}_2\text{TiO}_4}{\text{Fe}_3\text{O}_4 + \text{Fe}_2\text{TiO}_4}$	$0 \leq x \leq 1$	—————	—————	Akimoto, Katsura and Yoshida (1957).
$\frac{\text{Fe}}{\text{Fe} + \text{Ti}}$	$\frac{2}{3} \rightarrow 1$	$\frac{32(\text{Fe} + \text{Ti})}{\text{O}}$	19.2 → 24	Akimoto & Katsura (1959), Katsura & Kushiro (1961), Sasajima (1961), Verhoogen (1962).
$q = \frac{\text{Fe}_2\text{TiO}_4}{\text{Fe}_3\text{O}_4 + \text{Fe}_2\text{TiO}_4}$	$0 \leq q < 1$	$N = \text{Fe}^{2+}$ oxidized per initial 4 oxygens	$0 \leq n < 1 + q$	
$X = \frac{\text{Fe}}{\text{Fe} + \text{Ti}}$	$1 \leq X \leq \frac{2}{3}$	$\gamma = \frac{32(\text{Fe} + \text{Ti})}{\text{O}}$	$24 \leq \gamma \leq \frac{64}{4-X}$	Zeller & Babkine (1965), Zeller et al. (1967a,b).
$x = \frac{\text{Fe}_2\text{TiO}_4}{\text{Fe}_3\text{O}_4 + \text{Fe}_2\text{TiO}_4}$	$0 \leq x \leq 1$	$Z = \frac{\text{Fe}^{2+} \text{ oxidized}}{\text{Original Fe}^{2+}}$	$0 \leq z \leq 1$	O'Reilly and Banerjee (1966, 1967).
$x = \frac{\text{Fe}_2\text{TiO}_4}{\text{Fe}_3\text{O}_4 + \text{Fe}_2\text{TiO}_4}$	$0 \leq x \leq 1$	$N = \text{Fe}^{2+}$ oxidized per initial 4 oxygens	$0 \leq N \leq \frac{8}{7}x - 1.6$	Schult (1968).
$x = \frac{\text{Fe}_2\text{TiO}_4}{\text{Fe}_3\text{O}_4 + \text{Fe}_2\text{TiO}_4}$	$0 \leq x \leq 1$	$\gamma = \text{Excess of oxygen}$	—————	Hauptman (1974).
$x = \frac{\text{Fe}_2\text{TiO}_4}{\text{Fe}_3\text{O}_4 + \text{Fe}_2\text{TiO}_4}$	$0 \leq x \leq 1$	$N = \text{Fe}^{2+}$ oxidized per initial 4 oxygens	$0 \leq N \leq 1 + x$	Gidskehaug (1975).

constant during oxidation. Table 1.3 lists some of the parameters suggested by various authors to express the composition of a titanomaghemite. The formula  $(\text{Fe}_2\text{TiO}_4)/(\text{Fe}_3\text{O}_4 + \text{Fe}_2\text{TiO}_4)$ , for expressing the Fe/Ti ratio of the specimen is found to be particularly useful because it applies to the unoxidized titanomagnetite as well as the oxidation product. The oxidation parameter ( $z$ ), which expresses the ratio of  $\text{Fe}^{2+}$  ions oxidized to the original number of  $\text{Fe}^{2+}$  ions is the most useful parameter for defining the degree of oxidation of the specimen.

Oxidation of the parent titanomagnetite occurs when oxygen atoms adsorbed on the surface of the crystal are ionized by the mobile electrons transferring between  $\text{Fe}^{2+}$  and  $\text{Fe}^{3+}$  ions near to the surface of the crystal. These newly-formed oxygen ions then bond to the surface thereby forming new octahedral and tetrahedral sites. These newly-formed sites are then rapidly filled by the diffusion of cations from the titanomagnetite leaving cation vacancies. This oxidation mechanism is basically an extension of that described by Colombo et al. (1964) for the oxidation of magnetite. The process is shown schematically in figure 1.8. Akimoto and Katsura (1959) found that on oxidation, natural titanomagnetites retain their Fe/(Fe+Ti) ratio which suggests that the diffusing  $\text{Fe}^{3+}$  ions are retained by the newly expanded structure.

Early attempts to determine the cation distribution of the titanomaghemites led to the proposal (Dunn and Dey, 1937) of a hypothetical end-member, cubic  $\text{FeTiO}_3$ . This proposed end-member was later renamed  $V\text{-FeTiO}_3$  by Nicholls (1955) and again by Chevallier, Bolfa and Mathieu (1955) but was never found in nature or prepared artificially. The concept has since been discarded. More useful models for the cation distribution of the titanomaghemites take into account

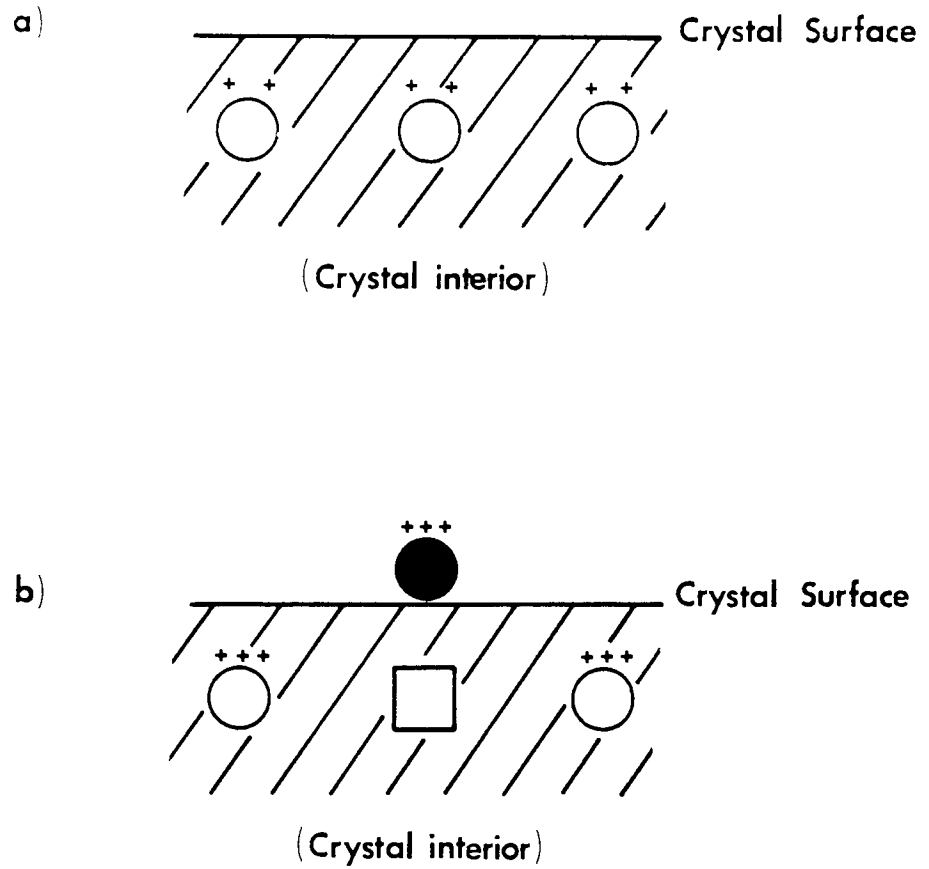


Figure 1.8 Schematic diagram to represent the oxidation of  $\text{Fe}^{2+}$  to  $\text{Fe}^{3+}$  leading to the production of titanomaghemite from titanomagnetite.  $\square$  represents a cation vacancy.

a) Before oxidation

b) After oxidation.

the distribution of cations in the unoxidized titanomagnetite and their redistribution as a result of oxidation.

It should be noted, because of the complexity of the problem, that the various authors have found it impossible to propose models for the cation distribution of intermediate members of this solid solution series without making assumptions. Four such models will now be considered and the assumptions and limitations involved in each will be discussed. The cation distribution of a natural titanomaghemite specimen, as found by experiment, is then compared with that predicted by the fourth model, since this really results from a combination of the other three.

i) Model 1 (Verhoogen, 1962)

The cation distribution predicted by this model assumes that the available  $\text{Fe}^{3+}$  ions enter tetrahedral sites until they are all fully occupied. Such an assumption has been supported by theoretical calculations (Goodenough and Loeb, 1955), but has been shown by O'Reilly and Banerjee (1965) not to be valid for some intermediate members of the solid solution series  $(1-x)\text{Fe}_3\text{O}_4 \cdot x\text{Fe}_2\text{TiO}_4$ , with  $0.2 < x < 0.8$ . This model is therefore too specific to be applicable to the titanomagnetites and titanomaghemites in general.

ii) Model 2 (O'Reilly and Banerjee, 1966)

This model takes account of cation distributions in the unoxidized titanomagnetite and the oxidation process, resulting from the ionization of oxygen atoms adsorbed to the crystal surface by the extra electrons

of the  $\text{Fe}^{2+}$  ions, after their oxidation to  $\text{Fe}^{3+}$ . The model assumes zero mobility for tetrahedral  $\text{Fe}^{2+}$  and  $\text{Fe}^{3+}$  ions and zero mobility for the  $\text{Ti}^{4+}$  ions. Cation vacancies are assumed to be restricted to octahedral sites.

The above model has several major drawbacks. Firstly, it has been assumed that only octahedral  $\text{Fe}^{2+}$  ions can be oxidized at the crystal surface because only octahedral  $\text{Fe}^{2+}$  can diffuse. But the oxidation of  $\text{Fe}^{2+}$  to  $\text{Fe}^{3+}$  need only involve the transfer of an electron to the adsorbed oxygen atoms at the crystal surface, charge balance being maintained by the diffusion of any sufficiently mobile cation to the surface. Secondly, as a result of the assumption of zero mobility for tetrahedral  $\text{Fe}^{2+}$ , the newly-formed tetrahedral sites at the surface must be occupied by  $\text{Fe}^{2+}$  and  $\text{Fe}^{3+}$  ions in the same ratio as the original sites in the unoxidized titanomagnetite. This is a highly unlikely occurrence. Sakamoto, Ince and O'Reilly (1968) for example, showed that some tetrahedral  $\text{Fe}^{2+}$  is oxidized. Thirdly, if only  $\text{Fe}^{2+}$  ions in octahedral sites were oxidized and diffuse into the newly-formed tetrahedral and octahedral sites, the product would be a spinel consisting of two separate phases, a titanomaghemite core surrounded by a mantle of maghemite, i.e. the product would be inhomogeneous. It is therefore only an approximation to assume that no tetrahedral  $\text{Fe}^{2+}$  oxidation takes place. Fourthly, for high degrees of oxidation, when only tetrahedral  $\text{Fe}^{2+}$  is being oxidized, it is possible for some vacancies to occur in tetrahedral sites.

iii) Model 3 (O'Reilly and Readman, 1971)

This third model helps to resolve some of the problems encountered by the other two models and includes important points used in previous models.

As stated above, ionization of the adsorbed oxygen atoms results in the formation of new tetrahedral and octahedral sites. The newly-formed tetrahedral sites are filled and the octahedral sites partially filled by the  $\text{Fe}^{3+}$  ions formed from diffused  $\text{Fe}^{2+}$  ions after oxidation at the crystal surface. Because of the low mobility of tetrahedral  $\text{Fe}^{2+}$  these ions come from octahedral sites leaving octahedral cation vacancies. The preference of  $\text{Fe}^{3+}$  for tetrahedral sites (Goodenough and Loeb, 1955) results in the newly-formed tetrahedral sites being filled with  $\text{Fe}^{3+}$  and the newly-formed octahedral sites being filled by  $5/6 \text{Fe}^{3+}$  and  $1/6$  vacancy. The diffusion process leads to the production of a mantle of magnetite at the crystal surface. The octahedral sublattice throughout the specimen then becomes homogeneous because of the diffusion of vacancies and  $\text{Fe}^{3+}$  into the crystal interior,  $\text{Fe}^{2+}$  and  $\text{Ti}^{4+}$  ions then diffuse out of the interior. Simultaneously, the tetrahedral sites become homogeneous because of a movement of electrons from the interior which is equivalent to moving  $\text{Fe}^{2+}$  from, and  $\text{Fe}^{3+}$  into the interior. Electron hopping between tetrahedral sites makes a contribution to this process but cannot account for oxidation alone since charge balance would not be maintained.

iv) Model 4 (Readman and O'Reilly, 1971)

Model 4 is based on Model 3 but the assumption of zero mobility for tetrahedral  $\text{Fe}^{2+}$  is replaced by a parameter which gives the probability of the availability of  $\text{Fe}^{2+}$  ions on tetrahedral and octahedral sites. This probability factor is based on the relative concentrations of  $\text{Fe}^{2+}$  on each site along with an additional term which defines the availability of  $\text{Fe}^{2+}$  ions depending upon their mobility. It was concluded that the availability of tetrahedral  $\text{Fe}^{2+}$  for oxidation was about 20% of the availability of octahedral site  $\text{Fe}^{2+}$ .

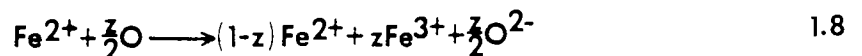
Taking the general formula for a stoichiometric titanomagnetite as:



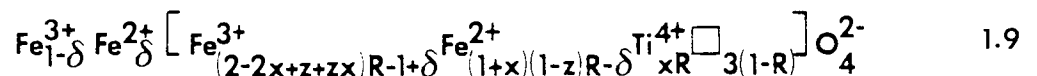
where  $0 < x < 1$ . If we define the oxidation parameter  $z$  as:

$$z = \frac{\text{number of Fe}^{2+} \text{ ions oxidized}}{\text{original number of Fe}^{2+} \text{ ions}} \quad 1.7$$

The oxidation reaction may be represented by:



where  $0 < z < 1$ . The cation distribution of any titanomaghemite may then be written as:



where  $R=8/[8+z(1+x)]$ ,  $x=Fe_2TiO_4/(Fe_3O_4+Fe_2TiO_4)$  and  $\delta$  is the total number of  $Fe^{2+}$  ions on tetrahedral sites. On oxidation the number of octahedral  $Fe^{2+}$  ions per molecule is reduced by  $z(1+x)R$  and the number of  $Fe^{3+}$  ions increased by  $z(1+x)R$ . The number of oxygen ions added for every four original oxygens is then equal to  $z/2(1+x)$ . The number of molecules in the sample is increased by a factor of  $(1/R)$ .

If  $f$  represents the fraction of  $Fe^{3+}$  ions formed from the oxidation of tetrahedral  $Fe^{2+}$ , assuming the electron hopping mechanism to operate then:

$$\delta = [\delta_0 - fz(1+x)] R \quad 1.10$$

The factor  $f$  is actually the product of a concentration factor  $f_c$  given by:

$$f_c = \frac{\delta}{(1+x)(1-z)R} \quad 1.11$$

where  $f_c$  is the ratio of the number of  $Fe^{2+}$  ions in tetrahedral sites to the total number of  $Fe^{2+}$  ions. The factor  $\alpha$  is a quantity which describes the availability of tetrahedral  $Fe^{2+}$  for oxidation. Substituting for  $f_c$  we get:

$$\delta = \frac{\delta_0(1-z)R}{1-z+\alpha z} \quad 1.12$$

when  $\alpha=1$  tetrahedral and octahedral  $Fe^{2+}$  are equally mobile and  $f=f_c$ . If the value of  $\alpha=0$  then  $Fe^{2+}$  in tetrahedral sites is immobile and not available for oxidation and Model 3 results.

## 1.11 Thesis Layout

Chapter 2 provides a review of the experimental evidence found by previous workers as regards the symmetry of the spinels in general. At an early stage of this work a body of X-ray intensity data, collected by Fleet (1981) from a natural magnetite crystal, became available. Since material had not been prepared for data collection at Aston an exercise was undertaken to examine this data under the space groups  $Fd\bar{3}m$  and  $F\bar{4}3m$ . Chapter 3 gives details of this examination. Chapter 4 gives details of a second refinement of the structure of magnetite under the space groups  $Fd\bar{3}m$  and  $F\bar{4}3m$ . The data used here were collected at Aston from a natural single crystal, and consisted of more than twice the number of X-ray intensities available for the refinement described in Chapter 3. This larger data set allowed a far more accurate determination of the structure parameters than was possible previously. A study of the intensities of Friedel related pairs of reflexions is a test which may be used to further substantiate  $F\bar{4}3m$  symmetry for magnetite. Chapter 5 gives details of this study. Chapter 6 is a study of the cation distribution and overall symmetry of a natural titanomaghemite specimen. Mössbauer spectroscopy and X-ray diffraction are the principal techniques employed in the solution of this problem. Chapter 7 provides a general discussion of the results obtained throughout the thesis, their implications, and suggestions for further work.

## CHAPTER 2

### REVIEW OF PUBLICATIONS RELATING TO THE SYMMETRY

#### OF THE SPINEL GROUP OF COMPOUNDS

##### 2.1 Review of Indirect Evidence in Favour of $F\bar{4}3m$ Symmetry for the Spinel

Many spinels are found to undergo a phase transition involving a change of structure but not of chemical composition (see for example Ohnishi and Teranishi, 1961; Goodenough, 1964; Brabers, 1971). The difference between the two structures above and below the transition comes about because of a slight readjustment of atom positions. In the spinels, a transition from cubic to tetragonal symmetry is common with a decrease in temperature. This is observed, for example, in  $\text{CuFe}_2\text{O}_4$  (Ohnishi and Teranishi, 1961),  $\text{FeCr}_2\text{O}_4$  (Wold et al. 1963) and in  $\text{Mn}_3\text{O}_4$  (Brabers, 1971). Dunitz and Orgel (1957) and Goodenough (1963) explained many of these transitions as being due to the presence of transition metal ions which exhibit the Jahn-Teller effect. These ions are orbitally degenerate but as the temperature is reduced local distortions occur which remove this degeneracy and lead to a reduction in symmetry (Finch et al. 1957). Direct physical evidence to support the above model has been observed by Cervinka (1965), Tanaka et al. (1966) and Brabers (1969). A review of the Jahn-Teller effect in spinels is given by Englman (1972) and also by Gehring and Gehring (1975).

In contrast to these compounds, spinels from the series  $\text{Mg}[\text{Cr}_x\text{Al}_{2-x}]\text{O}_4$  in which  $\text{Cr}^{3+}$  occupies the octahedral site are expected

to remain free from any structural distortions since  $\text{Cr}^{3+}$  is not a Jahn-Teller ion when in octahedral coordination. An X-ray diffraction study carried out by Grimes and Hilleard (1970) showed that an increase in  $x$  in this series led to a substantial increase in the Debye-Waller factor, similar to the results observed for the series  $\text{Mn}_x\text{Fe}_{3-x}\text{O}_4$  by Cervinka (1965). Grimes and Hilleard (1970) concluded that structural distortions occur in chrome spinels and that these distortions increase in magnitude with increasing chromium content. The suggestion that the anomalous behaviour of the chrome spinel series arises because the  $\text{Cr}^{3+}$  is in a low-spin state now seems incorrect since magnetic susceptibility measurements made on  $\text{MgCr}_2\text{O}_4$  by Lotgering (1962) showed that the values correspond to the normal spin-only value. This evidence from magnetic susceptibility measurements shows that  $\text{Cr}^{3+}$  is not a Jahn-Teller ion but does not show that structural distortions are absent. In fact there is a discrepancy noted by Lotgering (1962) which could only be accounted for if the trigonal component of the local crystal field is larger than that given by conventional symmetry.

Stahl-Brada and Low (1959) made electron spin resonance studies of the  $\text{Cr}^{3+}$  ion in natural single crystals of spinel and found that an exceptionally strong trigonal field is present with a  $[111]$  direction as an axis of symmetry. As pointed out by Henning and van den Boom (1973), electron spin resonance does not clearly distinguish between the trigonal point symmetries  $3m$  and  $\bar{3}m$ . The only indication of  $3m$  point symmetry they found was in the splitting of the  $\text{Cr}^{3+}$  ion energy levels deduced for zero magnetic field indicating a stronger trigonal field than expected for  $\bar{3}m$  symmetry. Lou and Ballentyne (1968), who studied the optical fluorescent spectra of a range of single crystals of  $\text{Mg}[\text{Cr}_x\text{Al}_{2-x}]\text{O}_4$  found that these distortions increased with increasing

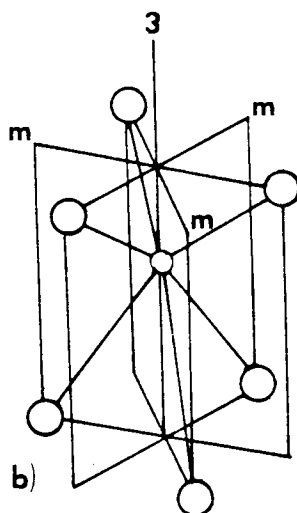
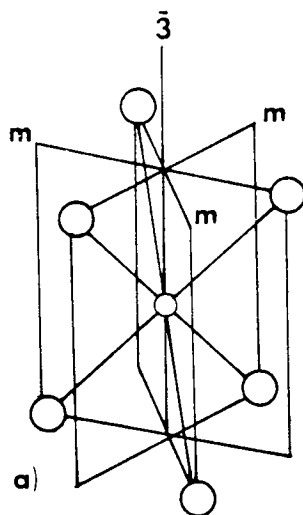


Figure 2.1 An illustration of the difference between the point symmetries a)  $\bar{3}m$

b)  $3m$  (after Grimes and Collett, 1971a).

chromium content. In addition, they noted that above a chromium content of 2wt% the point symmetry of the octahedral site is  $3m$ , a point symmetry not allowed under  $Fd\bar{3}m$ . Figure 2.1 shows the difference between the point symmetries  $\bar{3}m$  and  $3m$ . Had the local trigonal distortions been  $\bar{3}m$  then an increase in magnitude would be brought about by an increase in the oxygen positional parameter. X-ray diffraction studies of polycrystalline specimens of  $Mg[Cr_xAl_{2-x}]O_4$  by Grimes and Hilleard (1970) showed that no such change is observed. The increase in magnitude of the distortions with increasing chromium content shows up in an increase in the Debye-Waller factor, which for  $MgCr_2O_4$  is three times as large as that for  $MgAl_2O_4$ .

Grimes and Collett (1971a,b) pointed out that the results found from optical and X-ray measurements, carried out on the spinel series  $Mg[Cr_xAl_{2-x}]O_4$ , can be explained if the space group of these spinels is  $F\bar{4}3m$  rather than  $Fd\bar{3}m$ . Under this alternative space group, the point symmetry of the octahedral site is  $3m$ , as found by experiment, and allowance is made for the greatly increased trigonal component of the local crystal field which is needed to explain electron spin resonance measurements.

Studies made on the infrared spectra of the spinel series  $Zn_xMg_{1-x}Cr_2O_4$  by Tarte and Preudhomme (1963) showed that a decrease in complexity of the spectra is found with increasing zinc content. Assuming that this indicates a reduction in magnitude of the structural distortions in this series, then an almost distortion-free  $ZnCr_2O_4$  is expected. This is in fact found, since the Debye-Waller factor for this compound is found, by X-ray work, to be  $0.36 \text{ \AA}^2$  (Raccah, Bouchard and Wold, 1966) which is one third of that observed for  $MgCr_2O_4$ .

So far only structural distortions in the spinel series  $\text{Mg}(\text{Cr,Al})\text{O}_4$  have been explained by this alternative space group. It is highly unlikely that structural distortions are restricted to this series, Grimes (1972, 1973) has proposed that the spinel structure in general may be more correctly described by  $F\bar{4}3m$  symmetry. Polder (1950), for example, found that at low audio and radio frequencies the values for the dielectric constant of Mn-Zn and Ni-Zn ferrites rises by  $10^2$  to  $10^4$ ; this seems to be due to a permanent dipole moment, similar to that observed in  $\text{BaTiO}_3$  by Kay and Vousden (1949). Such behaviour, as pointed out by Fairweather, Roberts and Welch (1952), is not permitted by  $Fd3m$  symmetry.

These results indicate that the spinel structure exhibits a small deviation from  $Fd3m$  symmetry and that this deviation is associated with a displacement of the octahedral cations along a  $[111]$  direction, of the order of  $0.01$  to  $0.05 \text{ \AA}$  in oxides. The magnitude of this displacement is equivalent to that needed to produce the permanent dipole moment estimated by Peters and Standley (1958) to account for the dielectric constant observed in the Mg-Mn ferrites at  $200^\circ\text{C}$ .

Ultrasonic measurements by Kino and Lüthi (1971) made on  $\text{ZnCr}_2\text{O}_4$  gave a softening of the shear mode elastic constant  $c_{44}$  in the neighbourhood of  $40 \text{ K}$ . Similar effects have been observed for magnetite by Moran and Lüthi (1969) and for  $\text{NiFe}_2\text{O}_4$  by Gibbons (1957). Interpreting this softening using the selection rules of Nowick and Heller (1965) and Nowick (1968), a defect with trigonal distortion is indicated.

The almost exact agreement in frequency observed by O'Horo, Frisillo and White (1973) for  $\text{MgAl}_2\text{O}_4$  between that in the Raman spectrum at  $671 \text{ cm}^{-1}$  and the corresponding infrared absorption spectrum at

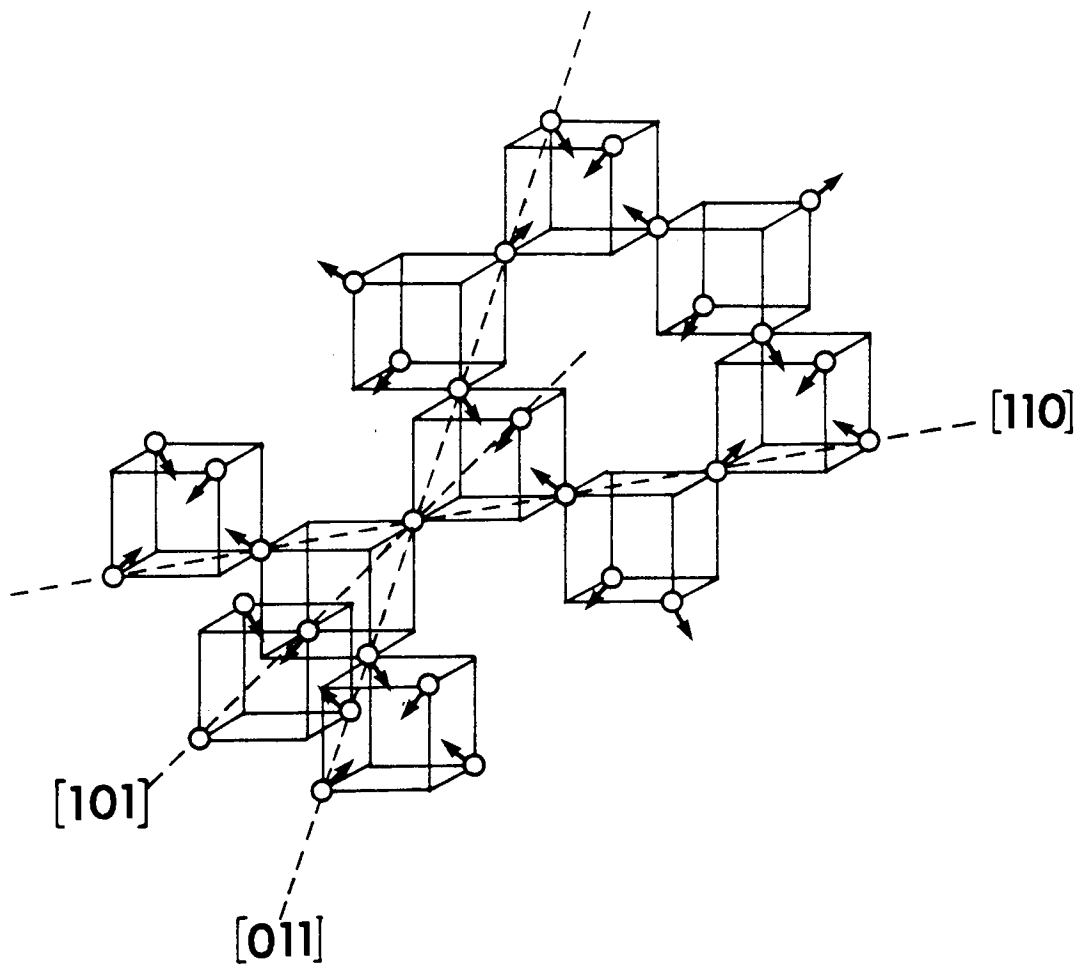


Figure 2.2 Octahedral ion sublattice of the spinel structure (after Grimes, 1973): arrows indicate the displacements which lead to  $F\bar{4}3m$  symmetry.

$670\text{ cm}^{-1}$  is a condition not allowed in a centrosymmetrical structure (Loudon, 1964). A similar situation has been observed in magnetite. Hart, Tenkin and Adams (1975) measured a Raman active mode at  $550\text{ cm}^{-1}$  and Boppart, Schlegel and Wachter (1980) found an infrared active mode at  $550\text{ cm}^{-1}$ . Again this agreement between frequencies in the infrared and Raman spectra is not permitted under a centrosymmetrical space group.

In order to explain the overall specific heat observed for  $\text{ZnFe}_2\text{O}_4$ , Grimes (1974) found it necessary to include a component which takes account of the off-centre  $\text{Fe}^{3+}$  ion in the octahedral site as occurs under  $F\bar{4}3m$  symmetry.

The symmetry proposed for the revised structure is  $F\bar{4}3m$ . The octahedrally coordinated metal ion sublattice is modified so that alternative groups expand and contract as shown in figure 2.2. These displacements occur along all  $\langle 111 \rangle$  directions simultaneously and do not lead to the property of ferroelectricity (Fairweather, Roberts and Welch, 1952) since the dipole moments which are created are arranged in the opposite sense and lead to antiferroelectricity (see sections 7.2 and 7.3 for details).

## 2.2 Double Diffraction

The phenomenon of double diffraction is referred to throughout section 2.3. This physical process will now be briefly considered to give some insight into how it arises and the effects produced.

Generally, reflexions present in the diffraction pattern produced by a given crystal are described mathematically by the kinematical theory of diffraction. When dealing with crystals of high symmetry,

using the short wavelength radiations necessary for detailed structure determination, it is possible for severe double diffraction to occur (Renninger, 1937), leading to the production of reflexions theoretically forbidden by symmetry.

Double diffraction occurs when the primary diffracted beams, formed inside the crystal specimen, act as secondary sources of diffraction. Many of the reflexions produced in this way coincide with existing primary diffraction reflexions; all newly-formed reflexions are due entirely to double diffraction. The Miller indices of these doubly diffracted reflexions are given by the sum of the indices of the two component primary reflexions. Hence, a reflexion of the type  $h_1+h_2$ ,  $k_1+k_2$ ,  $l_1+l_2$  is now possible, where  $h_1k_1l_1$  and  $h_2k_2l_2$  are any two allowed primary reflexions.

Theoretically, it is possible to test for double diffraction by rotating the crystal about the  $(h_1+h_2, k_1+k_2, l_1+l_2)$  scattering vector through the azimuthal or crystal angle. If the forbidden reflexion is real there should be no change in its intensity on rotation (within experimental error). On the other hand, if the reflexion is produced by double diffraction a large intensity variation will be observed. Ideally, the experiment should be carried out using a long wavelength radiation such as  $\text{CrK}\alpha$  ( $\lambda=2.291 \text{ \AA}$ ).

### 2.3 Diffraction Evidence

In theory, it should be possible to decide, using diffraction techniques, which of the two suggested space groups correctly describes the symmetry of the spinels since reflexions of the type  $\{hk0\}$  with  $h+k=4n+2$  are forbidden under  $Fd3m$  symmetry but allowed under  $F\bar{4}3m$ .

However, because the atomic displacements giving rise to  $F\bar{4}3m$  symmetry are small, the intensities of many of these reflexions are below the minimum detectable level. A further complication arises since reflexions of this type can be produced by the process of double diffraction, which leads to the production of otherwise forbidden reflexions (see section 2.2). The next step is to look in detail at the evidence found by previous authors for and against  $Fd\bar{3}m$  symmetry for the spinels, using electron, neutron and X-ray diffraction experiments.

### 2.3.1 Electron Diffraction Evidence

The use of electron diffraction to make a detailed study of the  $Fd\bar{3}m$  forbidden reflexions has been criticized because the short wavelength radiations and high voltages employed lead to considerable double diffraction. Whilst examining  $[001]$  orientated foils of  $MgAl_2O_4$  using transmission electron microscopy Hwang, Heuer and Mitchell (1973) observed  $\{200\}$  and  $\{420\}$  type  $Fd\bar{3}m$  forbidden reflexions. In addition, they examined foils of  $MgFe_2O_4$  and found  $200$  and  $420$  reflexions present in the diffraction patterns. They concluded that these reflexions could not have been produced by double diffraction in the orientation used and could not be caused by non-zero Laue zones.  $\{200\}$  and  $\{420\}$  type reflexions were also detected in  $MgFe_2O_4$  by Walters and Wirtz (1972). They concluded that these reflexions did not arise because of double diffraction but were produced because of superlattice formation. It is more likely that they are due to a departure from  $Fd\bar{3}m$  symmetry.

In an electron diffraction study of polycrystalline films of  $MnFe_2O_4$ , van den Berg, Lodder and Mensinga (1976) observed the

reflexions  $\bar{2} 0 0$ ,  $\bar{4} \bar{2} 0$  and  $\bar{6} 0 0$ . These reflexions were not thought to be produced by double diffraction and their observation was taken as support for  $F\bar{4}3m$  symmetry for this material.

Electron diffraction studies are not suitable for structure analysis but Heuer and Mitchell (1975) were able to compare the intensity ratio of the  $2 2 0$  reflexion with that of  $2 0 0$  for  $MgAl_2O_4$ . The result indicated that any off-centre displacement of the  $Al^{3+}$  ion in octahedral coordination was between  $0.006 \text{ \AA}$  and  $0.002 \text{ \AA}$ .

Mishra and Thomas (1977) heated a synthetic single crystal of  $MgAl_2O_4$  in the hot stage of a transmission electron microscope and found that at approximately  $450^\circ C$  the  $Fd3m$  forbidden reflexions disappeared and on cooling reappeared. From this observation they concluded that the symmetry of  $MgAl_2O_4$  at room temperature is  $F\bar{4}3m$ . The potential maximum through the octahedral site suggested by Grimes (1971) is the most likely explanation for this transition. Above  $450^\circ C$ , the octahedral ion has sufficient energy to overcome the potential barrier, the two non-equivalent positions under  $F\bar{4}3m$  become equivalent and the symmetry changes to  $Fd3m$  because of the increase in thermal vibration.

A natural single crystal of  $Mg_{0.85}Fe_{0.15}Al_2O_4$  was studied by Smith (1978) using electron diffraction, the electron beam being kept parallel to  $[001]$ ,  $\{200\}$  type reflexions were observed. In order to test for double diffraction the specimen was rotated about the  $[100]$  axis and the  $2 0 0$  reflexion observed. As the crystal rotated the reflexion was found to disappear and reappear. Similar results were found for a single crystal of magnetite. Smith (1978) concluded that the observed intensity of the  $2 0 0$  reflexion for these two materials was due almost entirely to double diffraction and that if a true Bragg peak exists then the

intensity of this peak must be far weaker than that found by Heuer and Mitchell (1975).

Tokonami and Horiuchi (1980) observed  $\{200\}$  type reflexions in  $\text{MgAl}_2\text{O}_4$  using electron diffraction and realized that double diffraction can occur not only because of reflexions from the zero order Laue-zone but also from the first order Laue-zone. They found that these reflexions were always observed along with  $\{1\ 21\ 1\}$  and  $\{3\ 21\ 1\}$  type reflexions from the first order Laue-zone. They concluded, since the  $\{200\}$  type reflexions disappeared with a minute change of orientation of the incident beam, that these reflexions were due entirely to double diffraction. They explained the results of Mishra and Thomas (1977) as being due to a decrease in the Debye-Waller factor with an increase in temperature, this was thought to give rise to a steady decrease in the intensity of the reflexion as the temperature increased. This interpretation does not really explain the disappearance of the  $2\ 0\ 0$  reflexion at  $450^\circ\text{C}$ ; if this theory is correct the reflexion should still be present if the X-ray exposure time is increased. However, this does not appear to be the case.

### 2.3.2 Neutron Diffraction Evidence

$\text{MgCr}_2\text{O}_4$  was examined by Infante and Fender (1973) using neutron diffraction. No additional reflexions were observed and no evidence was found to indicate a displacement of the  $\text{Cr}^{3+}$  ion along the  $\langle 111 \rangle$  direction. They carried out two structure refinements using the neutron diffraction data, one for  $Fd\bar{3}m$  symmetry and a second for  $F\bar{4}3m$ . The results obtained indicated that if the  $\text{Cr}^{3+}$  ion was displaced, the displacement must be less than  $0.02\ \text{\AA}$ .

Neutron time of flight studies of  $\text{Fe}_3\text{O}_4$  (Samuelsen, 1974) and  $\text{MgAl}_2\text{O}_4$  (Samuelsen and Steinsvoll, 1975) were found to support  $\text{Fd}\bar{3}\text{m}$  symmetry for these two materials. The crystal was rotated about the  $(200)$  scattering vector and it was found, in each case, that the intensity of the  $200$  reflexion varied. These results indicate that this reflexion was produced entirely by double diffraction. They concluded that any displacement of the octahedral site cation, if present, was less than  $0.004 \text{ \AA}$  in  $\text{Fe}_3\text{O}_4$  and less than  $0.0045 \text{ \AA}$  in  $\text{MgAl}_2\text{O}_4$ .

Rouse, Thomas and Willis (1976) made a neutron powder diffraction study of  $\text{MgAl}_2\text{O}_4$  and expected to observe the weak  $\text{Fd}\bar{3}\text{m}$  forbidden reflexions along with an enlarged Debye-Waller factor for the octahedrally coordinated cation, if  $\text{F}\bar{4}\bar{3}\text{m}$  symmetry is correct. Refinements of the neutron diffraction data were carried out under  $\text{Fd}\bar{3}\text{m}$  and  $\text{F}\bar{4}\bar{3}\text{m}$  symmetry but no indication of either of the above conditions was found. They concluded that the space group of  $\text{MgAl}_2\text{O}_4$  is  $\text{Fd}\bar{3}\text{m}$ .

In a neutron diffraction study carried out by Thompson and Grimes (1977) on a synthetic single crystal of  $\text{MgAl}_2\text{O}_4$  using a neutron wavelength which is suitable to reveal structural details, it was found that substantial double diffraction occurred. They realized that the effects of double diffraction could be greatly reduced if a longer wavelength was used, but concluded that neutron diffraction has severe limitations and is not really suitable for the determination of the space group of spinel by an examination of the weak forbidden reflexions.

In the experiments described in this section, none of the authors were able to positively identify any of the  $\text{Fd}\bar{3}\text{m}$  forbidden reflexions. This does not necessarily mean the space group of the spinels cannot be

$F\bar{4}3m$ , since, as pointed out by Heuer and Mitchell (1975), it is possible to get a combination of octahedral cation and anion shifts leading to an intensity below background for many of these forbidden reflexions.

### 2.3.3 X-Ray Diffraction Evidence

Electron density maps calculated from X-ray intensities for one natural and three synthetic single crystals of  $MgAl_2O_4$ , by Jagodzinski and Saalfeld (1958), showed that for all four samples there is a displacement of the octahedral cation from the  $Fd3m$  position, i.e. none of these crystals strictly obeyed the rules of  $Fd3m$  symmetry. However, no extra intensity peaks corresponding to a lower symmetry space group were observed.

Further evidence in favour of  $F\bar{4}3m$  symmetry for the spinels comes from a structural study carried out on  $\gamma$ - $Ni_2SiO_4$  by Marumo et al. (1974). The Fourier difference maps produced showed 8 peaks  $0.46 \text{ \AA}$  from the nickel atom, one in each of the 8  $[111]$  directions, the height of these peaks being approximately  $1.0 \text{ e\AA}^{-3}$ . These peaks were thought to occur because the nickel atom in the octahedral site vibrates with a larger amplitude along the body diagonal of the cube. Such an observation would be expected if this atom is restricted to an incorrect position by an erroneous choice of space group; i.e. it is far more likely that this effect is caused by the nickel atom being displaced along the  $[111]$  direction, as it would be if the space group was  $F\bar{4}3m$ .

Hilleard (1975), in a re-examination of data produced for  $MgCr_2O_4$  by Grimes and Hilleard (1970), gave further support to  $F\bar{4}3m$  symmetry for this particular spinel. The original value for the Debye-Waller factor found by Grimes and Hilleard (1970) of  $1.1 \text{ \AA}^2$  is rather high, a value of

around  $0.3 \text{ \AA}^2$  is expected (Grimes, 1972). The refinement of existing data by Hilleard (1975) under  $F\bar{4}3m$  symmetry led to a value of  $0.4 \text{ \AA}^2$  which is in good agreement with the value proposed by Grimes (1972) for this material.

In a single crystal X-ray diffraction study of a natural magnetite, Fleet (1981) observed weak reflexions of the type  $\{hk0\}$  with  $h+k=4n+2$ . He took these additional reflexions as being produced by double diffraction and rejected them since their intensity was found to vary if the conditions of diffraction were altered. Fleet (1981) therefore rejected the possibility of  $F\bar{4}3m$  symmetry for magnetite.

Grimes, Thompson and Kay (1983) made a single crystal X-ray diffraction study of synthetic  $\text{MgAl}_2\text{O}_4$  and observed  $Fd3m$  forbidden reflexions. The data obtained were refined under the space group  $Fd3m$  and then  $F\bar{4}3m$ , the forbidden reflexions being included in the latter refinement in an attempt to obtain a measure of the suspected deviations from  $Fd3m$  symmetry. A far better fit to the experimental data was found for the  $F\bar{4}3m$  refinement than that produced assuming  $Fd3m$  symmetry, even the weak forbidden reflexions gave a reasonable fit between observed and calculated structure factors. They came to the conclusion that the symmetry of this material is  $F\bar{4}3m$ .

Finally, it is worth mentioning that Higgins, Speer and Craig (1975) observed  $Fd3m$  forbidden reflexions on long exposure X-ray precession photographs of four thiospinels, namely, synthetic indite ( $\text{FeIn}_2\text{S}_4$ ), natural carrollite ( $\text{CuCo}_2\text{S}_4$ ), natural linnaeite ( $\text{CoCo}_2\text{S}_4$ ) and natural siegenite  $(\text{Co,Ni})_3\text{S}_4$ . These observations were taken to indicate that the symmetry of the thiospinels in general is lower than  $Fd3m$ .

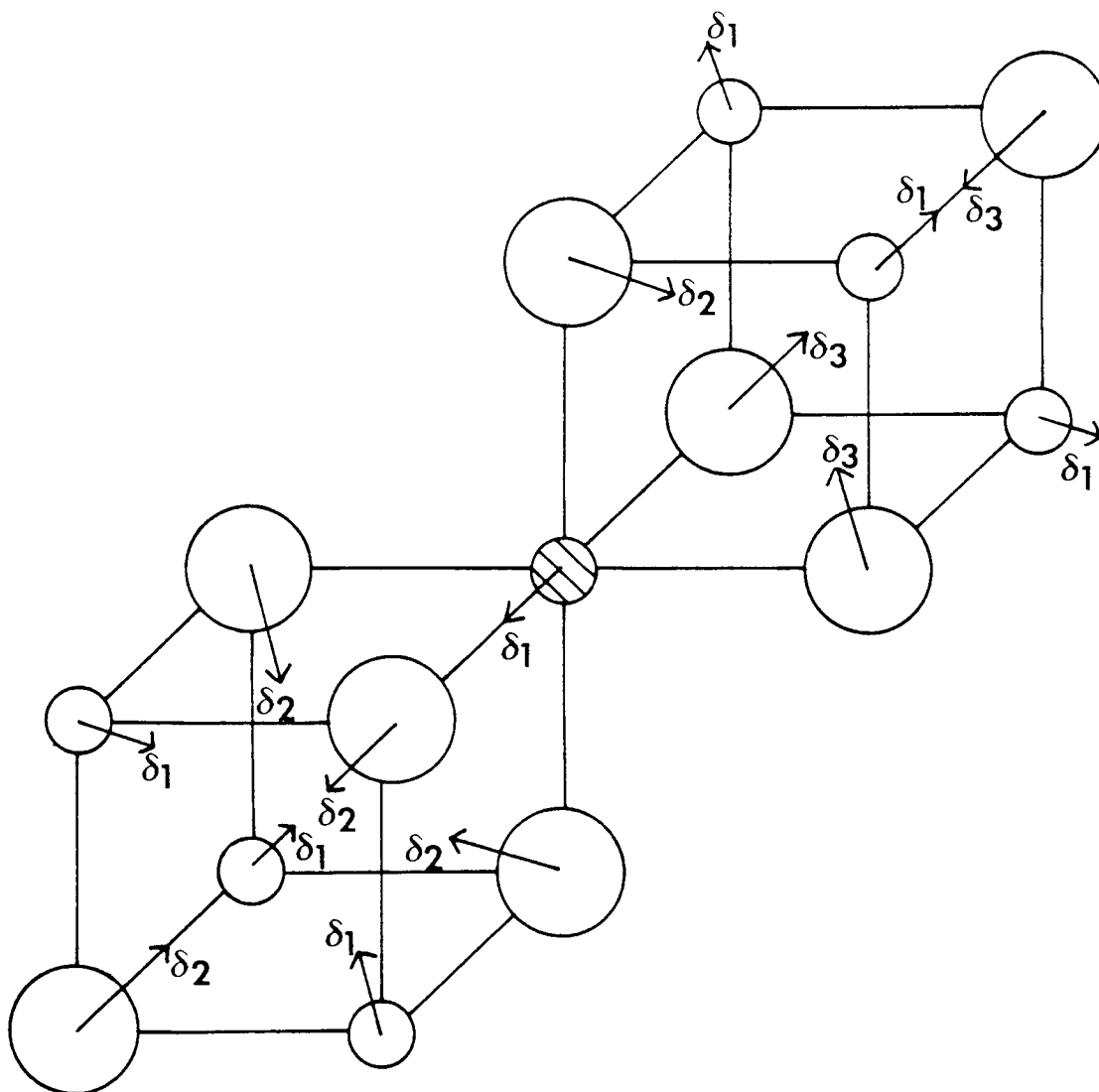


**Figure 2.3** The atom shifts occurring at an octahedral site in the spinel structure giving rise to  $F\bar{4}3m$  symmetry.  $\delta_1$  is the octahedral cation shift,  $\delta_2$  and  $\delta_3$  are the anion shifts from their  $Fd\bar{3}m$  positions. Large circles represent anions and small circles cations.

## 2.4 The Spinel's Under $F\bar{4}3m$ Symmetry

In order to explain the physical properties exhibited by a number of spinels, Grimes (1972, 1973) has proposed that the symmetry of this group of compounds can be more correctly described by the non-centrosymmetrical space group  $F\bar{4}3m$ , details of which are given in table 2.1

This alternative, lower symmetry space group, is obtained from the original by allowing the 32 anions to divide into two unique groups, the positional coordinates of each being given by the parameters  $u_2$  and  $u_3$ . The anions move along  $\langle 111 \rangle$  directions, each group moving in opposite directions thereby producing two separate tetrahedral sites. Cubic point symmetry ( $\bar{4}3m$ ) is retained and the cations may be regarded as dividing up into two groups, those on octahedral sites no longer occupy the centres of the anion octahedra but move along  $\langle 111 \rangle$  directions, their displacements being given by the parameter  $u_1$ . The point symmetry of the octahedral sites changes from the original  $\bar{3}m$  to  $3m$  with the loss of the d-glide planes.

Octahedral site cation positions are now controlled by the parameter  $u_1$ , where  $u_1 = 5/8 + \delta_1$ , and the two groups of anions by the parameters  $u_2$  and  $u_3$ , where  $u_2 = 3/8 + \delta_2$  and  $u_3 = 7/8 + \delta_3$  (see figure 2.3). If the structure does conform to  $Fd\bar{3}m$  symmetry, then  $\delta_1$  equals zero and  $\delta_2$  equals  $-\delta_3$ .

Table 2.1 Atom positions for the spinel structure according to  $F\bar{4}3m$  symmetry.

The symbols  $u_1$ ,  $u_2$  and  $u_3$  represent the three positional parameters.

Origin at  $\bar{4}3m$

The face centred cubic translations:-

$$(0,0,0; 0, \frac{1}{2}, \frac{1}{2}; \frac{1}{2}, 0, \frac{1}{2}; \frac{1}{2}, \frac{1}{2}, 0) +$$

Ion	Position	Point Symmetry	Coordinates of equivalent positions
$Fe^{3+}(1)$	4(a)	$\bar{4}3m$	0,0,0.
$Fe^{3+}(2)$	4(c)	$\bar{4}3m$	$\frac{1}{4}, \frac{1}{4}, \frac{1}{4}$ .
$Fe^{2.5+}$	16(e)	3m	$u_1, u_1, u_1; u_1, \bar{u}_1, \bar{u}_1;$ $\bar{u}_1, u_1, \bar{u}_1; \bar{u}_1, \bar{u}_1, u_1.$
$O^{2-}(1)$	16(e)	3m	$u_2, u_2, u_2; u_2, \bar{u}_2, \bar{u}_2;$ $\bar{u}_2, u_2, \bar{u}_2; \bar{u}_2, \bar{u}_2, u_2.$
$O^{2-}(2)$	16(e)	3m	$u_3, u_3, u_3; u_3, \bar{u}_3, \bar{u}_3;$ $\bar{u}_3, u_3, \bar{u}_3; \bar{u}_3, \bar{u}_3, u_3.$

## CHAPTER 3

### A RE-EXAMINATION OF STRUCTURE FACTOR DATA FOR MAGNETITE

#### 3.1 Introduction

Magnetite ( $\text{Fe}_3\text{O}_4$ ), has been found to exhibit the inverse spinel structure with  $Fd\bar{3}m$  symmetry (Bragg, 1915a,b; Claassen, 1926; Verwey and deBoer, 1936; Shull et al. 1951; Hamilton, 1958; Fleet, 1981). Under this centrosymmetrical space group the octahedrally coordinated cations occupy special positions at the centres of octahedral interstices in the oxygen framework. Grimes (1972, 1973) has proposed that the physical properties exhibited by a number of spinels, including magnetite, can be better explained if these cations are displaced from these ideal positions along  $\langle 111 \rangle$  directions; a displacement which has the effect of removing the centre of symmetry and giving rise to the space group  $F\bar{4}3m$ .

In the most recent X-ray diffraction study Fleet (1981) observed, on long exposure films, very weak sporadic reflexions with Miller indices of the type  $\{hk0\}$  with  $h+k=4n+2$ , e.g.  $002$  and  $024$  which are forbidden under  $Fd\bar{3}m$  symmetry. These additional reflexions were taken as arising from double diffraction and discarded, since their intensities were found to change if the conditions of diffraction were varied. The final structure parameters obtained by Fleet (1981) in this study were similar to the values found earlier by Hamilton (1958) in a neutron diffraction study of magnetite.

In a recent X-ray diffraction study of a synthetic single crystal of spinel ( $\text{MgAl}_2\text{O}_4$ ) by Grimes, Thompson and Kay (1983), it was found

that although Fd3m symmetry gave a good fit between observed and calculated structure factors, a far better fit was obtained using  $F\bar{4}3m$  symmetry. As a result, they concluded that the non-centrosymmetrical space group  $F\bar{4}3m$  correctly describes the symmetry of this material.

It was these observations on  $MgAl_2O_4$  that led to uncertainty over the true symmetry of magnetite. To try to solve this problem, a decision was made to re-examine the structure factor data published by Fleet (1981), firstly assuming conventional Fd3m symmetry and then for  $F\bar{4}3m$  symmetry. The use of existing data had two main advantages. Firstly, it was believed that although the Fd3m forbidden reflexions had been taken as due entirely to double diffraction and rejected by Fleet (1981), the remaining data were of good quality and still contained information, among the Fd3m allowed reflexions, on the deviations from conventional symmetry thought to be present in this mineral. Secondly, the long process of refining the structure parameters could continue while a suitable natural magnetite crystal was found, ground into a sphere as described in Appendix II, and a series of X-ray intensities collected (a much larger number than Fleet collected). The structure parameters obtained from refinement of Fleet's data, for each space group, could then be used as starting values for the refinement of the data collected from this new crystal.

### 3.2 Inspection of the Original Structure Factor Data

A copy of the structure factors calculated by Fleet (1981) for magnetite and deposited with the British Library Lending Division as Supplementary Publication No. SUP 35901 is given in Appendix VI. It should be noted that these data are not in standard form, that is, they

are not in absolute electron units and have not been corrected for secondary extinction or scale.

Two further difficulties must be mentioned. Firstly, no measurements were made for the intensities of the  $Fd3m$  forbidden reflexions. Secondly, under  $F\bar{4}3m$  symmetry there are 11 variable parameters, that is, 8 temperature factors and 3 atom positions. Fleet's original list of 132 independent reflexions, along with 15 reflexions below background level, are not really a large enough number to refine the values for these 11 variables with any degree of accuracy. However, as mentioned in the previous section, this re-examination of existing data was only being used as a method of finding approximate values for these variables. The values found could then be used as a starting point for the more detailed refinement reported in the next chapter.

At first sight, agreement between observed and calculated structure factors in Appendix VI appears to be quite good. Closer inspection shows the 6 reflexions 2 4 4, 2 4 8, 4 4 6, 4 4 10, 4 6 8 and 4 6 12 to have observed structure factors which are far larger than their calculated values. All 6 of these reflexions have Miller indices of the type  $4n$ ,  $4n$ ,  $4n+2$ , but under  $Fd3m$  symmetry these reflexions are produced by scattering from oxygen ions only, and would therefore be expected to be very weak indeed. For these to be as strong as observed here, there must have been a considerable contribution to the scattering from the ions on octahedral sites. This is only possible if the octahedral ion is displaced from its ideal position. Such a displacement is forbidden under  $Fd3m$  symmetry but allowed under  $F\bar{4}3m$ . A brief inspection therefore shows direct evidence in favour of  $F\bar{4}3m$  symmetry for magnetite on the basis of existing structure factor data.

### 3.3 Crystal Structure Refinement Procedure

Refinement of the structure parameters was carried out using the least squares program CRYLSQ from the crystallographic software package X-RAY 74 (see Appendix I). Because the structure factor data deposited by Fleet (1981) were not in standard form, it was necessary to determine values for scale and isotropic extinction correction using the least squares program. The initial refinement was carried out assuming conventional  $Fd\bar{3}m$  symmetry.

The extinction correction applied by X-RAY 74 is an isotropic correction based upon theory developed by Zachariasen (1967) for a mosaic crystal, the correction being given as a  $g$ -factor characteristic of that particular specimen. In this case the least squares refinement gave a  $g$ -factor of  $3.19(1) \times 10^3$ , a larger value than that obtained by Fleet (1981). This value suggests that the extinction for this crystal is Zachariasen type II, the mean domain radius within the crystal being  $2.265(10) \times 10^{-4}$  mm. Using this  $g$ -factor all the structure factors were now corrected for secondary extinction, thereby placing the data on an absolute scale and removing extinction as an adjustable parameter.

To maximize the sensitivity of the least squares program it was necessary to employ a non-linear weighting scheme. The scheme chosen was one which downweights low-angle and strong reflexions but allows more emphasis to be placed on the weak high-angle data, that is, those data most sensitive to atom position. The structure factor data were weighted according to the weighting scheme described in Appendix I. The variable  $Z$  was set equal to  $30.0$

Atomic scattering factors for  $Fe^{2+}$  and  $Fe^{3+}$  ions were taken from the International Tables for X-Ray Crystallography Vol. IV. Because of

the rapid electron hopping process taking place in magnetite between  $\text{Fe}^{2+}$  and  $\text{Fe}^{3+}$  ions on the octahedral site, it was necessary to average the  $\text{Fe}^{2+}$  and  $\text{Fe}^{3+}$  scattering factors to provide a value for the scattering produced by this site. Scattering factors for  $\text{O}^{2-}$  were those given by Tokonami (1965). Real and imaginary parts of the dispersion correction were taken from the International Tables for X-Ray Crystallography Vol.IV.

Least squares refinements were carried out for  $\text{Fd}3\text{m}$  symmetry until optimum values were found for the 5 temperature factors and the oxygen positional parameter. The next stage was to use the same values for scale, extinction correction and weighting scheme as before and repeat the process assuming  $\text{F}\bar{4}3\text{m}$  symmetry. For this second refinement the  $\text{Fd}3\text{m}$  forbidden reflexions, rejected by Fleet (1981), were included with intensities taken as being below threshold. It was necessary to include these forbidden reflexions in the refinement to give additional information to the least squares program, because, as stated earlier, the original data set of 147 independent reflexions does not give the least squares program sufficient information for the refinement of 8 temperature factors and 3 positional parameters of  $\text{F}\bar{4}3\text{m}$  symmetry.

The original structure factor data produced by Fleet (1981) do have some direct indications of the inadequacy of conventional  $\text{Fd}3\text{m}$  symmetry. If we examine table 3.1 it can be seen that there are six reflexions with Miller indices of the type  $4n, 4n, 4n+2$ . Under  $\text{Fd}3\text{m}$  symmetry these reflexions are produced by scattering from oxygen ions alone and should therefore be very weak. As table 3.1 shows all six of these reflexions, measured by Fleet, have observed structure factors which are far stronger than their calculated values. This result is only possible if there is a considerable contribution to the scattering by the ions on

Table 3.1 Weak reflexions taken from Fleet (1981) (SUP 35901)



Aston University

**Content has been removed for copyright reasons**



Aston University

**Content has been removed for copyright reasons**

the octahedral site which, in turn, is only possible if this cation is displaced from its ideal position. Such a displacement is forbidden under  $Fd\bar{3}m$  symmetry but allowed under  $F\bar{4}3m$ .

A test has been developed by Wilson (1949) to determine the presence or absence of a centre of symmetry in a crystal. This test depends upon the fact that a much larger percentage of small structure factors occurs in the diffraction pattern from a centrosymmetrical structure than in the corresponding pattern from a non-centrosymmetrical structure. Therefore, if the parameters of a crystal structure are refined under the constraints of a centrosymmetrical model when, in fact, a centre of symmetry is absent, the calculated structure factors for the weak reflexions tend to be too small. Table 3.1 lists the 20 weakest reflexions, arranged in order of strength, and taken directly from Fleet's results. Here it can be seen that in 15 out of the 20 cases, the values for the calculated structure factors are too small. In fact they are too small for the 11 weakest reflexions. This is the exact result to be expected if magnetite is non-centrosymmetrical but has been refined assuming it to be centrosymmetrical.

### 3.4 Results and Discussion

A complete list of structure factors for the  $Fd\bar{3}m$  and  $F\bar{4}3m$  refinements is given in Appendix V. The final values for anisotropic temperature factors and positional parameters (with the estimated standard deviation shown in brackets), along with those obtained by Fleet (1981), are presented in table 3.2. It should be noted that the results obtained from this analysis under  $Fd\bar{3}m$  symmetry differ very slightly from those obtained by Fleet (1981). On the whole, agreement

Table 3.2 Final structure parameters.

Positional and thermal parameters are multiplied by  $10^5$ .

Temperature factors are in the form

$$\exp \left\{ -(\beta_{11}h^2 + \beta_{22}k^2 + \beta_{33}l^2 + 2\beta_{12}hk + 2\beta_{13}hl + 2\beta_{23}kl) \right\}$$

		Fleet	Fd3m	F $\bar{4}$ 3m
<b>Tetrahedral site 1</b>	<b>Fe<sup>3+</sup></b>			
$x(-y-z)$			0	0
$\beta_{11}(-\beta_{22}=\beta_{33})$		124(5)	136(2)	138(5)
$\beta_{12}(-\beta_{13}=\beta_{23})$			0	0
<b>Tetrahedral site 2</b>	<b>Fe<sup>3+</sup></b>			
$x(-y-z)$			—	25000
$\beta_{11}(-\beta_{22}=\beta_{33})$			—	134(5)
$\beta_{12}(-\beta_{13}=\beta_{23})$			—	0
<b>Octahedral site</b>	<b>Fe<sup>2+</sup></b> <b>Fe<sup>3+</sup></b>			
$x(-y-z)$		62500	62500	62424(12)
$\beta_{11}(-\beta_{22}=\beta_{33})$		163(5)	176(2)	177(2)
$\beta_{12}(-\beta_{13}=\beta_{23})$		16(2)	19(2)	17(2)
<b>Oxygen site 1</b>				
$x(-y-z)$		37990(10)	37968(12)	86949(38)
$\beta_{11}(-\beta_{22}=\beta_{33})$		192(9)	172(4)	200(20)
$\beta_{12}(-\beta_{13}=\beta_{23})$		-1(6)	-15(6)	-16(20)
<b>Oxygen site 2</b>				
$x(-y-z)$			—	37896(38)
$\beta_{11}(-\beta_{22}=\beta_{33})$			—	155(20)
$\beta_{12}(-\beta_{13}=\beta_{23})$				-11(20)
<b>Overall R-factor</b> <b>(omitting less-thans)</b>		<b>2.40%</b>	<b>2.14%</b>	<b>1.94%</b>

between final structure parameters, when compared with those of Fleet (1981), is really quite good. In order to reproduce Fleet's results exactly it was necessary to assume a lower extinction correction than was found here, but this led to a significantly higher overall R-factor.

To help with analysis of the data a program known as WTANAL (see Appendix I) which allowed the structure factor data to be divided up into two groups, one in terms of  $F_0$  and a second in terms of  $\sin \theta/\lambda$ , was used. These two groups were then subdivided and an R-factor calculated for each subgroup. This R-factor breakdown facility was found to be a useful tool for identifying reflexions and groups of reflexions which were not fitting very well during the early stages of the refinement. It was found to be particularly useful when comparing structure factors produced for refinements made under the two different space groups. The structure factor data produced by the least squares program have been divided up using WTANAL and the results for the two refinements can be seen in tables 3.3.1 and 3.3.2.

Even though the results of the  $Fd\bar{3}m$  refinement are found to be in good agreement with those of the two previous authors, inspection of tables 3.3.1 and 3.3.2 shows that the refinement under  $F\bar{4}3m$  symmetry provides a far better fit to the experimental data. In fact, an overall R-factor of 2.14% was obtained for  $Fd\bar{3}m$  symmetry but for the equivalent refinement under  $F\bar{4}3m$  this value decreased to 1.94%. This improvement under  $F\bar{4}3m$  is achieved primarily by an improvement in the fitting of weak high-angle reflexions. Particularly noticeable are the 18 weakest reflexions with structure factors less than 10.0. The R-factor for this group changes from 30.8% to 16.7% with the change of space group. Because these 18 reflexions are all weak they suffer considerably from statistical errors; in fact, they are not expected to fit as well as the



Table 3.3.1 R-factor breakdown in terms of  $F_0$  and  $\sin \theta/\lambda$  for Fd3m symmetry.

<u>Overall agreement factors</u>		<u>R-factors</u>
No. of observations	132	Without reflexions below threshold 0.0214
No. of variables	6	With reflexion multiplicity 0.0198
No. below threshold	15	Of reflexions below threshold 0.0
No. calculating above threshold	0	Of $F^2$ (without reflexions below threshold) 0.0384

Results in terms of  $F_0$

Results in terms of  $\sin \theta/\lambda$

$F_0$	$\Sigma F_0$	$\Sigma \Delta F$	No. of Reflexions	R	$\sin \theta/\lambda$	$\Sigma F_0$	$\Sigma \Delta F$	No. of Reflexions	R
10.0	101.2	31.1	18	0.308	0.10	0.0	0.0	0	0.000
20.0	103.4	2.3	7	0.022	0.20	510.5	10.2	3	0.020
30.0	235.0	5.0	10	0.021	0.30	594.4	26.3	4	0.044
40.0	222.6	2.5	6	0.011	0.40	1366.2	20.9	8	0.015
50.0	491.8	7.5	11	0.015	0.50	1013.8	22.0	9	0.022
60.0	704.1	9.0	13	0.013	0.60	1269.0	25.6	15	0.020
70.0	837.0	12.9	13	0.015	0.70	1205.8	26.2	18	0.022
80.0	449.2	9.6	6	0.021	0.80	1510.6	25.7	22	0.017
90.0	1026.3	17.0	12	0.017	0.90	1459.1	34.7	26	0.024
100.0	5950.2	119.6	36	0.020	1.00	1191.4	25.0	27	0.021

Table 3.3.2 R-factor breakdown in terms of  $F_0$  and  $\sin \theta/\lambda$  for F43m symmetry.

<u>Overall agreement factors</u>	<u>R-factors</u>
No. of observations	Without reflexions below threshold 0.0194
No. of variables	With reflexion multiplicity 0.0175
No. below threshold	Of reflexions below threshold 0.0563
No. calculating above threshold	Of $F^2$ (without reflexions below threshold) 0.0375

Results in terms of  $F_0$

$F_0$	$\Sigma F_0$	$\Sigma \Delta F$	No. of Reflexions	R	$\sin \theta/\lambda$	$\Sigma F_0$	$\Sigma \Delta F$	No. of Reflexions	R
10.0	101.2	16.9	18	0.167	0.10	0.0	0.0	0	0.000
20.0	103.4	2.0	7	0.020	0.20	510.5	10.4	3	0.020
30.0	235.0	5.1	10	0.022	0.30	594.4	25.9	4	0.044
40.0	222.6	2.8	6	0.013	0.40	1366.2	19.9	8	0.015
50.0	491.8	6.2	11	0.013	0.50	1013.8	18.6	9	0.018
60.0	704.1	7.7	13	0.011	0.60	1269.0	25.6	15	0.020
70.0	837.0	11.6	13	0.014	0.70	1205.8	20.1	18	0.017
80.0	449.2	9.5	6	0.021	0.80	1510.6	23.2	22	0.015
90.0	1026.3	17.1	12	0.017	0.90	1459.1	32.9	26	0.023
100.0	5950.2	117.8	36	0.020	1.00	1191.4	20.0	27	0.017

Results in terms of  $\sin \theta/\lambda$

remaining group's but a fit as poor as 30.8% under Fd3m symmetry, when the overall R-factor is 2.14%, does strongly suggest that incorrect assumptions have been made in the original analysis. If we now examine the R-factor breakdown (shown in tables 3.3.1 and 3.3.2), in terms of  $\sin \theta/\lambda$ , it can be seen that the R-factor for the group of 27 reflexions with  $\sin \theta/\lambda$  lying between 0.9 and 1.0 changes from 2.1% under Fd3m to 1.7% under  $F\bar{4}3m$ . Again these data represent weak high-angle reflexions. This poor fit in R-factor for these weak high-angle reflexions under Fd3m implies that the atom positions imposed by this space group are incorrect. The dramatic improvement under  $F\bar{4}3m$  implies that this latter space group more correctly describes the symmetry of magnetite.

These results obtained for magnetite are similar to those obtained by Grimes et al. (1983) for spinel. Again, certain weak reflexions allowed under conventional symmetry are quite sensitive to the change of space group. A list of some of these sensitive reflexions is given in table 3.4. Six of the reflexions from this table have Miller indices of the type  $4n, 4n, 4n+2$ ; these are 2 4 4, 2 4 8, 4 4 6, 4 4 10, 4 6 8 and 4 6 12. For the Fd3m refinement, the fit between observed and calculated structure factors is poor, but under  $F\bar{4}3m$  the fits for 4 4 10, 4 6 8 and 4 6 12 are fairly good. Discrepancies in the other three have come about mainly because the least squares program has been unable to optimize the structure parameters, again this comes about because 147 independent reflexions is not enough data to refine the 11 variables needed to define the  $F\bar{4}3m$  structure.

Table 3.1 shows structure factors for the 20 weakest reflexions, arranged in order of strength, and taken directly from Fleet's original list. Examination of this table shows that for Fd3m symmetry the sign of  $(F_o - F_c)$  is positive for 15 of the 20 reflexions; in fact it is positive

Table 3.4 Some sensitive reflexions.

h	k	l	$F_o$	$F_c$	$F_{\bar{4}3m}$
				Fd3m	
1	7	7	9.6	9.2	9.4
2	4	4	3.8	0.5	1.3
2	4	8	4.2	0.8	1.3
3	3	7	13.3	12.5	13.4
3	3	15	3.3	1.3	3.6
3	7	11	5.8	2.8	5.4
3	7	13	9.6	8.7	9.0
4	4	6	3.3	0.4	3.3
4	4	10	3.3	0.3	3.7
4	6	8	3.3	0.6	2.4
4	6	12	5.0	0.6	2.1

for the 11 weakest. This implies that the scattering given by  $Fd3m$  symmetry is persistently too small to account for that measured by experiment. This is the effect predicted by Wilson (1949) in the absence of a centre of symmetry, i.e. a centrosymmetrical structure should possess a much larger percentage of small structure factors than a non-centrosymmetrical structure. Here 15 out of the 20 structure factors are larger which implies that magnetite is non-centrosymmetrical.

Final values found for the observed and calculated structure factors for the  $Fd3m$  forbidden reflexions are shown in table 3.5. It can be seen that although many of these reflexions did calculate below Fleet's threshold of approximately 3.3 electron units, six did calculate above. A point to note here is that the  $002$  reflexion, examined by Samuelsen (1974) in a neutron time of flight study, calculates out below threshold; a result which invalidates his assumption that  $F\bar{4}3m$  symmetry can be rejected for magnetite. In addition, the  $024$  reflexion, taken by Fleet (1981) as being produced entirely by double diffraction, also calculates as being below threshold.

These results for the  $002$  and  $024$  reflexions tend to enforce the idea put forward by Heuer and Mitchell (1975) that it is not possible to reject  $F\bar{4}3m$  symmetry on the basis of these  $Fd3m$  forbidden reflexions not being detected, since a combination of atom shifts to both octahedral cations and anions can result in negligible intensity for many of these forbidden reflexions.

In his analysis of magnetite specimen No. 633 Fleet (1981) observed residual electron density in a second tetrahedrally coordinated position. This was taken to be interstitial  $Fe^{3+}$  ions in equipoint 8(b), with corresponding vacancies in the octahedral site. Residual electron density was observed by Fleet (1981) at equipoints 96(g), 96(h) and

Table 3.5 Structure factors for the  $Fd\bar{3}m$  forbidden reflexions.

h	k	l	$F_c$
0	0	2	0.86
0	0	6	3.90
0	0	10	4.31
0	0	14	4.54
0	2	4	1.35
0	2	8	0.92
0	2	12	0.86
0	2	16	0.28
0	4	6	3.38
0	4	10	4.26
0	4	14	3.95
0	6	8	2.76
0	6	12	1.68
0	8	10	3.17

32(e), and taken as being produced by local displacements of the iron and oxygen ions respectively, from their ideal positions. The Fourier difference maps produced in the analysis described here, under  $Fd\bar{3}m$  symmetry, failed to reproduce these residual electron density peaks. Any variations in electron density observed were due entirely to experimental errors. The peaks observed by Fleet (1981) seem to be artifacts produced because the variable parameters had not been refined correctly by the least squares program. Further refinement of these parameters, as was done here, reduced these peaks to background noise.

Finally, it is worth mentioning that a similar analysis of structure factor data produced for magnetite crystal No. 2741 by Fleet (1982) did give a Fourier difference map with residual electron density peaks at equipoints 48(f) and 96(h), as predicted by Fleet (1982). This variation in electron density seems to represent a real effect corresponding to interstitial  $Fe^{3+}$  in a second tetrahedral and a second octahedral site.

### 3.5 Conclusions

Taking the limitations of the present analysis into account, and considering that this work was only being used as a preliminary examination before a more detailed study was made, the results obtained do support the idea of  $F\bar{4}3m$  symmetry for magnetite.

On the basis of the results found above, a decision was made to collect a new set of X-ray intensities from a natural single crystal and repeat the process described in this chapter, only in far more detail.

The analysis described in this chapter indicates that in order to find accurate values for the final structure parameters it will be

Table 3.6 Calculated bond lengths.

Fd3m		F $\bar{4}$ 3m	
Bond	Distance (Å)	Bond	Distance (Å)
Fe <sup>3+</sup> -O (Tetrahedral bond)	1.8854(4)	Fe <sup>3+</sup> (1)-O(2) Fe <sup>3+</sup> (2)-O(1)	1.898(2) 1.875(2)
Fe <sup>2+,3+</sup> -O (Octahedral bond)	2.0600(7)	Fe <sup>2+,3+</sup> -O(1) Fe <sup>2+,3+</sup> -O(2)	2.060(2) 2.059(2)
O-O	2.8566(7)	O(1)-O(1) O(2)-O(2)	2.874(3) 2.837(3)
O-O	2.9688(7)	O(1)-O(2)	2.969(3)
O-O	3.0789(7)	O(1)-O(1) O(2)-O(2)	3.062(3) 3.099(3)

necessary to use approximately ~~300~~ independent intensities, about twice as many as used by Fleet (1981). It is very unlikely that the values found for the final structure parameters, bond lengths (table 3.6) and for the intensities of the Fd3m forbidden reflexions will agree exactly with the values determined in this chapter. As discussed above, the accuracy of the structure parameters given in this chapter is fairly poor because of the limited amount of data available.

## CHAPTER 4

### REFINEMENT OF THE CRYSTAL STRUCTURE OF MAGNETITE

#### 4.1 Introduction

In theory, it should be possible to decide, using diffraction techniques, if the symmetry of magnetite is described by the space group  $Fd\bar{3}m$  or by the space group  $F\bar{4}3m$  because reflexions of the type  $\{hk0\}$  with  $h+k=4n+2$  are systematically absent under  $Fd\bar{3}m$  symmetry but allowed under  $F\bar{4}3m$ . However, because the atomic displacements giving rise to the difference in symmetry are small, the intensities of many of these reflexions are below the minimum detectable level. In addition, because of the high symmetry of magnetite, an effect known as double diffraction can lead to the production of these forbidden reflexions (see section 2.2).

It was decided to carry out three separate structure refinements; one under  $Fd\bar{3}m$  and two under  $F\bar{4}3m$  symmetry. The first  $F\bar{4}3m$  refinement was undertaken using the same intensity data as for the  $Fd\bar{3}m$  refinement so that the two data sets are directly comparable, the second using a data set including the  $Fd\bar{3}m$  forbidden reflexions. The structure parameters obtained from the two  $F\bar{4}3m$  refinements can then be compared to see if the addition of the extra reflexions has a significant effect on the refinement.

Table 4.1 Electron microprobe analysis of magnetite specimen BMDM11. These results are the average of 15 spot analyses.

Oxide	wt% oxides
FeO	31.04
Fe <sub>2</sub> O <sub>3</sub>	68.99
Al <sub>2</sub> O <sub>3</sub>	0.25
MnO	0.17

-----  
Total = 100.45

In addition, the elements Ca, Cr, Mg, Si and Ti were analysed for but not detected.

## 4.2 Electron Microprobe Analysis

The magnetite crystal chosen for the present investigation was a fragment taken off a larger natural single crystal from the British Museum's Duplicate Collection (this sample will be referred to hereafter as specimen BMDM11). Before carrying out an X-ray diffraction study of this specimen, it was necessary to examine the specimen initially using electron microprobe analysis and Mössbauer spectroscopy to ensure it is essentially end-member magnetite.

Experimental details of the microprobe analysis are given in Appendix III. Table 4.1 gives a list of the percentages of each oxide found in the analysis. The proportions of FeO and Fe<sub>2</sub>O<sub>3</sub> present were calculated by initially assuming all Fe to be present as FeO. This gave a value for the proportion of each cation present in the unit cell, from these values the contribution of each cation to the overall charge could then be calculated. Assuming charge balance, the difference between calculated cation charge and the theoretical value of 64<sup>+</sup> represents the proportion of FeO that is recalculated as Fe<sub>2</sub>O<sub>3</sub>. This recalculation has become a standard procedure for determining the proportions of FeO and Fe<sub>2</sub>O<sub>3</sub> in magnetite from electron microprobe data (see for example Kelly, 1985).

## 4.3 Mössbauer Spectrum of Magnetite Specimen BMDM11 at Room Temperature

Figure 4.1 shows that the Mössbauer spectrum produced by magnetite specimen BMDM11 at room temperature. It consists of two six peak hyperfine patterns, a result which is characteristic of magnetically ordered iron in two different sites. Reading from left to right (figure

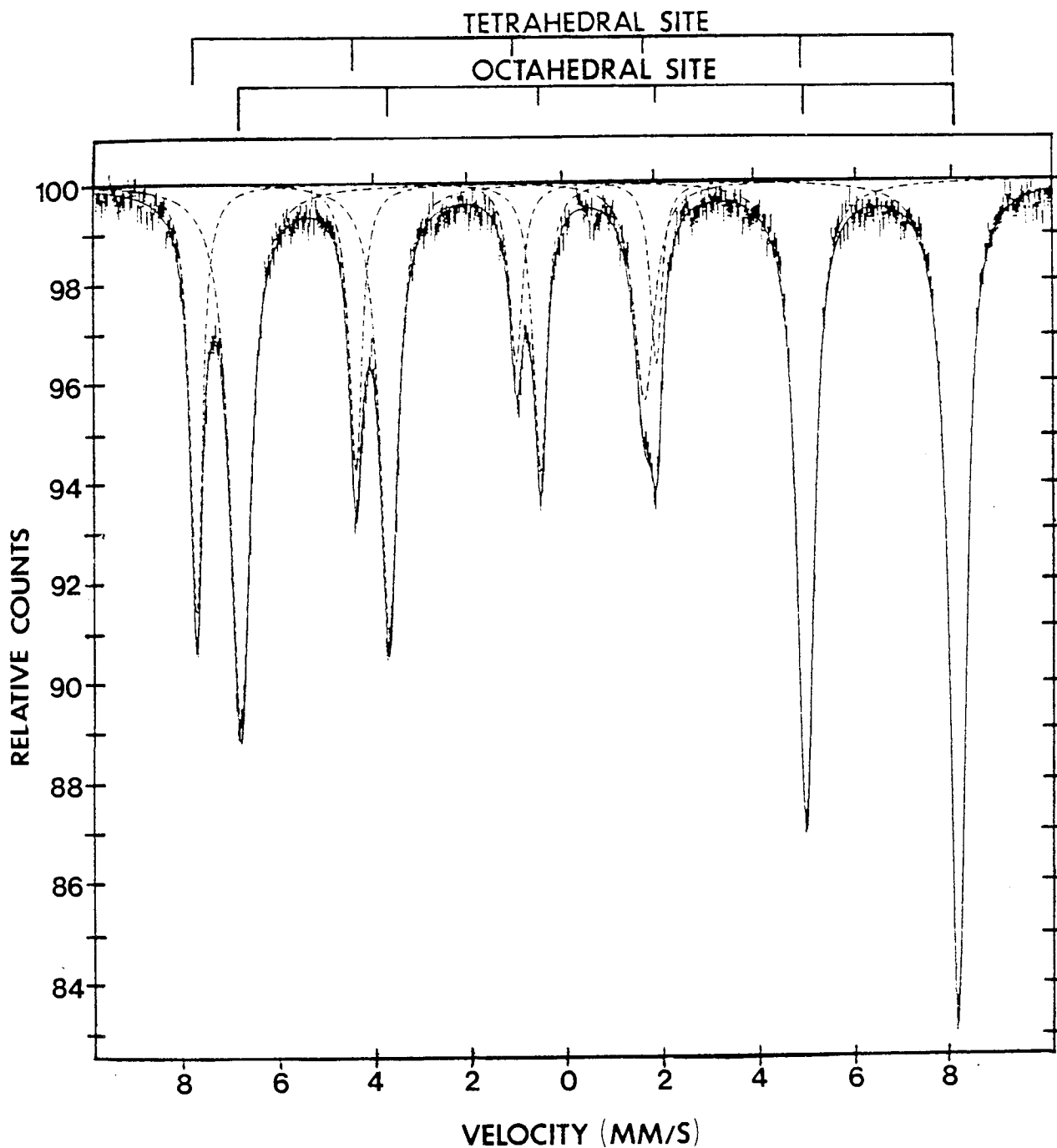


Figure 4.1 Mössbauer spectrum of magnetite specimen BMDM11 at room temperature. The solid lines represent least squares fits of the data points to superimposed Lorentzian curves.

Table 4.2 Values for the hyperfine field, quadrupole splitting and isomer shift, for magnetite specimen BMDM11, found by room temperature Mössbauer spectroscopy. Isomer shifts are quoted relative to iron metal absorber.

Site	Hyperfine Field (kOe)	Quadrupole Splitting (mm/s)	Isomer Shift (mm/s)
Tetrahedral	486(2)	-0.032(3)	0.244(3)
Octahedral	458(2)	0.025(3)	0.694(3)

4.1), the first set consists of peaks 1, 3, 5, 7, 9 and 10 and the second set, peaks 2, 4, 6, 8, 9 and 10, the two peaks combining to give peaks 9 and 10 are not resolved. Values for the hyperfine fields, quadrupole splittings and isomer shifts are given in table 4.2. The quadrupole splitting of each sub-spectrum was calculated by taking the difference in position between lines 1 and 2 and lines 5 and 6. From the intensity ratios and the values for the isomer shifts and hyperfine fields, it follows that the less intense spectrum is produced by  $\text{Fe}^{3+}$  in tetrahedral coordination and the more intense spectrum by  $\text{Fe}^{2+}$  and  $\text{Fe}^{3+}$  in octahedral coordination. Table 4.3 shows that the spectra and these assignments are in good agreement with the results found by previous authors. The observed broadening of the line spectra from the octahedral site is due to fast electron hopping between  $\text{Fe}^{2+}$  and  $\text{Fe}^{3+}$  ions at this site. The octahedral site sub-spectrum is therefore the average of that produced by  $\text{Fe}^{2+}$  and  $\text{Fe}^{3+}$ .

The ratio of the area of the spectrum from tetrahedral sites to that from octahedral sites was found to be 0.48(1). This ratio was obtained by fitting two Lorentzian curves to peaks 1 and 2; to obtain convergence, the areas of these two peaks were constrained in the ratio 1:2. When approximate areas were found the constraints were removed and the process repeated using these new values. This value of 0.48(1) is in good agreement with the theoretical value of 0.5 for end-member magnetite.

These results, along with the electron microprobe analysis which indicated that this specimen contains less than 0.3wt% impurities and the single crystal X-ray work (which gave a lattice constant of  $8.396(1) \text{ \AA}$ ), show that specimen BMDM11 is essentially end-member magnetite.

Table 4.3 Mössbauer parameters found by previous authors for magnetite at room temperature. The symbol A represents tetrahedral or A-sites and B octahedral or B-sites. Isomer shifts are quoted relative to iron metal absorber.

Site	Natural or Synthetic	Hyperfine Field (kOe)	Quadrupole Splitting (mm/s)	Isomer Shift (mm/s)	Reference
A	S	495(20)	0.1(2)	0.27(10)	Ito et al. (1963)
B		470(20)	-0.1(2)	0.68(10)	
A	S	497(2)	0.02(4)	0.29(4)	Daniels and Rosencwaig (1969)
B		462(2)	0.02(4)	0.67(4)	
A	N	493(3)	0.00(5)	0.25(2)	Evans and Hafner (1969)
B		460(1)	0.00(5)	0.65(2)	
A	S	491(1)	0.00(2)	0.27(3)	Evans and Hafner (1969)
B		460(1)	0.00(2)	0.67(3)	
A	S	491.8(5)	<0.025	0.27(1)	Kündig and Hargrove (1969)
B		460.7(5)	<0.025	0.66(1)	
A	S	489.9(5)	-	0.28(5)	Weber and Hafner (1971)
B		465.3(5)	-	0.67(5)	
A	S	495.1(2)	0.001(5)	0.27(5)	Annersten and Hafner (1973)
B		469.3(5)	0.24(3)	0.67(5)	
A	N	486(2)	-0.032(3)	0.244(3)	Present Study
B		458(2)	0.025(3)	0.694(3)	

#### 4.4 X-Ray Data Collection

Before choosing a specimen for investigation using single crystal X-ray diffraction it is necessary to consider the problems of X-ray attenuation by the specimen. Ideally this should be isotropic, and this is only possible if a spherical crystal is used. To simplify correction procedures the radius of the sphere should be such that  $\mu R < 2$ , where  $\mu$  is the linear absorption coefficient for the mineral under examination and  $R$  is the crystal radius (see International Tables for X-Ray Crystallography Vol.II, p300). Applying this simple rule to magnetite, where  $\mu = 14.36 \text{ mm}^{-1}$ , the ideal crystal radius is 0.14 mm. Unfortunately, it is not possible to produce spheres of precisely this radius, because the grinding process used to produce the spheres cannot be accurately controlled (see Appendix II). Thus, spheres as close as possible to radii of 0.14 mm were prepared. A sphere of radius 0.17(2) mm was chosen for the present investigation.

Integrated X-ray intensities were then collected from this crystal, at room temperature, using an Enraf-Nonius CAD-4 automated diffractometer (see figure 4.2), and employing the  $\omega$ - $2\theta$  scan technique. The radiation used was  $\text{MoK}\alpha$  ( $\lambda = 0.71069 \text{ \AA}$ ), monochromatized after reflexion by pyrolytic graphite with the monochromator angle  $\theta_m = 6.05^\circ$ . By operating the X-ray tube at 40 kV and 20 mA it was possible to prevent harmonic breakthrough. Least squares refinement of 25 centred reflexions gave the lattice constant for the specimen as  $8.396(1) \text{ \AA}$ , a value which is in good agreement with published values for stoichiometric magnetites (see for example Hamilton, 1958; Fleet, 1981).

All reflexions of the type  $h+k, k+l, l+h=2n$  in one hemisphere of reciprocal space, out to an angle of  $\theta = 70^\circ$ , were collected using a scan

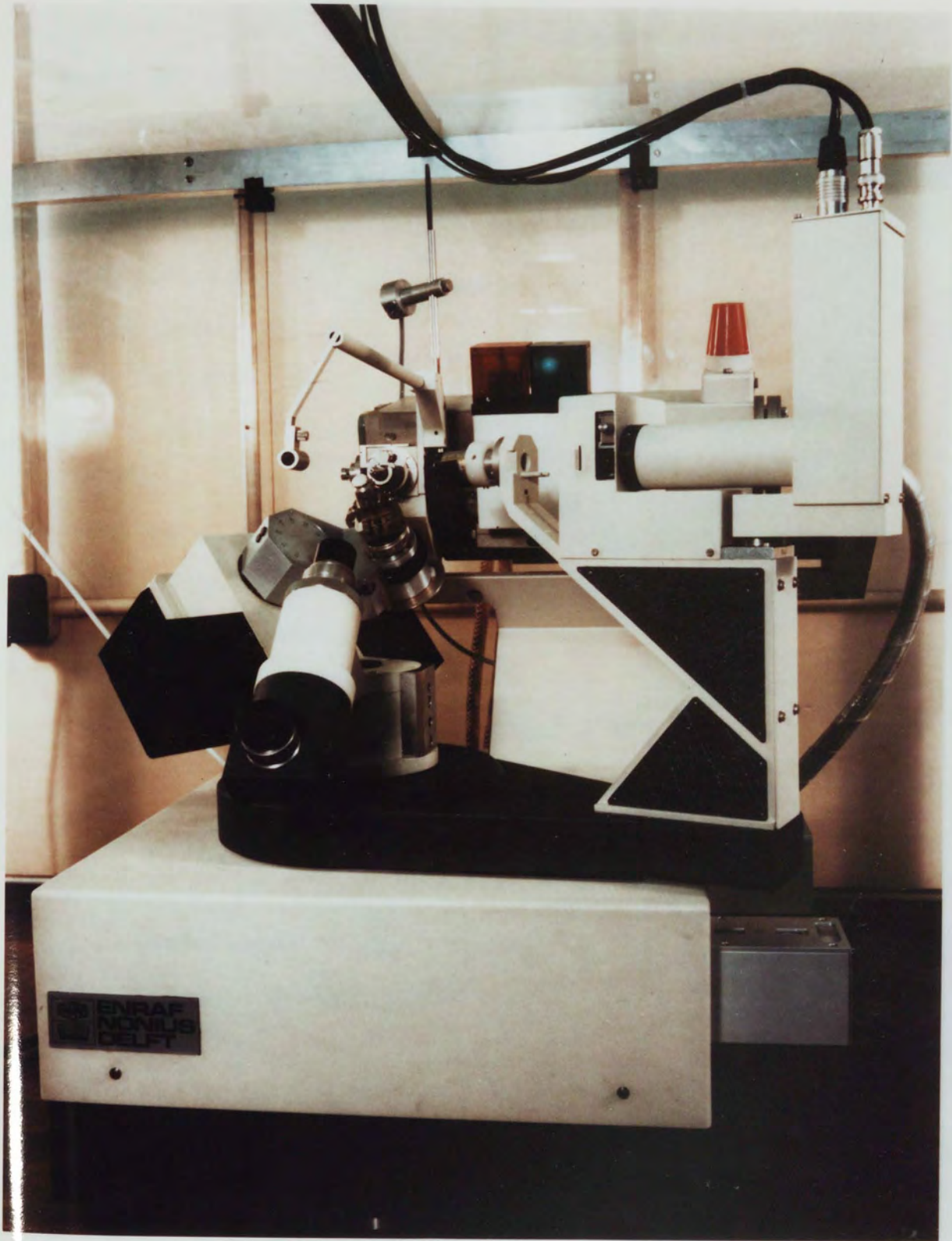


Figure 4.2 The CAD-4 diffractometer

speed of  $2\theta/6 \text{ deg min}^{-1}$ , giving a total of 5631 non-Friedel related reflexions.

During data collection, intensity and orientation control were maintained using the reflexions  $4\ 4\ 8$  and  $\bar{4}\ 2\ 2$ . These two reflexions were measured every 7200 seconds of X-ray exposure time and allowed the diffractometer to check the crystal orientation and, if necessary, stop data collection if the crystal was found to have moved significantly from its original position. In addition, after measuring every 200 reflexions the machine again returned and measured the intensity of the two control reflexions. Any fall-off in the intensity of the standards could then be used to correct all intensities by linear interpolation to the two control reflexions.

#### 4.5 Treatment of the X-Ray Data

Magnetite is a member of the cubic crystal system, therefore many of the observed intensities are crystallographically equivalent. In the measurements reported here one complete hemisphere of reciprocal space was examined, therefore reflexions of the general form  $\{hkl\}$  contain 24 equivalents, while  $\{hk0\}$  and  $\{hhl\}$  contain 12,  $\{hh0\}$  contain 6,  $\{hhh\}$  4 and  $\{h00\}$  only 3 equivalents. This means that the original list of 5631 observed integrated intensities can be collected into groups and reduced to 336 independent reflexions by averaging the equivalents within a group. Among the 336 unique reflexions, 27 were of the type  $\{hk0\}$  with  $h+k=4n+2$  and hence forbidden by conventional  $Fd3m$  symmetry (for example  $0\ 0\ 2$ ,  $0\ 2\ 4$  and  $0\ 0\ 6$ ). It should be noted that the intensities of these 27 additional reflexions are all very low.

For a number of the 336 groups of independent reflexions, a small number of weaker reflexions within those groups were found to have intensities inconsistent with those of the rest of the group. These inconsistencies are due to counting statistics. Similar intensity variations have been reported by Jagodzinski and Saalfeld (1958) and also by Grimes, Thompson and Kay (1983) for  $\text{MgAl}_2\text{O}_4$ .

In order to obtain a data set of high quality it was necessary to use an averaging process for the groups of weak and inconsistent reflexions described above. The following procedure was adopted for groups of weak reflexions containing 12 or more equivalents. The range of the observed intensities within each group was divided up into a number of intensity intervals and a histogram plotted with the frequency of intensity against the intensity interval as the y and x-axes respectively. The results of this analysis showed that the intensity variations within a group are approximately Gaussian, despite the small amounts of data involved. Integrated intensities for the structure refinement were taken to be the mean of the intensities enveloped by the Gaussian curve, any symmetry related reflexions lying outside this curve were rejected. Typical histograms obtained in this analysis are shown in figures 4.3 and 4.4. Use of the above criterion led to rejection of less than 3% of the measured data. For reflexions containing less than 12 equivalents a straightforward average intensity was taken. The number of equivalents used to calculate the observed intensity for each reflexion are shown in column 4 of Appendix VII.

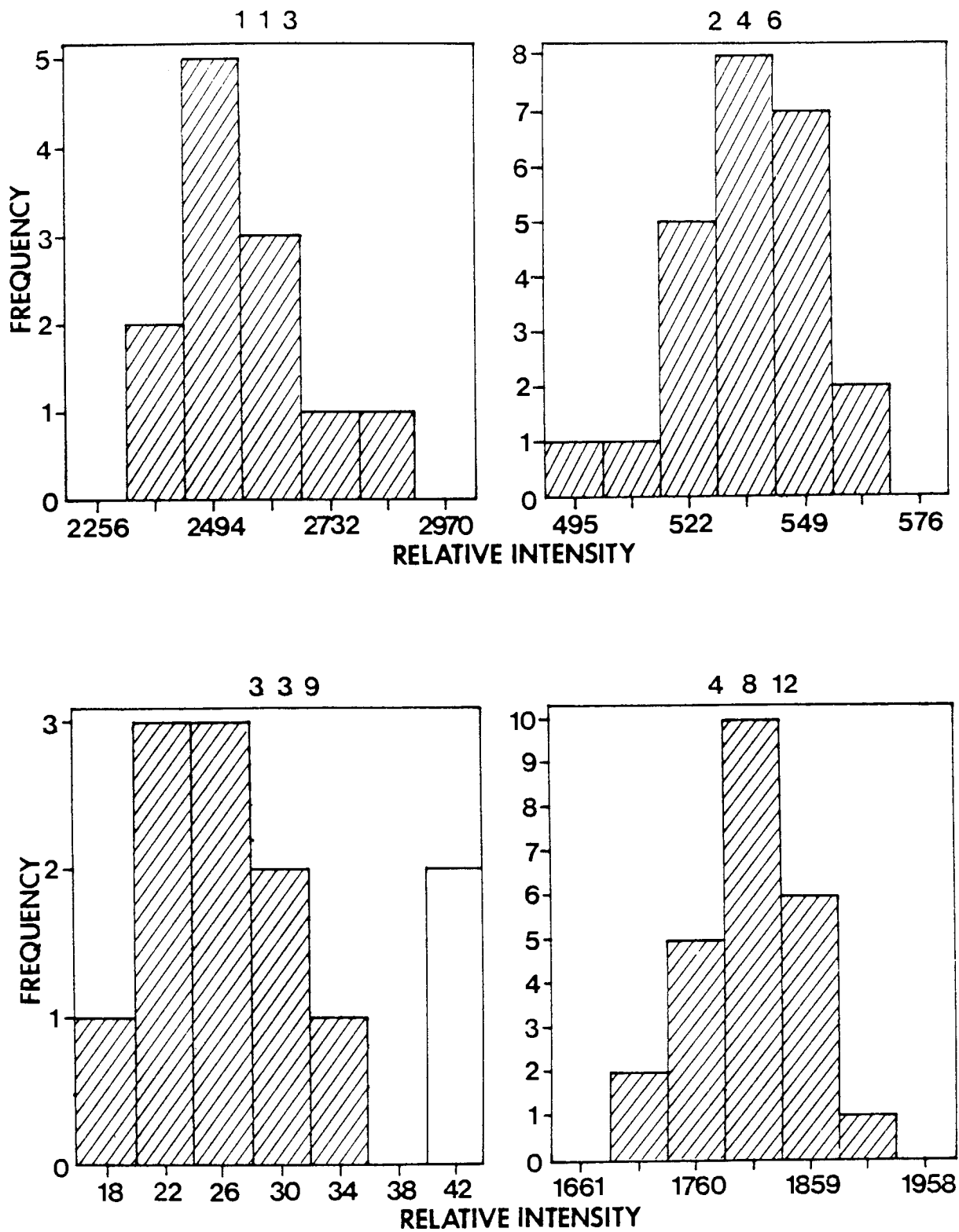


Figure 4.3 Histograms for four groups of equivalent reflexions showing the intensity distribution observed within a group. The shaded region indicates equivalents used to calculate the average intensity for each group. Any equivalents not shaded were rejected.

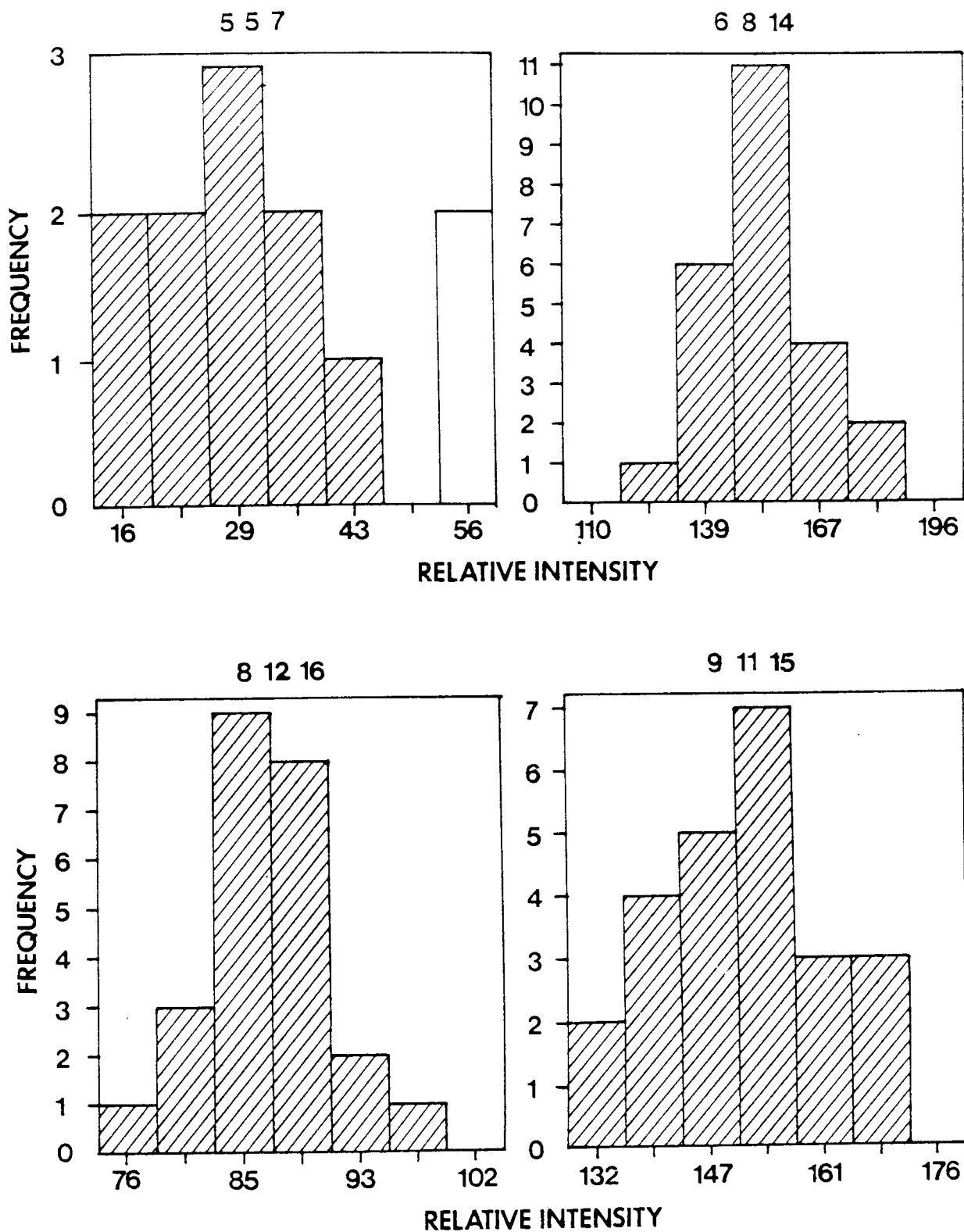


Figure 4.4 Histograms for four groups of equivalent reflexions showing the intensity distribution observed within a group. The shaded region indicates equivalent reflexions used to calculate the average intensity for each group. Any equivalent reflexions not shaded were rejected.

#### 4.6 Crystal Structure Refinement

Refinement of the structure parameters was carried out using the crystallographic least squares program CRYLSQ from the crystallographic software package X-RAY 74 (see Appendix I for details). The initial refinement was restricted to  $Fd\bar{3}m$  symmetry and the cation arrangement was assumed to be that of an inverse spinel. To begin with, only reflexions with intermediate range intensities were used so that approximate values for scale factor, oxygen positional parameter and anisotropic temperature factors could be found. These factors were then fixed, the remaining reflexions added and the extinction correction or g-factor refined separately. It was not possible to refine scale and extinction corrections simultaneously because of the close connections between these two parameters.

The least squares refinement gave a g-factor of  $1.45(1) \times 10^3$ , a value which suggests that the extinction for this crystal is Zachariasen type II, the mean domain radius within the crystal being  $1.03(1) \times 10^{-4}$  mm. Using this g-factor, all the structure factors were corrected for secondary extinction thereby placing the data on an absolute scale.

To maximize the sensitivity of the least squares refinement it was necessary to employ a non-linear weighting scheme. The scheme chosen was one which downweighted low-angle and strong reflexions but allowed more emphasis to be placed on the weak high-angle data, that is, those data most sensitive to atom position. The structure factor data were weighted according to the weighting scheme described in sub-section I.3 of Appendix I. The variable parameter Z in this weighting scheme was set equal to 200.0 for this refinement.

Atomic scattering factors for  $\text{Fe}^{2+}$  and  $\text{Fe}^{3+}$  ions were taken from the International Tables for X-Ray Crystallography Vol.IV. Because of the rapid electron hopping process taking place in magnetite between  $\text{Fe}^{2+}$  and  $\text{Fe}^{3+}$  ions on the octahedral site (see section 1.7), it was necessary to average the  $\text{Fe}^{2+}$  and  $\text{Fe}^{3+}$  scattering factors and use this new value as the scattering produced by this site. Scattering factors for  $\text{O}^{2-}$  were those given by Tokonami (1965). Real and imaginary parts of the dispersion correction were taken from the International Tables for X-Ray Crystallography Vol.IV. Absorption corrections applied were those given by Weber (1969) for spherical crystals. Least squares refinements were repeated until optimized values had been found for the scale, extinction correction, five temperature factors and the oxygen positional parameter.

The next step was to fix the scale and extinction correction at the values found in the  $\text{Fd}3\text{m}$  refinement, to use the same weighting scheme as before and repeat the process, this time for  $\text{F}\bar{4}3\text{m}$  symmetry. Under this alternative space group the number of variables increases from 6 (under  $\text{Fd}3\text{m}$ ), to 11, comprising of 8 temperature factors and 3 positional parameters. In an attempt to find approximate values for the 3 positional parameters,  $u_1$ ,  $u_2$ , and  $u_3$ , it was necessary to take the 76 most sensitive reflexions, all of which were weak and at high angles, and use them in a separate refinement. Here, only the positional parameters were refined, this process gave approximate values for all 3 parameters. These values were then used as starting positions for a refinement of all variables using the complete data set.

Because of the problems encountered in trying to obtain reliable intensity measurements for the 27  $\text{Fd}3\text{m}$  forbidden reflexions, it was necessary to make two separate refinements under  $\text{F}\bar{4}3\text{m}$  symmetry to see if

these values had any significant effect on the final structure parameters produced, assuming this alternative space group. In the first, the data set was exactly the same as that used for the Fd3m refinement. For the second, the extra 27 reflexions were added and the refinement repeated as before. The results produced by the former F $\bar{4}$ 3m refinement could therefore be compared directly with those produced in the refinement made assuming Fd3m symmetry. It was then possible to see if the goodness of fit of the structure improved with the change of space group.

Again, for these two data sets, a series of least squares refinements were made until values for the 11 variables had been optimized. The results obtained are discussed in the next section.

#### 4.7 Results and Discussion

A complete list of structure factors along with the number of equivalents used to calculate the observed intensity of each reflexion is given in Appendix VII. The final values for atom positions and anisotropic temperature factors for all three refinements, along with those found by Fleet (1981), have been summarized in table 4.4. As can be seen from this table, the results for the Fd3m refinement are in good agreement with those of Fleet (1981) who also worked on a natural magnetite crystal. The oxygen positional parameter of 0.3798(2) found by Hamilton (1958) for synthetic Fe<sub>3</sub>O<sub>4</sub> is also in good agreement with the value found here.

To help with analysis of the data a program known as WTANAL (see Appendix I), which allowed the structure factor data to be divided up into two groups, one in terms of F<sub>0</sub> and a second in terms of sin  $\theta/\lambda$ ,

Table 4.4 Final structure parameters.

Positional and thermal parameters are multiplied by  $10^5$ .

Temperature factors are in the form

$$\exp \left\{ -(\beta_{11}h^2 + \beta_{22}k^2 + \beta_{33}l^2 + 2\beta_{12}hk + 2\beta_{13}hl + 2\beta_{23}kl) \right\}$$

	Fleet (Fd3m)	Fd3m	$F\bar{4}3m$	$F\bar{4}3m^*$
<b>Tetrahedral site 1 Fe<sup>3+</sup></b>				
$x(-y-z)$		0	0	0
$\beta_{11}(-\beta_{22}=\beta_{33})$	124(5)	149(1)	120(1)	119(1)
$\beta_{12}(-\beta_{13}=\beta_{23})$		0	0	0
<b>Tetrahedral site 2 Fe<sup>3+</sup></b>				
$x(-y-z)$		—	25000	25000
$\beta_{11}(-\beta_{22}=\beta_{33})$		—	182(1)	183(1)
$\beta_{12}(-\beta_{13}=\beta_{23})$		—	0	0
<b>Octahedral site Fe<sup>2+</sup> Fe<sup>3+</sup></b>				
$x(-y-z)$	62500	62500	62480(6)	62483(6)
$\beta_{11}(-\beta_{22}=\beta_{33})$	163(5)	194(1)	196(1)	195(1)
$\beta_{12}(-\beta_{13}=\beta_{23})$	16(2)	17(1)	19(1)	19(1)
<b>Oxygen site 1</b>				
$x(-y-z)$	37990(10)	38005(5)	37972(18)	37968(18)
$\beta_{11}(-\beta_{22}=\beta_{33})$	192(9)	196(2)	208(5)	206(5)
$\beta_{12}(-\beta_{13}=\beta_{23})$	-1(6)	-10(3)	2(7)	-1(7)
<b>Oxygen site 2</b>				
$x(-y-z)$		—	86988(18)	86977(18)
$\beta_{11}(-\beta_{22}=\beta_{33})$		—	188(5)	190(5)
$\beta_{12}(-\beta_{13}=\beta_{23})$			-24(7)	-20(7)
<b>Overall R-factor (omitting less-thans)</b>	<b>2.40%</b>	<b>2.30%</b>	<b>1.55%</b>	<b>1.63%</b>

\* Structure parameters in this column were calculated with the 27 Fd3m forbidden reflexions included in the refinement

was used. These two groups were then subdivided, and an R-factor calculated for each subgroup. This R-factor breakdown facility was found to be a useful tool for identifying reflexions and groups of reflexions which were not fitting very well during the early stages of the refinement. It was found to be particularly useful when comparing structure factors produced for refinements made for the two different space groups. The structure factor data produced by the least squares program were divided up using WTANAL, the results for the three refinements can be seen in tables 4.5.1, 4.5.2 and 4.5.3.

Even though the results of the  $Fd\bar{3}m$  refinement are in good agreement with those found by previous authors, inspection of tables 4.5.1 and 4.5.2 shows the refinement under  $F\bar{4}3m$  symmetry to provide a far better fit to the experimental data. An overall R-factor of 2.30% was obtained for the  $Fd\bar{3}m$  refinement, for the equivalent refinement under  $F\bar{4}3m$  symmetry this value decreased to 1.55%. This improvement in fit under  $F\bar{4}3m$  was achieved primarily by an improvement in fit of the weak, high-angle reflexions. Particularly noticeable are the group of 76 weakest reflexions with structure factors less than 10.0, the R-factor here changing from 49.2% to 14.8% with the change of space group. These 76 reflexions are all weak and do suffer considerably from statistical errors, in fact they are not expected to fit as well as the remaining groups, but a fit of 49.2% under  $Fd\bar{3}m$  symmetry when the overall R-factor is 2.30% does strongly suggest that incorrect assumptions have been made in this original analysis. It is now necessary to consider in some detail why such a dramatic improvement in fit should occur to this particular group of reflexions.

Firstly, we must consider how the intensities of strong and weak reflexions are affected by atom positions. Strong reflexions occur when

Table 4.5.1 R-factor breakdown in terms of  $F_0$  and  $\sin \theta/\lambda$  for Fd3m symmetry.

<u>Overall agreement factors</u>	<u>R-factors</u>	
No. of observations	309	Without reflexions below threshold $0.0230$
No. of variables	6	With reflexion multiplicity $0.0250$
No. below threshold	12	Of reflexions below threshold $0.0$
No. calculating above threshold	0	Of $F^2$ (without reflexions below threshold) $0.0349$

Results in terms of  $F_0$

$F_0$	$\Sigma F_0$	$\Sigma \Delta F$	No. of Reflexions	R	$\sin \theta/\lambda$	$\Sigma F_0$	$\Sigma \Delta F$	No. of Reflexions	R
10.0	319.8	157.5	76	0.492	0.20	523.3	24.8	3	0.047
20.0	244.6	6.7	17	0.027	0.30	608.3	10.2	4	0.017
30.0	919.0	12.9	36	0.014	0.40	1386.5	30.9	7	0.022
40.0	1504.8	15.9	43	0.011	0.50	1005.4	11.8	8	0.012
50.0	1206.4	14.0	27	0.012	0.60	1251.8	14.7	14	0.012
60.0	1316.4	9.0	24	0.007	0.70	1194.5	17.1	18	0.014
70.0	837.5	9.6	13	0.011	0.80	1489.7	25.2	25	0.017
80.0	518.3	3.7	7	0.007	0.90	1403.0	22.6	27	0.016
90.0	1178.7	10.5	14	0.009	1.00	1169.6	33.1	32	0.028
100.0	6389.4	92.7	40	0.015	1.10	1517.2	45.5	44	0.030
					1.20	1374.3	46.7	49	0.034
					1.30	1511.3	49.8	66	0.033

Table 4.5.2 R-factor breakdown in terms of  $F_0$  and  $\sin \theta/\lambda$  for F43m symmetry.

<u>Overall agreement factors</u>	<u>R-factors</u>
No. of observations	Without reflexions below threshold 0.0155
No. of variables	With reflexion multiplicity 0.0148
No. below threshold	Of reflexions below threshold 0.0
No. calculating above threshold	Of $F^2$ (without reflexions below threshold) 0.0349

Results in terms of  $F_0$

$F_0$	$\Sigma F_0$	$\Sigma \Delta F$	No. of Reflexions	R	$\sin \theta/\lambda$	$\Sigma F_0$	$\Sigma \Delta F$	No. of Reflexions	R
10.0	319.8	47.2	76	0.148	0.20	523.3	24.5	3	0.047
20.0	244.6	8.1	17	0.033	0.30	608.3	9.9	4	0.016
30.0	919.0	14.2	36	0.015	0.40	1386.5	31.0	7	0.022
40.0	1504.8	14.3	43	0.009	0.50	1005.4	13.2	8	0.013
50.0	1206.4	14.4	27	0.012	0.60	1251.8	14.7	14	0.012
60.0	1316.4	10.1	24	0.008	0.70	1194.5	11.6	18	0.010
70.0	837.5	8.3	13	0.010	0.80	1489.7	16.3	25	0.011
80.0	518.3	3.2	7	0.006	0.90	1403.0	18.3	27	0.013
90.0	1178.7	10.7	14	0.009	1.00	1169.6	17.1	32	0.015
100.0	6389.4	93.8	40	0.015	1.10	1517.2	20.9	44	0.014
					1.20	1374.3	19.8	49	0.014
					1.30	1511.3	26.9	66	0.018

Results in terms of  $\sin \theta/\lambda$

Table 4.5.3 R-factor breakdown in terms of  $F_0$  and  $\sin \theta/\lambda$  for F43m symmetry, with the 27 Fd3m forbidden reflexions included in the refinement.

Overall agreement factors	R-factors	
No. of observations	336	Without reflexions below threshold 0.0164
No. of variables	11	With reflexion multiplicity 0.0156
No. below threshold	24	Of reflexions below threshold 0.0274
No. calculating above threshold	3	Of $F^2$ (without reflexions below threshold) 0.0350

Results in terms of  $\sin \theta/\lambda$

$F_0$	$\Sigma F_0$	$\Sigma \Delta F$	No. of Reflexions	R	$\sin \theta/\lambda$	$\Sigma F_0$	$\Sigma \Delta F$	No. of Reflexions	R
10.0	379.9	60.5	91	0.159	0.20	523.3	24.5	3	0.047
20.0	244.6	8.0	17	0.033	0.30	608.3	9.9	4	0.016
30.0	919.0	14.7	36	0.016	0.40	1386.5	31.1	7	0.022
40.0	1504.8	13.9	43	0.009	0.50	1005.4	13.3	8	0.013
50.0	1206.4	14.2	27	0.012	0.60	1251.8	14.7	14	0.012
60.0	1316.4	10.0	24	0.008	0.70	1198.4	13.6	19	0.011
70.0	837.5	8.4	13	0.010	0.80	1497.0	17.3	27	0.012
80.0	518.3	3.2	7	0.006	0.90	1406.4	18.4	28	0.013
90.0	1178.7	10.7	14	0.009	1.00	1177.6	18.2	34	0.015
100.0	6389.4	94.0	40	0.015	1.10	1534.7	24.8	48	0.016
					1.20	1382.7	23.2	51	0.017
					1.30	1523.0	28.9	69	0.018

all the atoms of a crystal scatter X-rays cooperatively. If a number of atoms are slightly displaced from these positions then the change in intensity that results is small, making strong reflexions insensitive to small changes in atom position. Low-angle reflexions are also insensitive because the interplanar spacings associated with them are large compared with the displacements themselves. On the other hand, weak high-angle reflexions are extremely sensitive to small shifts in atom position.

The fact that the group of weakest reflexions fits so badly under  $Fd\bar{3}m$  symmetry tends to support the idea that the atom positions imposed on the structure by the conventional space group are incorrect. Changes that occur in the remaining groups in terms of  $F_0$  are not as dramatic as with this first group, but they do cause the R-factor for all groups to become more evenly distributed than before. If we now examine the R-factor breakdown (tables 4.5.1 and 4.5.2) in terms of  $\sin \theta/\lambda$ , it can be seen that for all groups of reflexions with  $\sin \theta/\lambda$  lying between 0.9 and 1.3 the R-factor for each group is approximately halved by the change of space group. Again, the data in these groups correspond to weak high-angle reflexions. This result, therefore, tends to reinforce the idea that the space group  $F\bar{4}3m$  more correctly describes the symmetry of magnetite.

It seems that these inconsistencies were not noticed by Hamilton (1958) or Fleet (1981), primarily because they failed to carry out sufficient numbers of measurements to high enough angles in reciprocal space. Fleet (1981) for example, measured reflexions out to  $\theta=45^\circ$ , whereas the measurements here were made out to  $\theta=70^\circ$ . Hamilton (1958), in his neutron diffraction study did measure reflexions out to  $\theta=70^\circ$ , but he only measured strong reflexions and his complete data set

consisted of just 60 reflexions, too small a number to reveal any consistent discrepancies.

The suggestion that the structure of magnetite is non-centrosymmetrical, with space group  $F\bar{4}3m$ , can be further substantiated by applying a statistical test. Because a centre of symmetry does not produce systematic absences among the X-ray intensities, it is necessary to perform a statistical survey of the distribution of these intensities to reveal the presence or absence of this symmetry element. The distribution taking a different form in each case.

If the structure factors of a crystal are plotted in the complex  $x$ ,  $y$ -plane then they exhibit a Gaussian distribution. If the structure is centrosymmetrical, and the centre of symmetry taken as the origin, then the structure factors are confined to the  $x$ -axis alone, again with a Gaussian distribution. This occurs because the projection of the imaginary parts of the structure factor on the  $y$ -axis for two atoms related by a centre of symmetry cancel each other out. When the crystal lacks a centre of symmetry, there are projections of the structure factors on both  $x$  and  $y$ -axes. For a centrosymmetrical structure the projection of the structure factor on the  $x$ -axis must be small for a weak reflexion to occur. In the non-centrosymmetrical case, the resultant projections on both axes must be small to produce a weak reflexion, but here, when one is small the other is likely to be large.

The above means that if the reflexions are plotted against their intensities, then a centrosymmetrical structure will possess a much larger percentage of reflexions with small structure factors than a non-centrosymmetrical structure. Theoretically, the difference between the two distributions is sufficient to determine the presence or absence of a centre of symmetry. Using this statistical test, known as Wilson's

criterion (Wilson, 1949), it should be possible to determine whether the structure of magnetite is centrosymmetrical or non-centrosymmetrical by making a survey of the {hkl} type reflexions.

Unfortunately, because of lattice centering, three quarters of the possible reflexions in magnetite are systematically absent. Additionally, because the changes in atom position from the centrosymmetrical structure are small, it is found that any statistical survey of X-ray intensities normally suitable for detecting the presence or absence of a centre of symmetry (see for example Wilson, 1949, 1952; Howells et al. 1950; Srinivasan et al. 1966) proves inconclusive. The failure of these statistical tests under such conditions is well known, see for example Srinivasan and Vijayalakshmi (1972).

Particularly interesting reflexions are the 40 shown in table 4.6 with Miller indices of the type  $4n, 4n, 4n+2$ , for example  $2\ 4\ 12$ ,  $4\ 8\ 10$  and  $6\ 12\ 12$ . Under  $Fd3m$  symmetry, these reflexions are produced by scattering from oxygen ions only. Because of the low atomic number of  $O^{2-}$ , we would expect the observed structure factors for these 40 reflexions to be small. This is not so; in fact, in all 40 cases the observed structure factor for the  $Fd3m$  refinement is far stronger than the calculated value. This result could only occur if there is a considerable contribution to the structure factor from the cations on the octahedral site, a situation only possible if this cation is displaced from its ideal position. Such a displacement is forbidden under  $Fd3m$  symmetry but allowed under  $F\bar{4}3m$ . Inspection of the column labelled  $F_c$  for the  $F\bar{4}3m$  refinement, again in table 4.6, shows the greatly improved fit obtained using this non-centrosymmetrical space group. It is worth noting that the improvement in fit for all 40 reflexions is achieved by an increase in  $F_c$ , which is the result

Table 4.6 Reflexions produced by oxygen only scattering under Fd3m symmetry.

h	k	l	Number of Equivalents	F <sub>o</sub>		F <sub>c</sub>	
						Fd3m	F $\bar{4}$ 3m
2	4	4	10	<	4.34	0.08	1.60
2	4	8	22	<	4.00	0.23	1.83
2	4	12	22		3.61	0.24	2.78
2	4	16	24		3.22	0.21	3.04
2	4	20	24		4.06	0.20	3.39
2	8	8	9	<	3.75	0.38	2.72
2	8	12	18		3.42	0.38	2.74
2	8	16	21		3.09	0.38	3.48
2	8	20	24		2.77	0.36	3.21
2	12	12	9		4.49	0.46	3.50
2	12	16	24		2.90	0.49	3.18
4	4	6	9	<	4.10	0.10	1.18
4	4	10	9		3.75	0.08	3.05
4	4	14	12	<	3.37	0.04	2.42
4	4	18	10		3.01	0.03	3.61
4	6	8	20		3.83	0.19	2.69
4	6	12	19	<	3.48	0.19	2.64
4	6	16	24		3.13	0.19	3.19
4	6	20	24		2.80	0.18	3.42
4	8	10	20		3.54	0.12	2.31
4	8	14	22		3.22	0.08	3.39
4	8	18	22		2.90	0.06	3.14
4	10	12	24		3.27	0.14	3.17
4	10	16	23		2.98	0.15	3.39
4	12	14	21		3.01	0.10	3.23
4	12	18	24		3.87	0.07	3.28
4	14	16	24		2.77	0.11	3.16
6	8	8	9	<	3.61	0.29	2.37
6	8	12	24		3.32	0.33	3.21
6	8	16	20		3.01	0.34	3.25
6	12	12	10		3.09	0.40	3.16
6	12	16	24		2.83	0.44	3.49
8	8	10	9	<	3.37	0.20	3.20
8	8	14	12		4.37	0.14	3.05
8	8	18	12		2.80	0.11	3.40
8	10	12	21		3.13	0.25	3.11
8	10	16	24		2.87	0.27	3.30
8	12	14	24		4.11	0.19	3.34
10	12	12	12		2.94	0.33	3.38
12	12	14	12		2.73	0.24	3.34

expected by Wilson's criterion if magnetite lacks a centre of symmetry because a centrosymmetrical structure contains a larger percentage of smaller structure factors than a non-centrosymmetrical structure.

Table 4.7 shows the structure factors for the 76 weakest reflexions. Examination of the column labelled  $(F_o - F_c)$  shows that for the refinement made assuming  $Fd\bar{3}m$  symmetry, the sign of  $(F_o - F_c)$  is positive for 65 of the 76 reflexions. Prima facie, one would expect a value of approximately 38, i.e. even numbers of plus and minus signs. This result implies that scattering given assuming  $Fd\bar{3}m$  symmetry is persistently too small to account for that measured experimentally. For the  $F\bar{4}3m$  refinement, the balance of plus and minus signs changes to the ratio 34:42, i.e. it becomes more evenly distributed. Again, this is not an exact balance but it is reasonable considering the number of data points taken into account. Such an observation is not really a statistical test, mainly because of the small number of reflexions considered, but it is the effect predicted by Wilson's criterion if magnetite lacks a centre of symmetry.

It is a well-known fact that in any crystal structure refinement, the introduction of extra variables into the least squares refinement will usually lead to a better fit between observed and calculated structure factors, simply because there are fewer constraints on the model. This means that it is not possible to come to any statistically valid conclusions regarding the symmetry of magnetite by just examining the final structure parameters and estimated standard deviations produced by the least squares refinement. To decide whether the improvement in fit under  $F\bar{4}3m$  is statistically significant, or just a consequence of the addition of extra variables into the argument, two standard statistical tests have been applied to the experimental data.

Table 4.7 Structure factors for the 76 weakest reflexions.

h	k	l	Number of Equivalents	$F_o$	$F_c$		$(F_o - F_c)$	
					Fd3m	$\bar{F}43m$	Fd3m	$\bar{F}43m$
1	1	15	12	4.77	2.01	4.12	+	+
1	3	11	20	6.50	5.86	6.42	+	+
1	3	19	24	2.98	1.87	2.79	+	+
1	3	21	24	6.27	6.68	6.63	-	-
1	5	11	24	9.01	8.45	8.95	+	+
1	5	19	24	2.94	0.96	3.54	+	-
1	5	21	24	8.76	9.05	9.24	-	-
1	7	7	12	8.76	8.14	8.68	+	+
1	7	17	24	4.32	7.31	7.33	-	-
1	9	15	19	4.44	2.31	3.79	+	+
1	11	11	10	3.32	0.99	1.99	+	+
1	11	13	24	5.51	5.63	5.99	-	-
1	11	19	24	2.74	2.57	3.08	+	-
1	15	15	12	3.96	2.49	2.95	+	+
2	4	12	22	3.61	0.24	2.78	+	+
2	4	16	24	3.22	0.21	3.04	+	+
2	4	20	24	4.06	0.20	3.39	+	+
2	8	12	18	3.42	0.38	2.74	+	+
2	8	16	21	3.09	0.38	3.48	+	-
2	8	20	24	2.77	0.36	3.21	+	-
2	12	12	9	4.49	0.46	3.50	+	+
2	12	16	24	2.90	0.49	3.18	+	-
3	3	15	12	3.32	1.01	3.98	+	-
3	3	17	9	7.02	8.61	8.70	-	-
3	5	15	24	3.27	1.36	2.68	+	+
3	7	11	24	3.55	1.79	4.39	+	-
3	7	13	24	8.93	8.31	8.42	+	+
3	7	19	21	2.87	2.60	4.51	+	-
3	9	11	24	4.85	5.36	5.76	-	-
3	11	15	24	4.27	2.36	4.46	+	-
3	11	17	24	2.87	2.54	3.45	+	-
3	13	17	24	9.18	8.99	8.95	+	+
4	4	10	9	3.75	0.08	3.05	+	+
4	4	18	10	3.01	0.03	3.61	+	-
4	6	8	20	3.83	0.19	2.69	+	+
4	6	16	24	3.13	0.19	3.19	+	-
4	6	20	24	2.80	0.18	3.42	+	-
4	8	10	20	3.54	0.12	2.31	+	+
4	8	14	22	3.22	0.08	3.39	+	-
4	8	18	22	2.90	0.06	3.14	+	-
4	10	12	24	3.27	0.14	3.17	+	+
4	10	16	23	2.98	0.15	3.39	+	-
4	12	14	21	3.01	0.10	3.23	+	-
4	12	18	24	3.87	0.07	3.28	+	+
4	14	16	24	2.77	0.11	3.16	+	-
5	5	15	12	4.56	3.00	4.30	+	+
5	7	11	20	3.49	3.17	3.86	+	-
5	7	19	24	2.84	2.02	2.94	+	-

h	k	l	Number of Equivalents	$F_o$	$F_c$		$(F_o - F_c)$	
					Fd3m	$F\bar{4}3m$	Fd3m	$F\bar{4}3m$
5	9	11	24	5.84	8.04	8.29	-	-
5	9	19	24	2.77	0.35	2.96	+	-
5	11	15	21	2.98	1.60	2.53	+	+
5	11	17	24	4.01	4.33	4.62	-	-
5	13	15	24	4.06	2.23	3.30	+	+
6	8	12	24	3.32	0.33	3.21	+	+
6	8	16	20	3.01	0.34	3.25	+	-
6	12	12	10	3.09	0.40	3.16	+	-
6	12	16	24	2.83	0.44	3.49	+	-
7	7	7	4	6.37	2.77	5.04	+	+
7	7	9	12	7.93	6.86	7.11	+	+
7	7	15	12	4.38	2.27	4.49	+	-
7	7	17	10	4.16	3.26	3.94	+	+
7	9	17	20	6.42	7.59	7.60	-	-
7	11	11	10	4.50	2.09	4.45	+	+
7	11	13	21	3.05	2.00	3.07	+	-
7	13	13	12	7.78	8.73	8.74	-	-
8	8	14	12	4.37	0.14	3.05	+	+
8	8	18	12	2.80	0.11	3.40	+	-
8	10	12	21	3.13	0.25	3.11	+	+
8	10	16	24	2.87	0.27	3.30	+	-
8	12	14	24	4.11	0.19	3.34	+	+
9	9	15	12	4.16	2.80	3.74	+	+
9	11	11	10	3.10	0.63	2.34	+	+
9	11	13	24	4.21	6.01	6.22	-	-
10	12	12	12	2.94	0.33	3.38	+	-
11	11	15	12	3.92	2.78	4.66	+	-
12	12	14	12	2.73	0.24	3.34	+	-

The first of these tests was devised by Hamilton (1965) and is used to examine the crystallographic R-factor. In this particular test, the ratio  $R_1/R_0$  is examined using linear hypothesis theory. Theoretically, this analysis should be made using the generalized R-factor ( $R_G$ ) which is given by :

$$R_G = \left\{ \frac{\sum_i \sum_j W_{ij} (|F_i|_o - |F_i|_c)(|F_i|_o - |F_i|_c)}{\sum_i \sum_j W_{ij} |F_i|_o |F_i|_o} \right\}^{1/2} \quad 4.1$$

Hamilton (1965) states that the ratio  $R_1/R_0$  is relatively insensitive to the method of calculation of the R-factors and that it is therefore permissible to use the conventional crystallographic R-factor.

Application of this ratio test to the data produced for magnetite specimen BMDM11, taking  $R_1$  as the  $Fd\bar{3}m$  R-factor and  $R_0$  as the  $F\bar{4}3m$  R-factor, showed the hypothesis that the space group of magnetite is  $F\bar{4}3m$  to be correct with at least 99.50% certainty.

The second test involves the examination of bond lengths calculated for each space group. This is necessary because, before any definite conclusions can be drawn, it is important to initially make an estimation of any errors occurring. Unless a standard procedure is followed for this estimation, it is possible that conclusions drawn may be based on differences which are due entirely to experimental errors.

Assuming that the experimental and computational errors have been estimated correctly, then the probability distribution of these errors is Gaussian.

Table 4.8 Comparison of bond lengths calculated in the refinement under  $Fd3m$  symmetry with those found by previous authors (all distances given are in Angstrom units).

Bond	Present Study	Hamilton (1958)	Fleet (1981)	Fleet*
$Fe^{3+}-O$ (Tetrahedral bond)	1.8912(2)	1.8871(29)	1.8883(17)	1.8854(4)
$Fe^{2+,3+}-O$ (Octahedral bond)	2.0575(2)	2.0590(16)	2.0584(9)	2.0600(17)
O-O	2.8485(3)	2.8538(46)	2.8519(27)	2.8566(7)
O-O	2.9696(3)	2.9689(3)	2.9689(3)	2.9688(7)
O-O	3.0884(3)	3.0817(46)	3.0836(27)	3.0789(7)

\* This refers to the re-examination of data collected by Fleet (1981), as discussed in Chapter 3.

The probability that the error lies between  $x$  and  $x+dx$  is given by :

$$\frac{1}{(2\pi\sigma^2)^{1/2}} \exp(-x^2/2\sigma^2) dx \quad 4.2$$

where  $\sigma$  is the standard deviation of the error.

In the results shown in table 4.9, it has been found that a bond length under  $F\bar{4}3m$  symmetry, with standard deviation  $\sigma_A$ , differs from a similar bond length under  $Fd3m$  symmetry, with standard deviation  $\sigma_B$ , by an amount  $\delta l$ . It is then necessary to ask the question: is there a real difference between these two bond lengths or does the difference occur because of random errors? To test this the numerical significance levels suggested by Cruickshank (1949), which are ideal for crystallographic purposes, may be used.

If  $P$  represents the probability that a bond length under  $F\bar{4}3m$  symmetry, having standard deviation  $\sigma_A$ , is observed as differing from the same bond length under  $Fd3m$  symmetry with standard deviation  $\sigma_B$ , then :

- If  $P > 5\%$              $\delta l$  is not significant
- If  $5\% > P > 1\%$     $\delta l$  is of possible significance
- If  $P < 1\%$              $\delta l$  is significant
- If  $P < 0.1\%$          $\delta l$  is highly significant

If  $\sigma = (\sigma_A^2 + \sigma_B^2)^{1/2}$  for the various values of  $P$  for a Gaussian distribution and if  $\delta l / \sigma = \sqrt{2} \cdot x$  then :

$$P = \frac{1}{2} - \frac{1}{\sqrt{\pi}} \int_0^x e^{-t^2} dt = \frac{1}{2} [1 - \text{erf}(x)] \quad 4.3$$

Table 4.9 Calculated bond lengths.

Fd3m		F $\bar{4}$ 3m	
Bond	Distance (Å)	Bond	Distance (Å)
Fe <sup>3+</sup> -O (Tetrahedral bond)	1.8912(2)	Fe <sup>3+</sup> (1)-O(2) Fe <sup>3+</sup> (2)-O(1)	1.8923(2) 1.8864(2)
Fe <sup>2+, 3+</sup> -O (Octahedral bond)	2.0575(2)	Fe <sup>2+, 3+</sup> -O(1) Fe <sup>2+, 3+</sup> -O(2)	2.0584(2) 2.0586(2)
O-O	2.8485(3)	O(1)-O(1) O(2)-O(2)	2.8563(3) 2.8468(3)
O-O	2.9696(3)	O(1)-O(2)	2.9696(3)
O-O	3.0884(3)	O(1)-O(1) O(2)-O(2)	3.0805(3) 3.0901(3)

Table 4.10 The significance (P) of differences in bond lengths between the Fd3m and F43m structure refinements.

Bond	Difference ( $\overset{\circ}{\text{A}}$ )	x	P
Fe <sup>3+</sup> (1)-O(2)	0.0011	2.75	< 0.1%
Fe <sup>3+</sup> (2)-O(1)	0.0048	12.00	< 0.1%
Fe <sup>2+,3+</sup> -O(1)	0.0009	2.25	< 0.1%
Fe <sup>2+,3+</sup> -O(2)	0.0011	2.75	< 0.1%
O(1)-O(1)	0.0078	13.00	< 0.1%
O(2)-O(2)	0.0017	2.83	< 0.1%
O(1)-O(1)	0.0079	13.17	< 0.1%
O(2)-O(2)	0.0017	2.83	< 0.1%

Table 4.11 Some sensitive reflexions.

h	k	l	Number of Equivalents	$F_o$	$F_c$	
					Fd3m	$\bar{F}43m$
1	3	11	20	6.50	5.86	6.42
1	3	19	24	2.98	1.87	2.79
1	5	11	24	9.01	8.45	8.95
1	7	7	12	8.76	8.14	8.68
2	4	16	24	3.22	0.21	3.04
3	11	15	24	4.27	2.36	4.46
4	6	16	24	3.13	0.19	3.19
4	8	14	22	3.22	0.08	3.39
4	10	12	24	3.27	0.14	3.17
4	12	14	21	3.01	0.10	3.23
5	5	15	12	4.56	3.00	4.30
5	7	19	24	2.84	2.02	2.94
5	9	19	24	2.77	0.35	2.96
6	8	12	24	3.32	0.33	3.21
6	8	16	20	3.01	0.34	3.25
6	12	12	10	3.09	0.40	3.16
7	7	15	12	4.38	2.27	4.49
7	11	11	10	4.50	2.09	4.45
7	11	13	21	3.05	2.00	3.07
8	10	12	21	3.13	0.25	3.11

Bond lengths for the two refinements along with their estimated standard deviations are shown in table 4.9. Inspection shows them to differ by  $0.0009 \text{ \AA}$  to  $0.0079 \text{ \AA}$  from the corresponding  $Fd\bar{3}m$  values. The bond length differences found between the two space groups have been compared with the numerical significance levels suggested by Cruickshank (1949), and the results of this comparison are shown in table 4.10. Examination of these bond length differences using Cruickshank's significance tests showed all differences to be highly significant; a result which again supports the idea that magnetite is more correctly described by the non-centrosymmetrical space group  $F\bar{4}3m$ .

All of the calculations described above were performed on the data produced in the refinement made under  $F\bar{4}3m$  symmetry and not including the additional 27  $Fd\bar{3}m$  forbidden reflexions. This was done so that the various statistical tests were applied to two directly comparable data sets (i.e. two data sets with the same number of data points), the only difference being the space group used for the calculations in each case.

Table 4.4 gives atom positions and temperature factors for all three refinements. The structure factors for all three refinements are given in Appendix VII; R-factor breakdowns for all three refinements are given in tables 4.5.1, 4.5.2 and 4.5.3. Structure factors for the 27 forbidden reflexions, after convergence of the least squares program, are given in table 4.12. Table 4.4 shows that the temperature factors for the  $F\bar{4}3m$  refinement remain practically unaltered when the 27 forbidden reflexions are included in the refinement. The three atom positions  $u_1$ ,  $u_2$  and  $u_3$  do change slightly with the addition of these extra reflexions, but again this change is very small. The R-factor breakdown is practically unaltered and the overall R-factor changes from

Table 4.12 Structure factors for the 27 Fd3m forbidden reflexions.

h	k	l	Number of Equivalents	$F_o$	$F_c$
0	0	2	3	< 4.64	0.11
0	0	6	3	< 4.34	1.23
0	0	10	3	< 3.91	2.65
0	0	14	3	< 3.48	2.81
0	0	18	3	4.37	3.61
0	0	22	3	3.87	3.52
0	2	4	9	< 4.48	0.99
0	2	8	12	< 4.10	1.99
0	2	12	10	3.67	2.75
0	2	16	10	3.27	3.24
0	2	20	12	4.11	3.68
0	4	6	11	< 4.22	1.90
0	4	10	10	3.83	2.24
0	4	14	10	3.42	3.24
0	4	18	12	4.32	3.46
0	6	8	9	< 3.91	2.26
0	6	12	10	< 3.54	2.83
0	6	16	9	4.49	3.61
0	6	20	12	< 2.83	3.38
0	8	10	12	3.61	2.86
0	8	14	10	< 3.27	3.33
0	8	18	9	< 2.94	3.54
0	10	12	10	4.69	3.40
0	10	16	12	4.26	3.29
0	12	14	11	4.32	3.35
0	12	18	11	3.91	3.76
0	14	16	10	3.96	3.88

1.55% to 1.65%. On the whole, the addition of these forbidden reflexions seems to make very little difference to the final analysis.

The 27  $Fd\bar{3}m$  forbidden reflexions are again direct evidence in favour of  $F\bar{4}3m$  symmetry for magnetite. Structure factors for these reflexions are given in table 4.12, 12 of the 27 were found to have an intensity below the minimum detectable level of 100 counts. Agreement between observed and calculated structure factors for these reflexions really is quite good, especially when it is considered how weak they are. Of the reflexions calculated as less than threshold only three, namely  $0\ 2\ 20$ ,  $0\ 8\ 14$  and  $0\ 8\ 18$  calculated above, and then only marginally so. The overall R-factor for these reflexions is 17.0%, which is reasonable since it is only slightly worse than the group of 76 reflexions with structure factors less than 10.0

Finally, the small atom shifts which give rise to  $F\bar{4}3m$  symmetry in magnetite can be seen in figures 4.5 and 4.6. Figure 4.5 shows both tetrahedral sites and figure 4.6 shows the surroundings of the octahedral site ion, which is normally located at  $5/8, 5/8, 5/8$ . The arrows indicate the displacements that occur along  $\langle 111 \rangle$  directions, giving rise to the lowering of crystal symmetry from  $Fd\bar{3}m$  to  $F\bar{4}3m$ . These diagrams are drawn for the ideal configuration, with the origin at an octahedral site. Figure 4.7 shows how the two sections of the structure labelled R (figure 4.5) and S (figure 4.6) relate to the unit cell.

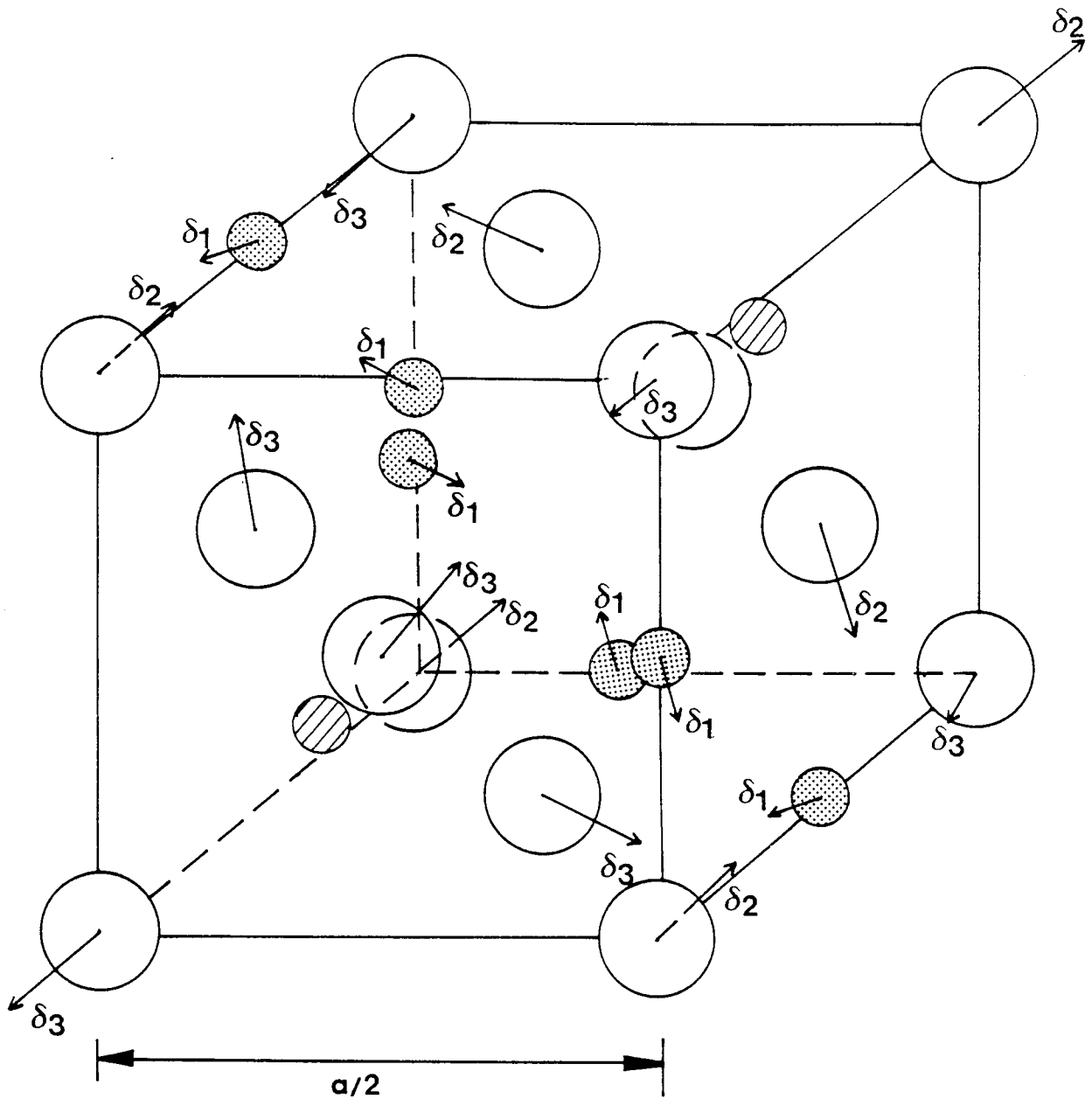


Figure 4.5 Atom shifts in magnetite giving rise to  $F\bar{4}3m$  symmetry in one eighth of the unit cell are shown. The symbols  $\delta_1$ ,  $\delta_2$  and  $\delta_3$  represent the shifts of the octahedral site cations and the two anions respectively, along  $\langle 111 \rangle$  directions, from their  $Fd\bar{3}m$  positions. The small hatched circles represent iron atoms in tetrahedral sites, the small dotted circles iron atoms in octahedral sites and the large open circles oxygen atoms. This diagram represents the regions labelled R in figure 4.7.

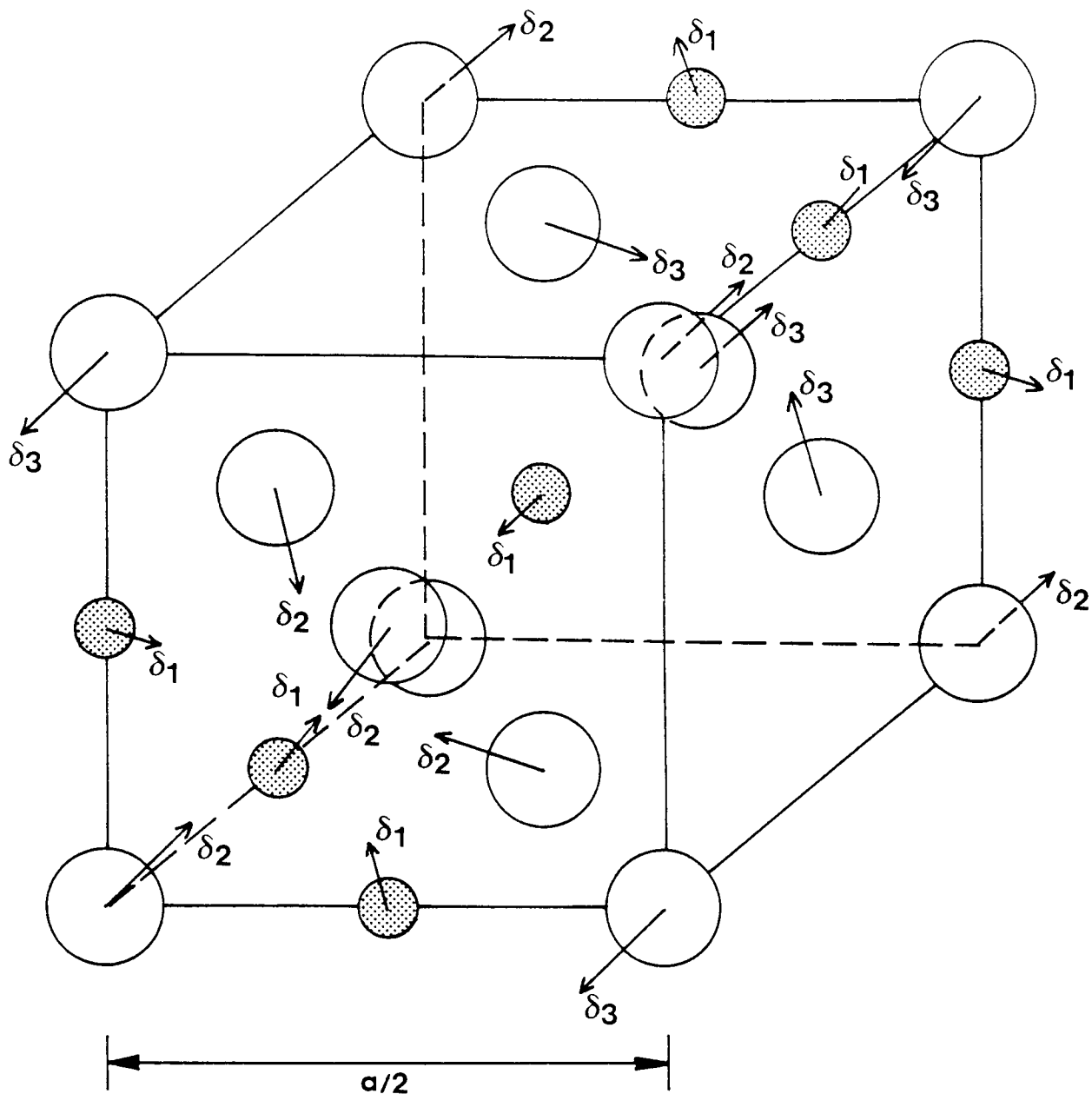


Figure 4.6 Atom shifts in magnetite giving rise to  $F\bar{4}3m$  symmetry in one eighth of the unit cell are shown. The symbols  $\delta_1$ ,  $\delta_2$  and  $\delta_3$  represent the shifts of the octahedral site cations and the two anions respectively, along  $\langle 111 \rangle$  directions, from their  $Fd\bar{3}m$  positions. The small dotted circles represent iron atoms in octahedral sites and the large open circles oxygen atoms. This diagram represents the regions labelled S in figure 4.7.

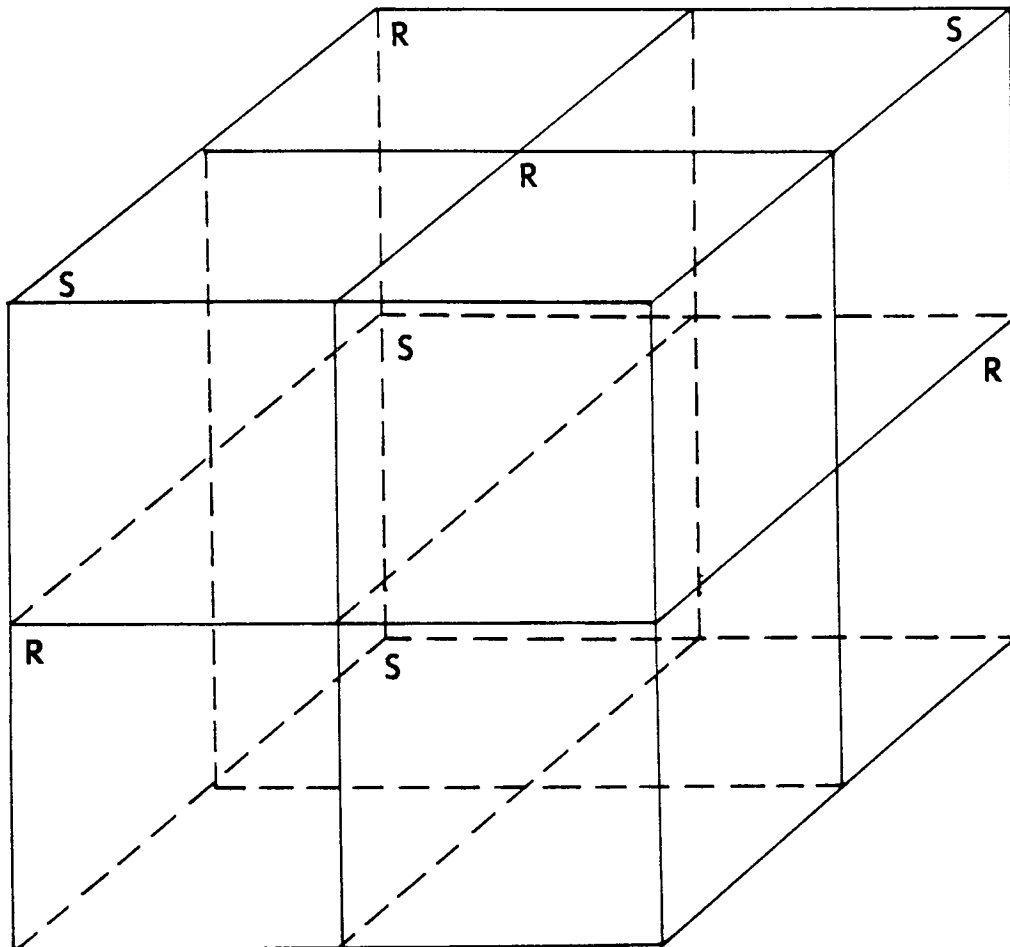


Figure 4.7 A unit cell of magnetite. The regions labelled R and S are the one eighths of the unit cell shown in figures 4.5 and 4.6 respectively.

## CHAPTER 5

### THE USE OF X-RAY ANOMALOUS SCATTERING IN STUDIES OF THE SYMMETRY OF MAGNETITE

#### 5.1 Introduction

X-ray anomalous scattering techniques have attracted increasing interest in crystal structure determination in recent years, mainly because the increase in precision of intensity measuring procedures means that the small effects produced can be measured with reasonable accuracy. The most common use of anomalous scattering is in the determination of phase angles and absolute molecular configurations. A less common use of anomalous scattering is in distinguishing between centrosymmetrical and non-centrosymmetrical structures. It is this latter application which is discussed in this chapter. Before considering how anomalous scattering can be used, it is necessary to look at the effects it has on the structure factors of Friedel related pairs of reflexions in centrosymmetrical and non-centrosymmetrical structures.

Normally in a diffraction study, the wavelength of the radiation used is somewhat different to that of an absorption edge of any atom in the structure. If this is the case then the intensities of a Friedel pair of reflexions, that is to say, reflexions with Miller indices  $hkl$  and  $\bar{h}\bar{k}\bar{l}$ , are equal even in a non-centrosymmetrical structure. This is Friedel's law and may be stated as: the diffraction symmetry of a crystal is the point symmetry plus a centre of symmetry. Nishikawa and

Matukawa (1928) and Coster, Knol and Prins (1930) were able to demonstrate, in a non-centrosymmetrical structure, that as the wavelength of the incident radiation approaches that of an absorption edge of one of the atoms in the crystal, then the scattering factor becomes complex, a phase change results and Friedel's law breaks down. The intensities of a Friedel pair of reflexions with Miller indices  $hkl$  and  $\bar{h}\bar{k}\bar{l}$  are no longer equal.

The anomalous phase shifts and the differences in intensity between the reflexions  $hkl$  and  $\bar{h}\bar{k}\bar{l}$  are greatest when an X-ray wavelength slightly shorter than an absorption edge of one atom is used. Hönl (1935a,b) was able to show that these effects are still appreciable even at much shorter wavelengths; a result which means that with accurate intensity measurements, the most commonly available radiations can be used to examine differences between Friedel related pairs of reflexions in non-centrosymmetrical structures.

For any mineral crystallizing in the cubic system, in one complete hemisphere of reciprocal space the general reflexion  $hkl$  has 48 symmetry related equivalents. If the mineral is non-centrosymmetrical and contains one or more anomalous scatterers in the unit cell, then these equivalent reflexions divide into two separate groups, each containing 24 equivalents. A unique intensity is found for each group. An extensive search through the literature on anomalous scattering has revealed much confusion in the terminology used to refer to the equivalent reflexions within a group. To prevent further confusion the term 'Friedel pair' is used throughout this chapter to refer solely to the reflexions  $hkl$  and  $\bar{h}\bar{k}\bar{l}$  and the term 'Laue-equivalents' is used to refer to the equivalent reflexions making up a specific group. The intensity of one member of a

Friedel pair is calculated by averaging the Laue-equivalents for that particular reflexion.

We will now consider in detail how anomalous scattering arises and what effect it has on the structure factors of Friedel pairs of reflexions in centrosymmetrical and non-centrosymmetrical structures.

## 5.2 Anomalous Scattering

When calculating structure factors, it is assumed that the scattering factor for an element is independent of the wavelength of the incident radiation, provided  $\sin \theta/\lambda$  is constant. This is not true if the wavelength of the incident radiation is near to that of an absorption edge for the scattering element. In this case, an anomalous phase change occurs on scattering. Physically, this change arises because of a resonance effect induced in the K-shell electrons by the incident radiation. It has the effect of advancing the phase of the wave scattered by this atom relative to that scattered by other atoms in the structure. This effect is known as anomalous scattering and causes the scattering factor to become complex (Woolfson, 1979). Figure 5.1 shows how the real and imaginary components of anomalous scattering for iron vary with the ratio  $\lambda/\lambda_k$  where  $\lambda$  is the wavelength of the incident radiation and  $\lambda_k$  is the wavelength of the K-absorption edge.

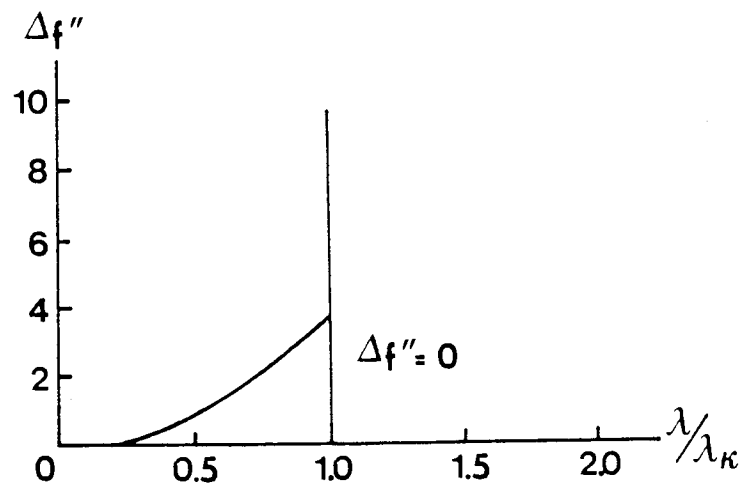
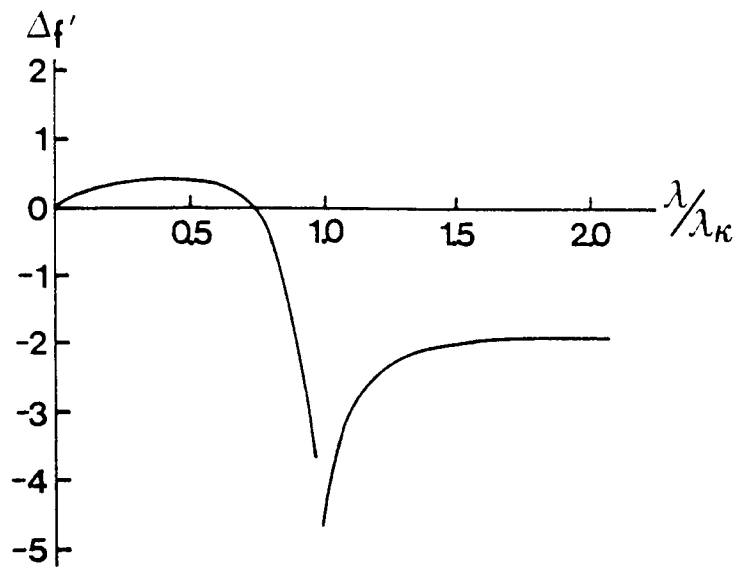


Figure 5.1 Variation of the real ( $\Delta f'$ ) and imaginary ( $\Delta f''$ ) anomalous scattering components for iron with  $\lambda/\lambda_K$ , from quantum mechanical theory (after Woolfson, 1979).

The scattering factor ( $f$ ) can be represented by :

$$f = f_0 + \Delta f' + i\Delta f'' = f' + i\Delta f'' \quad 5.1$$

where  $f_0$  represents the normal scattering factor,  $\Delta f'$  and  $\Delta f''$  are the real and imaginary components of anomalous scattering. An important point to note here is that because the diffracting power of an atom decreases with increasing  $\sin \theta/\lambda$ , the anomalous scattering effects, which are approximately independent of angle, are much greater for weak high-angle reflexions than those which are strong and at low angles.

It is possible to represent anomalous scattering by a series of vector diagrams. Figure 5.2 shows the situation in a centrosymmetrical structure which consists of several atoms which do not, and two atoms which do scatter anomalously.  $F_w$  represents the scattering produced by the atoms which do not scatter anomalously,  $f'$  and  $\Delta f''$  are the real and imaginary parts of the scattering factor for each atom which scatters anomalously. From figure 5.2 it can be seen that the phases of the Friedel pair of reflexions  $hkl$  and  $\bar{h}\bar{k}\bar{l}$  are still equal but that they now differ from  $0$  or  $\pi$ . The structure factors become complex but Friedel's law still holds and  $|F_{hkl}| = |F_{\bar{h}\bar{k}\bar{l}}|$ .

A similar situation for a non-centrosymmetrical structure is shown in figure 5.3. As above  $F_w$  represents the resultant of scattering from the atoms without anomalous scattering but  $f'$  and  $\Delta f''$  are now the resultants of scattering from one or more identical atoms which scatter anomalously. Figure 5.3a shows  $F_{hkl}$  and  $F_{\bar{h}\bar{k}\bar{l}}$  on the same diagram but in figure 5.3b  $F_{\bar{h}\bar{k}\bar{l}}$  is reflected across the real axis so that the difference between  $|F_{hkl}|$  and  $|F_{\bar{h}\bar{k}\bar{l}}|$  can be easily seen. From these

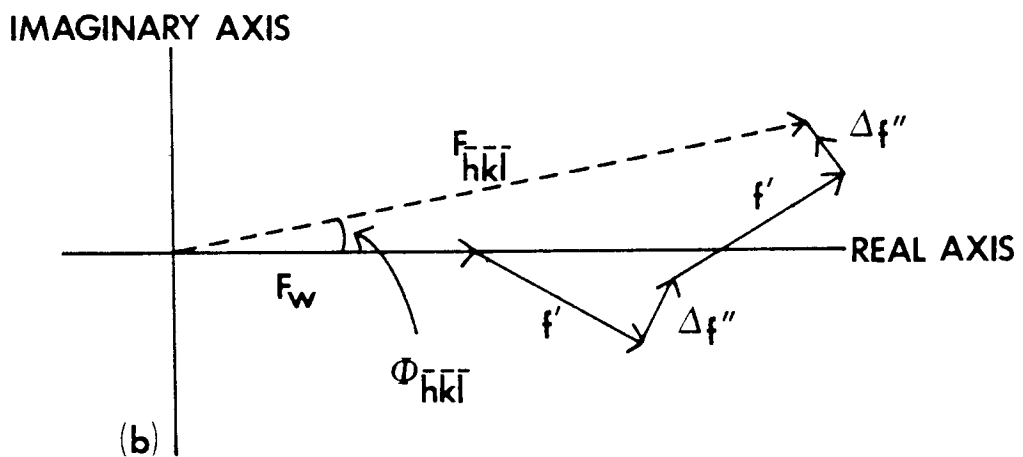
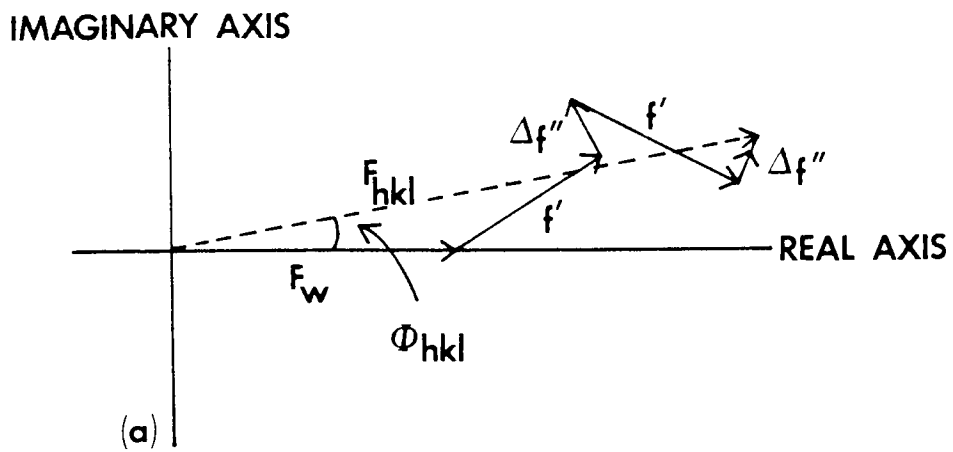


Figure 5.2 Vector representation of a Friedel pair of reflections for a centrosymmetrical structure when anomalous scattering is present;  $|F_{hkl}| = |F_{\bar{h}\bar{k}\bar{l}}|$  (after Stout and Jensen, 1968).

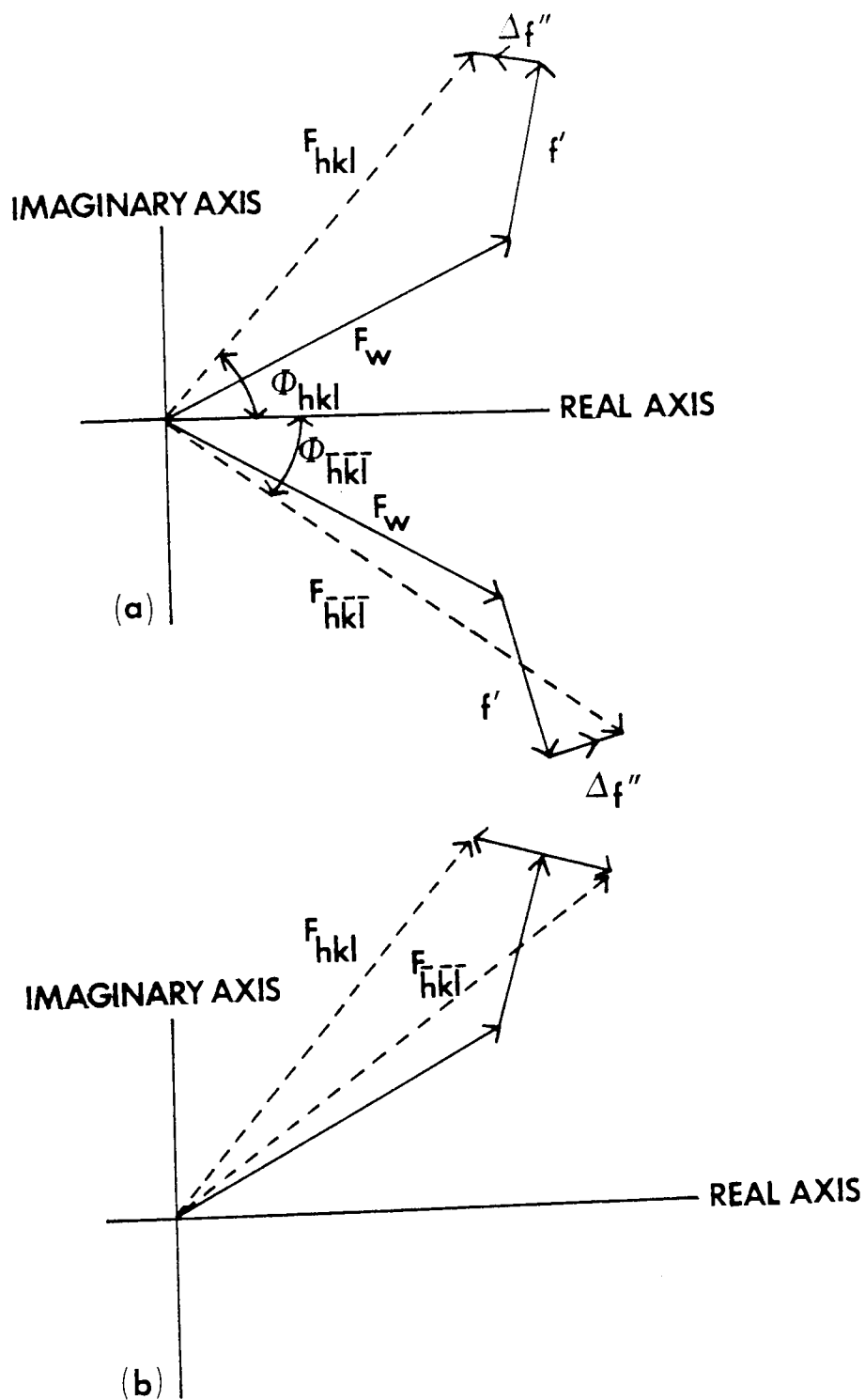
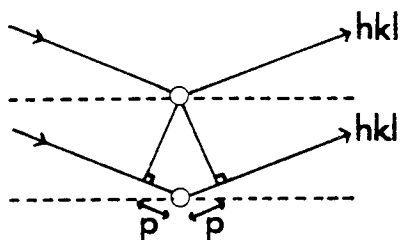


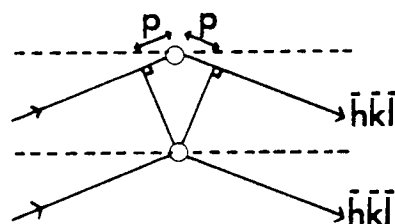
Figure 5.3 Vector representation of a Friedel pair of reflections for a non-centrosymmetrical structure when anomalous scattering is present;  $|F_{hkl}| \neq |F_{\bar{h}\bar{k}\bar{l}}|$  (after Stout and Jensen, 1968).

(a) WITHOUT ANOMALOUS SCATTERING



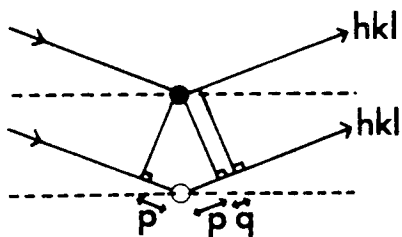
PHASE DIFFERENCE =  $2p$

$$|F_{hkl}| = |F_{\bar{h}\bar{k}\bar{l}}|$$



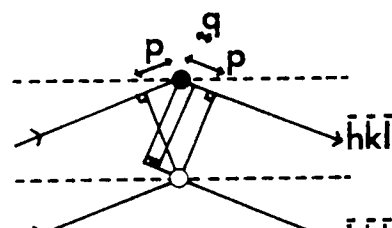
PHASE DIFFERENCE =  $2p$

(b) WITH ANOMALOUS SCATTERING



PHASE DIFFERENCE =  $2p+q$

$$|F_{hkl}| \neq |F_{\bar{h}\bar{k}\bar{l}}|$$



PHASE DIFFERENCE =  $2p-q$

Figure 5.4 Phase differences arising in a non-centrosymmetrical structure (a) without (b) with an anomalous scatter (after Glusker and Trueblood, 1972).

diagrams it can be seen that Friedel's law is violated in a non-centrosymmetrical structure with one or more atoms that scatter anomalously and  $|F_{hkl}| \neq |F_{\bar{h}\bar{k}\bar{l}}|$ .

Diffraction with and without anomalous scattering by a non-centrosymmetrical structure is shown schematically in figure 5.4. Figure 5.4a shows the arrangement if no anomalous scattering is present. Here the phase differences on scattering for the  $hkl$  and  $\bar{h}\bar{k}\bar{l}$  reflexions are both  $2p$  and  $|F_{hkl}| = |F_{\bar{h}\bar{k}\bar{l}}|$ . Figure 5.4b shows the situation when an anomalous scatterer is present. For a particular reflexion, the anomalous scatterer (shown as the dark atom) causes a phase difference of  $q$  in addition to the original value of  $2p$ . In this case the phase difference for the  $hkl$  reflexion is  $2p+q$  and for  $\bar{h}\bar{k}\bar{l}$  it is  $2p-q$ . Because the intensity of the diffracted beam depends on the phase difference between waves scattered by various atoms within the unit cell, the result is that Friedel's law is violated in a non-centrosymmetrical structure in the presence of anomalous scattering and  $|F_{hkl}| \neq |F_{\bar{h}\bar{k}\bar{l}}|$ .

### 5.3 Practical Difficulties Arising When Using Anomalous Scattering

In practice, to determine whether magnetite lacks a centre of symmetry using anomalous scattering it is necessary to measure, with a high degree of accuracy, groups of very weak Friedel related pairs of reflexions in a mineral which strongly absorbs X-rays. The problems of making consistent intensity measurements of equivalent reflexions in absorbing crystals are well known. These problems arise partly because of difficulties arising over inaccuracies in the absorption corrections applied and partly because of the differences in the quality of the

outer layers of the crystal produced in the grinding process (Boehm, Prager and Barnea, 1974).

In order to draw significant conclusions from an examination of Friedel pairs of reflexions, it is necessary to look at the factors which lead to errors in the X-ray intensity measurements and how these errors may be overcome.

### 5.3.1 Absorption

Anisotropic absorption can have a significant influence on the intensity of Friedel related pairs of reflexions and must therefore be avoided. This was achieved in the present study by using a spherical crystal specimen for data collection, which meant that the reflexions  $hkl$  and  $\bar{h}\bar{k}\bar{l}$  had the same absorption correction. In addition, a short wavelength radiation ( $MoK\alpha$ ) was used which helped to reduce X-ray absorption by the specimen.

### 5.3.2 Extinction

The effect of anisotropic extinction differs for the Friedel related reflexions in a non-centrosymmetrical structure. To reduce this problem it is necessary to make measurements on weak reflexions which are not affected by extinction. This problem was easily resolved because the Friedel pairs showing the largest differences are all extremely weak.

### 5.3.3 Double Diffraction

The effects of double diffraction depend upon geometrical factors such as crystal orientation. This means that the effects of double diffraction can be reduced by measuring the reflexions  $hkl$  and  $\bar{h}\bar{k}\bar{l}$  under identical experimental conditions. Double diffraction is not really a problem for weak reflexions at high angles so again this is overcome by the nature of the reflexions being measured.

### 5.3.4 Thermal Diffuse Scattering

Errors due to thermal diffuse scattering were overcome by using identical experimental conditions to measure each member of the Friedel pair.

### 5.3.5 Counting Statistics

Counting statistics were improved by using a counting time of 600 seconds for each reflexion. The use of a small crystal reduced X-ray absorption by the specimen and also helped to improve counting statistics.

### 5.3.6 Inhomogeneous X-Ray Beam

Using a graphite monochromator placed between the X-ray tube and sample can cause the incident beam to become inhomogeneous. Hope (1975) found that this effect could be minimized by using a crystal specimen less than 0.4 mm in diameter. The specimen used was 0.34 mm in diameter.

With all these possible sources of error minimized the intensities of a number of Friedel pairs of reflexions produced by a natural single crystal of magnetite were measured. If magnetite does lack a centre of symmetry then the intensities of each member of a Friedel pair should not be equal.

#### 5.4 Data Collection

For consistency, the same spherical crystal specimen (specimen BMDM11), used for the structure refinement described in the previous chapter, was used in the study of anomalous scattering. Integrated X-ray intensities were collected from the crystal at room temperature, using the CAD-4 diffractometer. Structure factor calculations predicted that, for  $\text{MoK}\alpha$  radiation, 13 pairs of Friedel related reflexions have differences in intensity between each member of the pair that are large enough to be detected. This is a far greater number showing such a difference than arises for any other commonly used radiation. If magnetite is non-centrosymmetrical, then in the presence of anomalous scattering these 13 pairs of reflexions become 26 unique reflexions, since  $I_{hkl}$  is no longer equal to  $I_{\bar{h}\bar{k}\bar{l}}$ .  $\text{MoK}\alpha$  radiation which had been monochromatized after reflexion by pyrolytic graphite was therefore chosen. The X-ray tube was operated at a voltage of 40 kV and a current of 20 mA.

Normally, for a cubic mineral which is non-centrosymmetrical, in a complete sphere of reciprocal space the general reflexion  $hkl$  contains 48 equivalents. In the presence of anomalous scattering, these divide into 2 groups, each group containing 24 Laue-equivalents. The first group corresponds to the  $hkl$  reflexion and the second to  $\bar{h}\bar{k}\bar{l}$ . For

reflexions of the type  $\{hhl\}$ , which normally contain 24 equivalents, in the presence of anomalous scattering, we get 2 groups, each containing 12 Laue-equivalents. The first group corresponds to  $hhl$  and the second to  $\bar{h}\bar{h}\bar{l}$ .

All of the Laue-equivalents for each of the 26 reflexions were measured using a scan time of 600 seconds for each reflexion, this gave a total of 480 intensities. These intensities were then collected into 26 groups, each group containing all the Laue-equivalents for that particular reflexion. Because all 26 reflexions were extremely weak, a number of reflexions within these groups were found to be below threshold; these data consisted of 27% of the data set and were rejected. In addition, for several groups a small number of reflexions within a group were found to have intensities inconsistent with those of the rest of the group. These inconsistencies appear to be due to poor counting statistics, despite the long scan time used. In order to obtain a data set of the extremely high quality needed, it was necessary to use an averaging process for the groups of reflexions found to exhibit these inconsistencies. The following procedure was adopted: the range of observed relative intensities within a group was divided up into a number of intensity intervals and a histogram plotted with the frequency of intensity against the interval as the y and x-axes respectively. Typical histograms produced in this analysis are shown in figure 5.5. As can be seen from these four histograms, the results of the analysis gave an intensity variation within a group which is approximately Gaussian, despite the small number of reflexions used in each case. Integrated intensities for the calculations were taken to be the mean of the intensities enveloped by the Gaussian curve. Any reflexions lying outside this curve (those in figure 5.5 not shaded) were rejected. Use

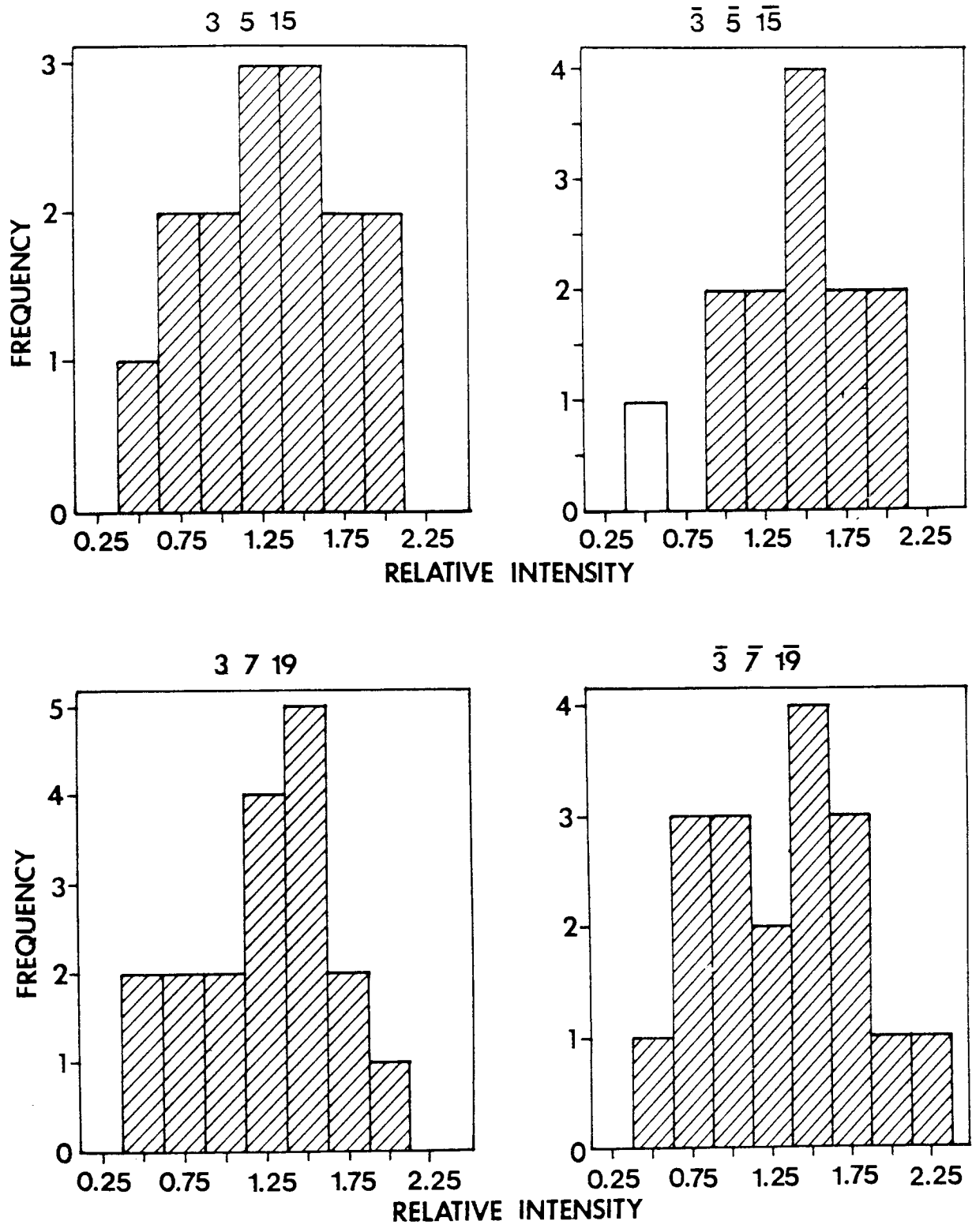


Figure 5.5 Histograms for two Friedel pairs of reflections showing the intensity distribution of the Laue-equivalents for each member of the pair.

of this criterion led to the rejection of 2% of the observed intensity data.

## 5.5 Results and Discussion

Observed and calculated structure factors for all 26 reflexions, along with the number of Laue-equivalents used to calculate the observed intensity in each case, are shown in table 5.1. These structure factors were calculated using the atom positions and temperature factors found in the  $F\bar{4}3m$  structure refinement reported in the previous chapter. The calculations were performed using the data reduction program DATRDN, the atom loading program LOADAT, and the program FC to calculate structure factors, all from X-RAY 74.

These 26 reflexions were all weak with structure factors less than 5.0, despite using a counting time of 600 seconds they still suffer considerably from statistical errors. Nevertheless, table 5.1 shows that agreement between observed and calculated structure factors for all 26 is really quite good. In fact, the R-factor of 18.6% is only slightly worse than that of 14.8% obtained for the 76 reflexions with structure factors less than 10.0 reported in the previous chapter. Agreement between observed and calculated structure factors as to which member of the Friedel pair, either  $F_{hkl}$  or  $F_{\bar{h}\bar{k}\bar{l}}$ , has the larger structure factor is correct in 11 out of 13 cases. Ideally we would expect agreement for all 13 pairs but considering that the reflexions are all very weak, the results are still very satisfactory. Of the two pairs of reflexions which disagree, the 9 11 11 pair have observed structure factors which are so close, that their relative magnitudes could be reversed within experimental error.

Table 5.1 Structure factors for Friedel pairs of reflexions.

h	k	l	Number of Equivalents	$F_o$	$F_c$
1	1	15	12	4.12	4.13
$\bar{1}$	$\bar{1}$	$\bar{15}$	12	3.70	3.09
1	3	19	19	2.97	2.80
$\bar{1}$	$\bar{3}$	$\bar{19}$	16	3.15	4.11
1	5	19	11	3.26	3.55
$\bar{1}$	$\bar{5}$	$\bar{19}$	13	3.03	2.69
1	7	15	24	2.99	2.12
$\bar{1}$	$\bar{7}$	$\bar{15}$	16	3.54	3.93
1	11	11	12	3.16	2.01
$\bar{1}$	$\bar{11}$	$\bar{11}$	9	3.76	3.92
3	3	15	6	3.91	4.00
$\bar{3}$	$\bar{3}$	$\bar{15}$	12	2.96	2.07
3	5	15	15	3.48	2.69
$\bar{3}$	$\bar{5}$	$\bar{15}$	12	3.75	3.77
3	7	11	14	3.59	4.41
$\bar{3}$	$\bar{7}$	$\bar{11}$	15	3.43	2.64
3	7	19	18	2.93	4.52
$\bar{3}$	$\bar{7}$	$\bar{19}$	18	3.08	3.02
5	7	11	15	3.85	3.86
$\bar{5}$	$\bar{7}$	$\bar{11}$	15	3.93	4.72
7	7	15	8	3.37	4.50
$\bar{7}$	$\bar{7}$	$\bar{15}$	8	2.93	2.46
7	11	11	9	3.44	4.46
$\bar{7}$	$\bar{11}$	$\bar{11}$	8	3.41	2.19
9	11	11	12	2.77	2.35
$\bar{9}$	$\bar{11}$	$\bar{11}$	12	2.73	3.34

If magnetite does possess a centre of symmetry, then the values of observed structure factors for each Friedel pair should be equal, at least within experimental error. Table 5.1 shows that this is not the case, the difference in intensity between each member of a pair is far greater than could be explained by experimental error. The results obtained therefore support the idea that the crystal structure of magnetite is non-centrosymmetrical since there are significant differences in intensity between Friedel pairs; a result which is only possible in a non-centrosymmetrical material. The results found here, along with those of the last chapter, strongly support the idea that the space group of magnetite is  $F\bar{4}3m$ .

## CHAPTER 6

### THE CRYSTAL STRUCTURE OF TITANOMAGHEMITE SPECIMEN BML929,1687

#### 6.1 Review of Publications Relating to the Symmetry of Maghemite

The fact that  $\gamma\text{-Fe}_2\text{O}_3$  is a polymorph of  $\text{Fe}_2\text{O}_3$  was realized by Sosman and Posnjak (1925). In this paper they described a number of ways of preparing  $\gamma\text{-Fe}_2\text{O}_3$  and were the first to record its occurrence as a mineral, in a specimen taken from a gossan deposit at Iron Mountain, Shasta County, California. Sosman and Posnjak (1925) also studied the physical properties exhibited by this mineral and noted that the X-ray powder diffraction patterns it produces are practically identical to those of magnetite. The name maghemite was suggested by Wagner (1927) for naturally occurring  $\gamma\text{-Fe}_2\text{O}_3$ .

Welo and Baudisch (1925) found that they were able to completely oxidize magnetite at  $200^\circ\text{C}$  without any change in magnetic properties. An examination of the X-ray powder diffraction pattern of the oxide revealed that a chemical change had occurred but no change in structure. On further heating, the oxide was found to retain its magnetic properties until  $550^\circ\text{C}$  where a transformation took place and the structure reverted to that of  $\alpha\text{-Fe}_2\text{O}_3$ . The idea was put forward that the unit cell of maghemite is similar to that of magnetite but with four additional oxygen anions. This suggestion was investigated in greater detail by Thewlis (1931) who used X-ray intensity measurements, atomic dimensions and rules of coordination to determine the symmetry of maghemite. Only two space groups were found to agree with the measured

X-ray intensities. Thewlis (1931) was unable to distinguish between the two because both gave the same calculated intensities. It was concluded that the space group of  $\gamma$ -Fe<sub>2</sub>O<sub>3</sub> was either the enantiomorphous pair P4<sub>1</sub>32-P4<sub>3</sub>32 or P2<sub>1</sub>3 and that the iron and oxygen ions occupy the same sites as in magnetite but that there are four additional oxygen ions in the structure. It was pointed out by Verwey (1935a,b) that the measured density of  $\gamma$ -Fe<sub>2</sub>O<sub>3</sub> is in good agreement with a unit cell containing 32 oxygen ions and that the addition of four extra oxygens is contradictory to all previous crystallographic results found for similar structures.

Hägg (1935a,b), Kordes (1935) and Verwey (1935a,b) independently proposed that maghemite is an iron-deficient spinel with the chemical formula Fe<sub>21.33</sub>O<sub>32</sub>. Hägg (1935b) concluded from X-ray intensities that the cation vacancies were randomly distributed over the octahedral sites and that the structural formula is Fe<sup>3+</sup>[Fe<sup>3+</sup><sub>1.67</sub>□<sub>0.33</sub>]<sub>4</sub>O<sub>4</sub><sup>2-</sup>, where □ indicates a cation vacancy. The unit cell is found by multiplying the above formula by eight since each cell contains eight molecules. The new structure was found to agree well with both X-ray data and the physical properties exhibited by maghemite.

An X-ray powder diffraction study of ordered LiFe<sub>5</sub>O<sub>8</sub> made by Braun (1952) revealed that this compound is primitive cubic with space group P4<sub>1</sub>32(or P4<sub>3</sub>32) and that the structure is that of a spinel but with cation vacancies. This alternative space group, apart from small changes in atom position, corresponds to that normally assumed for the spinel structure, but with a special arrangement of iron and lithium ions on octahedral sites. Braun (1952) proposed an ordered arrangement of lithium and iron atoms in the ratio of 1:3 over octahedral sites. The 16 octahedral sites are occupied by 4 lithium and 12 iron atoms in such a way that each lithium atom is surrounded by 6 iron atoms in a deformed

octahedron and each iron atom is surrounded by 4 iron and 2 lithium atoms. Braun (1952) also noted that samples of  $\gamma$ -Fe<sub>2</sub>O<sub>3</sub> give a very similar powder diffraction pattern to that of LiFe<sub>5</sub>O<sub>8</sub>. To account for this he suggested that the iron and the vacancies on octahedral sites are arranged in a similar manner to the iron and lithium atoms in LiFe<sub>5</sub>O<sub>8</sub>. The proposed unit cell for  $\gamma$ -Fe<sub>2</sub>O<sub>3</sub> is Fe<sub>8</sub>[Fe<sub>13.33</sub>□<sub>2.67</sub>]<sub>32</sub>O<sub>32</sub> (Hägg, 1935b) with the ratio of vacancies to iron atoms being 1:5. Braun (1952) realized that the ideal ratio of 1:3 would occur if water molecules were incorporated into the structure giving the composition Fe<sub>8</sub>[Fe<sub>12</sub>H<sub>4</sub>]<sub>32</sub>O<sub>32</sub> and also noted that his specimens did contain some water but did not give details of the amount.

A detailed study carried out by David and Welch (1956) showed  $\gamma$ -Fe<sub>2</sub>O<sub>3</sub> could not be prepared by oxidation of Fe<sub>3</sub>O<sub>4</sub> without the presence of a small percentage of water. From this observation they concluded that water forms part of the structure. They suggested that this water is present in the structure in the form of hydroxyl ions and proposed the formula Fe<sub>8</sub>[Fe<sub>12</sub>□<sub>4</sub>](OH)<sub>4</sub>O<sub>28</sub> for  $\gamma$ -Fe<sub>2</sub>O<sub>3</sub>.

Henry and Boehm (1956) used a sample motion ballistic method to determine the magnetic moment of  $\gamma$ -Fe<sub>2</sub>O<sub>3</sub>. A moment of 1.18(2) $\mu_{\beta}$  ( $\mu_{\beta}$ =Bohr magneton) per atom of iron was found in comparison with the value of 1.19 $\mu_{\beta}$  predicted if the vacancies were restricted to octahedral sites. A value of 1.66 $\mu_{\beta}$  is predicted from theory if the vacancies are distributed randomly over tetrahedral and octahedral sites. These results disagree with Braun's formula given above since a value of 1.0 $\mu_{\beta}$  per atom of iron would be expected if his formula were correct. The formula given by Braun (1952) was supported to some extent by Davey and Scott (1957) who found that their samples contained 3 to 4wt% water

which is in reasonable agreement with the value of 2.21wt% predicted by Braun's formula.

A maghemite prepared by van Oosterhout and Rooijmans (1958) was found to be tetragonal and contained less than 0.5wt% water. The unit cell was found to be based on that of spinel but contained 32 molecules of  $\text{Fe}_2\text{O}_3$ , the ratio  $c/a = 3$ , and the space group is  $P4_1$  (or  $P4_3$ ) which is a sub-group of  $P4_132$  (or  $P4_332$ ). If we take the unit cell proposed by Braun (1952) to be  $\text{Fe}_8[(\text{Fe}_{1.33} \square_{2.67})\text{Fe}_{12}]_{32}\text{O}_{32}$ , then this is trebled in the tetragonal case and the  $3 \times 1.33 = 4$  iron atoms and  $3 \times 2.67 = 8$  vacancies are ordered on the  $3 \times 4 = 12$  available octahedral sites. van Oosterhout and Rooijmans (1958) expected to produce a verification of their proposed structure but this was never published.

Strickler and Roy (1961) attempted to confirm Braun's formula,  $\text{HFe}_5\text{O}_8$ , for maghemite but found their results were inconclusive. The problem was approached in two ways: firstly they studied the weight loss of their samples with increase in temperature, and secondly attempted to prepare  $\text{HFe}_5\text{O}_8$  under high water pressure and at low temperature. Neither technique allowed unquestionable confirmation of Braun's formula. They came to the conclusion that if maghemite does contain 2.21wt% water, even after removal of that water the structure and magnetic properties remain unaltered.

A great deal of confusion seems to exist as to whether synthetic  $\gamma\text{-Fe}_2\text{O}_3$  contains water molecules in the structure. It appears that water helps in the formation of maghemite but it seems to serve only as a catalyst. Colombo et al. (1964, 1965) for example were able to oxidize magnetite to maghemite without the presence of water.

The intensity ratio of the  $400$  reflexion to that of  $440$  was examined by Ferguson and Hass (1958) in a neutron diffraction study of

$\gamma$ -Fe<sub>2</sub>O<sub>3</sub>. If the cation vacancies are distributed randomly this ratio is 0.482, for vacancies on tetrahedral sites only it is 0.580 and for vacancies restricted to octahedral sites 0.433. A ratio of 0.443 was observed indicating that the cation vacancies are largely restricted to octahedral sites.

X-ray and neutron diffraction was employed by Ueda and Hasegawa (1962) in a further attempt to determine the vacancy distribution of maghemite. Intensity calculations were performed to estimate the effect of various vacancy distributions on the diffracted intensities. Cation vacancies were found to be restricted to octahedral sites but in a manner leading to P2<sub>1</sub>3 symmetry.

Armstrong, Morrish and Sawatzky (1966) carried out a Mössbauer study of  $\gamma$ -Fe<sub>2</sub>O<sub>3</sub> in applied magnetic fields. This allowed a direct determination of the vacancy distribution since the relative numbers of iron atoms on the tetrahedral and octahedral sites can be obtained by a direct comparison of the intensity ratio of Lorentzian curves produced by each site. An average intensity ratio of tetrahedral to octahedral sites of 0.62(5) was found. A value of 0.33 is expected if the vacancies are entirely located on tetrahedral sites and 0.60 for octahedral vacancies. They concluded that the vacancies are restricted to octahedral sites.

Takei and Chiba (1966) made an X-ray diffraction study of single crystal films of  $\gamma$ -Fe<sub>2</sub>O<sub>3</sub> epitaxially grown onto MgO and found no evidence of vacancy ordering. They found a net magnetic moment per iron atom of  $1.45\mu_{\beta}$ , a value of  $1.66\mu_{\beta}$  is predicted by Henry and Boehm (1956) for a maghemite containing a random distribution of vacancies on tetrahedral and octahedral sites. This measured magnetic moment suggests

that 20% of the cation vacancies occur on tetrahedral sites and the remaining 80% are on octahedral sites.

High purity magnetite was reacted with sulphur by Kullerud and Donnay (1967) who found that iron was removed from the magnetite to form stoichiometric pyrite and an iron-deficient magnetite. An X-ray diffraction study of the iron-deficient magnetite showed that the cell parameter remains unchanged and that approximately 50% of the cation vacancies occur on tetrahedral sites. Kullerud, Donnay and Donnay (1968, 1969) proposed that natural maghemites are omission solid solutions between magnetite and two end-members; one with all vacancies on tetrahedral sites which they named 'kenotetrahedral magnetite'; and a second with vacancies restricted to octahedral sites which they called a 'kenooctahedral magnetite'. A Mössbauer study of the vacancy distribution of a kenotetrahedral magnetite was made by Weber and Hafner (1971). Here the intensity ratio of the two magnetic hyperfine patterns were examined and they concluded that the vacancies were statistically distributed over tetrahedral and octahedral sites with a ratio of 1:2 respectively.

Haul and Schoon (1939) carried out an X-ray powder diffraction study of a number of synthetic maghemites and observed reflexions forbidden by the space group  $Fd\bar{3}m$  normally assigned to the spinels. These additional reflexions were thought to be due to ordering of the cation vacancies on octahedral sites leading to an alternative symmetry from that previously assumed.

Four different maghemites were prepared by Bernal, Dasgupta and Mackay (1959); one with the spinel structure; one which was tetragonal with  $c/a = 3$ ; one which was primitive cubic with space group  $P4_132$  (or  $P4_332$ ); and a fourth which was also primitive cubic but showed reflexions such as  $002$  and  $006$  not permitted by  $P4_132$  (or  $P4_332$ ).

Table 6.1 Cell parameters and space groups reported for a number of natural and synthetic maghemites

Cell Parameter (Å)	Crystal System	Space Group	Natural or Synthetic	Reference
8.30	Cubic	Fd3m	S	Welo and Baudisch (1925)
8.40	Cubic	$P4_132(P4_332)$ or $P2_13$	S	Thewlis (1931)
8.339	Cubic	Fd3m <sup>1</sup>	S	Hägg (1935b)
8.32	Cubic		N	Newhouse and Glass (1936)
8.343	Cubic		N	Newhouse and Glass (1936)
8.333	Cubic		S	Haul and Schoon (1939)
8.342	Cubic		S	Mason (1943)
8.337	Cubic		N	Mason (1943)
8.33	Cubic	$P4_132(P4_332)$	S	Braun (1952)
8.348	Cubic		S	David and Welch (1956)
8.35	Cubic		S	Davey and Scott (1957)
8.322	Tetragonal		S	Behar and Collongues (1957)
8.33	Tetragonal	$P4_1(P4_3)$	S	van Oosterhout and Rooijmans (1958)
8.34	Tetragonal	$P4_1(P4_3)$	S	Rooksby (1961)
8.320	Cubic		S	Ueda and Hasegawa (1962)
8.33	Tetragonal	$P4_1(P4_3)$	S	Schrader and Büttner (1963)
8.35	Cubic		S	Takei and Chiba (1966)
8.39	Cubic	$P4_132(P4_332)$	N	Smith (1979)

Natural maghemite was studied by Smith (1979) using electron diffraction. The structure was found to be similar to that of ordered lithium ferrite with the vacancies taking the place of the lithium atoms, the space group was found to be given by the enantiomorphous pair  $P4_132-P4_332$ .

A range of values have been reported for the unit cell parameter of maghemite; this variation seems to arise because much of the material under examination was not adequately characterized chemically. A list of some reported cell parameters for maghemite along with the reported space group is given in table 6.1. A continuous solid solution series exists between magnetite and maghemite so many of the higher cell parameters reported are probably due to the samples containing some  $Fe_3O_4$ . A realistic cell parameter for pure end-member maghemite seems to be somewhere between 8.330 and 8.340 Å.

An extensive search through the existing literature has revealed that no previous attempts have been made to determine the space group of a natural or synthetic titanomaghemite specimen. The purpose of the work reported in this chapter is to carry out such a determination using a combination of Mössbauer spectroscopy, X-ray diffraction and electron microprobe analysis.

## 6.2 Mössbauer Spectrum of Maghemite

Bauminger et al. (1961) and Kelly et al. (1961) made the first  $^{57}Fe$  Mössbauer studies of maghemite ( $\gamma-Fe_2O_3$ ). They found that the sub-spectra produced by tetrahedral and octahedral sites at room temperature completely overlapped, that is, they observed a single six-peak hyperfine pattern instead of two, as would be expected if the

tetrahedral and octahedral sites were distinguishable. Similar observations have been made in other oxides containing  $\text{Fe}^{3+}$  ions. This overlap arises primarily because the  $\text{Fe}^{3+}$  ion is relatively insensitive to its environment and therefore exhibits similar splittings whether in tetrahedral or octahedral coordination.

Armstrong, Morrish and Sawatzky (1966) found that it is possible to separate the two sub-lattice contributions by the application of an external magnetic field, thereby allowing unambiguous assignment of the patterns to each site. Cations on tetrahedral and octahedral sites were found to align parallel and antiparallel respectively to the applied field. The resulting two fields differ in magnitude and therefore become distinguishable.

The site occupancies of a magnetite specimen may be determined from the areas of the sub-spectra produced by iron atoms on each of the two sites, provided the absorber is thin, the temperature low and the recoil free fractions of tetrahedral and octahedral sites equal. This latter assumption was investigated by Sawatzky, van der Woude and Morrish (1969) who studied the recoil free fraction of iron in tetrahedral and octahedral sites in the spinel structure. They made a comparison of the relative areas of the respective sub-spectra and found a ratio of recoil free fraction for tetrahedral to that of octahedral sites equal to 0.94(2) at room temperature and 0.99(1) at 0 K. Sawatzky et al. (1969) concluded that the site populations could not be simply determined at room temperature but at liquid helium temperatures the recoil free fractions of tetrahedral and octahedral sites were approximately equal. This result means that a comparison of the relative areas of the sub-spectra from tetrahedral and octahedral sites gives a good estimate of the respective site occupancies.

It is the aim of this Mössbauer study to use maghemite specimens M1 and M2, which are essentially end-members, to obtain values for the relative areas of the spectra produced by tetrahedral and octahedral sites and then use these values to make a comparison with the areas found for titanomaghemite specimen BM1929,1687 and hence determine the cation and vacancy distribution of this latter specimen. The results obtained are then compared with those found for this specimen by single crystal X-ray diffraction.

### 6.3 Mössbauer Spectra of Maghemite Specimens M1 and M2 at Room Temperature

The room temperature Mössbauer spectra of maghemite specimens M1 and M2 can be seen in figures 6.1 and 6.2 respectively. Each spectrum consists of two superimposed six-peak hyperfine patterns, a condition which is characteristic of magnetically ordered iron in two different sites. The outer two peaks in figure 6.1 arise because of the presence of a small percentage (approximately 12%) of  $\alpha\text{-Fe}_2\text{O}_3$ . These two peaks actually form part of a six-peak hyperfine pattern due to the presence of  $\text{Fe}^{3+}$  ions on octahedral sites in  $\alpha\text{-Fe}_2\text{O}_3$ . Because of overlap with the maghemite spectrum it was not possible to fit these remaining four peaks. Attempts to fit two six-peak hyperfine patterns to the spectra for specimens M1 and M2 proved unsuccessful, mainly because the difference in splittings between the spectra from tetrahedral and octahedral sites is too small. The rather poor value for the goodness of fit of the spectrum for specimen M1 ( $\chi^2=1254$ ) arises firstly because it was not possible to fit two six-peak hyperfine spectra to the data and secondly because of the presence of the four unfitted peaks due to the

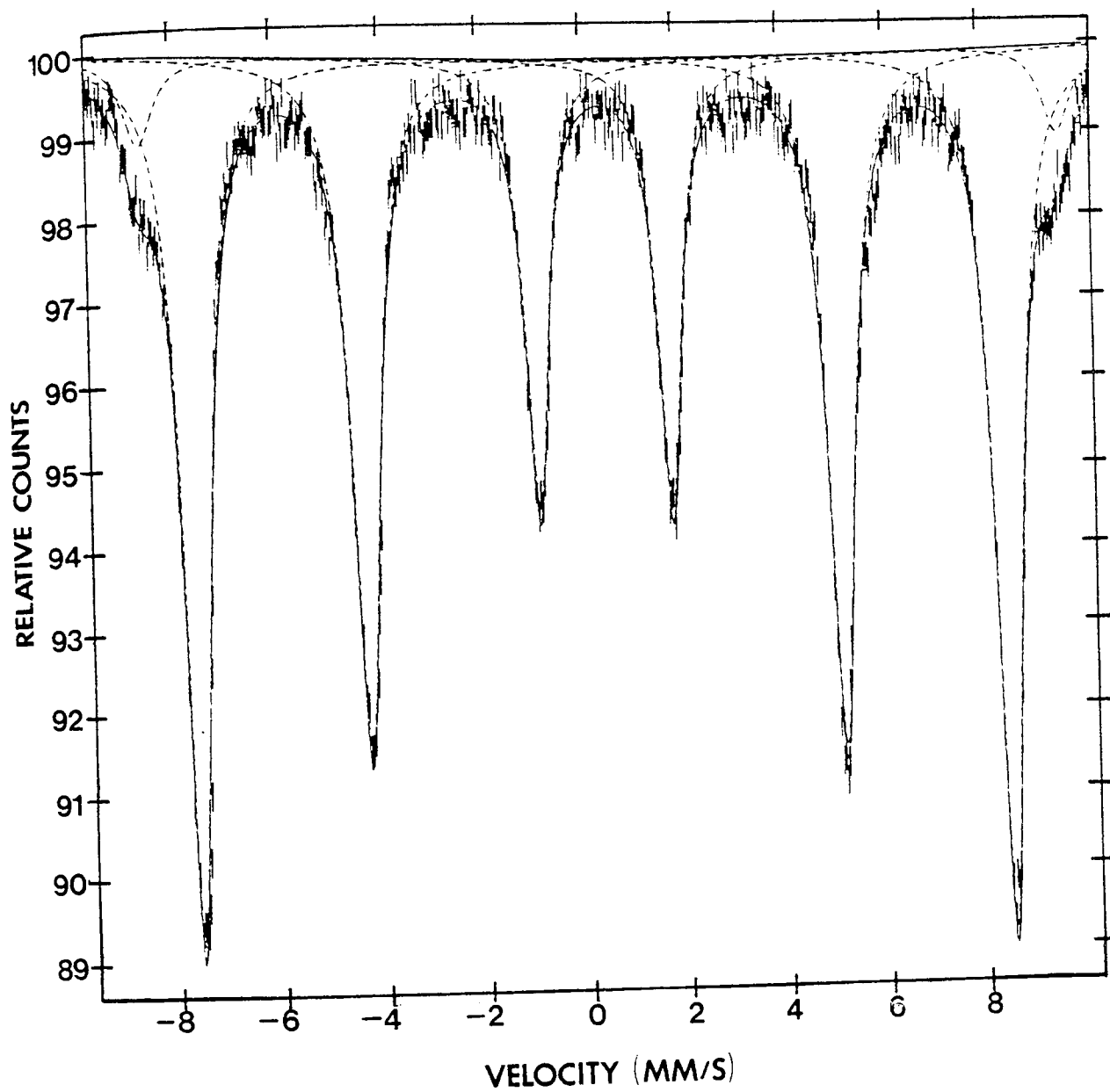


Figure 6.1 Mössbauer spectrum of maghemite specimen M1 at room temperature. The outermost doublet is due to the presence of a small percentage of  $\alpha\text{-Fe}_2\text{O}_3$ . The solid lines represent least squares fits of the data points to superimposed Lorentzian curves.

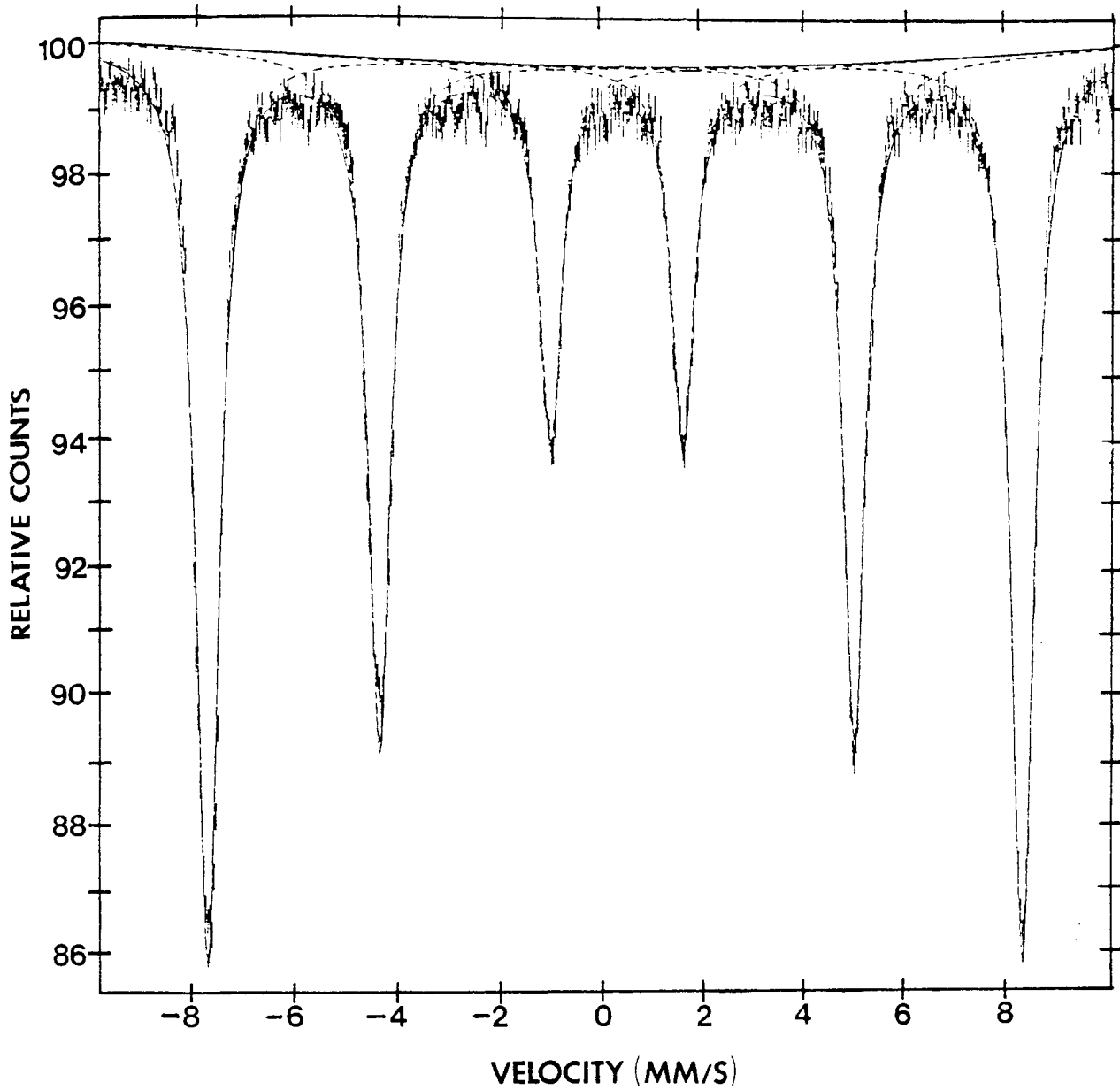


Figure 6.2 Mössbauer spectrum of maghemite specimen M2 at room temperature. The solid lines represent least squares fits of the data points to superimposed Lorentzian curves.

Table 6.2 Mössbauer parameters for maghemite specimen M1 a) at room temperature b) at 4.2 K in an applied magnetic field of 4.2 T. Isomer shifts are quoted relative to iron metal absorber.

a)

Ion	Hyperfine Field (kOe)	Quadrupole Splitting (mm/s)	Isomer Shift (mm/s)	Relative Area
Fe <sup>3+</sup> * (A and B-sites)	496.7(5)	0.001(5)	0.309(5)	100.00

b)

Ion	Hyperfine Field (kOe)	Quadrupole Splitting (mm/s)	Isomer Shift (mm/s)	Relative Area
Fe <sup>3+</sup> (A-site)	553.3(5)	0.015(5)	0.348(5)	39.53
Fe <sup>3+</sup> (B-site)	490.4(5)	-0.000(5)	0.489(5)	60.47

\* At room temperature the A and B-sites were not resolved.

Table 6.3 Mössbauer parameters for magnetite specimen M2 a) at room temperature b) at 4.2 K in an applied magnetic field of 4.2 T. Isomer shifts are quoted relative to iron metal absorber.

a)

Ion	Hyperfine Field (kOe)	Quadrupole Splitting (mm/s)	Isomer Shift (mm/s)	Relative Area
Fe <sup>3+</sup> * (A and B-sites)	494.7(5)	0.003(5)	0.313(5)	100.00

b)

Ion	Hyperfine Field (kOe)	Quadrupole Splitting (mm/s)	Isomer Shift (mm/s)	Relative Area
Fe <sup>3+</sup> (A-site)	553.7(5)	0.003(5)	0.356(5)	39.43
Fe <sup>3+</sup> (B-site)	490.6(5)	0.002(5)	0.487(5)	60.57

\* At room temperature the A and B-sites were not resolved.

$\alpha$ -Fe<sub>2</sub>O<sub>3</sub> impurity. The goodness of fit ( $\chi^2=1595$ ) for specimen M2 is again poor and also arises because it was not possible to fit individual spectra due to tetrahedral and octahedral sites to the data.

The spectra were fitted with four variable parameters, the line position, hyperfine field, isomer shift and quadrupole splitting ( $\epsilon$ ), where  $4\epsilon=(6-5)-(2-1)$ , the numbers 1,2,5 and 6 refer to line positions. The quadrupole splittings are very close to zero, a result expected for a polycrystalline ferrite. Area ratios of the lines were constrained to the theoretical values of 3:2:1 initially, when approximate areas had been found these constraints are removed. Values for the hyperfine field, quadrupole splitting and isomer shifts for each specimen are given in tables 6.2 and 6.3. All of these parameters quoted are effectively an average of the values produced by tetrahedral and octahedral sites since the individual sites are unresolved. These parameters are found to agree well with those found by previous authors (see table 6.4).

#### 6.4 Mössbauer Spectra of Maghemite Specimens M1 and M2 at 4.2 K in a Longitudinal Magnetic Field of 4.2 T

In order to resolve the sub-spectra produced by tetrahedral and octahedral sites the temperature was reduced to 4.2 K and a longitudinal magnetic field of 4.2 T applied to each specimen. These new experimental conditions cause the spectrum to split into separate Fe<sup>3+</sup> (tetrahedral site) and Fe<sup>3+</sup> (octahedral site) patterns. In a strong external magnetic field the spins of ions on tetrahedral and octahedral sites align parallel to the direction of the applied field. If all spins align

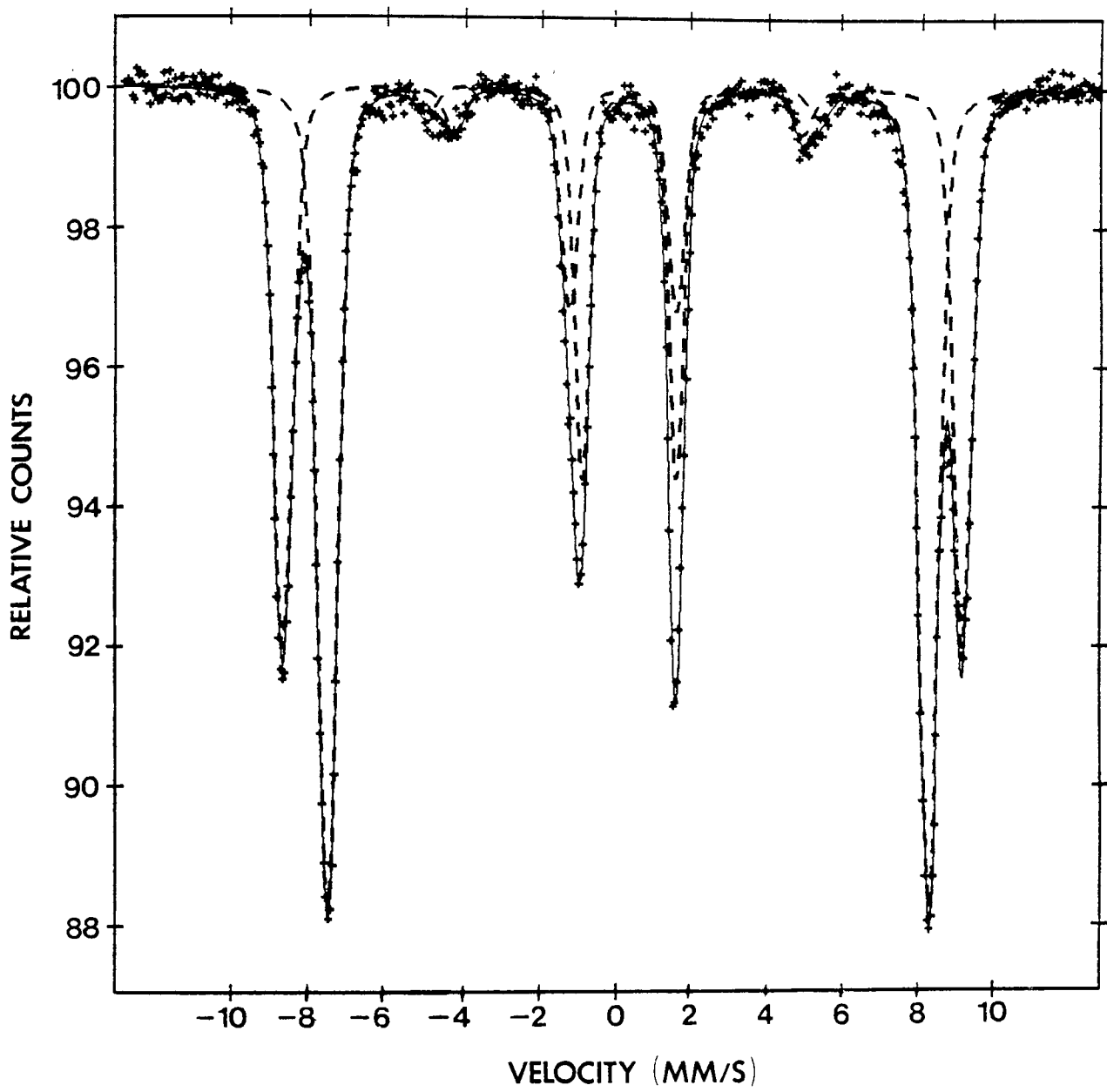


Figure 6.3 Mössbauer spectrum of maghemite specimen M1 at 4.2K in a longitudinal magnetic field of 4.2T. The solid lines represent least squares fits of the data points to superimposed Lorentzian curves.

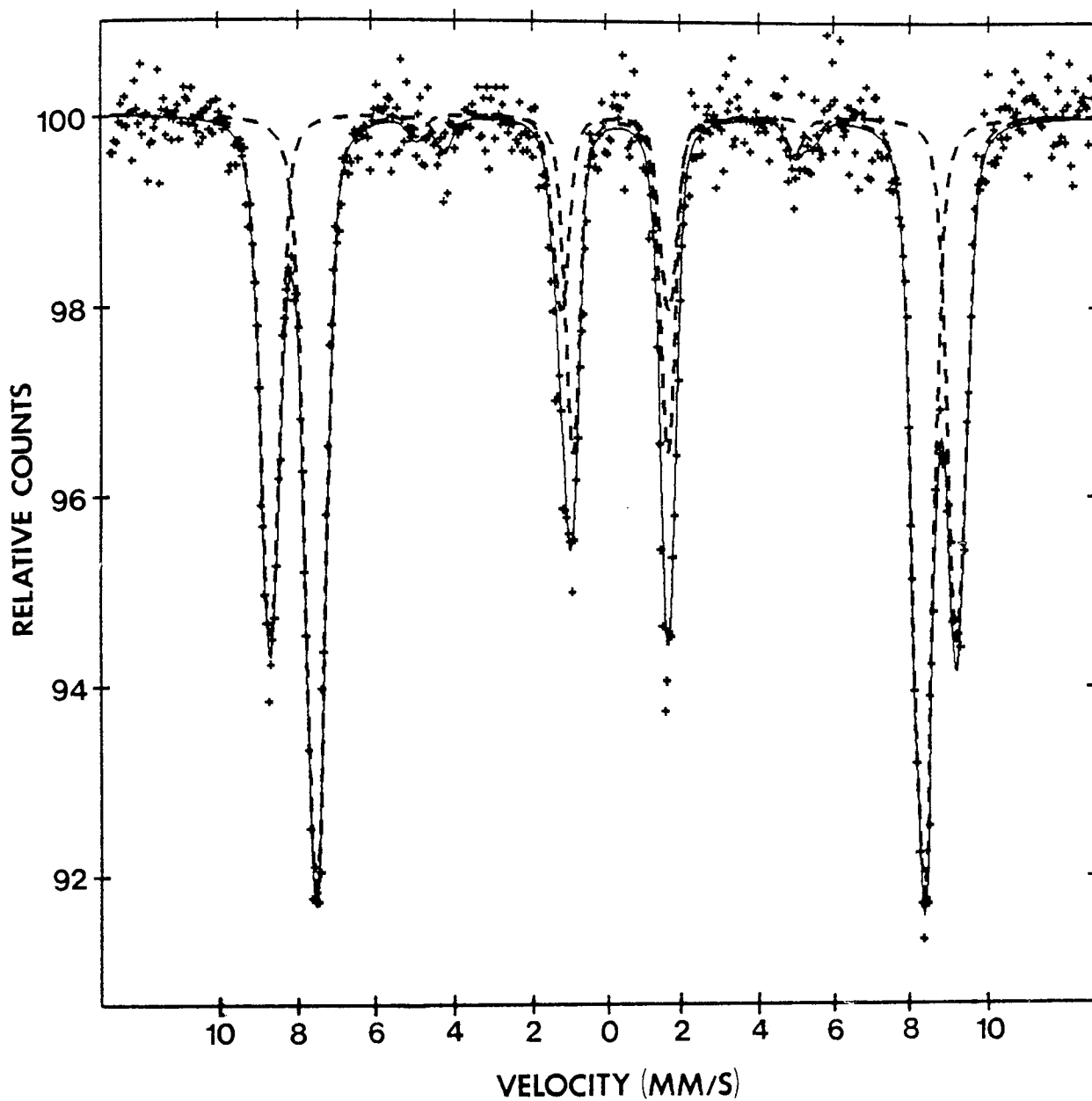


Figure 6.4 Mössbauer spectrum of maghemite specimen M2 at 4.2K in a longitudinal magnetic field of 4.2T. The solid lines represent least squares fits of the data points to superimposed Lorentzian curves.

parallel then peaks 2 and 5 of tetrahedral and octahedral site sub-spectra are absent. This effect has been observed in bulk specimens of  $\gamma$ - $\text{Fe}_2\text{O}_3$  (Coey and Khalafalia, 1972). Inspection of the spectra produced by specimens M1, M2 and BM1929,1687 in an external field (figures 6.3, 6.4, 6.5) show clearly that peaks 2 and 5 are present in all three cases, though greatly reduced in intensity. This arises because the spins of ions in the core of each specimen arrange themselves parallel to the applied field whereas those at the surface are inclined at an angle to the applied field. This effect is known as spin canting and occurs in other ferrimagnetic materials and specimens consisting of ultrafine particles (Coey and Khalafalia, 1972).

The spectra produced by specimens M1 and M2 can be seen in figures 6.3 and 6.4. Two sets of hyperfine patterns can be clearly seen indicating the presence of two magnetic substructures with ions arranged antiparallel. The six-peak hyperfine pattern due to the  $\alpha$ - $\text{Fe}_2\text{O}_3$  impurity in specimen M1 was not resolved. This additional spectrum is produced by octahedral  $\text{Fe}^{3+}$  in the  $\alpha$ - $\text{Fe}_2\text{O}_3$  and is superimposed on top of the spectrum due to octahedral  $\text{Fe}^{3+}$  in the  $\gamma$ - $\text{Fe}_2\text{O}_3$ . Because of almost complete overlap of these two spectra it was not possible to fit peaks to the  $\alpha$ - $\text{Fe}_2\text{O}_3$  spectrum. The presence of the unresolved  $\alpha$ - $\text{Fe}_2\text{O}_3$  spectrum therefore introduces an error into the value for the relative area of the spectrum produced by octahedral  $\text{Fe}^{3+}$  for maghemite specimen M1.

To fit the experimental data it was necessary to assume that each of the doublets was the sum of two Lorentzian curves superimposed on a linear background. The lines comprising each doublet were constrained to have equal halfwidths initially and then the constraints were removed. The outer lines of each spectrum are found to correspond to  $\text{Fe}^{3+}$  on tetrahedral sites and the inner to  $\text{Fe}^{3+}$  on octahedral sites. This is

Table 6.4 Mössbauer parameters found by previous authors for maghemite. The symbol A represents tetrahedral or A-sites and B octahedral or B-sites. Isomer shifts are quoted relative to iron metal absorber.

Site	Temperature (K)	Hyperfine Field (kOe)	Isomer Shift (mm/s)	Reference
A and B	300	505(20)	0.31(5)	Bauminger et al. (1961)
A and B	300	496(20)	0.32(9)	Kelly et al. (1961)
A B	300	499 505	0.35 0.46	Coey et al. (1971)
A B	4.2	488(5) 499(5)	0.36(4) 0.50(4)	Armstrong et al. (1966)

confirmed from the relative areas of these lines since a larger number of ions must occupy the octahedral sites than tetrahedral sites, regardless of the vacancy distribution. Values for the hyperfine field, quadrupole splitting and isomer shift for each specimen are shown in tables 6.2 and 6.3. Values for isomer shift are quoted relative to iron metal. The Mössbauer parameters shown in tables 6.2 and 6.3 are in good agreement with those found by previous authors (see table 6.4).

The goodness of fit ( $\chi^2=952$ ) for specimen M1 is rather high but as stated earlier this arises because of unresolved peaks due to the presence of a small percentage of  $\alpha\text{-Fe}_2\text{O}_3$ . The fit for specimen M2 ( $\chi^2=560$ ) is quite good.

The vacancy distribution of each specimen was determined from the results shown in tables 6.2 and 6.3. This was possible because the relative numbers of  $\text{Fe}^{3+}$  ions on each of the two sites is given by the ratio of the area of the line from the tetrahedral site to that from the octahedral site, assuming the recoil free fraction for each site to be equal (see section 6.2). This ratio was found to be 0.65(5) for each specimen. If all vacancies are located on octahedral sites this value would be 0.6, 0.33 for all vacancies on tetrahedral sites and 0.5 for equal numbers of vacancies on each site. The result found here suggests that within experimental error the cation vacancies in maghemite specimens M1 and M2 are restricted to octahedral sites.

## 6.5 Mössbauer Spectrum of Titanomaghemite Specimen BM1929,1687 at Room Temperature

The room temperature spectrum of titanomaghemite specimen BM1929,1687 is shown in figure 6.5. This spectrum consists of three six-peak hyperfine patterns along with two superimposed quadrupole split doublets. The first of these doublets has an isomer shift of  $1.063(5)$  mm/s and a quadrupole splitting of  $0.476(5)$  mm/s and the second an isomer shift of  $0.365(5)$  mm/s and a quadrupole splitting of  $0.360(5)$  mm/s.

Examination of a polished block of this specimen using reflected light microscopy indicates that there is an additional phase present with optical properties characteristic of ilmenite ( $\text{FeTiO}_3$ ) i.e. brownish grey in colour, exhibits weak reflection pleochroism and is strongly anisotropic. These optical properties along with the isomer shifts and quadrupole splittings found in the Mössbauer work indicate that this additional phase is in fact an intermediate member of the solid solution series  $(1-x)\text{FeTiO}_3 \cdot x\text{Fe}_2\text{O}_3$ , with a value of  $x$  lying between 0.12 and 0.21 (see table 6.5). Because the two end-members of this series, ilmenite and haematite, contain  $\text{Fe}^{2+}$  and  $\text{Fe}^{3+}$  ions respectively, this intermediate member must also contain iron in the two valence states. The former central doublet therefore corresponds to  $\text{Fe}^{2+}$  and the latter to  $\text{Fe}^{3+}$  in this additional phase.

The three hyperfine patterns are found to have isomer shifts and hyperfine fields characteristic of  $\text{Fe}^{3+}$  in tetrahedral coordination,  $\text{Fe}^{3+}$  in octahedral coordination and  $\text{Fe}^{2+}$  in octahedral coordination. Values for the Mössbauer parameters along with the relative areas of each sub-spectrum are given in table 6.6 and are found to be in good

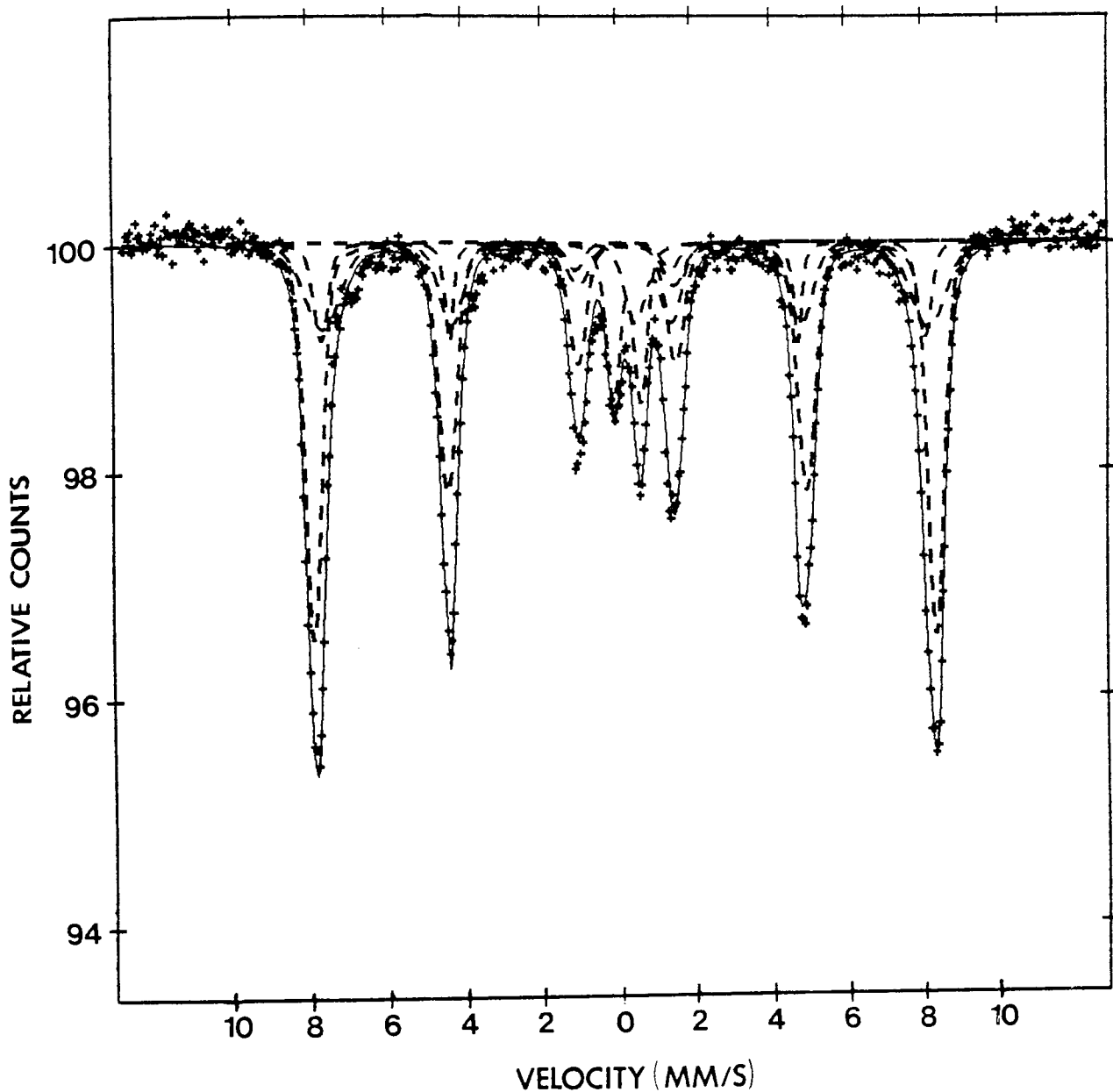


Figure 6.5 Mössbauer spectrum of titanomaghemite specimen BM1929, 1687 at room temperature. The innermost pair of doublets arise because of the presence of a small percentage of an intermediate member of the solid solution series  $(1-x)\text{FeTiO}_3-x\text{Fe}_2\text{O}_3$ . The solid lines represent least squares fits of the data points to superimposed Lorentzian curves.

Table 6.5 Mössbauer parameters for members of the solid solution series  $(1-x)\text{FeTiO}_3 \cdot x\text{Fe}_2\text{O}_3$  at room temperature. Isomer shifts are quoted relative to iron metal absorber (after Shirane et al. 1962).

x	$\text{Fe}^{3+}$		$\text{Fe}^{2+}$	
	Isomer Shift (mm/s)	Quadrupole Splitting (mm/s)	Isomer Shift (mm/s)	Quadrupole Splitting (mm/s)
1.00	0.38	0.20	-	-
0.70	0.46	0.25	-	-
0.50	0.46	0.25	1.11	0.35
0.33	0.41	0.20	1.11	0.35
0.21	0.36	0.20	1.11	0.35
0.12	0.36	0.20	1.11	0.35
0.00	-	-	1.09	0.33

Table 6.6 Mössbauer parameters for titanomaghemite specimen BM1929,1687  
a) at room temperature b) at 4.2 K in an applied magnetic field of  
4.2 T. Isomer shifts are quoted relative to iron metal absorber.

a)

Ion	Hyperfine Field (kOe)	Quadrupole Splitting (mm/s)	Isomer Shift (mm/s)	Relative Area
Fe <sup>3+</sup> (A-site)	491.2(5)	-0.003(5)	0.352(5)	25.86
Fe <sup>3+</sup> (B-site)	504.5(5)	-0.021(5)	0.338(5)	60.90
Fe <sup>2+</sup> (B-site)	489.5(5)	-0.002(5)	0.281(5)	13.25

b)

Ion	Hyperfine Field (kOe)	Quadrupole Splitting (mm/s)	Isomer Shift (mm/s)	Relative Area
Fe <sup>3+</sup> (A-site)	551.3(5)	0.012(5)	0.364(5)	40.38
Fe <sup>3+</sup> (B-site)	492.4(5)	-0.028(5)	0.514(5)	48.35
Fe <sup>2+</sup> (B-site)	433.6(5)	0.069(5)	0.406(5)	11.27

agreement with those found for maghemite specimens M1 and M2. The fitting procedure was similar to that described in section 6.3. The goodness of fit ( $\chi^2=895$ ) is rather poor but when the complexity of the spectrum is taken into account this value is quite acceptable. No peaks corresponding to tetrahedral site  $\text{Fe}^{2+}$  were observed.

#### 6.6 Mössbauer Spectrum of Titanomaghemite Specimen BM1929,1687 at 4.2 K in a Longitudinal Magnetic Field of 4.2 T

In order to improve the resolution of the tetrahedral and octahedral site sub-spectra and thus accurately determine the vacancy distribution of this specimen it was necessary to repeat the experiment at 4.2 K in a magnetic field of 4.2 T. The fitting procedure adopted has already been described in section 6.4. Mössbauer parameters obtained are given in table 6.6 and the spectra in figure 6.6. A goodness of fit ( $\chi^2$ ) of 607 was obtained which is a great improvement on the value of 895 obtained at room temperature.

An electron microprobe study of this specimen has shown it to contain 54.36wt% iron and 8.82wt% titanium (these values represent the average of 10 spot analyses). The elements Al, Ca, Cr, Mg, Mn and Si were also analysed for but not detected (see Appendix III for experimental details of this study). Unfortunately,  $^{57}\text{Fe}$  Mössbauer spectroscopy does not detect the presence of titanium. A review of existing literature reveals that the titanium is likely to occupy octahedral sites. Neutron diffraction studies, for example, made by Ishikawa et al. (1971) along with magnetic measurements (O'Reilly and Banerjee, 1965; Stephenson, 1969) indicate that  $\text{Ti}^{4+}$  always occupies octahedral sites in titanomagnetites and titanomaghemites. In addition,

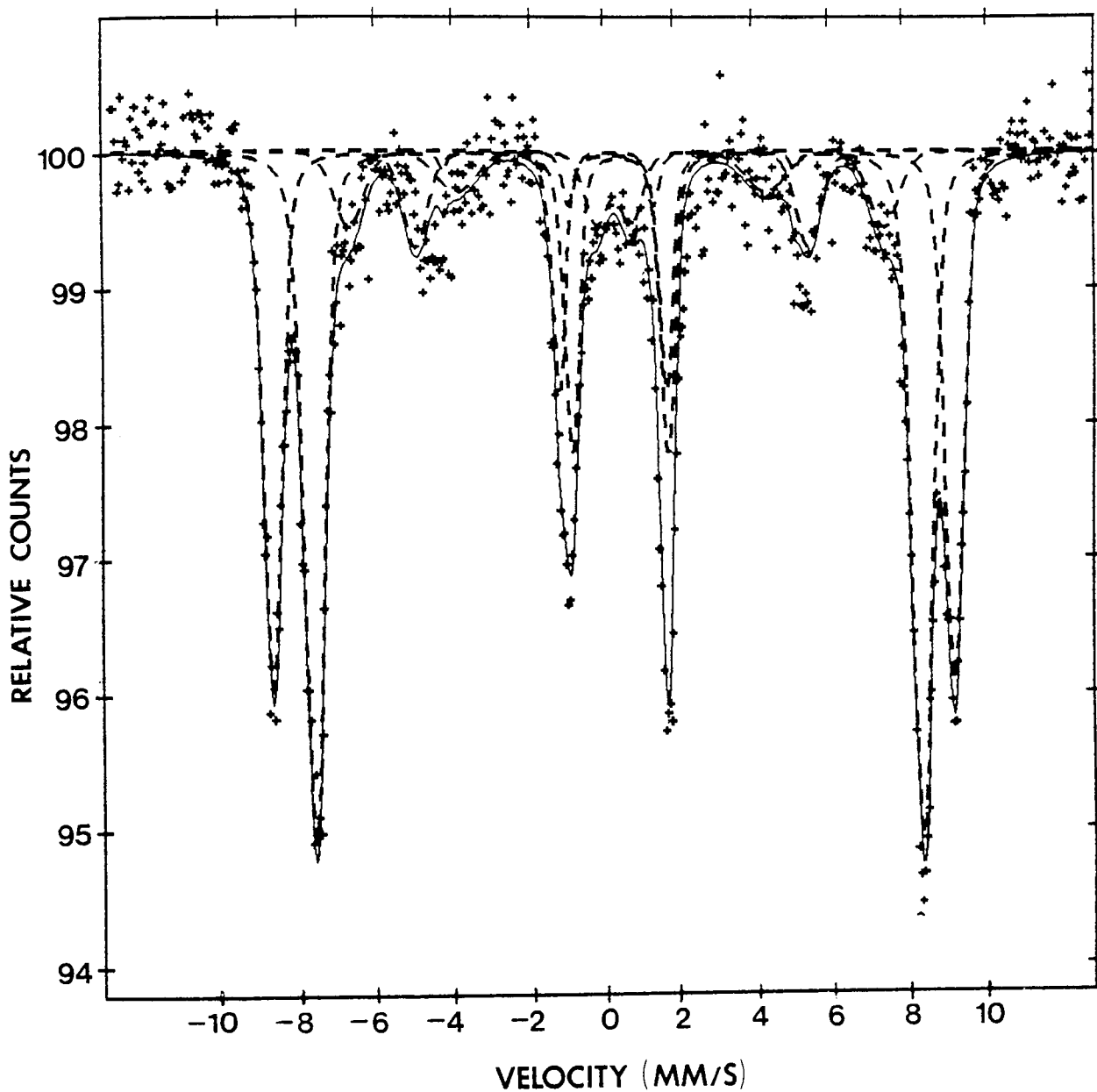


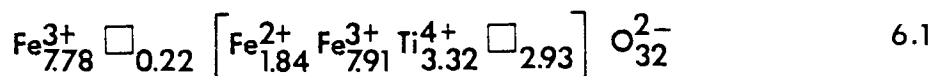
Figure 6.6 Mössbauer spectrum of titanomaghemite specimen BM1929, 1687 at 4.2K in a longitudinal magnetic field of 4.2T. The solid lines represent least squares fits of data points to superimposed Lorentzian curves.

Table 6.7 Calculation of the structural formula for titanomaghemite specimen BM1929,1687 from Mössbauer and electron microprobe data.

Oxide	wt% of oxides	Mol. prop. of oxides	Atom. prop. of oxygen from each mol.	No. of anions on basis of 32 per unit cell	No. of ions in formula
Fe <sub>2</sub> O <sub>3</sub> (Tetrahedral)	34.49	0.2160	0.6480	11.67	7.78
Fe <sub>2</sub> O <sub>3</sub> (Octahedral)	35.06	0.2195	0.6585	11.85	7.91
FeO (Octahedral)	7.36	0.1024	0.1024	1.84	1.84
TiO <sub>2</sub> (Octahedral)	14.71	0.1841	0.3682	6.63	3.32

By difference, the number of cation vacancies = 3.15

The above calculation leads to the structural formula:



where  $\square$  represents a cation vacancy.

existing models for cation distributions in titanomaghemites (see section 1.10) have suggested that all  $Ti^{4+}$  occupies octahedral sites.

Initially, it was assumed that the amount of  $Fe^{3+}$  on tetrahedral sites is the same as in end-member maghemite i.e. 24.12wt%. This is a reasonable first approximation since the relative area of the tetrahedral site spectrum for maghemite specimen M2 of 39.43, which is essentially end-member, agrees within experimental error with that of 40.38 found for this titanomaghemite specimen. The remaining octahedral site iron (30.24wt%) found in the microprobe study was then divided up in the ratio 48.35:11.27, a ratio given by the relative areas of the sub-spectra produced by  $Fe^{3+}$  and  $Fe^{2+}$  on octahedral sites. The concentration of octahedral  $Fe_2O_3$  and FeO could then be determined. The amount of  $TiO_2$  was taken directly from the microprobe data. The results obtained have been tabulated and are shown in table 6.7. Using these results and the procedure described by Deer, Howie and Zussman (1966, p515) the structural formula of titanomaghemite specimen BM1929,1687 was calculated, details of this calculation are shown in table 6.7.

In order to see if this titanomaghemite does conform to  $P4_332$  symmetry, to confirm the presence of cation vacancies on tetrahedral sites, and to determine the distribution of cations and cation vacancies over the two octahedral sites, it was necessary to carry out a detailed examination of this specimen using single crystal X-ray diffraction.

## 6.7 Data Collection

The titanomaghemite crystal chosen for the present investigation was a fragment taken from British Museum specimen BM1929,1687, which was ground into a sphere using the procedure described in Appendix II. A

preliminary examination, made using the CAD-4 diffractometer, indicated that the Bravais lattice is primitive cubic and the reflexions observed are consistent with the space group  $P4_132$  (or  $P4_332$ ). No reflexions of the type  $\{h00\}$  with  $h=2n$ , e.g.  $002$  and  $006$  were observed and so the alternative space group  $P2_13$  was immediately ruled out. It is possible that other natural and synthetic titanomaghemites exhibit a variety of structures as was found to occur for end-member maghemite (see section 6.1), depending upon the geological history or, for synthetic material, the method of preparation.

The assumed space group ( $P4_332$ ) was then used in a crystal structure refinement of X-ray intensity data collected from this specimen. Observed and calculated structure factors were compared to see if this space group does correctly describe the symmetry of this sample. Results from the analysis were then used to determine the cation and vacancy distribution over tetrahedral and octahedral sites.

Integrated X-ray intensities were collected from this crystal, at room temperature, using the CAD-4 diffractometer and employing the  $\omega-2\theta$  scan technique. The radiation was  $\text{MoK}\alpha$  ( $\lambda=0.71069 \text{ \AA}$ ) monochromatized after reflexion by pyrolytic graphite with a monochromator angle  $\theta_m=6.05^\circ$ . The X-ray tube was operated at 40 kV and 20 mA. Least squares refinement of 25 centred reflexions gave the lattice constant for the specimen of  $8.341(1) \text{ \AA}$ , a value which is in good agreement with that found by Basta (1959) for a titanomaghemite specimen taken from the same locality.

All reflexions in one hemisphere of reciprocal space out to an angle of  $\theta=30^\circ$  were collected, using a scan time of  $20/6 \text{ deg min}^{-1}$  giving a total of 3543 non-Friedel related reflexions. Under  $P4_332$  symmetry reflexions of the type  $\{h00\}$  with  $h=4n$  are systematically

absent, these reflexions were still measured as a check to ensure they really are of zero intensity. In fact, reflexions of this type were found to be absent and were therefore rejected from the data set.

During data collection, intensity control was maintained using the reflexions  $\bar{5} \bar{1} 1$ ,  $\bar{5} \bar{3} 3$  and  $\bar{8} \bar{4} 4$ , and orientation control using  $\bar{4} \bar{4} 4$ ,  $\bar{7} \bar{1} 3$  and  $\bar{8} \bar{4} 4$ . After measuring every 200 reflexions, the diffractometer returned and measured the intensity of the three intensity control reflexions. Any fall-off in the intensity of these standards detected was then employed to correct all intensities, using linear interpolation to the control reflexions. The three orientation control reflexions were measured every 7200 seconds of X-ray exposure time and allowed the diffractometer to check the crystal orientation, and if necessary, stop data collection if the crystal was found to have moved significantly from its original position.

#### 6.8 Treatment of the X-Ray Data

It has been established that the titanomagnetite specimen is primitive cubic, this means that many of the observed intensities are crystallographically equivalent. In the measurements reported here, one complete hemisphere of reciprocal space was examined, therefore reflexions of the general form  $\{hkl\}$  contain 24 equivalents, while  $\{hk0\}$  and  $\{hhl\}$  contain 12,  $\{hh0\}$  contain 6,  $\{hhh\}$  4 and  $\{h00\}$  only 3 equivalents. The original list of 3543 observed integrated intensities could therefore be collected into groups and reduced to 197 independent reflexions by averaging the equivalents within a group.

For several of the 197 groups of independent reflexions, a small number of weaker reflexions within these groups were found to have

reflexions inconsistent with the rest of the group. These consisted of less than 1% of the data, too small a number to have any significant effect, therefore all measured intensities were included and the integrated intensity was taken to be the average intensity for each group.

### 6.9 Crystal Structure Refinement

Refinement of the structure parameters was carried out using the crystallographic least squares program CRYLSQ from X-RAY 74 (see Appendix I for details). To begin with, only reflexions with intermediate range intensities were used so that approximate values for the scale factor could be found. Initial parameters for atom positions and anisotropic temperature factors were taken from those published by Tomas, Laruelle, Dormann and Norques (1983) for ordered  $\text{LiFe}_5\text{O}_8$ . This compound is found to have the same space group and a very similar arrangement of atoms to that of maghemite (Braun, 1952).

The least squares refinement gave a small extinction correction (or g-factor) of  $0.03(1) \times 10^3$ . This result indicates that the arrangement of the mosaic blocks within the crystal is such as to approach that of the ideally imperfect crystal as described by Zachariasen (1967). The averaged intensities were then corrected for secondary extinction using the above g-factor.

As with the refinement of the structure of magnetite, it was necessary to employ a weighting scheme which downweights low-angle and strong reflexions but allows more emphasis to be placed on the weak high-angle data which is more sensitive to atom positions. The weighting

scheme used is described in Appendix I, the parameter Z used in the equations was set equal to 100.0 for the refinement reported here.

Atomic scattering factors for  $\text{Fe}^{2+}$ ,  $\text{Fe}^{3+}$  and  $\text{Ti}^{4+}$  ions were taken from the International Tables for X-Ray Crystallography Vol.IV and those for  $\text{O}^{2-}$  from Tokonami (1965). Real and imaginary parts of the dispersion correction were taken from the International Tables for X-Ray Crystallography Vol.IV. Absorption corrections applied were those given by Weber (1969) for spherical crystals. The value of  $\mu_R=2.3$ .

Least squares refinements were repeated until optimized values had been found for scale, the 7 atom positions and 16 temperature factors.

#### 6.10 Results and Discussion

Under  $P4_32$  symmetry, two separate octahedral sites exist, these are represented in table 6.8 by the symbols Fe(1) and Fe(3), with positions 12(d) and 4(b) respectively. The presence of three different types of cations ( $\text{Fe}^{2+}$ ,  $\text{Fe}^{3+}$  and  $\text{Ti}^{4+}$ ) and cation vacancies on the two unique octahedral sites, along with the similarity in scattering factors for the three ions meant that it was impossible to determine the precise distribution of individual cations between these two octahedral sites.

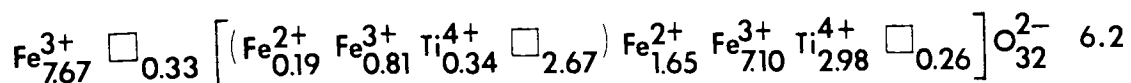
In order to simplify this problem it was necessary to make several assumptions, this will introduce errors into the argument but unless some form of simplification is made the problem becomes insoluble using simple techniques. The precise distribution of individual cations on each of the two octahedral sites has no real bearing on the problem since we are concerned primarily with the overall symmetry of the specimen and to some extent the vacancy distribution. The average cation distribution is therefore sufficient for present purposes.

Table 6.8 Atom positions for the titanomaghemite specimen according to P4<sub>3</sub>2 symmetry. The symbols x, x<sub>1</sub>, x<sub>2</sub>, x<sub>3</sub>, y and z represent the 6 positional parameters.

Ion	Position	Point Symmetry	Coordinates of Equivalent Positions
Fe(1)	12(d)	2	$\frac{1}{8}, x_1, \frac{1}{4}-x_1, \frac{3}{8}, \bar{x}_1, \frac{3}{4}-x_1, \frac{5}{8}, \frac{1}{2}-x_1, \frac{3}{4}+x_1, \frac{7}{8}, \frac{1}{2}+x_1, \frac{1}{4}+x_1,$ $\frac{1}{4}-x_1, \frac{1}{8}, x_1, \frac{3}{4}-x_1, \frac{3}{8}, \bar{x}_1, \frac{3}{4}+x_1, \frac{5}{8}, \frac{1}{2}-x_1, \frac{1}{4}+x_1, \frac{7}{8}, \frac{1}{2}+x_1,$ $x_1, \frac{1}{4}-x_1, \frac{1}{8}, \bar{x}_1, \frac{3}{4}-x_1, \frac{3}{8}, \frac{1}{2}-x_1, \frac{3}{4}+x_1, \frac{5}{8}, \frac{1}{2}+x_1, \frac{1}{4}+x_1, \frac{7}{8}.$
Fe(2)	8(c)	3	$x_2, x_2, x_2, \frac{1}{4}-x_2, \frac{1}{4}-x_2, \frac{1}{4}-x_2, \frac{1}{2}+x_2, \frac{1}{2}-x_2, \bar{x}_2, \frac{3}{4}-x_2, \frac{1}{4}+x_2, \frac{3}{4}+x_2,$ $\bar{x}_2, \frac{1}{2}+x_2, \frac{1}{2}-x_2, \frac{3}{4}+x_2, \frac{3}{4}-x_2, \frac{1}{4}+x_2, \frac{1}{2}-x_2, \bar{x}_2, \frac{1}{2}+x_2, \frac{1}{4}+x_2, \frac{3}{4}+x_2,$ $\frac{3}{4}-x_2.$
O(1)	8(c)	3	$x_3, x_3, x_3, \frac{1}{4}-x_3, \frac{1}{4}-x_3, \frac{1}{4}-x_3, \frac{1}{2}+x_3, \frac{1}{2}-x_3, \bar{x}_3, \frac{3}{4}-x_3, \frac{1}{4}+x_3, \frac{3}{4}+x_3,$ $\bar{x}_3, \frac{1}{2}+x_3, \frac{1}{2}-x_3, \frac{3}{4}+x_3, \frac{3}{4}-x_3, \frac{1}{4}+x_3, \frac{1}{2}-x_3, \bar{x}_3, \frac{1}{2}+x_3, \frac{1}{4}+x_3, \frac{3}{4}+x_3,$ $\frac{3}{4}-x_3.$
O(2)	24(e)	1	$x, y, z, \frac{1}{2}+x, \frac{1}{2}-y, \bar{z}, \bar{x}, \frac{1}{2}+y, \frac{1}{2}-z, \frac{1}{2}-x, \bar{y}, \frac{1}{2}+z,$ $z, x, y, \frac{1}{2}+z, \frac{1}{2}-x, \bar{y}, \bar{z}, \frac{1}{2}+x, \frac{1}{2}-y, \frac{1}{2}-z, \bar{x}, \frac{1}{2}+y,$ $y, z, x, \frac{1}{2}+y, \frac{1}{2}-z, \bar{x}, \bar{y}, \frac{1}{2}+z, \frac{1}{2}-x, \frac{1}{2}-y, \bar{z}, \frac{1}{2}+x,$ $\frac{1}{4}-x, \frac{1}{4}-z, \frac{1}{4}-y, \frac{3}{4}+x, \frac{3}{4}-z, \frac{1}{4}+y,$ $\frac{1}{4}-y, \frac{1}{4}-x, \frac{1}{4}-z, \frac{3}{4}+y, \frac{3}{4}-x, \frac{1}{4}+z,$ $\frac{1}{4}-z, \frac{1}{4}-y, \frac{1}{4}-x, \frac{3}{4}+z, \frac{3}{4}-y, \frac{1}{4}+x,$ $\frac{3}{4}-x, \frac{1}{4}+z, \frac{3}{4}+y, \frac{1}{4}+x, \frac{3}{4}+z, \frac{3}{4}-y,$ $\frac{3}{4}-y, \frac{1}{4}+x, \frac{3}{4}+z, \frac{1}{4}+y, \frac{3}{4}+x, \frac{3}{4}-z,$ $\frac{3}{4}-z, \frac{1}{4}+y, \frac{3}{4}+x, \frac{1}{4}+z, \frac{3}{4}+y, \frac{3}{4}-x.$
Fe(3)	4(b)	2	$\frac{5}{8}, \frac{5}{8}, \frac{5}{8}, \frac{1}{8}, \frac{7}{8}, \frac{3}{8}, \frac{3}{8}, \frac{1}{8}, \frac{7}{8}, \frac{7}{8}, \frac{3}{8}, \frac{1}{8}.$

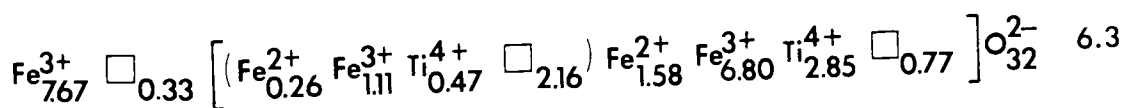
No lines corresponding to tetrahedral  $\text{Fe}^{2+}$  were observed in the Mössbauer study and the presence of  $\text{Ti}^{4+}$  on tetrahedral sites is highly unlikely (see section 6.6). Initially it was assumed that the tetrahedral sites were occupied by 8  $\text{Fe}^{3+}$  ions. The population parameter for this site was then refined and converged on a value of 0.96, indicating the presence of 4% tetrahedral vacancies, that is 7.67  $\text{Fe}^{3+}$  tetrahedral cations per unit cell, a value which is in good agreement with that of 7.78 found in the Mössbauer work. The numbers of octahedral  $\text{Fe}^{2+}$ ,  $\text{Fe}^{3+}$ ,  $\text{Ti}^{4+}$  ions and cation vacancies were taken to be 1.84, 7.91, 3.32 and 2.93 respectively (the values found in the Mössbauer and microprobe studies). As a first approximation it was assumed that 2.67 cation vacancies were present on octahedral site Fe(3). This is the number of cation vacancies present on this site in end-member maghemite and is therefore likely to be a reasonable initial value. The remaining 0.26 cation vacancies were assumed to be present on octahedral site Fe(1). Octahedral sites Fe(1) and Fe(3), when fully occupied contain 12 and 4 cations respectively. We have already assumed Fe(1) to have 0.26 and Fe(3) 2.67 sites vacant, the remaining sites must therefore be occupied by  $\text{Fe}^{2+}$ ,  $\text{Fe}^{3+}$  and  $\text{Ti}^{4+}$  ions. The 1.84  $\text{Fe}^{2+}$ , 7.91  $\text{Fe}^{3+}$  and 3.32  $\text{Ti}^{4+}$  octahedral cations found in the Mössbauer and microprobe studies were therefore divided between the octahedral sites Fe(1) and Fe(3) in the ratio 11.74:1.33, where this ratio represents the numbers of each octahedral site occupied.

The following structural formula results:



where  $\square$  represents a cation vacancy. Atomic scattering factors for each octahedral site were calculated on the basis of the above formula.

The population parameter for octahedral site Fe(3) was then refined, the results obtained indicated that the cation distribution given in the above formula underestimated the scattering produced by this site by approximately 27%. This result meant that the number of cation vacancies on site Fe(3) was less than the value of 2.67 assumed initially and the number of cations greater than the assumed value. Keeping the overall number of octahedral cations and vacancies constant (at the value found in the Mössbauer and microprobe studies), the numbers of  $\text{Fe}^{2+}$ ,  $\text{Fe}^{3+}$  and  $\text{Ti}^{4+}$  ions on octahedral site Fe(3) were increased by 27%, and those on octahedral site Fe(1) reduced by the appropriate amount, to account for the observed population parameters. The number of vacancies for sites Fe(1) and Fe(3) were found by difference. The following structural formula results:



The arrangement of cations and cation vacancies on the two octahedral sites is similar to that observed in  $\text{LiFe}_5\text{O}_8$  by Famery et al. (1979), i.e.  $(0.26\text{Fe}^{2+} + 1.11\text{Fe}^{3+} + 0.47\text{Ti}^{4+} + 2.16\square)$  and  $(1.58\text{Fe}^{2+} + 6.80\text{Fe}^{3+} + 2.85\text{Ti}^{4+} + 0.77\square)$  occupy the octahedral positions 4(b) and 12(d) in a statistical manner. No evidence of ordering of cations or cation vacancies on the octahedral sites, leading to a lower symmetry

Table 6.9 Final values for atom positions obtained for a) Titanomaghemite specimen BM1929,1687 b)  $\text{LiFe}_5\text{O}_8$  (Tomas et al. 1983) c)  $\text{LiAl}_5\text{O}_8$  (Famery et al. 1979).

a)

Atom	Position	x	y	z
Fe(1)	12(d)	0.12500	0.36623(6)	-0.11623(6)
Fe(2)	8(c)	-0.00444(6)	-0.00444(6)	-0.00444(6)
O(1)	8(c)	0.3862(3)	0.3862(3)	0.3862(3)
O(2)	24(e)	0.1179(3)	0.1304(3)	0.3837(3)
Fe(3)	4(b)	0.62500	0.62500	0.62500

b)

Atom	Position	x	y	z
Fe(1)	12(d)	0.12500	0.36735(6)	-0.11735(6)
Fe(2)	8(c)	-0.00235(7)	-0.00235(7)	-0.00235(7)
O(1)	8(c)	0.3853(3)	0.3853(3)	0.3853(3)
O(2)	24(e)	0.1166(3)	0.1284(3)	0.3839(3)
Li(1)	4(b)	0.62500	0.62500	0.62500

c)

Atom	Position	x	y	z
Al(1)	12(d)	0.1250	0.3636(1)	-0.1186(1)
Al(2)	8(c)	-0.025(1)	-0.025(1)	-0.025(1)
O(1)	8(c)	0.3859(1)	0.3859(1)	0.3859(1)
O(2)	24(e)	0.1146(1)	0.1329(1)	0.3847(1)
Li(1)	4(b)	0.6250	0.6250	0.6250

Table 6.10 Final values for anisotropic temperature factors obtained for a) Titanomagnetite specimen BM1929,1687 b)  $\text{LiFe}_5\text{O}_8$  (Tomas et al. 1983) c)  $\text{LiAl}_5\text{O}_8$  (Famery et al. 1979).

a)

Atom	$\beta_{11}$	$\beta_{22}$	$\beta_{33}$	$\beta_{12}$	$\beta_{13}$	$\beta_{23}$
Fe(1)	335(9)	200(5)	200(5)	-28(5)	-28(5)	-77(7)
Fe(2)	183(3)	183(3)	183(3)	-3(5)	-3(5)	-3(5)
O(1)	203(18)	203(18)	203(18)	36(25)	36(25)	36(25)
O(2)	225(26)	535(33)	230(28)	-40(22)	24(20)	76(35)
Fe(3)	381(14)	381(14)	381(14)	8(16)	8(16)	8(16)

b)

Atom	$\beta_{11}$	$\beta_{22}$	$\beta_{33}$	$\beta_{12}$	$\beta_{13}$	$\beta_{23}$
Fe(1)	191(14)	151(9)	151(9)	14(9)	14(9)	-43(11)
Fe(2)	146(9)	146(9)	146(9)	3(9)	3(9)	3(9)
O(1)	286(34)	286(34)	286(34)	-23(43)	-23(43)	-23(43)
O(2)	263(54)	460(54)	274(51)	-43(40)	-14(40)	43(57)
Li(1)	-	-	-	-	-	-

c)

Atom	$\beta_{11}$	$\beta_{22}$	$\beta_{33}$	$\beta_{12}$	$\beta_{13}$	$\beta_{23}$
Al(1)	182(14)	231(8)	231(8)	-30(8)	-30(8)	32(10)
Al(2)	188(2)	188(2)	188(2)	0(1)	0(1)	0(1)
O(1)	241(8)	241(8)	241(8)	12(10)	12(10)	12(10)
O(2)	249(12)	429(12)	265(10)	-26(10)	22(8)	89(12)
Li(1)	138(20)	138(20)	138(20)	-20(20)	-20(20)	-20(20)

space group was found. New atomic scattering factors for each octahedral site were then calculated on the basis of the new cation distribution predicted by the above formula. Refinement of the population parameters for each octahedral site indicated that the observed parameters agreed with those given by this above formula to within 2%. The population parameter for tetrahedral sites was found to agree within 2% of that predicted by the Mössbauer and microprobe studies.

A complete list of observed and calculated structure factors obtained for the specimen under  $P4_332$  symmetry is given in Appendix VIII. Atom positions (table 6.9) are found to be in good agreement with those found by Tomas et al. (1983) and Famery et al. (1979) for the compounds  $LiFe_5O_8$  and  $LiAl_5O_8$  respectively, which are each found to crystallize with the same space group as this particular titanomaghemite specimen. Anisotropic temperature factors for all three structures are shown in table 6.10, agreement in all three cases is good. Calculated bond lengths are shown in table 6.11.

Inspection of the R-factor breakdown (table 6.12) in terms of the observed structure factor and  $\sin \theta/\lambda$  for the refinement shows that agreement between observed and calculated structure factors for  $P4_332$  symmetry is good. Apart from the group of 43 weakest reflexions, with  $R=14.3\%$ , the R-factors for the remaining groups are all similar indicating no anomalies. These weakest reflexions are expected to give a high R-factor because they suffer considerably from counting statistics. The overall R-factor found in the analysis was 2.38%.

Table 6.11 Bond lengths calculated for titanomaghemite specimen BM1929,1687 under  $P4_32$  symmetry.

Bond	Distance ( $\text{\AA}$ )
Fe(2)-O(2)	1.8789(2)
Fe(2)-O(1)	1.9038(2)
(Tetrahedral cation to oxygen)	
Fe(1)-O(2)	1.9581(2)
Fe(1)-O(2)	2.0209(2)
Fe(1)-O(1)	2.0670(2)
(Octahedral cation to oxygen)	
Fe(3)-O(2)	2.1327(3)
(Octahedral cation to oxygen)	
O(2)-O(2)	3.0641(3)
O(2)-O(1)	3.0928(3)
O(2)-O(2)	2.8672(3)
O(2)-O(2)	2.9198(3)
O(2)-O(2)	2.9678(3)
O(1)-O(2)	2.7265(3)
O(1)-O(2)	2.8722(3)
O(1)-O(1)	2.9549(3)
O(1)-O(2)	3.0928(3)

Table 6.12 R-factor breakdown in terms of  $F_0$  and  $\sin \theta/\lambda$  for  $P4_32$  symmetry.

<u>Overall agreement factors</u>	<u>R-factors</u>
No. of observations	Without reflexions below threshold
No. of variables	With reflexion multiplicity
No. below threshold	Of reflexions below threshold
No. calculating above threshold	Of $F^2$ (without reflexions below threshold)
	0.0235
	0.0250
	0.0342
	0.0281

Results in terms of  $F_0$

$F_0$	$\Sigma F_0$	$\Sigma \Delta F$	No. of Reflexions	R	$\sin \theta/\lambda$	$\Sigma F_0$	$\Sigma \Delta F$	No. of Reflexions	R
10.0	281.6	39.8	43	0.141	0.10	20.6	1.0	1	0.048
20.0	922.5	34.2	62	0.037	0.20	504.4	9.4	7	0.019
30.0	732.9	18.1	29	0.025	0.30	563.2	21.0	13	0.037
40.0	261.3	6.7	8	0.026	0.40	1399.3	21.9	24	0.016
50.0	140.7	2.6	3	0.019	0.50	1163.8	37.3	33	0.032
60.0	224.5	5.5	4	0.024	0.60	1366.6	22.0	45	0.016
70.0	331.2	3.1	5	0.009	0.70	1413.7	39.0	55	0.028
80.0	222.5	1.7	3	0.008					
90.0	167.2	1.6	2	0.010					
100.0	3147.2	38.1	19	0.012					

## 6.11 Summary of Conclusions

The space group of titanomaghemite specimen BM1929,1687 is  $P4_32$  (no. 212). The presence of 4(1)% tetrahedral cation vacancies is confirmed by both single crystal X-ray diffraction and  $^{57}\text{Fe}$  Mössbauer spectroscopy. The octahedral site as a whole contains 18(2)% cation vacancies. There is no evidence of tetrahedral  $\text{Fe}^{2+}$  or  $\text{Ti}^{4+}$ . It is not possible to accurately determine the distribution of  $\text{Fe}^{2+}$ ,  $\text{Fe}^{3+}$  and  $\text{Ti}^{4+}$  between the two unique octahedral sites using X-ray diffraction because of the similar scattering factors for each ion, neither can the site populations of  $\text{Fe}^{2+}$  and  $\text{Fe}^{3+}$  be resolved by Mössbauer spectroscopy of iron in these two very similar sites.

## CHAPTER 7

### DISCUSSION AND CONCLUSIONS

#### 7.1 Summary of Major Conclusions on the Structure and Symmetry of Magnetite

According to the conventional description, magnetite possesses the inverse spinel structure with the centrosymmetrical space group  $Fd\bar{3}m$ . Under  $Fd\bar{3}m$  symmetry the metal cations on octahedral sites occupy special positions at the centres of the octahedral interstices. This description has been shown in this work to be an oversimplification of the situation. The octahedral site cations have been found to be displaced along  $\langle 111 \rangle$  directions leading to the non-centrosymmetrical space group  $F\bar{4}3m$ .

This conclusion results from a study of existing X-ray intensity data, which is described in Chapter 3, and also from a study of a newly collected, more extensive data set (see Chapter 4). Values for atom positions and anisotropic temperature factors for the refinement of existing data are listed in table 3.2. Table 3.6 gives values obtained for the bond lengths and a complete list of structure factors determined in this particular refinement is given in Appendix V. Table 4.4 lists values for the atom positions and anisotropic temperature factors determined in the study of new X-ray data, collected from natural magnetite specimen BMDM11. Bond lengths determined in this latter study are given in table 4.9 and a list of structure factors is tabulated in Appendix VII. Further support for  $F\bar{4}3m$  symmetry for magnetite comes from

the observation of 27 reflexions with Miller indices of the type  $\{hk0\}$  with  $h+k=4n+2$ , forbidden under  $Fd\bar{3}m$  symmetry but allowed under  $F\bar{4}3m$ . The observed and calculated structure factors for the 27  $Fd\bar{3}m$  forbidden reflexions are given in table 4.12

Measurements of the intensities of Friedel related pairs of reflexions, known from structure factor calculations to show significant differences in intensity between each member of the pair if magnetite is non-centrosymmetrical, have also shown the structure to be non-centrosymmetrical. Observed and calculated structure factors obtained by studying Friedel related pairs of reflexions are given in table 5.1

## 7.2 A Proposed Displacement Mechanism giving rise to $F\bar{4}3m$ Symmetry in Magnetite

It has been established that the metal cations occupying the octahedral sites in magnetite are not situated at the geometrical centres as was previously thought, but are displaced along  $\langle 111 \rangle$  directions from these symmetrical positions leading to  $F\bar{4}3m$  symmetry. The mechanism leading to the displacement seems to be very similar to that responsible for the displacement of small impurity atoms in the alkali halides. Lombardo and Pohl (1965) realized that the dielectric behaviour observed in single crystals of KCl doped with lithium could only be explained if the small lithium ions occupy a position off-centre from that normally exactly filled by the larger  $K^+$  ion in ideal KCl. The doped material was found to exhibit a permanent dipole moment not possessed by the parent compound (Sack and Moriarty, 1965). In addition, it was noted that the ionic conductivity of KCl was unaltered by the addition of the lithium impurity. To explain this observation Lombardo

and Pohl (1965) suggested that this dielectric behaviour could only occur if the lithium ion occupies a position off-centre from the conventional lattice site. This proposal was confirmed by Byer and Sack (1966) who found that acoustic relaxations occur in doped KCl, but only at velocities involving the  $c_{44}$  elastic constant. They concluded that the lithium ions were displaced along the  $\langle 111 \rangle$  directions. Calculations performed by Wilson et al. (1967) showed that the potential conditions at the site occupied by the lithium ions is such that a weak maximum occurs at the centre of the site giving rise to two equivalent positions of minimum energy. A large ion such as  $K^+$  is held at the centre of the site but  $Li^+$ , which is small, moves to one of the positions of minimum energy.

The results of the X-ray diffraction studies reported in Chapters 3, 4 and 5, along with a relaxation of the  $c_{44}$  elastic constant reported by Moran and Lüthi (1969), indicate that the octahedral site cations in magnetite are displaced in a manner similar to that described above for alkali halides containing impurities. This comes about because of the existence of an electrostatic potential maximum along the  $[111]$  direction at the centre of the octahedral site. The potential conditions at the octahedral site can be seen in figure 7.1. The potential maximum, of height  $\Delta$ , forces the cation to sit in either of the two positions of minimum energy. The precise position is determined by a balance between the local potential gradient and the repulsive interactions of the ion cores, while the ions surrounding the cation relax to positions of minimum energy. This distortion produces fields at all ion sites which polarize the ions and produce electronic dipole moments. A cation with large ionic radius would be held at the centre of the octahedral site because of the repulsive interactions with neighbouring anions, but

$\triangle$  = Barrier height

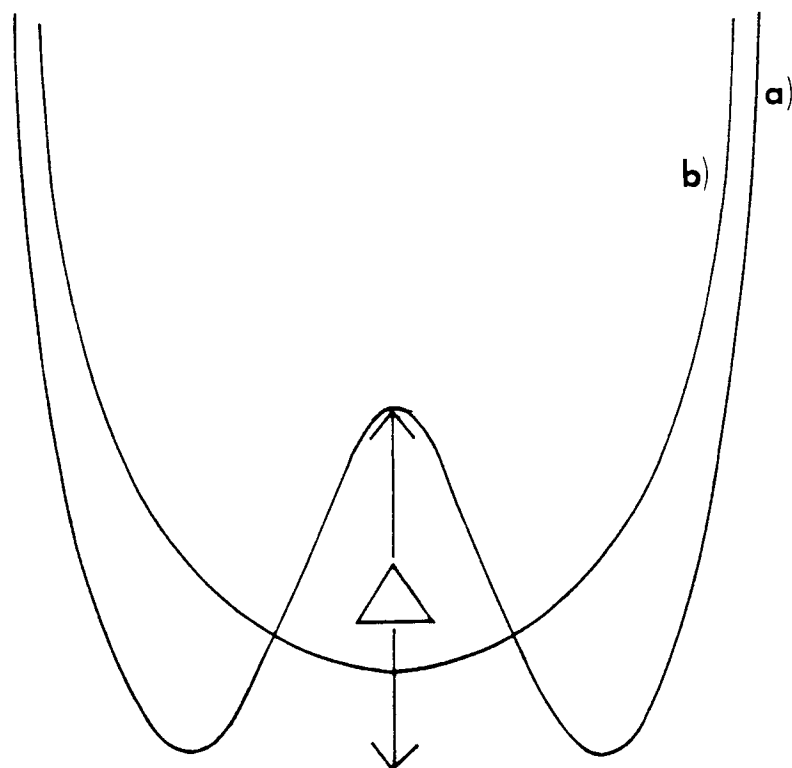


Figure 7.1 Potential conditions which exist at the octahedral site  
a) at room temperature  
b) at elevated temperatures.

smaller cations such as  $\text{Fe}^{2+}$  and  $\text{Fe}^{3+}$  are found to move to the positions of minimum energy and thus become displaced. Because most natural spinels have cations with a small ionic radius occupying the octahedral sites it is likely that they exhibit  $F\bar{4}3m$  symmetry at room temperature,  $Fd3m$  symmetry would then be possible in synthetic spinels with cations of larger ionic radii occupying octahedral sites. It is likely that at elevated temperatures the off-centre octahedral cations possess sufficient energy to overcome the potential barrier, effectively making the two possible positions of minimum energy equivalent, and resulting in a second-order solid state phase transition to  $Fd3m$  symmetry (figure 7.1).

A second-order phase transition such as this arises when a second structure is derived from the original by a continuous and ordered process of atomic displacements, these displacements being small enough so that no bonds involved in the cohesion of the structure are broken. An important feature of such a transition is that a change of symmetry occurs and the low-temperature structure closely resembles the high-temperature structure. Atomic displacements required for the transition are propagated by the same sort of mechanism as a thermal wave and not by atomic diffusion. The transition will occur rapidly and the path from the  $F\bar{4}3m$  structure to the  $Fd3m$  structure is reversible. Close to the transition, atomic positions become indeterminate and fluctuating and the structure no longer vibrates as if it were truly periodic. As the temperature increases, the amplitude of vibration of the octahedral site cation increases until it reaches a critical value at the transition temperature. Unless a change in frequency occurs then there is an abrupt increase in energy, and by Boltzmann's principle a redistribution of

energy must occur and the two minima in the potential energy curve change to a single minimum at the transition point (figure 7.1).

This transition is similar to that observed by Mishra and Thomas (1977) in  $\text{MgAl}_2\text{O}_4$ , i.e. it was found that at room temperature the structure of  $\text{MgAl}_2\text{O}_4$  conforms to  $F\bar{4}3m$  symmetry but above  $450^\circ\text{C}$  the structure reverts to  $Fd3m$ . It is possible that most spinels containing octahedral site cations with a small ionic radius exhibit the  $F\bar{4}3m$  to  $Fd3m$  reversible transition, but in some cases it may take place below room temperature.

A second mechanism, known as the co-operative Jahn-Teller effect, can also lead to off-centre displacements of the cations in spinels. This effect leads to a phase transition and occurs when transition metal ions such as  $\text{Cu}^{2+}$ ,  $\text{Fe}^{2+}$  or  $\text{Mn}^{3+}$ , which have orbitally degenerate ground states, are present in the structure. An interaction between the degenerate states and the lattice vibrations (phonons) leads to a coupling between the electronic states of different cations. If the Jahn-Teller active ions are present in sufficiently high concentrations and the coupling is strong, then the electronic states order and a phase transition from cubic to lower symmetry occurs. This transition is of the first-order and the lower symmetry phase is only stable below a critical temperature ( $T_{JT}$ ). When the Jahn-Teller active ions occupy the octahedral sites the lower symmetry phase is tetragonal with an axial ratio  $c/a > 1$ , as is the case in  $\text{Mn}_3\text{O}_4$  (Brabers, 1971) and  $\text{CuFe}_2\text{O}_4$  (Ohnishi and Teranishi, 1961). If the Jahn-Teller active ions occupy tetrahedral sites the situation tends to be more varied. Tetragonal symmetry with  $c/a > 1$  and  $c/a < 1$  may occur as is found in the series  $\text{Fe}_{3-x}\text{Cr}_x\text{O}_4$  (Goodenough, 1964); orthorhombic symmetry has also been reported for the series  $\text{Fe}_x\text{NiCr}_{2-x}\text{O}_4$  (Arnott, Wold and Rogers, 1964). If

the concentration of the Jahn-Teller active ions is less than the critical value then the macroscopic symmetry remains cubic but local displacements, due to the Jahn-Teller effect, can still occur (Kubo et al. 1969; Kozhuhar et al. 1973).

Ultrasonic measurements made on magnetite by Moran and Lüthi (1969) indicate a softening of the shear mode elastic constant ( $c_{44}$ ). If this is interpreted using the selection rules of Nowick and Heller (1965), this implies a distortion with trigonal symmetry and not tetragonal as would be expected if it arises because of the presence of Jahn-Teller active  $Fe^{2+}$  ions in the octahedral sites. The presence of a distortion with trigonal symmetry tends to rule out the possibility of Jahn-Teller distortions leading to  $F\bar{4}3m$  symmetry in magnetite. It is possible, however, that the potential maximum is surrounded by more than two positions of minimum energy because of local distortions due to the Jahn-Teller effect, in addition to the distortions due to the local potential conditions.

Magnetic exchange interactions in spinels exist mutually between the octahedral (B-site) cations, these are referred to as BB interactions. Similarly, between the tetrahedral (A-site) cations there are AA interactions and between the ions on A and B-sites, AB interactions (see section 1.8). If both the tetrahedral and octahedral sites are occupied by transition metal ions the AB interaction is far stronger than either the AA or BB interactions. The resultant effect of these interactions is that the spins of octahedral site ions align antiparallel with those of tetrahedral site ions, the net magnetic moment arises because the octahedral site contains twice as many cations as the tetrahedral site. The above description is known as the uniaxial model and was proposed by Néel (1948) in his theory of ferrimagnetism. Since the work of Néel

(1948), however, a number of different modifications to his theory have been proposed in an attempt to fully explain the magnetic properties exhibited by the spinels. These theories have been of increasing complexity and have led to the inclusion of more complex interactions; unfortunately, no theory has proved entirely successful.

The magnitude of the AB interaction depends strongly on the degree of cation-cation overlap and decreases rapidly with increasing separation of the cations. It has been suggested (Bloch, 1966) that the strength of this interaction varies as the inverse tenth power of the cation-cation separation. The small displacements of the octahedral cations in spinels ( $\sim 0.0002 \text{ \AA}$ ) would therefore have a considerable effect on the magnetic properties of these materials and may well account for some of the anomalies observed. It is likely that these displacements show up as anomalies in the magnetostriction (magnetostriction is a general term applied to a phenomenon which occurs when ferrimagnetic materials are magnetized and undergo small changes in dimensions). In fact anomalously large magnetostriction has been observed in ulvöspinel ( $\text{Fe}_2\text{TiO}_4$ ) (Ishikawa and Syono, 1971; Klerk et al. 1977). An explanation of this observation, based on the presence of  $\text{Fe}^{2+}$  ions in tetrahedral sites which produce a co-operative Jahn-Teller distortion, has been put forward, but long-range magnetic order tends to suppress this distortion. Nevertheless, a distortion does still occur. Similar anomalous magnetostriction is observed in members of the solid solution series between  $\text{Fe}_3\text{O}_4$  and  $\text{Fe}_2\text{TiO}_4$  (Syono, 1965).

Much of the detailed work on the magnetic properties of the spinels has been restricted to studies of the chromium chalcogenides, mainly because they are normal spinels with the chromium ions exclusively occupying the octahedral sites and usually a diamagnetic ion on

tetrahedral sites, i.e. the only magnetic exchange interactions present are those between octahedral site cations. Srivastava (1969), for example, studied the volume dependence of the exchange interaction in  $\text{CdCr}_2\text{Se}_4$ ,  $\text{HgCr}_2\text{Se}_4$ ,  $\text{CdCr}_2\text{S}_4$  and  $\text{HgCr}_2\text{S}_4$  and found the properties of  $\text{HgCr}_2\text{S}_4$  to be quite different to those of the other three compounds, an unusual result considering the similarity of all four materials. Martin et al. (1969) observed large shifts in the optical absorption edges of  $\text{CdCr}_2\text{S}_4$  and  $\text{CdCr}_2\text{Se}_4$  as the temperature decreased below the Curie temperature. These shifts were taken to arise because of large local distortions occurring during exchangestriction (exchangestriction is a quantity which gives a measure of the variation of the exchange interaction with strain). Bindloss (1971) studied the variation of lattice constant with temperature and the pressure dependence of the Curie temperature in  $\text{CdCr}_2\text{S}_4$  and  $\text{CdCr}_2\text{Se}_4$  and noted that the exchangestriction was considerably less than that given by thermodynamic predictions. Bindloss (1971) realized that this anomalous behaviour arises because of small atomic displacements within the unit cell which have the effect of modifying the magnetic exchange integral.

The presence of these small atomic shifts leads to the possibility of a simplified interpretation of the magnetic exchange interactions in spinels. The possibility then emerges of a self consistent interaction scheme capable of accounting for the properties observed across the whole range of spinel compounds, or at least a unified theory for specific groups such as ferrites or thiospinels, without the need to consider the more complex exchange interactions.

### 7.3 Physical Properties Exhibited by a Non-Centrosymmetrical Material

It has been established that magnetite, and probably many other spinels, conforms to the non-centrosymmetrical space group  $F\bar{4}3m$ . Entirely new properties which cannot arise in centrosymmetrical materials such as ferroelectricity, piezoelectricity, pyroelectricity and non-linear optical properties like frequency doubling, are now possible. Each of these properties will now be considered briefly.

#### 7.3.1 Ferroelectricity

A crystal which possesses the property of ferroelectricity shows a spontaneous polarization. This polarization may be reversed by the application of a sufficiently large electric field. The electric field causes a small relative shift of the atoms in the crystal and so reverses the direction of polarization. Ferroelectricity disappears above the Curie point ( $T_c$ ). At this temperature, the crystal changes from its low-temperature polarized form to its high-temperature unpolarized form. A crystal in its ferroelectric state, with a spontaneous polarization, is in a lower symmetry form than the same crystal in its non-polarized state.

It has been shown in magnetite that the octahedral site cations are displaced from their  $Fd3m$  positions, so that neighbouring rows of ions are displaced in the opposite sense, leading to  $F\bar{4}3m$  symmetry. This arrangement will give rise to a special form of ferroelectricity known as antiferroelectricity. Unlike ferroelectricity, antiferroelectricity does not give a spontaneous polarization but it is accompanied by an

increase in the dielectric constant of the crystal. Has such an increase been observed in spinel oxides? Such an increase has been observed in Mn-Zn ferrites, i.e. a rise in the dielectric constant of  $10^2$ - $10^4$  occurs at low radio and audio frequencies (Polder, 1950). The occurrence of such unusually large low-frequency dielectric constants in these materials tends to infer the presence of antiferroelectricity, which in turn means that they must be non-centrosymmetrical.

### 7.3.2 Piezoelectricity

This is a property which arises whereby a material, when placed in an electric field, undergoes a mechanical strain and conversely when mechanically strained it becomes electrically polarized and produces an electric field. The detection of piezoelectricity denotes the absence of a centre of symmetry. Unfortunately, the inability to detect piezoelectricity does not necessarily mean the material is centrosymmetrical since in many cases the effect is very weak.

### 7.3.3 Pyroelectricity

Non-centrosymmetrical crystals have the property of developing an electric polarization when the temperature is changed. Alternatively, if a spontaneous polarization is already present a change in temperature alters it. A pyroelectric crystal possesses a permanent polarization which suggests the presence of electric dipoles within the crystal. The additional polarization which arises on heating is due to asymmetric oscillation of these dipoles. This effect occurs at all temperatures, including room temperature. In practice the polarization does not

persist because imperfect insulation leads to its neutralization by the migration of charges to the crystal surface. The presence of pyroelectricity in spinels may therefore be difficult to detect without careful measurements.

#### 7.3.4 Frequency Doubling

Light is propagated in materials by inducing vibrations in the charged components (usually electrons) of the material. If there is some form of asymmetry around a small element of charge then the vibration induced by this element is anharmonic. The effect is that when a beam of light of frequency  $\nu$  passes into the crystal then a second harmonic of frequency  $2\nu$  is generated. This harmonic generation is only appreciable at very high intensities of incident light, it therefore requires light from a pulsed laser for the effect to be observed. This effect is known as frequency doubling and can only occur in a non-centrosymmetrical structure. The detection of frequency doubling can therefore be used as a means for detecting a lack of a centre of symmetry in spinels.

The detection of any one of the above properties in a compound means that the structure of that compound must be non-centrosymmetrical. There are no reports in the literature of any of these properties being observed in spinels (apart from the presence of large dielectric constants in Mn-Zn ferrites, which implies the presence of antiferroelectricity in these compounds), but because it is generally accepted that spinels are centrosymmetrical, it is unlikely that serious attempts have been made to detect such properties.

#### 7.4 The Structure and Symmetry of Titanomaghemite: Major Conclusions

A single crystal X-ray diffraction study of titanomaghemite specimen BM1929,1687 has shown it to possess a primitive cubic Bravais lattice with the space group  $P4_332$ . Atom positions, temperature factors and bond lengths found in the structure refinement under  $P4_332$  symmetry are listed in tables 6.9, 6.10 and 6.11 respectively. A complete list of structure factors obtained in this refinement is given in Appendix VIII. The structural formula determined for this specimen, by a combination of Mössbauer spectroscopy, X-ray diffraction and electron microprobe analysis, is given in section 6.10. This formula shows that cation vacancies are present within the structure on both tetrahedral and octahedral sites, the majority being restricted to octahedral sites, and that no tetrahedral site  $Fe^{2+}$  or  $Ti^{4+}$  occurs.

Because this space group does not contain any symmetry operations involving inversion or reflection it is possible for the crystals to exist in both right and left-handed forms. These two forms have different space groups, in this case  $P4_132$  and  $P4_332$ . Two space groups such as this are referred to as an enantiomorphous pair. Without having to resort to precise measurements of Friedel related pairs of reflexions it is impossible to distinguish between the two different forms of the structure, so for simplicity, the space group  $P4_332$  was assumed throughout the study described in Chapter 6.

It is possible for the two enantiomorphous forms of such a structure to exist within an apparent single crystal, as is found in  $LiFe_5O_8$  (van der Biest and Thomas, 1975). These two forms occur as small domains, the exact domain size is dependent upon the previous history of the sample but is usually of the order of  $0.1 \mu m$  in diameter. The

interface between the domains can be described by a set of geometrical operations which convert the structure on one side of the interface into the structure on the other side.

A domain structure as described above has been observed in dark-field electron micrographs of a natural maghemite crystal (Smith, 1979). These domains arise because of a phase transition involving a decrease in overall crystal symmetry from  $Fd\bar{3}m$  to the enantiomorphous pair of space groups  $P4_132$ - $P4_332$ . The domain structure observed by Smith (1979) was identical with that found in ordered  $LiFe_5O_8$  by van der Biest and Thomas (1975), which also arises because of a symmetry change from  $Fd\bar{3}m$  to  $P4_132$ (or  $P4_332$ ). Within the crystal it is possible for a total of seven crystallographically distinct types of domain boundary to occur, three of these involve translation, three inversion and translation and one involves pure inversion (for details see van der Biest and Thomas, 1975).

If additional information is required, such as the characterization of domain boundaries and the positions of specific domains, then it is possible to use contrast electron microscopy (dark-field imagery) to characterize the interface between any two domains. There is a difference in the phase-angle of a particular reflexion for the two forms of the structure (i.e. Friedel's law is violated), which means that it is possible to identify the two enantiomorphous forms on either side of a domain boundary (van der Biest and Thomas, 1975).

For present purposes it is sufficient to know of the existence of the two enantiomorphous forms within an apparent single crystal. The precise details of the positions of domain boundaries and the identification of the space group of specific domains has no real

bearing on the overall symmetry and cation distribution of the crystal under investigation.

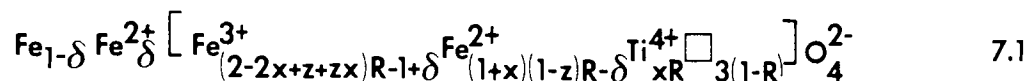
A synthetic maghemite which was tetragonal with the axial ratio  $c/a=3$ , showing reflexions forbidden by the space group  $P4_332$  was prepared by van Oosterhout and Rooijmans (1958). In this tetragonal modification, the basic primitive cubic unit cell was trebled and the vacancies and iron atoms on octahedral site 4(b) were ordered leading to the space group  $P4_1$  (or  $P4_3$ ), which is a sub-group of  $P4_332$  (or  $P4_332$ ). No reflexions inconsistent with  $P4_332$  symmetry were observed in the study of titanomaghemite specimen BM1929,1687 and so the possibility of vacancy ordering, leading to a tetragonal unit cell was ruled out. It is possible, however, that synthetic titanomaghemites exhibit vacancy ordering on octahedral sites leading to a tetragonal unit cell, as is observed in synthetic maghemites. Unfortunately, no previous attempts have been made to determine the symmetry of synthetic titanomaghemites using X-ray diffraction and so at the present time no data are available to confirm or deny this possibility.

#### 7.5 A Comparison of the Observed Cation Distribution in Titanomaghemite Specimen BM1929,1687 with that Predicted by Theory

The work carried out in Chapter 6 leads to a model for the cation distribution in titanomaghemite specimen BM1929,1687. This observed distribution can now be compared with that predicted by Readman and O'Reilly (1971) (see Model 4 in section 1.10). This particular model is generally accepted as giving the most reliable predictions for the cation distribution in titanomaghemites. Two different formulae for the

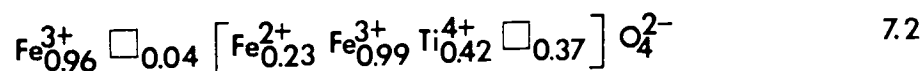
cation distribution in the parent titanomagnetite can also be determined using two recently proposed models and the merits of these models will now be discussed.

According to Readman and O'Reilly (1971) the general formula for the cation distribution of any titanomagnhemite is:

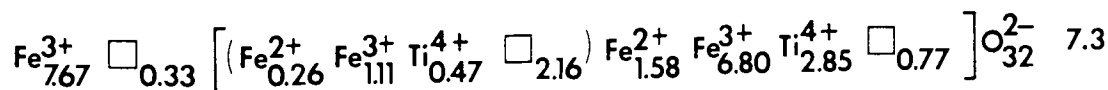


where  $x$  expresses the iron/titanium ratio,  $z$  gives the degree of oxidation,  $R$  is the spinel stoichiometry parameter and  $\delta$  represents the number of  $\text{Fe}^{2+}$  ions on tetrahedral sites (see section 1.10 for further details of these four parameters). The four parameters  $x$ ,  $z$ ,  $R$  and  $\delta$  are sufficient to define the composition of any titanomagnhemite. The above equation assumes that cation vacancies and  $\text{Ti}^{4+}$  ions are restricted to octahedral sites. This latter assumption agrees with the experimental evidence presented in Chapter 6.

From the study reported in Chapter 6 it has been established that the structural formula for titanomagnhemite specimen BM1929,1687 is:

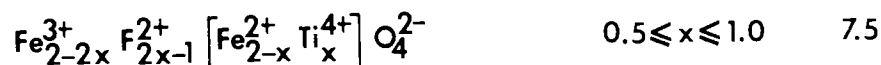


with a unit cell content of:

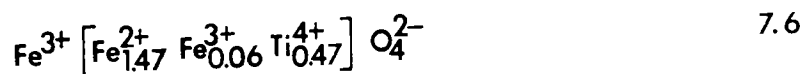


Substituting values from equation 7.2 into equation 7.1, it follows that  $x=0.47(2)$ ,  $z=0.82(2)$ ,  $R=0.88(2)$  and  $\delta=0$ .

Titanomaghemites form, under suitable conditions, from the oxidation of titanomagnetites; the oxidation process is referred to as 'maghemitization'. Néel (1955) and Chevallier et al. (1955) each proposed models for the cation distribution in titanomagnetites in which all the  $Ti^{4+}$  enters the octahedral sites and the  $Fe^{2+}$  first replaces the  $Fe^{3+}$  in octahedral sites and only then  $Fe^{3+}$  in tetrahedral sites. This model leads to the following structural formulae:



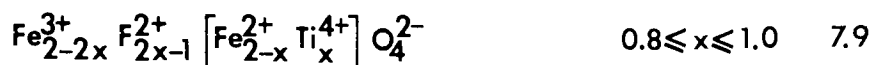
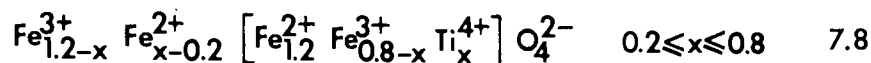
In the Néel-Chevallier model, no tetrahedral  $Fe^{2+}$  exists in the parent titanomagnetite for  $x < 0.5$ . It has been established that  $x = 0.47(2)$  in titanomaghemite specimen BM1929,1687, this value for  $x$  also applies to the titanomagnetite parent. The above model therefore stipulates that no tetrahedral  $Fe^{2+}$  should occur in either the parent titanomagnetite or the titanomaghemite; the latter is as observed experimentally. Substituting values for  $x$  into equation 7.4 gives:



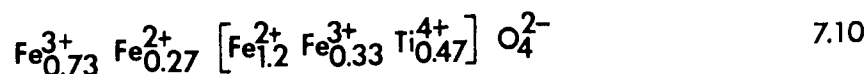
for the parent titanomagnetite.

Unfortunately, this model does not fit many of the physical properties observed in titanomagnetites particularly well. This led to the proposal of another model by O'Reilly and Banerjee (1965). In the O'Reilly-Banerjee model the tetrahedral  $Fe^{2+}$  begins to occupy the tetrahedral sites at  $x > 0.2$ . This model is similar to the Néel-Chevallier model over the compositional ranges  $0 < x < 0.2$  and  $0.8 < x < 1.0$  but varies continuously

over  $x=0.2$  and  $0.8$  with no discontinuities at  $x=0.5$ . The following structural formulae result:



There is a significant amount of evidence indicating the correctness of the latter model, found from the physical properties exhibited by the titanomagnetites: graphs of the electrical conductivity, activation energy of conduction, unit cell dimensions and Curie temperature all show a change in gradient near  $x=0.2$  and  $0.8$ . In the vicinity of  $x=0.2$  there are changes in the coercive force, remanent magnetization in uniform fields, and in magnetostriction and magnetocrystalline anisotropy constants (for a detailed study of the variation of these properties see Readman and O'Reilly, 1972). The O'Reilly-Banerjee model, because of the good agreement with observed physical properties, appears to give a more accurate prediction of the cation distribution in titanomagnetites than the Néel-Chevallier model. On the assumption of the O'Reilly-Banerjee model the following structural formula results for the parent titanomagnetite:



Unfortunately, the presence of tetrahedral  $\text{Fe}^{2+}$  in the parent titanomagnetite, predicted by the above formula, implies that it should also occur in the titanomaghemite, but no tetrahedral site  $\text{Fe}^{2+}$  was detected in the titanomaghemite. This inability to detect the presence

of tetrahedral  $\text{Fe}^{2+}$  does not necessarily mean that it is absent. It is possible that all the tetrahedral  $\text{Fe}^{2+}$  present in the parent titanomagnetite has been oxidized during the formation of the titanomaghemite. This is highly unlikely since the availability of tetrahedral  $\text{Fe}^{2+}$  in the parent titanomagnetite for oxidation is 20% that of octahedral  $\text{Fe}^{2+}$  (see section 1.10), which implies that as long as octahedral  $\text{Fe}^{2+}$  remains there should always be a percentage of tetrahedral  $\text{Fe}^{2+}$  present. It is possible that a small percentage of tetrahedral  $\text{Fe}^{2+}$  does occur which was not detected in the Mössbauer study, i.e. the corresponding peak was not resolved since it is low in intensity and superimposed on the other iron peaks. O'Reilly (1983) gives a table of  $\delta$  values ( $\delta$  equals the number of  $\text{Fe}^{2+}$  ions per molecule in tetrahedral sites) for titanomaghemites for various values of  $x$  and  $z$ . For the composition found here  $x=0.47(2)$  and  $z=0.82(2)$ ,  $\delta$  should be approximately equal to 0.2. Because 0.23  $\text{Fe}^{2+}$  ions per molecule of titanomaghemite on octahedral sites were detected in the Mössbauer study, it seems probable that 0.2 tetrahedral  $\text{Fe}^{2+}$ , if present, should also have been detected. The inability to detect the presence of tetrahedral  $\text{Fe}^{2+}$  suggests that the Néel-Chevallier model for the cation distribution of the parent titanomagnetite gives a more accurate description than the O'Reilly-Banerjee model. Since the Néel-Chevallier model predicts that no tetrahedral  $\text{Fe}^{2+}$  occurs in the parent titanomagnetite for  $x=0.47(2)$ , then no tetrahedral site  $\text{Fe}^{2+}$  will occur in the oxidation product, i.e. in the titanomaghemite. Because errors occur in the calculated values of  $x$  and  $z$  the possibility of the O'Reilly-Banerjee model accurately describing the cation distribution in the parent titanomagnetite cannot be ruled out entirely.

During oxidation of the parent titanomagnetite, octahedral site  $\text{Fe}^{2+}$  diffuses to the crystal surface where it is oxidized by adsorbed oxygen ions forming new tetrahedral and octahedral sites (see section 1.10 for details). The majority of these vacancies are then filled by diffusing  $\text{Fe}^{3+}$  ions, but for high degrees of oxidation some tetrahedral sites will remain vacant. The presence of tetrahedral site vacancies in the titanomaghemite, although not allowed for in equation 7.1, was not ruled out entirely as a possibility by Readman and O'Reilly (1971). They found it necessary to make assumptions in the formulation of this model, in order to simplify an already complex problem, and one such assumption was that all cation vacancies were restricted to octahedral sites, but they noted that tetrahedral site cation vacancies were likely in highly oxidized samples.

#### 7.6 Suggestions for Further Work

During the course of the present study, use has been made of the violation of Friedel's law which occurs in a non-centrosymmetrical structure, in the presence of anomalous scattering. This involves making a comparison of the intensity of each member of a Friedel pair of reflexions, i.e. a comparison of the observed intensities  $I_{hkl}$  and  $I_{\bar{h}\bar{k}\bar{l}}$ , and provides a relatively quick method for determining if a structure lacks a centre of symmetry. Similar studies of the Friedel pairs could be used to search for other spinels which may also conform to  $F\bar{4}3m$  symmetry. Because the spinels are such an extensive range of compounds (more than 200 are known to exist), it would be necessary to make a study of selected spinels. A study, for example of spinels containing octahedral site cations with large ionic radius and a similar study of

spinel containing octahedral site cations with small ionic radius might prove to be the most useful approach. Spinel such as  $\text{FeAl}_2\text{O}_4$ ,  $\text{ZnAl}_2\text{O}_4$ ,  $\text{FeCr}_2\text{O}_4$  and  $\text{MgCr}_2\text{O}_4$  containing octahedral site ions with a small ionic radius would then be expected to show displacements leading to  $F\bar{4}3m$  symmetry, whereas,  $\text{MnRh}_2\text{O}_4$ ,  $\text{CuRh}_2\text{O}_4$  and  $\text{WNa}_2\text{O}_4$ , containing octahedral site cations which fill the available interstice, would not be expected to show any significant difference in intensity between  $I_{hkl}$  and  $I_{\bar{h}\bar{k}\bar{l}}$ . Because the Friedel pairs showing the greatest difference in intensity are all weak, it would be more practical to carry out the measurements at low temperatures, since a reduction in temperature has the effect of reducing the loss in diffracted beam intensity due to thermal vibration, leading to a higher count rate and thus improved counting statistics.

A study of the structure of magnetite at elevated temperatures could also be made to see if the  $Fd3m$  forbidden reflexions disappear on heating and reappear on cooling as is observed in  $\text{MgAl}_2\text{O}_4$  (Mishra and Thomas, 1977). This is due to a reversible transition from  $F\bar{4}3m$  to  $Fd3m$ , brought about because the off-centre cation has sufficient energy to overcome the potential barrier at elevated temperatures. If such a change is observed, it should be accompanied by a change in the magnetic properties and could confirm the proposed displacement mechanism (section 7.2).

Magnetite and its derivatives are used extensively in the determination of natural remanent magnetization (NRM) in rocks. An increase in hydrostatic pressure or a decrease in temperature, leading to volume contraction, is expected to lead to a reduction of the displacement of the octahedral site cation. This is observed in KCl doped with lithium (Wilson et al. 1967) where it is found that a uniform hydrostatic pressure forces the displaced ion to return to its original

position. This result indicates that the effect of increased hydrostatic pressure can be sufficient to force the displaced cation to return to its  $Fd3m$  position (see section 7.2). Considering the usefulness of this extensive range of minerals and the fact that their magnetic properties are very much dependent upon the positions of the cations, a study of the structure and magnetic properties of magnetite, at high pressure would be interesting.

Aluminium is the most abundant cation species, apart from iron and titanium, found in titanomaghemites. A clear understanding of the cation distribution, oxidation process, and magnetic properties of titanomaghemites, is necessary for an accurate interpretation of palaeomagnetic data. A study of the crystal structure and hence cation distribution of a series of aluminium substituted titanomaghemites should help to give a better understanding of the physical properties exhibited by these materials. An X-ray diffraction study, preferably carried out in conjunction with neutron diffraction, since the neutron scattering cross-sections for iron, titanium and aluminium are sufficiently different, would allow a precise determination of the distribution of individual cations within the structure.

Finally, it is known that the cation distribution of a titanomaghemite is not a unique function of composition, but depends upon the path by which maghemitization has taken place (O'Reilly, 1983). In addition, it has been found that the process of maghemitization in nature is not the same as that which has been simulated in the laboratory. A study of the cation distribution in natural and synthetic titanomaghemites, for a range of compositions, would be expected to lead to a better understanding of natural and laboratory simulated

magnetization mechanisms and in turn the magnetic properties exhibited by these materials.

## APPENDIX I

### DATA REDUCTION PROCEDURES AND THE CRYSTALLOGRAPHIC SOFTWARE USED IN THE STRUCTURE REFINEMENTS

#### I.1 Introduction

All of the crystallographic calculations reported in this thesis, with the exception of data reduction, were carried out using the crystallographic software package X-RAY 74 (Stewart et al. 1974) which is stored at Manchester University's Regional Computer Centre.

Files containing the data necessary to perform the calculations were initially stored at Aston on an ICL 1904S computer and then transmitted to Manchester using the UASWAN link. At Manchester they were queued on a second, front-end, ICL 1904S before being processed on a CDC 7600 computer system. Replacement of Manchester's 1904S with an AMDAHL 470/V8 in April 1985, before completion of the titanomagemite crystal structure refinement gave direct access from Aston to Manchester. The AMDAHL was therefore used for storing data files for the final stages of the titanomagemite refinement before they were processed on the CDC 7600.

#### I.2 Data Reduction

Integrated X-ray intensities collected using the four circle diffractometer form the raw data from which a crystal structure is determined. These intensities represent all the information which is

obtained by physical measurements made on the crystal and the solution of a structure is dependent upon the accurate retrieval of this information. The initial manipulation of the data is referred to as data reduction.

Data reduction was carried out at Aston on a HARRIS 500 computer system using a program written by DR. T.A. Hamor and modified by D.J. Stops. The program takes raw intensity data and applies corrections for background counts, Lorentz and polarization effects and corrects for any drop in intensity of the X-ray beam during data collection. Output from the program is in the form of the Miller indices for each reflexion, the relative structure factor ( $F_R$ ) and its standard deviation  $\sigma(F_R)$  calculated on the basis of counting statistics and including a correction for variation of the X-ray beam with time.

The next four sub-sections describe the corrections applied using the data reduction program.

### I.2.1 Subtraction of Background Counts

The raw intensity data were corrected for background using the method described by Stout and Jensen (1968). The background is measured on either side of the peak for one half the time used to count the peak. The net peak count is given by :

$$N_{PK} = N_T - r(N_{BL} + N_{BR}) \quad 1.1$$

where  $N_T$  is the total peak count and  $N_{BL}$  and  $N_{BR}$  are the background counts to the left and right of the peak respectively, each collected over a period of  $1/r \times$  peak count time.

### 1.2.2 Standard Deviation of Peak

The standard deviation in  $N_{PK}$  due to counting statistics is given by the expression :

$$\sigma_{PK}^2 = \sigma_I^2 + \sigma_{BL}^2 + \sigma_{BR}^2 \quad 1.2$$

where  $\sigma_I^2 = N_I$  and  $\sigma_{BL} = r\sqrt{N_{BL}}$ . The expression for the standard deviation of the peak must include an additional expression which takes account of any variation of the X-ray beam with time, this is carried out as follows :

$$\sigma_I^2 = \sigma_{PK}^2 + (fN_{PK})^2 \quad 1.3$$

where  $f$  is a parameter which depends on the constancy of the X-ray beam and is dependent upon the X-ray generator and mains supply used.

### 1.2.3 Intensity Control and Orientation

During data collection, two control reflexions are measured repeatedly. If a monotonic decrease in intensity of these reflexions is observed this indicates a deterioration of the crystal in the X-ray beam, and for a sudden drop in intensity a change in crystal alignment is indicated. Any small change in the intensity of the control reflexions is then used to estimate a value for the parameter  $f$  of equation 1.3. This is achieved by attributing any part of the variation in intensity of the control reflexions not accounted for by counting statistics, to variation in intensity of the main beam.

If  $\bar{N}$  is the mean count for  $n$  measurements and  $\sigma^2(N)$  the variance of the counts (a value expected on the basis of counting statistics to be  $\bar{N} / n-1$ ) then :

$$\sigma^2(N) = \frac{\bar{N}}{n-1} + (f\bar{N})^2 \quad 1.4$$

rearranging equation 1.4 we get :

$$f = \frac{1}{\bar{N}} \left( \sigma^2(N) - \frac{\bar{N}}{n-1} \right)^{1/2} \quad 1.5$$

Using equation 1.5 it is possible to find an accurate value for  $f$ .

#### 1.2.4 Lorentz and Polarization Corrections

The relationship between the observed structure factor,  $F_o$ , and the square root of the intensity measured for each reflexion depends upon a number of geometrical factors which relate to the individual reflexion and to the apparatus used to measure the intensity. Two such factors are important, the Lorentz factor ( $L$ ) and the polarization factor ( $p$ ). The Lorentz factor arises because the time required for a reciprocal lattice point to pass through the sphere of reflexion is not constant but varies with its position in reciprocal space and with the direction in which it approaches the sphere. The polarization factor arises because of the nature of the X-ray beam and the manner in which its reflecting efficiency varies with the reflexion angle.

The Lorentz factor depends on the precise measurement technique and is a function of  $2\theta$  (see International Tables for X-ray Crystallography Vol.II, p266).

For the  $\omega$ - $2\theta$  scan technique used here :

$$L = \frac{1}{\sin 2\theta} \quad 1.6$$

In the presence of a graphite monochromator, the polarization factor is given by :

$$P = \frac{\cos^2 \theta_m + \cos^2 2\theta}{2} \quad 1.7$$

where  $\theta_m$  is the monochromator angle.

Combining equations 1.6 and 1.7 we get :

$$L_p = \frac{\cos^2 \theta_m + \cos^2 2\theta}{2 \sin 2\theta} \quad 1.8$$

Output from the data reduction program for each reflexion consists of the Miller indices, the relative structure factor ( $F_R$ ) and  $\sigma(F_R)$ . The structure factor data are not on any fixed scale and must therefore be rescaled to convert into observed structure factors ( $F_o$ ). Scaling between  $F_R$  and  $F_o$  is by comparison of  $F_R$  with the calculated structure factor,  $F_c$  (see section 1.3.5). This procedure adds an additional parameter, the scaling factor, which is dependent upon the crystal size and the beam intensity, but does not affect the accuracy of the final results.

### 1.3 X-RAY 74

X-RAY 74, commonly referred to as the X-RAY SYSTEM, is a library of programs, written in FORTRAN, and designed to carry out the calculations

required for the solution of a crystal structure from diffraction data. The following description gives a brief outline of the programs used and the calculations performed by each.

i) DATRDN

The raw intensity data, after being corrected for Lorentz and polarization effects as described in section I.2.4, were arranged into groups of equivalent reflexions and an average intensity found for each group (for details see section 4.5 and 6.8). Using the data reduction program DATRDN these data were then organized into a condensed form to allow all the remaining programs to run automatically. The program requires the following data :

- a) Unit cell dimensions.
- b) Atomic scattering factors.
- c) The general symmetry operations of the space group.
- d) Identification of the unit cell as centric or acentric and the lattice type.
- e) Dispersion corrections.
- f) The physical orientation of the crystal.
- g) Absorption corrections.
- h) Intensity data.

(ii) LOADAT

The atomic parameters such as atom type, scattering factor, atomic coordinates, population parameter and temperature factors are loaded

into the X-RAY SYSTEM using the atom loading program LOADAT. This program places all these parameters into their appropriate arrays and is needed before structure factor calculations may be performed.

(iii) WTLSSQ

In order to achieve rapid convergence of the least squares program individual weights were assigned to each reflexion according to the expression :

$$W_i = XY;$$

If  $\sin \theta > \lambda$  then  $X = 1$  otherwise  $X = \sin \theta / \lambda$ ,

and if  $F_o > Z$  then  $Y = Z / F_o$  but if  $F_o \leq Z$  then  $Y = 1.0$

This non-linear weighting scheme was applied using the weighted least squares program WTLSSQ.

(iv) CRYLSQ

Refinement of the structure parameters was achieved using the crystallographic least squares program CRYLSQ. To achieve convergence the program attempts to minimize the function :

$$R_W = \sum_{i=1}^S W_i (|F_o| - |F_c|)^2 \quad 1.9$$

where  $W_i$  is the weight applied to the  $i$ th reflexion and  $S$  is the number of reflexions measured.

The refinement is carried out in a number of cycles. After each cycle values for anisotropic temperature factors, atom positions along with estimated standard deviations, overall R-factor, R-factor for the reflexions below threshold (less-thans), weighted R-factor and various intensity statistics are given.

(v) WTANAL

Analysis of the R-factor for various groups of reflexions was achieved using WTANAL, a program designed to examine  $\sum W_i |\Delta F_i|^2$  and  $|\Delta F|^2$  as a function of  $F_o$  and  $\sin \theta$ . During various stages of the structure refinement WTANAL allowed any groups of reflexions with an abnormally large R-factor to be identified.

(vi) BONDLA

The objectives of this program are to calculate bond lengths and bond angles within the structure, including those of atoms related by symmetry, and to estimate the errors in these calculated quantities based upon results obtained in the least squares refinement.

(vii) FOURR

The refinement procedure was helped by the use of various Fourier maps. Any reflexion flagged as a less-than was excluded from the Fourier summations. The maps were produced with a suppressed background so as to improve resolution.

### I.3.1 Atomic Scattering Factors

Output from the data reduction program serves as input to the X-RAY SYSTEM. This program is used to perform structure factor calculations on the basis of an assumed atomic arrangement, these calculated structure factors are then compared with those observed experimentally.

In order to carry out the necessary calculations the program must firstly be given a table of scattering factors for each atom type. Values for these scattering factors, taken from the International Tables for X-ray Crystallography Vol.IV are read into the X-RAY SYSTEM for a series of values of  $\sin \theta/\lambda$ , a table is then stored for each atom. Accurate values of the scattering factor for each reflexion are then determined by a four point interpolation using Aitken's method as described by Milne (1949).

### I.3.2 Temperature Factors

Usually atomic scattering factors are calculated with the assumption that the atom is at rest, in reality it vibrates about a mean position. This vibration must be taken into account in any structure factor calculation where observed and calculated values are being compared. The magnitude of the vibration is dependent upon the temperature, the mass of the atom and the strength of the atomic bonds. The overall effect of this motion is to cause the scattering power of an atom to fall off more rapidly than it would if the atom were at rest.

The effect of thermal vibration on the diffracted intensities was treated by Cruickshank (1956) by introducing the concept of anisotropic vibrations. A number of different conventions have been followed in the

crystallographic literature for the definition of temperature factors. Within the X-RAY SYSTEM the Debye-Waller Beta factor for the anisotropic mode is used. The temperature factor is given by :

$$\exp\left\{-\left(\beta_{11}h^2 + \beta_{22}k^2 + \beta_{33}l^2 + 2\beta_{12}hk + 2\beta_{13}hl + 2\beta_{23}kl\right)\right\} \quad 1.10$$

The anisotropic thermal motion of each atom is represented by a vibrational ellipsoid for which the individual temperature factors  $\beta_{11}$ ,  $\beta_{22}$ ,  $\beta_{33}$ ,  $\beta_{12}$ ,  $\beta_{13}$  and  $\beta_{23}$  define the principal axes and their direction cosines. These six parameters form a nine element matrix in which the number of independent parameters may be reduced by the symmetry of the environment of each atom.

### I.3.3 Absorption Correction

Incorrect absorption corrections can lead to large systematic errors in a highly refined structure. It is therefore important to minimize these errors in the work carried out here.

In order to make an accurate correction, it is necessary to calculate the absorption arising for the actual path length travelled within the crystal by the beam reflected off each plane and to integrate these values over the entire crystal volume. This calculation is far too complex for a crystal of random shape. The practical approach employed here to simplify the calculation was to use a spherical crystal for data collection. In addition, to reduce X-ray absorption by the specimen a penetrating radiation ( $\text{MoK}\alpha$ ) was used. The absorption correction applied was that given for spheres by Weber (1969).

#### I.3.4 Extinction Correction

In addition to absorption, a second physical process leads to a reduction in intensity of the diffracted beam. Darwin (1922) named this effect extinction and realized that two different types occur, these are primary and secondary extinction.

Primary extinction is an interference process which reduces the intensity of the X-ray beam as it passes through the crystal; it is said to occur in crystals which are ideally perfect. Experiments have shown that primary extinction effects are negligible even for the strongest reflexions of most crystals. In reality crystals are made up of small mosaic blocks so that the concept of an ideally imperfect crystal is entirely theoretical. Attenuation of the diffracted beam between these mosaic blocks is known as secondary extinction. Small crystals suffer less from secondary extinction than large ones and crystals in which the mosaic blocks are not well aligned suffer less than those in which the alignment is more or less parallel. Secondary extinction is more prevalent at low angles where the intensities tend to be stronger. Secondary extinction effects can be quite large, especially for low angle strong reflexions, and result in the observed structure factors for strong reflexions being lower than their calculated values.

X-RAY 74 applies an isotropic extinction correction to the calculated structure factors using the procedure described by Larson (1967), which is based on theory developed by Zachariasen (1967) for a mosaic crystal. The symbol  $g$  is used to represent the secondary extinction factor, its value is given by the two equations shown below and may be refined, using CRYLSQ, as a least squares parameter. The value found for  $g$  during least squares refinement is closely connected

with the scale and temperature factors and cannot be refined simultaneously with these parameters.

If  $FC_E$  represents the calculated structure factor corrected for secondary extinction then :

$$FC_E = |FC| (1.0 + 2.0g\Delta FC^2)^{-1/4} \quad 1.11$$

where  $\Delta$  is obtained from a knowledge of physical and diffraction parameters and is given by :

$$\Delta = \frac{(\rho^2 \lambda^3 L p_2 \bar{T})}{(V^2 p_1 \sin 2\theta)} \quad 1.12$$

where  $p_n = 1 + (\cos 2\theta)^n$ ,  $\bar{T}$  is the average path length through the crystal,  $V$  is the volume of the unit cell and  $\rho$  is the classical radius of an electron.

Zachariasen (1967) realized that two types of real crystal exist; he named these type I and type II. For type I the extinction depends upon the mosaic spread of the diffracted beam and in type II it depends on the mean domain radius of the mosaic blocks. For both types of crystal the extinction depends on the mean path length through the crystal ( $\bar{T}$ ), i.e. it depends upon the shape of the crystal. The use of a spherical crystal for data collection therefore makes the calculation far simpler since  $\bar{T}$  can be considered constant.

### 1.3.5 Scale Factor

The necessity for a scale factor arises because the observed intensity data are not initially on the same scale as the calculated

data. In the X-RAY SYSTEM the scale factor applied is such as to place the values of the relative structure factor ( $F_R$ ) on the same scale as the calculated structure factor ( $F_c$ ) as described in the International Tables for X-ray Crystallography Vol.I. Scale is a quantity which is refined using the least squares program.

#### I.3.6 Less-Thans

This term is used throughout this thesis to refer to reflexions of very low intensity but it does not apply to space group dependent systematic absences. As the name suggests it is used to set a threshold of observability. This threshold is set on the basis of counting statistics. When the estimated standard deviation of the intensity is of the same order of magnitude as the intensity then a reflexion is considered to be a less-than.

## APPENDIX II

### SPECIMEN PREPARATION FOR SINGLE CRYSTAL X-RAY STUDIES

Spherical crystal specimens of magnetite and titanomagnetite used for the crystal structure refinements were produced by grinding small crystal fragments taken from much larger single crystals. The grinding apparatus is based on that described by Bond (1951) and is shown in figure II.1.

The air driven grinder consists of a square brass plate of sides 40 mm and 5 mm thick with a 20 mm diameter hole drilled through its centre. Emery paper 5 mm wide lining the 20 mm hole was used as the abrasive. One end of the emery paper was pushed into slot S, thereby preventing the compressed air from passing under the paper, the other end was held in place by soft wax placed between the paper and the brass plate. Two perspex plates cover the faces of the brass plate, one having a 10 mm diameter hole drilled in it with a fine silk screen across the hole. This prevents any build up of pressure by allowing the air to escape from the equipment.

Compressed air was brought into the apparatus tangentially as shown in figure II.1 through a 0.5 mm diameter air jet labelled H. The air intake and the slot S enter the 20 mm hole slightly above the lowest point thus preventing the crystal from falling into the air intake or the slot when the air is switched off. This latter feature is important because the crystals used in the work reported here were smaller than either the air hole or the slot (S).

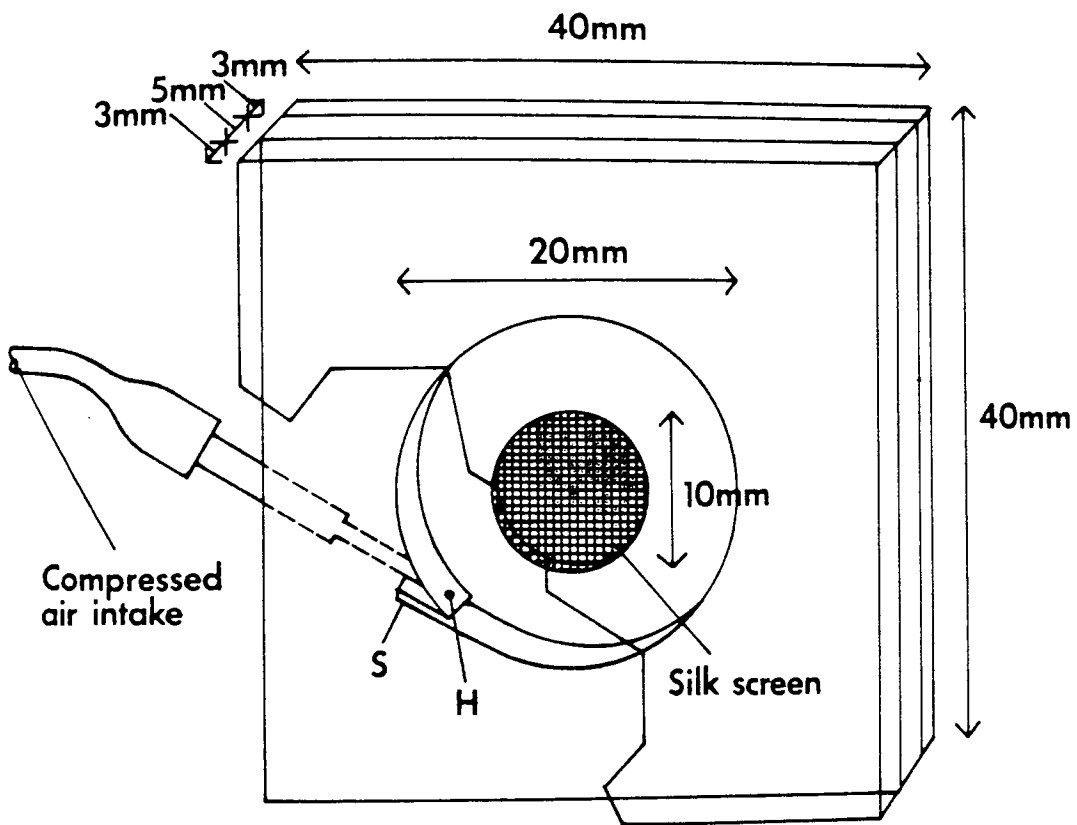


Figure II.1 Air Driven Sphere Grinder.

Several small crystal fragments of the order of 1 mm in diameter were broken off the larger single crystals and one individual fragment at a time was placed into the air driven sphere grinder. The introduction of more than one fragment at a time proved unsuccessful, i.e. it was found that the fragments tended to splinter because of contact with one another during the grinding process. Compressed air at a pressure of 70 p.s.i., from a compressed air cylinder, was injected into the device through air intake (H). Initially 240  $\mu\text{m}$  grade emery paper was used as an abrasive, this was found to be ideal for removing any rough edges but did reduce the size of the fragments quite rapidly. When the crystal was approximately spherical the 240  $\mu\text{m}$  grade emery paper was replaced by 400  $\mu\text{m}$  which was used to produce the finished spheres, the air pressure being reduced to 60 p.s.i. for this final stage. It was necessary to use a lower pressure here because it was noted that the spheres, now approximately 0.4 mm in diameter, tended to disintegrate if higher pressures were used.

The apparatus was checked periodically and the crystal examined under an optical microscope to ensure that cracks had not developed during the grinding process. It was found that a good spherical crystal could be produced in approximately six hours using the procedure described above. The grinding process was repeated several times until a number of spherical crystals of each specimen, suitable for examination by single crystal X-ray diffraction, had been produced.

### APPENDIX III

#### ELECTRON MICROPROBE ANALYSIS

Electron microprobe analysis of magnetite specimen BMDM11 and titanomagnetite specimen BM1929,1687 were carried out using a Cambridge Instruments Microscan MK5 microprobe.

A fragment of each of the crystals was mounted in separate araldite blocks and polished using 6  $\mu\text{m}$ , 1  $\mu\text{m}$  and finally 1/4  $\mu\text{m}$  diamond paste until the surface was relatively free from scratches. Specimen and standard were each coated with a carbon film approximately 250  $\mu\text{m}$  thick. This allowed the specimen to conduct, thereby preventing a build up of charge which could lead to a deflection of the electron beam and also prevented any errors due to a difference in thickness of the carbon coat between standard and specimen. The accelerating voltage was 15 kV with a beam current of approximately 0.05  $\mu\text{A}$ . A counting time of 100 seconds was used for each analysis. Background readings for each element were taken 2° either side of the peak.

Peak and background counts were corrected for dead time. Each count was then corrected for atomic number, absorption and fluorescence effects (Z.A.F.) using the procedure described by Sweatman and Long (1969).

Pure metal standards were used to analyse for the elements Cr, Fe and Ti. For Al a synthetic  $\text{Al}_2\text{O}_3$  standard was used, for Mg synthetic  $\text{MgO}$ , for Ca and Si synthetic  $\text{CaSiO}_3$  and for Mn synthetic  $\text{Mn}_3\text{O}_4$ . The minimum detectable level was found to vary from 0.05wt% to 0.10wt% depending upon the atomic weight of the element.

## APPENDIX IV

### MÖSSBAUER SPECTROSCOPY

Magnetite specimen BMDM11 and titanomagnetite specimen BM1929,1687 were studied using  $^{57}\text{Fe}$  Mössbauer spectroscopy. A constant acceleration type spectrometer was employed in which a range of velocities is scanned linearly and repeatedly. The  $\gamma$ -rays were detected using a gas filled proportional counter, counts being recorded on 512 channels of an Ino-Tech 5200 multichannel analyser such that the velocity interval per channel is constant. The source was  $^{57}\text{Co}$  diffused into a palladium foil, the spectrometer being calibrated relative to iron metal (all isomer shifts quoted are relative to iron metal).

Assuming the absorption line shapes to be Lorentzian the parameters; position, height, area of each line and standard deviation of these three parameters were obtained by computer fitting the experimental data on an ICL 1904S computer system using a program written by A. J. Stone which follows the procedure described by Bancroft et al. (1967). This program uses Gaussian non-linear regression analysis with a facility for constraining any set of parameters or combination of parameters in order to obtain convergence.

The absorber consisted of a crushed single crystal, prepared by grinding under acetone, spread out to a disc of thickness such that the average sample concentration was  $25 \text{ mg/cm}^2$  and held rigidly between thin card.

APPENDIX V

STRUCTURE FACTORS FOR MAGNETITE PRODUCED BY A RE-EXAMINATION OF  
EXPERIMENTAL DATA PUBLISHED BY FLEET (1981)

h	k	l	$F_o$	$F_c$	$F_{d3m}$	$F_{\bar{4}3m}$
			After Fleet	Absolute Electron Units		
0	0	2	-	-	-	0.9
0	0	4	467	295.5	313.2	312.9
0	0	6	-	-	-	3.9
0	0	8	582	327.0	334.2	333.6
0	0	10	-	-	-	4.3
0	0	12	203	87.0	89.7	88.9
0	0	14	-	-	-	4.5
0	0	16	299	132.9	138.5	137.7
0	2	2	323	173.4	166.2	166.3
0	2	4	-	-	-	1.4
0	2	6	241	107.7	110.7	110.7
0	2	8	-	-	-	0.9
0	2	10	164	69.7	71.0	71.1
0	2	12	-	-	-	0.9
0	2	14	108	45.3	45.6	45.5
0	2	16	-	-	-	0.3
0	4	4	680	473.2	473.6	473.2
0	4	6	-	-	-	3.4
0	4	8	293	130.9	132.6	132.0
0	4	10	-	-	-	4.3
0	4	12	402	186.7	191.0	190.3
0	4	14	-	-	-	4.0
0	4	16	129	54.3	55.2	54.3
0	6	6	202	87.2	88.8	88.9
0	6	8	-	-	-	2.8
0	6	10	129	54.3	55.4	55.3
0	6	12	-	-	-	1.7
0	6	14	-	46.6	46.7	46.8
0	6	16	111	46.6	46.7	46.8
0	8	8	447	214.2	220.1	219.4
0	8	10	-	-	-	3.2
0	8	12	-	65.7	68.9	68.1
0	8	14	155	65.7	68.9	68.1
0	8	16	125	52.6	52.2	52.3
0	10	10	125	52.6	52.2	52.3
1	1	1	145	66.6	67.4	67.5
1	1	3	437	270.5	268.2	268.1
1	1	5	422	227.5	233.0	233.1
1	1	7	51	21.3	21.2	21.0
1	1	9	71	29.7	30.2	30.4
1	1	11	223	96.2	98.0	97.8
1	1	13	215	92.3	93.4	93.3

			$F_o$				$F_c$
After Fleet			Absolute Electron Units	Fd3m	$F_{43m}$		
h	k	l					
1	1	15	< 8	< 3.3	2.8		2.9
1	3	3	73	30.7	30.6		30.6
1	3	5	88	37.0	37.3		37.3
1	3	7	334	153.5	149.6		149.5
1	3	9	291	129.3	130.2		130.0
1	3	11	16	6.7	6.9		7.0
1	3	13	39	16.3	16.5		16.7
1	3	15	144	60.8	61.7		61.7
1	5	5	99	41.6	41.8		42.1
1	5	7	301	135.4	137.8		137.6
1	5	9	284	125.3	125.8		125.7
1	5	11	22	9.2	9.2		8.9
1	5	13	51	21.3	21.2		21.3
1	5	15	143	60.4	60.7		60.4
1	7	7	23	9.6	9.2		9.4
1	7	9	36	15.0	15.2		15.1
1	7	11	175	74.4	76.8		76.8
1	7	13	172	73.1	74.0		73.7
1	7	15	< 8	< 3.3	1.0		1.2
1	9	9	58	24.2	24.6		24.7
1	9	11	170	72.2	73.8		73.5
1	9	13	177	75.3	77.1		76.8
1	11	11	< 8	< 3.3	1.3		1.7
2	2	2	277	134.0	126.3		126.4
2	2	4	285	134.1	133.2		133.3
2	2	6	272	123.1	124.6		124.6
2	2	8	196	84.4	85.6		86.2
2	2	10	190	81.3	83.3		83.3
2	2	12	130	54.8	55.3		55.6
2	2	14	130	54.8	55.0		55.0
2	2	16	96	40.2	39.5		40.2
2	4	4	9	3.8	0.5		1.3
2	4	6	226	98.8	98.1		98.4
2	4	8	10	4.2	0.8		1.3
2	4	10	148	62.6	62.5		62.4
2	4	12	< 8	< 3.3	0.8		0.8
2	4	14	112	47.0	46.2		46.3
2	4	16	< 8	< 3.3	0.7		1.0
2	6	6	230	100.1	101.1		101.2
2	6	8	161	68.3	68.5		68.7
2	6	10	164	69.6	70.8		70.8
2	6	12	120	50.4	50.1		50.7
2	6	14	118	49.6	49.7		49.7
2	8	8	< 8	< 3.3	1.2		1.2
2	8	10	125	52.6	53.4		53.7
2	8	12	< 8	< 3.3	1.2		1.4
2	8	14	91	38.1	38.2		38.2
2	10	10	128	53.9	55.1		55.0
2	10	12	94	39.4	40.1		40.4

			$F_o$		$F_c$	
After Fleet			Absolute Electron Units	Fd3m	$\bar{F}43m$	
h	k	l				
3	3	3	404	209.2	204.8	204.6
3	3	5	380	184.7	182.2	182.2
3	3	7	32	13.3	12.5	13.4
3	3	9	49	20.4	19.1	19.2
3	3	11	206	88.2	87.9	87.8
3	3	13	195	83.2	82.4	82.5
3	3	15	8	3.3	1.3	3.6
3	5	5	363	170.0	166.1	166.0
3	5	7	37	15.4	15.4	15.3
3	5	9	58	24.2	23.8	24.0
3	5	11	200	85.4	84.5	84.5
3	5	13	199	85.0	83.3	83.0
3	5	15	9	3.8	2.0	1.9
3	7	7	238	103.2	103.7	103.7
3	7	9	220	94.6	94.7	94.7
3	7	11	14	5.8	2.8	5.4
3	7	13	23	9.6	8.7	9.0
3	9	9	216	92.8	93.4	93.2
3	9	11	14	5.8	5.9	6.0
3	9	13	39	16.3	16.3	16.5
3	11	11	135	56.9	57.8	57.8
4	4	4	383	184.9	182.7	182.1
4	4	6	8	3.3	0.4	3.3
4	4	8	534	270.3	263.1	262.4
4	4	10	8	3.3	0.3	3.7
4	4	12	187	79.6	78.0	77.2
4	4	14	< 8	< 3.3	0.1	4.2
4	6	6	175	74.5	73.3	73.2
4	6	8	8	3.3	0.6	2.4
4	6	10	142	59.9	59.2	59.4
4	6	12	12	5.0	0.6	2.1
4	6	14	91	38.1	37.3	37.3
4	8	8	207	88.7	89.7	89.0
4	8	10	< 8	< 3.3	0.4	3.3
4	8	12	340	152.8	152.6	151.8
4	8	14	< 8	< 3.3	0.3	3.3
4	10	10	94	39.4	39.9	39.8
4	10	12	< 8	< 3.3	0.5	2.5
5	5	5	344	157.6	155.6	155.5
5	5	7	48	20.0	19.2	19.1
5	5	9	70	29.3	29.1	29.2
5	5	11	197	84.1	82.8	82.5
5	5	13	205	87.6	85.0	84.7
5	5	15	12	5.0	3.7	3.4
5	7	7	232	100.1	98.0	98.0
5	7	9	221	94.9	93.3	93.1
5	7	11	11	4.6	3.9	3.9
5	7	13	29	12.1	12.2	12.4
5	9	9	224	96.3	94.6	94.4

			$F_o$		$F_c$	
After Fleet			Absolute Electron Units	Fd3m	$\bar{F}43m$	
h	k	l				
5	9	11	19	7.9	8.7	8.6
5	9	13	49	20.4	20.6	20.5
5	11	11	132	55.6	56.2	56.3
6	6	6	197	84.3	83.4	83.4
6	6	8	153	64.6	61.7	62.1
6	6	10	148	62.5	61.8	61.8
6	6	12	105	44.0	43.1	43.3
6	6	14	109	45.8	45.4	45.4
6	8	8	< 8	< 3.3	1.0	2.4
6	8	10	108	45.3	43.9	44.0
6	8	12	< 8	< 3.3	1.1	1.7
6	10	10	119	50.0	49.8	49.8
6	10	12	97	40.7	40.2	40.5
7	7	7	< 8	< 3.3	4.0	6.9
7	7	9	17	7.1	7.3	7.4
7	7	11	152	64.3	63.7	63.8
7	7	13	144	60.8	60.6	60.7
7	9	9	36	15.0	14.2	14.3
7	9	11	145	61.2	60.8	60.9
8	8	8	389	177.2	169.6	168.8
8	8	10	< 8	< 3.3	0.7	2.7
8	8	12	128	53.9	55.2	54.4
8	10	10	109	45.7	43.6	43.8
9	9	9	58	24.2	23.3	23.1

APPENDIX VI

STRUCTURE FACTORS FOR MAGNETITE PRODUCED BY FLEET (1981)

h	k	l	F <sub>o</sub>	F <sub>c</sub>	h	k	l	F <sub>o</sub>	F <sub>c</sub>	h	k	l	F <sub>o</sub>	F <sub>c</sub>
0	0	4	467	473	2	2	4	285	284	4	4	10	8	0
0	0	8	582	605	2	2	6	272	272	4	4	12	187	183
0	0	12	203	211	2	2	8	196	199	4	4	14	0	0
0	0	16	299	315	2	2	10	190	193	4	6	6	175	171
0	2	2	323	314	2	2	12	130	132	4	6	8	8	0
0	2	6	241	249	2	2	14	130	132	4	6	10	142	142
0	2	10	164	168	2	2	16	96	95	4	6	12	12	0
0	2	14	108	108	2	4	4	9	1	4	6	14	91	88
0	4	4	680	648	2	4	6	226	225	4	8	8	207	210
0	4	8	293	303	2	4	8	10	0	4	8	10	0	0
0	4	12	402	421	2	4	10	148	147	4	8	12	340	342
0	4	16	129	129	2	4	12	0	0	4	8	14	0	0
0	6	6	202	207	2	4	14	112	111	4	10	10	94	94
0	6	10	129	130	2	4	16	0	0	4	10	12	0	0
0	6	14	111	113	2	6	6	230	229	5	5	5	344	343
0	8	8	447	465	2	6	8	161	161	5	5	7	48	46
0	8	12	155	162	2	6	10	164	166	5	5	9	70	70
0	10	10	125	126	2	6	12	120	119	5	5	11	197	194
1	1	1	145	147	2	6	14	118	120	5	5	13	205	199
1	1	3	437	424	2	8	8	0	1	5	5	15	12	9
1	1	5	422	432	2	8	10	125	127	5	7	7	232	227
1	1	7	51	50	2	8	12	0	1	5	7	9	221	218
1	1	9	71	74	2	8	14	91	91	5	7	11	11	9
1	1	11	223	227	2	10	10	128	132	5	7	13	29	29
1	1	13	215	219	2	10	12	94	96	5	9	9	224	220
1	1	15	0	6	3	3	3	404	398	5	9	11	19	21
1	3	3	73	72	3	3	5	380	377	5	9	13	49	48
1	3	5	88	89	3	3	7	32	27	5	11	11	132	135
1	3	7	334	327	3	3	9	49	47	6	6	6	197	192
1	3	9	291	296	3	3	11	206	204	6	6	8	153	146
1	3	11	16	15	3	3	13	195	195	6	6	10	148	146
1	3	13	39	40	3	3	15	8	1	6	6	12	105	102
1	3	15	144	146	3	5	5	363	358	6	6	14	109	110
1	5	5	99	101	3	5	7	37	37	6	8	8	0	0
1	5	7	301	307	3	5	9	58	58	6	8	10	108	104
1	5	9	284	288	3	5	11	200	199	6	8	12	0	0
1	5	11	22	22	3	5	13	199	196	6	10	10	119	120
1	5	13	51	51	3	5	15	9	5	6	10	12	97	97
1	5	15	143	144	3	7	7	238	237	7	7	7	0	7
1	7	7	23	21	3	7	9	220	221	7	7	9	17	19
1	7	9	36	37	3	7	11	14	5	7	7	11	152	150
1	7	11	175	180	3	7	13	23	22	7	7	13	144	146
1	7	13	172	176	3	9	9	216	218	7	9	9	36	34
1	7	15	0	1	3	9	11	14	15	7	9	11	145	146
1	9	9	58	59	3	9	13	39	38	8	8	8	389	372
1	9	11	170	175	3	9	13	39	38	8	8	10	0	0
1	9	13	177	181	3	11	11	135	137	8	8	12	128	130
1	11	11	0	2	4	4	4	383	385	8	10	10	109	105
2	2	2	277	289	4	4	6	8	0	9	9	9	58	54
					4	4	8	534	523					

## APPENDIX VII

STRUCTURE FACTORS FOR MAGNETITE SPECIMEN BMDM11

h	k	l	Number of Equivalents	F <sub>o</sub>	F <sub>c</sub>		
					Fd3m	F $\bar{4}$ 3m	F $\bar{4}$ 3m*
0	0	4	3	310.70	311.86	311.89	311.90
0	0	8	3	334.89	330.13	330.01	330.00
0	0	12	3	87.14	86.24	86.31	86.31
0	0	16	3	129.94	131.88	131.78	131.76
0	0	20	3	32.03	32.63	32.61	32.60
0	2	2	6	174.37	166.22	166.18	166.19
0	2	6	12	110.08	109.94	109.85	109.84
0	2	10	12	69.77	70.21	70.13	70.13
0	2	14	12	43.85	44.26	44.16	44.14
0	2	18	12	33.63	33.61	33.58	33.59
0	2	22	12	20.94	21.14	21.17	21.17
0	4	4	6	495.24	470.71	470.62	470.61
0	4	8	12	131.72	129.80	129.87	129.87
0	4	12	12	183.83	185.25	185.13	185.11
0	4	16	12	50.95	51.16	51.20	51.19
0	4	20	12	82.33	83.22	83.20	83.20
0	6	6	6	88.40	88.31	88.24	88.26
0	6	10	12	54.03	54.01	53.88	53.85
0	6	14	12	46.04	45.67	45.62	45.64
0	6	18	12	26.53	26.29	26.24	26.22
0	8	8	6	215.94	214.78	214.65	214.64
0	8	12	12	64.88	65.10	65.16	65.16
0	8	16	12	108.03	109.02	108.96	108.94
0	8	20	12	26.03	26.19	26.14	26.12
0	10	10	6	51.66	51.27	51.22	51.25
0	10	14	12	29.71	29.34	29.25	29.22
0	10	18	12	30.80	30.69	30.74	30.77
0	12	12	6	120.31	119.73	119.65	119.64
0	12	16	12	32.56	32.72	32.71	32.70
0	14	14	6	33.66	33.67	33.70	33.73
1	1	1	4	67.89	71.08	70.73	70.73
1	1	3	12	280.99	267.52	267.57	267.56
1	1	5	12	234.90	232.95	232.56	232.56
1	1	7	10	22.74	20.34	20.66	20.63
1	1	9	12	30.00	30.16	29.99	30.00
1	1	11	12	95.22	95.72	95.78	95.76
1	1	13	12	89.86	91.29	91.00	91.00
1	1	15	12	4.77	2.01	4.12	3.94
1	1	17	12	14.23	13.45	13.46	13.49
1	1	19	12	40.76	40.77	40.89	40.87
1	1	21	12	43.03	43.15	43.03	43.04
1	3	3	10	30.45	29.53	29.91	29.90

\* Structure factors in this column were produced with the Fd3m forbidden reflexions included in the refinement

h	k	l	Number of Equivalents	F <sub>o</sub>	F <sub>c</sub>		
					Fd3m	F $\bar{4}$ 3m	F $\bar{4}$ 3m*
1	3	5	22	37.91	37.25	37.11	37.11
1	3	7	24	147.46	147.49	147.71	147.71
1	3	9	24	127.18	128.72	128.44	128.43
1	3	11	20	6.50	5.86	6.42	6.38
1	3	13	24	16.63	16.04	15.90	15.89
1	3	15	24	58.57	59.02	59.19	59.21
1	3	17	24	59.35	59.95	59.78	59.77
1	3	19	24	2.98	1.87	2.79	2.69
1	3	21	24	6.27	6.68	6.63	6.61
1	5	5	12	43.48	42.13	41.90	41.90
1	5	7	24	136.42	136.13	136.01	135.99
1	5	9	24	125.18	124.27	124.00	123.98
1	5	11	24	9.01	8.45	8.95	8.86
1	5	13	24	20.91	20.53	20.49	20.49
1	5	15	24	57.31	58.12	58.12	58.10
1	5	17	24	60.66	61.44	61.29	61.27
1	5	19	24	2.94	0.96	3.54	3.36
1	5	21	24	8.76	9.05	9.24	9.26
1	7	7	12	8.76	8.14	8.68	8.65
1	7	9	24	15.01	14.76	14.76	14.73
1	7	11	24	74.10	74.20	74.45	74.45
1	7	13	24	71.01	71.76	71.54	71.53
1	7	15	20	< 3.23	1.11	2.11	2.05
1	7	17	24	4.32	7.31	7.33	7.29
1	7	19	24	35.37	35.31	35.58	35.60
1	9	9	12	25.01	24.00	23.96	23.96
1	9	11	24	71.00	71.47	71.33	71.31
1	9	13	24	74.11	74.28	74.16	74.12
1	9	15	19	4.44	2.31	3.79	3.59
1	9	17	24	12.98	13.30	13.44	13.45
1	11	11	10	3.32	0.99	1.99	1.96
1	11	13	24	5.51	5.63	5.99	5.89
1	11	15	24	42.49	41.91	42.21	42.23
1	11	17	24	41.04	41.21	41.11	41.10
1	11	19	24	2.74	2.57	3.08	3.08
1	13	13	12	14.97	15.09	15.23	15.23
1	13	15	24	40.71	40.62	40.56	40.55
1	13	17	24	43.96	44.41	44.49	44.43
1	15	15	12	3.96	2.49	2.95	2.96
2	2	2	4	132.00	126.32	126.33	126.33
2	2	4	12	135.13	132.72	132.65	132.62
2	2	6	12	122.68	124.03	123.93	123.92
2	2	8	12	86.21	84.88	84.87	84.89
2	2	10	12	80.56	82.29	82.34	82.34
2	2	12	12	53.87	54.17	54.04	54.01
2	2	14	12	53.04	53.73	53.55	53.54
2	2	16	12	39.51	38.19	38.28	38.29
2	2	18	12	36.87	36.94	37.16	37.17
2	2	20	12	26.21	26.57	26.54	26.52
2	4	4	10	< 4.34	0.08	1.60	1.44

\* Structure factors in this column were produced with the Fd3m forbidden reflexions included in the refinement

h	k	l	Number of Equivalents	F <sub>o</sub>	F <sub>c</sub>		
					Fd3m	F $\bar{4}$ 3m	F $\bar{4}$ 3m*
2	4	6	24	98.55	97.58	97.55	97.56
2	4	8	22	< 4.00	0.23	1.83	1.99
2	4	10	24	61.13	61.36	61.22	61.20
2	4	12	22	3.61	0.24	2.78	2.84
2	4	14	24	44.86	45.00	44.98	44.98
2	4	16	24	3.22	0.21	3.04	3.15
2	4	18	24	29.81	29.81	29.73	29.73
2	4	20	24	4.06	0.20	3.39	3.53
2	6	6	12	99.58	100.29	100.32	100.32
2	6	8	24	67.68	67.52	67.38	67.36
2	6	10	24	68.82	69.65	69.50	69.49
2	6	12	24	49.24	48.97	49.01	49.02
2	6	14	24	48.35	48.39	48.57	48.57
2	6	16	24	34.40	34.52	34.42	34.40
2	6	18	24	33.88	34.05	33.91	33.91
2	6	20	24	25.11	25.05	25.24	25.25
2	8	8	9	< 3.75	0.38	2.72	2.74
2	8	10	24	52.63	52.36	52.36	52.37
2	8	12	18	3.42	0.38	2.74	2.85
2	8	14	24	37.01	36.79	36.66	36.65
2	8	16	21	3.09	0.38	3.48	3.59
2	8	18	24	29.15	28.79	28.88	28.88
2	8	20	24	2.77	0.36	3.21	3.30
2	10	10	12	53.04	53.78	53.95	53.95
2	10	12	24	38.57	38.80	38.67	38.65
2	10	14	24	40.29	40.28	40.13	40.12
2	10	16	24	30.93	30.53	30.67	30.67
2	10	18	24	29.21	29.06	29.39	29.40
2	12	12	9	4.49	0.46	3.50	3.60
2	12	14	24	32.34	32.02	32.13	32.12
2	12	16	24	2.90	0.49	3.18	3.27
2	12	18	24	21.90	22.14	22.09	22.10
2	14	14	12	31.73	31.50	31.82	31.82
2	14	16	24	23.02	23.18	23.13	23.13
3	3	3	4	203.73	202.53	203.07	203.05
3	3	5	12	181.96	180.95	180.81	180.83
3	3	7	12	10.88	11.09	12.07	12.04
3	3	9	10	19.18	18.86	18.76	18.79
3	3	11	12	84.39	85.28	85.59	85.57
3	3	13	12	79.92	80.41	80.05	80.09
3	3	15	12	3.32	1.01	3.98	3.93
3	3	17	9	7.02	8.61	8.70	8.72
3	3	19	12	38.47	38.32	38.55	38.55
3	3	21	12	38.19	38.65	38.43	38.50
3	5	5	12	166.84	165.05	164.77	164.76
3	5	7	24	13.89	14.73	14.90	14.90
3	5	9	24	23.61	23.44	23.30	23.29
3	5	11	24	81.88	82.22	82.18	82.21
3	5	13	24	80.61	80.96	80.77	80.75
3	5	15	24	3.27	1.36	2.68	2.53

\* Structure factors in this column were produced with the Fd3m forbidden reflexions included in the refinement

h	k	l	Number of Equivalents	$F_o$	$F_c$		
					Fd3m	$\bar{F}43m$	$\bar{F}43m^*$
3	5	17	22	11.16	11.69	11.57	11.56
3	5	19	24	37.32	37.53	37.62	37.67
3	5	21	24	38.93	39.56	39.60	39.59
3	7	7	12	101.50	101.06	101.47	101.46
3	7	9	24	92.65	92.78	92.52	92.57
3	7	11	24	3.55	1.79	4.39	4.40
3	7	13	24	8.93	8.31	8.42	8.43
3	7	15	24	49.94	49.90	50.21	50.21
3	7	17	24	49.78	49.16	48.84	48.92
3	7	19	21	2.87	2.60	4.51	4.52
3	9	9	12	91.07	91.22	91.04	91.01
3	9	11	24	4.85	5.36	5.76	5.72
3	9	13	24	16.04	15.35	15.25	15.23
3	9	15	24	48.47	48.36	48.26	48.32
3	9	17	24	51.09	51.31	51.34	51.30
3	9	19	22	< 2.80	1.27	2.78	2.62
3	11	11	12	54.99	54.92	55.27	55.27
3	11	13	24	53.33	53.12	52.85	52.93
3	11	15	24	4.27	2.36	4.46	4.50
3	11	17	24	2.87	2.54	3.45	3.38
3	13	13	12	56.46	56.06	56.09	56.04
3	13	15	20	< 2.91	0.80	2.64	2.47
3	13	17	24	9.18	8.99	8.95	8.93
3	15	15	12	31.64	31.02	31.32	31.35
4	4	4	4	180.58	180.34	180.40	180.40
4	4	6	9	< 4.10	0.10	1.18	1.65
4	4	8	12	262.38	258.27	258.13	258.13
4	4	10	9	3.75	0.08	3.05	2.73
4	4	12	12	74.88	74.31	74.36	74.36
4	4	14	12	< 3.37	0.04	2.42	2.90
4	4	16	12	118.91	119.69	119.59	119.58
4	4	18	10	3.01	0.03	3.61	3.45
4	4	20	12	29.67	29.24	29.19	29.18
4	6	6	12	73.25	72.15	72.00	71.97
4	6	8	20	3.83	0.19	2.69	2.54
4	6	10	24	58.16	58.38	58.35	58.37
4	6	12	19	< 3.48	0.19	2.64	2.85
4	6	14	24	36.08	35.80	35.66	35.64
4	6	16	24	3.13	0.19	3.19	3.30
4	6	18	24	32.36	32.20	32.25	32.27
4	6	20	24	2.80	0.18	3.42	3.50
4	8	8	12	87.53	86.28	86.34	86.34
4	8	10	20	3.54	0.12	2.31	2.68
4	8	12	24	146.60	146.17	146.05	146.04
4	8	14	22	3.22	0.08	3.39	3.26
4	8	16	24	40.40	40.84	40.84	40.83
4	8	18	22	2.90	0.06	3.14	3.45
4	8	20	24	68.78	69.89	69.89	69.89
4	10	10	12	38.89	38.38	38.23	38.19

\* Structure factors in this column were produced with the Fd3m forbidden reflexions included in the refinement

h	k	l	Number of Equivalents	F <sub>o</sub>	F <sub>c</sub>		
					Fd3m	F $\bar{4}$ 3m	F $\bar{4}$ 3m*
4	10	12	24	3.27	0.14	3.17	3.16
4	10	14	24	39.14	38.96	39.00	39.02
4	10	16	23	2.98	0.15	3.39	3.52
4	10	18	24	20.18	20.00	19.94	19.93
4	12	12	12	46.76	45.71	45.72	45.72
4	12	14	21	3.01	0.10	3.23	3.47
4	12	16	24	83.33	83.31	83.27	83.27
4	12	18	24	3.87	0.07	3.28	3.33
4	14	14	12	21.27	21.01	20.92	20.90
4	14	16	24	2.77	0.11	3.16	3.29
5	5	5	4	154.48	154.51	154.24	154.20
5	5	7	10	20.35	18.70	18.70	18.67
5	5	9	12	29.06	28.67	28.60	28.59
5	5	11	12	80.55	80.49	80.38	80.35
5	5	13	12	82.60	82.37	82.23	82.18
5	5	15	12	4.56	3.00	4.30	4.09
5	5	17	12	15.27	15.12	15.22	15.23
5	5	19	12	36.75	37.02	37.07	37.04
5	7	7	12	97.09	95.89	95.88	95.91
5	7	9	24	91.89	91.25	91.05	91.02
5	7	11	20	3.49	3.17	3.86	3.80
5	7	13	24	11.98	11.54	11.50	11.46
5	7	15	24	49.14	48.90	48.99	49.03
5	7	17	24	50.06	49.99	49.92	49.89
5	7	19	24	2.84	2.02	2.94	2.85
5	9	9	12	92.73	92.23	92.10	92.04
5	9	11	24	5.84	8.04	8.29	8.20
5	9	13	24	19.63	19.49	19.57	19.56
5	9	15	24	47.74	48.21	48.18	48.14
5	9	17	24	53.02	52.92	52.94	52.88
5	9	19	24	2.77	0.35	2.96	2.78
5	11	11	12	53.79	53.72	53.82	53.86
5	11	13	24	53.61	53.49	53.39	53.36
5	11	15	21	2.98	1.60	2.53	2.47
5	11	17	24	4.01	4.33	4.62	4.54
5	13	13	12	58.26	57.82	57.85	57.78
5	13	15	24	4.06	2.23	3.30	3.14
5	13	17	24	11.61	11.55	11.79	11.79
5	15	15	12	30.40	30.16	30.38	30.43
6	6	6	4	83.30	82.32	82.19	82.18
6	6	8	12	61.38	60.81	60.81	60.82
6	6	10	12	60.85	60.58	60.74	60.73
6	6	12	12	42.87	41.73	41.60	41.57
6	6	14	12	44.28	44.01	43.86	43.84
6	6	16	12	33.91	33.56	33.68	33.69
6	6	18	12	31.59	31.45	31.79	31.78
6	6	20	12	22.07	22.18	22.16	22.14
6	8	8	9	< 3.61	0.29	2.37	2.60
6	8	10	24	43.16	42.54	42.38	42.35

\* Structure factors in this column were produced with the Fd3m forbidden reflexions included in the refinement

h	k	l	Number of Equivalents	F <sub>o</sub>	F <sub>c</sub>		
					Fd3m	$\overline{F43m}$	$\overline{F43m}^*$
6	8	12	24	3.32	0.33	3.21	3.26
6	8	14	24	38.79	38.33	38.39	38.40
6	8	16	20	3.01	0.34	3.25	3.36
6	8	18	24	22.88	22.74	22.66	22.65
6	10	10	12	49.27	48.44	48.30	48.28
6	10	12	24	39.47	38.92	39.01	39.02
6	10	14	24	37.12	37.03	37.38	37.36
6	10	16	24	26.37	25.96	25.88	25.86
6	10	18	24	26.84	26.88	26.82	26.81
6	12	12	10	3.09	0.40	3.16	3.27
6	12	14	24	26.37	26.16	26.06	26.05
6	12	16	24	2.83	0.44	3.49	3.64
6	14	14	12	29.35	29.11	29.05	29.04
6	14	16	24	23.77	24.01	24.22	24.22
7	7	7	4	6.37	2.77	5.04	5.07
7	7	9	12	7.93	6.86	7.11	7.10
7	7	11	12	61.96	60.78	61.20	61.20
7	7	13	12	59.21	58.40	58.10	58.18
7	7	15	12	4.38	2.27	4.49	4.54
7	7	17	10	4.16	3.26	3.94	3.89
7	7	19	12	31.27	30.93	31.25	31.27
7	9	9	12	12.83	13.47	13.43	13.39
7	9	11	24	58.72	58.45	58.31	58.38
7	9	13	24	60.10	59.79	59.73	59.69
7	9	15	24	< 3.02	0.49	2.40	2.24
7	9	17	20	6.42	7.59	7.60	7.56
7	11	11	10	4.50	2.09	4.45	4.53
7	11	13	21	3.05	2.00	3.07	2.97
7	11	15	24	37.55	36.50	36.87	36.89
7	11	17	24	34.00	34.56	34.35	34.45
7	13	13	12	7.78	8.73	8.74	8.70
7	13	15	24	34.87	34.47	34.36	34.46
8	8	8	4	166.03	163.44	163.30	163.29
8	8	10	9	< 3.37	0.20	3.20	3.13
8	8	12	12	52.66	51.23	51.24	51.24
8	8	14	12	4.37	0.14	3.05	3.33
8	8	16	12	90.62	91.02	90.95	90.96
8	8	18	12	2.80	0.11	3.40	3.41
8	10	10	12	42.86	42.42	42.47	42.48
8	10	12	21	3.13	0.25	3.11	3.30
8	10	14	24	25.31	25.27	25.15	25.13
8	10	16	24	2.87	0.27	3.30	3.45
8	10	18	24	26.15	26.27	26.43	26.44
8	12	12	12	100.04	99.57	99.48	99.48
8	12	14	24	4.11	0.19	3.34	3.41
8	12	16	24	25.74	26.26	26.18	26.18
8	14	14	12	28.47	28.77	28.91	28.93
9	9	9	4	22.78	22.19	22.26	22.25
9	9	11	12	58.63	58.60	58.51	58.47
9	9	13	12	63.54	63.27	63.29	63.21

\* Structure factors in this column were produced with the Fd3m forbidden reflexions included in the refinement

h	k	l	Number of Equivalents	F <sub>o</sub>	F <sub>c</sub>		
					Fd3m	F $\bar{4}$ 3m	F $\bar{4}$ 3m*
9	9	15	12	4.16	2.80	3.74	3.57
9	9	17	12	13.14	13.04	13.26	13.26
9	11	11	10	3.10	0.63	2.34	2.21
9	11	13	24	4.21	6.01	6.22	6.14
9	11	15	24	35.06	34.84	34.87	34.95
9	13	13	12	15.19	14.71	14.92	14.91
9	13	15	24	33.94	34.49	34.56	34.52
10	10	10	4	41.15	40.31	40.67	40.64
10	10	12	12	28.05	27.65	27.53	27.51
10	10	14	12	31.19	31.52	31.46	31.44
10	10	16	12	26.19	26.28	26.47	26.47
10	12	12	12	2.94	0.33	3.38	3.50
10	12	14	24	28.25	28.38	28.55	28.55
11	11	11	4	42.49	39.68	40.09	40.11
11	11	13	12	37.65	37.57	37.42	37.53
11	11	15	12	3.92	2.78	4.66	4.74
11	13	13	12	38.09	38.38	38.47	38.42
12	12	12	4	30.48	29.34	29.27	29.27
12	12	14	12	2.73	0.24	3.34	3.45

\* Structure factors in this column were produced with the Fd3m forbidden reflexions included in the refinement

APPENDIX VIII

STRUCTURE FACTORS FOR TITANOMAGHEMITE SPECIMEN BM1929,1687

h	k	l	F <sub>o</sub>	F <sub>c</sub>	h	k	l	F <sub>o</sub>	F <sub>c</sub>
0	0	4	244.88	237.09	0	6	10	53.88	53.18
0	0	8	272.74	260.15	0	7	7	3.64	3.23
0	1	1	20.61	21.60	0	7	8	27.58	27.50
0	1	2	23.48	25.49	0	7	9	7.78	8.69
0	1	3	25.11	25.05	0	8	8	157.17	157.03
0	1	4	11.98	13.07	1	1	1	30.68	29.14
0	1	5	8.30	8.70	1	1	2	28.52	30.93
0	1	6	27.49	25.64	1	1	3	222.93	221.74
0	1	7	12.49	11.54	1	1	4	8.45	8.16
0	1	8	34.15	33.00	1	1	5	192.70	191.44
0	1	9	< 3.73	4.08	1	1	6	18.97	17.70
0	1	10	< 3.62	0.67	1	1	7	3.94	2.74
0	1	11	23.05	23.05	1	1	8	7.67	8.83
0	2	2	155.32	156.52	1	1	9	10.54	10.09
0	2	3	18.14	18.10	1	1	10	6.27	7.75
0	2	4	< 4.21	0.31	1	1	11	69.24	69.49
0	2	5	30.01	29.93	1	2	2	18.32	19.29
0	2	6	106.43	104.83	1	2	3	11.28	9.40
0	2	7	< 3.93	1.92	1	2	4	26.20	26.99
0	2	8	< 3.82	0.69	1	2	5	36.32	37.69
0	2	9	15.76	15.28	1	2	6	16.58	16.98
0	2	10	61.00	59.28	1	2	7	11.09	12.77
0	2	11	3.50	2.22	1	2	8	16.63	16.57
0	3	3	11.95	11.59	1	2	9	29.66	29.84
0	3	4	26.62	29.11	1	2	10	24.69	24.48
0	3	5	15.26	13.89	1	2	11	14.41	13.70
0	3	6	< 3.99	1.18	1	3	3	4.21	3.51
0	3	7	31.85	31.88	1	3	4	15.52	14.99
0	3	8	18.94	18.50	1	3	5	12.87	12.55
0	3	9	3.68	4.04	1	3	6	7.96	6.64
0	3	10	13.87	14.45	1	3	7	114.63	112.97
0	3	11	< 3.48	3.86	1	3	8	13.64	13.32
0	4	4	387.88	388.79	1	3	9	101.69	101.51
0	4	5	17.06	17.43	1	3	10	< 3.58	3.27
0	4	6	< 3.93	0.58	1	3	11	12.03	10.23
0	4	7	12.74	12.24	1	4	4	30.03	31.94
0	4	8	81.18	80.30	1	4	5	10.61	9.98
0	4	9	< 3.64	0.72	1	4	6	11.11	10.50
0	4	10	< 3.54	0.52	1	4	7	24.56	24.17
0	5	5	5.59	4.58	1	4	8	12.95	12.74
0	5	6	10.95	10.89	1	4	9	14.56	13.93
0	5	7	16.49	15.92	1	4	10	15.02	15.36
0	5	8	5.22	5.78	1	5	5	16.73	15.20
0	5	9	24.66	24.16	1	5	6	22.86	22.62
0	5	10	15.66	16.32	1	5	7	107.80	107.99
0	6	6	73.50	73.52	1	5	8	5.21	5.86
0	6	7	10.50	10.77	1	5	9	91.34	91.85
0	6	8	< 3.63	1.55	1	6	6	29.59	29.50
0	6	9	16.22	16.64	1	6	7	8.29	8.74

h	k	l	F <sub>o</sub>	F <sub>c</sub>	h	k	l	F <sub>o</sub>	F <sub>c</sub>
1	6	8	14.94	14.89	3	4	6	17.31	16.94
1	6	9	23.98	24.04	3	4	7	6.55	7.18
1	7	7	10.90	10.86	3	4	8	33.01	32.79
1	7	8	9.41	10.79	3	4	9	6.23	9.37
1	7	9	4.91	4.20	3	4	10	6.06	7.34
1	8	8	28.50	27.54	3	5	5	131.32	132.26
2	2	2	55.38	51.98	3	5	6	17.03	16.39
2	2	3	5.99	5.72	3	5	7	< 3.73	2.55
2	2	4	124.25	125.84	3	5	8	11.51	11.21
2	2	5	7.08	5.46	3	5	9	6.15	6.96
2	2	6	72.70	71.27	3	5	10	9.78	10.77
2	2	7	6.75	8.27	3	6	6	7.48	8.53
2	2	8	76.29	76.00	3	6	7	12.68	12.85
2	2	9	9.76	9.72	3	6	8	11.88	10.87
2	2	10	47.16	46.86	3	6	9	19.15	18.68
2	2	11	< 3.48	0.67	3	7	7	69.73	69.13
2	3	3	13.88	13.60	3	7	8	19.25	19.83
2	3	4	13.03	13.42	4	4	4	121.89	121.98
2	3	5	24.27	24.28	4	4	5	3.90	4.89
2	3	6	22.03	22.05	4	4	6	< 3.82	2.00
2	3	7	18.93	19.72	4	4	7	23.64	23.78
2	3	8	13.57	13.84	4	4	8	195.05	196.05
2	3	9	24.84	24.49	4	4	9	10.68	10.19
2	3	10	15.92	15.52	4	4	10	< 3.47	1.16
2	3	11	17.64	17.72	4	5	5	17.58	18.53
2	4	4	4.06	3.51	4	5	6	19.91	20.05
2	4	5	21.10	20.67	4	5	7	12.76	12.56
2	4	6	86.01	86.78	4	5	8	23.34	22.33
2	4	7	8.53	9.27	4	5	9	< 3.52	2.57
2	4	8	5.26	4.30	4	6	6	69.74	70.04
2	4	9	16.60	16.04	4	6	7	5.12	6.50
2	4	10	55.74	56.04	4	6	8	< 3.54	3.45
2	5	5	35.28	35.68	4	6	9	9.16	9.43
2	5	6	24.60	23.36	4	7	7	24.89	25.25
2	5	7	14.06	13.51	4	7	8	17.06	16.20
2	5	8	15.56	15.90	5	5	5	114.22	116.44
2	5	9	29.05	28.99	5	5	6	27.50	26.89
2	5	10	17.75	17.02	5	5	7	5.14	4.35
2	6	6	59.48	58.40	5	5	8	< 3.56	4.05
2	6	7	7.38	7.52	5	5	9	6.94	6.10
2	6	8	61.53	61.31	6	6	6	45.50	47.55
2	6	9	9.31	9.76	6	6	7	15.34	15.07
2	7	7	20.78	20.87	6	6	8	48.04	48.33
2	7	8	7.92	9.70	6	7	7	18.62	18.46
2	7	9	17.29	17.39					
3	3	3	159.52	158.35					
3	3	4	29.69	29.25					
3	3	5	145.42	147.29					
3	3	6	8.77	9.60					
3	3	7	13.26	13.64					
3	3	8	5.28	6.72					
3	3	9	5.14	5.89					
3	3	10	5.00	3.46					
3	4	4	17.52	17.67					
3	4	5	8.83	8.13					

## REFERENCES

Aharoni, A., Frei, E.H., and Schieber, M. 1962. Curie point and origin of weak ferromagnetism in haematite. *Phys. Rev.* 127, 439-441.

Akimoto, S., and Katsura, T. 1959. Magneto-chemical study of the generalized titanomagnetite in volcanic rocks. *J. Geomag. Geoelect.* 3, 69-90.

Akimoto, S., Katsura, T., and Yoshida, M. 1957. Magnetic properties of the  $\text{Fe}_2\text{TiO}_4$ - $\text{Fe}_3\text{O}_4$  system and their change with oxidation. *J. Geomag. Geoelect.* 9, 165-178.

Annersten, H., and Hafner, S.S. 1973. Vacancy distribution in synthetic spinels of the series  $\text{Fe}_3\text{O}_4$ - $\gamma$ - $\text{Fe}_2\text{O}_3$ . *Z. Krist.* 137, 321-340.

Armstrong, R.J., Morrish, A.H., and Sawatzky, G.A. 1966. Mössbauer study of ferric ions in a spinel. *Phys. Lett.* 23, 414-416.

Arnott, R.J., Wold, A., and Rogers, D.B. 1964. Electron ordering transitions in several chromium spinel systems. *J. Phys. Chem. Solids* 25, 161-166.

Balko, B., and Hoy, G.R. 1977. Selective excitation double Mössbauer studies (SEDM) of the electron hopping in magnetite ( $\text{Fe}_3\text{O}_4$ ). *Physica* 86-88B, 953-954.

Bancroft, G.M., Maddock, A.G., Ong, W.K., Prince, R.H., and Stone, A.J. 1967. Mössbauer spectra of iron III diketone complexes. *J. Chem. Soc.* A1976, 1966-1971.

Barth, T.F.W., and Posnjak, E. 1931. Spinel structure: an example of variate-atom equipoints. *J. Washington Acad. Sci.* 21, 255-258.

Basta, E.Z. 1959. Some mineralogical relationships in the system  $\text{Fe}_2\text{O}_3$ - $\text{Fe}_3\text{O}_4$  and the composition of titanomaghemite. *Econ. Geol.* 54, 698-719.

Bauminger, R., Cohen, S.G., Marinov, A., Ofer, S., and Segal, E. 1961. Study of the low-temperature transition in magnetite and the internal fields acting on iron nuclei in some spinel ferrites, using Mössbauer absorption. *Phys. Rev.* 122, 1447-1450.

Behar, I., and Collongues, R. 1957. Sur la transformation ordre-désordre dans la phase sesquioxyde de fer cubique. C.R. Acad. Sci. (Paris) 244, 617-619.

Bernal, J.D., Dasgupta, D.R., and Mackay, A.L. 1957. Oriented transformations in iron oxides and hydroxides. Nature 180, 645-647.

Bernal, J.D., Dasgupta, D.R., and Mackay, A.L. 1959. The oxides and hydroxides of iron and their structural interrelationships. Clay. Min. Bull. 4, 15-30.

Bindloss, W. 1971. Anomalous exchangestriction in ferromagnetic pyrite and chromium chalcogenide spinel compounds. J. Appl. Phys. 42, 1474-1475.

Blasse, G. 1964. Crystal chemistry and some magnetic properties of mixed metal oxides with spinel structure. Philips Res. Rep. Suppl. no. 3.

Bleaney, B.I., and Bleaney, B. 1978. Electricity and Magnetism. Revised edition, Oxford University Press, Oxford.

Bloch, D. 1966. The  $10/3$  law for the volume dependence of superexchange. J. Phys. Chem. Solids 27, 881-885.

Boehm, J.M., Prager, P.R., and Barnea, Z. 1974. The effect of surface damage on the intensity of X-rays diffracted by ground spherical single crystals. Acta Cryst. A30, 335-337.

Bond, W.L. 1951. Making small spheres. Rev. Sci. Inst. 22, 344-345.

Boppart, H., Schlegel, A., and Wachter, P. 1980. Optical properties of magnetite,  $Fe_3O_4$ . Phil. Mag. B42, 431-432.

Borrelli, N.F. 1975. Uniaxial anisotropy in  $MgFe_{2-\gamma}Al_{\gamma}O_4$ . J. Appl. Phys. 46, 430-435.

Brabers, V.A.M. 1969. Infrared spectra of cubic and tetragonal manganese ferrites. Phys. Stat. Solidi 33, 563-572.

Brabers, V.A.M. 1971. Cation migration, cation valencies and the cubic-tetragonal transition in  $Mn_xFe_{3-x}O_4$ . J. Phys. Chem. Solids 32, 2181-2191.

Bragg, W.H. 1915a. The structure of magnetite and the spinels. *Nature* 95, 561.

Bragg, W.H. 1915b. The structure of the spinel group of crystals. *Phil. Mag.* 30, 305-315.

Braun, P. 1952. A superstructure in spinels. *Nature* 170, 1123.

Buddington, A.F., Fahey, J., and Vlisidis, A. 1955. Thermometric and petrogenetic significance of titaniferous magnetite. *Am. J. Sci.* 253, 497-532.

Buddington, A.F., and Lindsley, D.H. 1964. Iron-titanium oxide minerals and synthetic equivalents. *J. Petrol.* 5, 310-357.

Byer, N.E., and Sack, H.S. 1966. Symmetry of paraelectric defects in alkali halides ( $\text{Li}^+$  in KCl). *Phys. Rev. Lett.* 17, 72-74.

Cervinka, L. 1965. Comparison of lattice vibrations in nickel and manganese-ferrite single crystals. *Czech. J. Phys.* B15, 425-427.

Cervinka, L., and Vetterkind, D. 1968. The influence of low temperature (293 K-4.5 K) on the structure of manganese-rich manganese ferrite. *J. Phys. Chem. Solids* 29, 171-179.

Chevallier, R.J., Bolfa, J., and Mathieu, S. 1955. Titanomagnétites et ilmenites ferromagnétiques (1). Etude optique, radiocristallographique, chimique. *Bull. Soc. Franc. Mineral. Crist.* 78, 307-346.

Chikazumi, S., Chiba, K., Suzuki, K., and Yamada, T. 1971. Electron-microscopic observation of the low-temperature phase of magnetite. *Proceedings of the International Ferrite Conference*, Tokyo University Press, Japan.

Claassen, A.A. 1926. The scattering power of oxygen and iron for X-rays. *Proc. Phys. Soc.* 38, 482-487.

Coey, J.M.D., and Khalafalla, D. 1972. Superparamagnetic  $\gamma\text{-Fe}_2\text{O}_3$ . *Phys. Stat. Solidi* 11, 229-241.

Coey, J.M.D., Morrish, A.H., and Sawatzky, G.A. 1971. Mössbauer study of conduction in magnetite. *J. Phys. (Paris) Colloq.* 32, C271-C273.

Colombo, U., Fagherazzi, G., Gazzarrini, F., Lanzavecchia, G., and Sironi, G. 1964. Mechanisms in the first stage of oxidation of magnetites. *Nature* 202, 175-176.

Colombo, U., Gazzarrini, F., Lanzavecchia, G., and Sironi, G. 1965. Magnetite oxidation: a proposed mechanism. *Science* 147, 1033.

Coster, D., Knol, K.S., and Prins, J.A. 1930. Reflexion of X-rays from zinc blende. *Z. Phys.* 63, 345-369.

Creer, K.M., and Ibbetson, J.D. 1970. Electron microprobe analyses and magnetic properties of non-stoichiometric titanomagnetites in basaltic rocks. *Geophys. J. R. Astron. Soc.* 21, 485-511.

Cruickshank, D.W.J. 1949. Accuracy of electron density maps in X-ray analysis. *Acta Cryst.* 2, 65-82.

Cruickshank, D.W.J. 1956. The determination of the anisotropic thermal motion of atoms in crystals. *Acta Cryst.* 9, 747-753.

Daniels, J.M., and Rosencwaig, A. 1969. Mössbauer spectroscopy of stoichiometric and non-stoichiometric magnetite. *J. Phys. Chem. Solids* 30, 1561-1571.

Darwin, C.G. 1922. The reflexion of X-rays from imperfect crystals. *Phil. Mag.* 43, 800-829.

Davey, P.T., and Scott, T.R. 1957. Preparation of maghemite by electrolysis. *Nature* 179, 1363.

David, I., and Welch, A.J.E. 1956. The oxidation of magnetite and related spinels. Constitution of gamma ferric oxide. *Trans. Faraday Soc.* 52, 1642-1650.

Day, R., O'Reilly, W., and Banerjee, S.K. 1970. Rotational hysteresis study of oxidized basalts. *J. Geophys. Res.* 75, 375-386.

Deer, W.A., Howie, R.A., and Zussman, J. 1962. *Rock-Forming Minerals: Volume 5. Non-Silicates.* Longman, New York.

Deer, W.A., Howie, R.A., and Zussman, J. 1966. *An Introduction to the Rock-Forming Minerals.* Longman, New York.

Dunitz, J.D., and Orgel, L.E. 1957. Electronic properties of transition metal oxides I. Distortions from cubic symmetry. *J. Phys. Chem. Solids* 3, 20-29.

Dunn, J.A., and Dey, A.K. 1937. Vanadium-bearing titaniferous iron ores in Singhbhum and Mayurbharji, India. *Trans. Mining Geol. Inst. India* 31, 117-184.

Elder, T. 1965. Particle-size effect in oxidation of natural magnetite. *J. Appl. Phys.* 36, 1012-1013.

Elsdon, R. 1975. Iron-titanium oxide minerals in igneous and metamorphic rocks. *Min. Sci. Eng.* 7, 48-70.

Englman, R. 1972. *The Jahn-Teller Effect in Molecules and Crystals*. Wiley, New York.

Evans, B.J., and Hafner, S.S. 1969.  $^{57}\text{Fe}$  hyperfine fields in magnetite ( $\text{Fe}_3\text{O}_4$ ). *J. Appl. Phys.* 40, 1411-1413.

Evans, B.J., Hafner, S.S., and Weber, H.P. 1971. Electric field gradients at  $^{57}\text{Fe}$  in  $\text{ZnFe}_2\text{O}_4$  and  $\text{CdFe}_2\text{O}_4$ . *J. Chem. Phys.* 55, 5282-5288.

Fairweather, A., Roberts, F.F., and Welch, A.J.E. 1952. Ferrites. *Rep. Prog. Phys.* 15, 142-172.

Famery, R., Queyroux, F., and Gilles, J.C. 1979. Etude structurale de la forme ordonnée de  $\text{LiAl}_5\text{O}_8$ . *J. Solid State Chem.* 30, 257-263.

Feitknecht, W. 1965. Einfluss der teilchen grösse auf den mechanismus von festkörperreactionen. *Pure and Appl. Chem.* 9, 423-440.

Feitknecht, W., and Lehmann, H.W. 1959. Über die oxidation von magnetit zu  $\gamma\text{-Fe}_2\text{O}_3$ . *Helv. Chim. Acta* 42, 2035-2039.

Ferguson, G.A., and Hass, M. 1958. Magnetic structure and vacancy distribution in  $\gamma\text{-Fe}_2\text{O}_3$  by neutron diffraction. *Phys. Rev.* 112, 1130-1131.

Finch, G.I., Sinha, A.P.B., and Sinha, K.P. 1958. Crystal distortion in ferrite-manganites. *Proc. Roy. Soc.* A242, 28-35.

Fleet, M.E. 1981. The structure of magnetite. *Acta Cryst.* B37, 917-920.

Fleet, M.E. 1982. The crystal structure of magnetite: defect structure II. Acta Cryst. B38, 1718-1723.

Frölich, F. and Vollstaedt, H. 1967. Untersuchungen zur bestimmung der Curie temperatur von maghemit ( $\gamma$ - $\text{Fe}_2\text{O}_3$ ). Mon. Deut. Akad. Wiss. (Berlin) 9, 180-186.

Gehring, G.A., and Gehring, K.A. 1975. Co-operative Jahn-Teller effects. Rep. Prog. Phys. 38, 1-89.

Gibbons, D.F. 1957. Acoustic relaxations in ferrite single crystals. J. Appl. Phys. 28, 810-814.

Gidskehaug, A. 1975. Method to determine the degree of non-stoichiometry of iron-titanium oxides. Geophys. J. R. Astron. Soc. 41, 255-259.

Gilleo, M.A. 1958. Superexchange interaction energy for  $\text{Fe}^{3+}$ -O- $\text{Fe}^{3+}$  linkages. Phys. Rev. 109, 777-781.

Goodenough, J.B. 1963. Magnetism and the Chemical Bond. Interscience, London.

Goodenough, J.B. 1964. Jahn-Teller distortions induced by tetrahedral site  $\text{Fe}^{2+}$  ions. J. Phys. Chem. Solids 25, 151-160.

Goodenough, J.B., and Loeb, A.L. 1955. Theory of ionic ordering, crystal distortion, and magnetic exchange due to covalent forces in spinels. Phys. Rev. 98, 391-408.

Gorter, E.W. 1954. Saturation magnetization and crystal chemistry of ferrimagnetic oxides. Philips Res. Rep. 9, 295-365.

Greig, J.W., Posnjak, E., Merwin, H.E., and Sosman, R.B. 1935. Equilibrium relationships of  $\text{Fe}_3\text{O}_4$ ,  $\text{Fe}_2\text{O}_3$ , and oxygen. Am. J. Sci. 30, 239-316.

Grimes, N.W. 1971. Structural distortions in  $\text{MgCr}_2\text{O}_4$ . J. Phys. C4, L342-L344.

Grimes, N.W. 1972. 'Off-centre' ions in compounds with spinel structure. Phil. Mag. 26, 1217-1226.

Grimes, N.W. 1973. Antiferroelectricity among compounds with spinel structure. J. Phys. C6, L78-L79.

Grimes, N.W. 1974. On the specific heat of compounds with the spinel structure II. Zinc ferrite, a paramagnetic compound with magnetic ion occupying the octahedral site. Proc. Roy. Soc. A338, 223-233.

Grimes, N.W. 1975. The spinels: versatile materials. Phys. Techn. 6, 22-27.

Grimes, N.W., and Collett, A.J. 1971a. Correlation of infrared spectra with structural distortions in the spinel series  $Mg[Cr_xAl_{2-x}]O_4$ . Phys. Stat. Solidi 43, 591-599.

Grimes, N.W., and Collett, A.J. 1971b. Infrared absorption spectra of ferrites. Nature 230, 158.

Grimes, N.W., and Hilleard, R.J. 1970. X-ray diffraction studies of the spinel series  $Mg[Cr_xAl_{2-x}]O_4$  I. Lattice parameters and structure. J. Phys. C3, 861-871.

Grimes, N.W., Thompson, P., and Kay, H.F. 1983. New symmetry and structure for spinel. Proc. Roy. Soc. A386, 333-345.

Hägg, G. 1935a. The spinels and the cubic sodium tungsten bronzes as new examples of structures with vacant lattice points. Nature 135, 874.

Hägg, G. 1935b. Die kristallstruktur des magnetischen ferrioxys,  $\gamma$ - $Fe_2O_3$ . Z. Phys. Chem. B29, 95-103.

Hamilton, W.C. 1958. Neutron diffraction investigation of the 119 K transition in magnetite. Phys. Rev. 110, 1050-1057.

Hamilton, W.C. 1965. Significance tests on the crystallographic R-factor. Acta Cryst. 18, 502-510.

Hart, T.R., Temkin, H., and Adams, S.B. 1975. In: Light Scattering in Solids (ed. M. Balkanski). Flammarion, Paris.

Haul, R., and Schoon, T. 1939. Zur struktur des ferromagnetischen eisen (III)-oxys  $\gamma$ - $Fe_2O_3$ . Z. Phys. Chem. B44, 216-226.

Hauptman, Z. 1974. High-temperature oxidation, range of non-stoichiometry and Curie point variation of cation-deficient titanomagnetite  $Fe_{2.4}Ti_{0.6}O_{4+\gamma}$ . Geophys. J. R. Astron. Soc. 38, 29-47.

Henning, J.C.M., and van den Boom, H. 1973. ESR investigations of nearest-neighbour  $\text{Cr}^{3+}$ - $\text{Cr}^{3+}$  interactions in Cr-doped spinel  $\text{MgAl}_2\text{O}_4$ . Phys. Rev. B8, 2255-2262.

Henry, W.E., and Boehm, M.J. 1956. Intradomain magnetic saturation and magnetic structure of  $\gamma$ - $\text{Fe}_2\text{O}_3$ . Phys. Rev. 101, 1253-1255.

Heuer, A.H., and Mitchell, T.E. 1975. Further discussion on the space group of spinel. J. Phys. C8, L541-543.

Higgins, J.B., Speer, J.A., and Craig, J.R. 1975. A note on thiospinel space group assignment. Phil. Mag. 30, 683-685.

Hilleard, R.J. 1975. Concerning the structure of  $\text{MgCr}_2\text{O}_4$ . J. Phys. C8, L193-L194.

Hönl, H. 1933a. Atomfaktor für Röntgenstrahlen auf problem der dispersionstheorie (K-schale). Ann. de Phys. 18, 625-655.

Hönl, H. 1933b. Zur dispersionstheorie der Röntgenstrahlen. Z. Phys. 84, 1-16.

Hope, H. 1975. Intensity measurements. In: Anomalous Scattering (ed. S. Ramaseshan and S.C. Abrahams). Munksgaard, Copenhagen.

Howells, E.R., Phillips, D.C., and Rogers, D. 1950. The probability distribution of X-ray intensities II. Experimental investigation and the detection of centres of symmetry. Acta Cryst. 3, 210-214.

Hudson, A., and Whitfield, H.J. 1967. Electric field gradients in normal spinels. Mol. Phys. 12, 165-172.

Hwang, L., Heuer, A.H., and Mitchell, T.E. 1973. On the space group of  $\text{MgAl}_2\text{O}_4$  spinel. Phil. Mag. 28, 241-243.

Iida, S., Yamamoto, M., and Umemura, S. 1973. Detailed study on the electronic transition of  $\text{Fe}_3\text{O}_4$ . A.I.P. Conf. Proc. (U.S.A.) 18, 913-917.

Iizumi, M., Koetzle, T.F., Shirane, G., Chikazumi, S., Matsui, M., and Todo, S. 1982. Structure of magnetite ( $\text{Fe}_3\text{O}_4$ ) below the Verwey transition. Acta Cryst. B38, 2121-2133.

Iizumi, M., and Shirane, G. 1975. Crystal symmetry of the low-temperature phase of magnetite. Solid State Comm. 17, 433-436.

Infante, C., and Fender, B.E.F. 1973. Off-centre displacements in spinels: a neutron diffraction examination of  $\text{MgCr}_2\text{O}_4$ . J. Phys. C6, L333-L335.

International Tables for X-Ray Crystallography, 1952. Four volumes (ed. N.F.M. Henry and K. Lonsdale). Kynoch Press, Birmingham.

Ishikawa, Y., Sato, S., and Syono, Y. 1971. Neutron and magnetic studies of a single crystal of  $\text{Fe}_2\text{TiO}_4$ . J. Phys. Soc. Japan 31, 452-460.

Ito, A., Ono, K., and Ishikawa, Y. 1963. A study of the low-temperature transition in magnetite. J. Phys. Soc. Japan 18, 1465-1473.

Jagodzinski, H., and Saalfeld, H. 1958. Kationenverteilung und strukturbedingungen zu Mg-Al-spinellen. Z. Krist. 110, 197-218.

Johnson, H.P., and Merrill, R.T. 1972. Magnetic and mineralogical changes associated with the low-temperature oxidation of magnetite. J. Geophys. Res. 77, 334-341.

Johnson, H.P., and Merrill, R.T. 1973. Low-temperature oxidation of a titanomagnetite and the implications to palaeomagnetism. J. Geophys. Res. 78, 4938-4949.

Johnson, H.P., and Merrill, R.T. 1974. Low-temperature oxidation of a single-domain magnetite. J. Geophys. Res. 79, 5533-5534.

Kachi, S., Momiyama, K., and Shimizu, S. 1963. An electron diffraction study and a theory of the transformation from  $\gamma\text{-Fe}_2\text{O}_3$  to  $\alpha\text{-Fe}_2\text{O}_3$ . J. Phys. Soc. Japan 18, 106-116.

Katsura, T., and Kushiro, I. 1961. Titanomagnetite in igneous rocks. Am. Miner. 46, 134-145.

Kay, H.F., and Vousden, P. 1949. Symmetry changes in barium titanate at low-temperatures and their relation to its ferroelectric properties. Phil. Mag. 40, 1019-1040.

Keefer, C.M., and Shive, P.N. 1981. Curie temperature and lattice constant reference contours for synthetic titanomagnetites. J. Geophys. Res. 86, 987-998.

Kelly, D.P. 1985. Ph.D. Thesis, University of Aston.

Kelly, W.H., Folen, V.J., Hass, M., Schreiner, W.N., and Beard, G.B. 1961. Magnetic field at the nucleus in spinel-type crystals. Phys. Rev. 124, 80-86.

Kino, Y., and Lüthi, B. 1971. Magnetic and elastic properties of zinc chromite. Solid State Comm. 9, 805-808.

Klerk, J., Brabers, V.A.M., and Kuipers, A.J.M. 1977. Magnetostriction of the mixed series iron titanium oxide ( $\text{Fe}_{3-x}\text{Ti}_x\text{O}_4$ ). J. Phys. (Paris) Colloq. 38, 187-189.

Koops, C.G. 1951. On the dispersion of resistivity and dielectric constant of some semiconductors at audiofrequencies. Phys. Rev. 83, 121-124.

Kordes, E. 1935. Kristallchemische untersuchungen über aluminium verbindungen mit spinellartigem gitterbau und über  $\gamma$ - $\text{Fe}_2\text{O}_3$ . Z. Krist. 91, 193-228.

Kozhuhar, A.Y., Tsintsadze, G.A., Shapovalov, V.A., and Seleznev, V.N. 1973. The Jahn-Teller effect in a lithium gallium spinel. Phys. Lett. A42, 377-378.

Kubo, T., Hirai, A., and Abe, H. 1969.  $^{55}\text{Mn}$  nuclear magnetic resonance of the  $\text{Mn}^{3+}$  ion located at the B-site in manganese ferrite single crystals - anisotropic hyperfine field due to the local Jahn-Teller distortion. J. Phys. Soc. Japan 26, 1094-1109.

Kullerud, G., and Donnay, G. 1967. Sulphide-oxide relations. Carn. Inst. Wash. Year Book 65, 356-357.

Kullerud, G., Donnay, G., and Donnay, J.D.H. 1968. Omission solid solutions in magnetite. Carn. Inst. Wash. Year Book 66, 497-498.

Kullerud, G., Donnay, G., and Donnay, J.D.H. 1969. Omission solid solution in magnetite: kenotetrahedral magnetite. Z. Krist. 128, 1-17.

Kündig, W., and Hargrove, R.S. 1969. Electron hopping in magnetite. Solid State Comm. 7, 223-227.

Kushiro, I. 1960.  $\gamma$ - $\alpha$  transition in  $\text{Fe}_2\text{O}_3$  with pressure. J. Geomag. Geoelect. 11, 148-151.

Larson, A.C. 1967. Inclusion of secondary extinction in least squares calculations. Acta Cryst. 23, 664-665.

Laves, F., Bayer, G., and Panagos, A. 1963. Strukturelle beziehungen zwischen den typen  $\alpha$ - $\text{PbO}_2$ ,  $\text{FeWO}_4$  (wolframit) und  $\text{FeNb}_2\text{O}_4$  (columbit), und über die polymorphie des  $\text{FeNbO}_4$ . Schw. Min. Petrog. Mitt. 43, 217-234.

Lindsley, D.H. 1963. Fe-Ti oxides in rocks as thermometers and oxygen barometers. Carn. Inst. Wash. Year Book 62, 60-66.

Lindsley, D.H. 1965. Iron-titanium oxides. Carn. Inst. Wash. Year Book 64, 144-148.

Lindsley, D.H. 1976. The crystal chemistry and structure of oxide minerals as exemplified by the Fe-Ti oxides. In: Reviews in Mineralogy Volume 3: Oxide Minerals (ed. D. Rumble). Mineralogical Society of America.

Lippens, B.C., and deBoer, J.H. 1964. Study of phase transformations during calcination of aluminium hydroxide by selected area electron diffraction. Acta Cryst. 17, 1312-1321.

Lombardo, G., and Pohl, R.O. 1965. Electrocaloric effect and a new type of impurity mode. Phys. Rev. Lett. 15, 291-293.

Lotgering, F.K. 1962. Paramagnetic susceptibilities of  $\text{Fe}^{2+}$  and  $\text{Ni}^{2+}$  ions at tetrahedral or octahedral sites of oxides. J. Phys. Chem. Solids 23, 1153-1167.

Lou, F.H., and Ballentyne, D.W.G. 1968. Visible and ultraviolet emission and absorption spectra of  $\text{MgAl}_2\text{O}_4:\text{Cr}$ . J. Phys. Cl, 608-613.

Loudon, R. 1964. The Raman effect in crystals. Adv. Phys. 13, 423-482.

Marshall, M., and Cox, A. 1972. Magnetic changes in pillow basalt due to sea-floor weathering. J. Geophys. Res. 77, 6459-6469.

Martin, G.W., Kellogg, A.K., White, R.L., White, R.M., and Pinch, H. 1969. Exchangestriction in  $\text{CdCr}_2\text{S}_4$  and  $\text{CdCr}_2\text{Se}_4$ . J. Appl. Phys. 40, 1015-1016.

Marumo, F., Isobe, M., Saito, Y., Yagi, T., and Akimoto, S. 1974. Electron density distribution in crystals of  $\text{V-Ni}_2\text{SiO}_4$ . Acta Cryst. B30, 1904-1906.

Mason, B. 1943. Mineralogical aspects of the system  $\text{FeO-Fe}_2\text{O}_3\text{-MnO-Mn}_2\text{O}_3$ . Geol. Fören. Förh. (Stockholm) 65, 97-180.

Maxwell, L.R., Smart, J.S., and Brunauer, S. 1949. Dependence of the intensity of magnetization and the Curie point of certain iron oxides upon the ratio of  $\text{Fe}^{2+}/\text{Fe}^{3+}$ . Phys. Rev. 76, 459-460.

McClure, D.S. 1957. The distribution of transition metal cations in spinels. J. Phys. Chem. Solids 3, 311-317.

Michel, A., and Chaudron, G. 1935. Étude du sesquioxyde de fer cubique stabilisé. C. R. Acad. Sci. (Paris) 201, 1191-1193.

Miles, P.A., Westphal, W.B., and von Hippel, A. 1957. Dielectric spectroscopy of ferromagnetic semiconductors. Rev. Mod. Phys. 29, 279-307.

Miller, A. 1959. Distribution of cations in spinels. J. Appl. Phys. Suppl. 30, 24S-26S.

Milne, W.E. 1949. Numerical Calculus. Princeton University Press, Princeton.

Mishra, R.K., and Thomas, G. 1977. Structural phase transition in the spinel  $\text{MgAl}_2\text{O}_4$ . Acta Cryst. A33, 678.

Moran, T.J., and Lüthi, B. 1969. Elastic and magnetoelastic effects in magnetite. Phys. Rev. 187, 710-714.

Mott, N.F. 1969. Conduction in non-crystalline materials III. Localized states in a pseudogap and near extremities of conduction and valence bands. Phil. Mag. 19, 835-852.

Muller, O., and Roy, R. 1974. The Major Ternary Structural Families. Springer Verlag, New York.

Nagata, T. 1961. Rock Magnetism. Revised edition. Maruzen Co. Ltd., Tokyo.

Navrotsky, A., and Kleppa, O.J. 1967. The thermodynamics of cation distributions in simple spinels. J. Inorg. Nucl. Chem. 29, 2701-2714.

Néel, L. 1948. Propriétés magnétiques des ferrites; ferrimagnétisme et antiferromagnétisme. Ann. de Phys. 3, 137-198.

Néel, L. 1955. Some theoretical aspects of rock magnetism. Adv. Phys. 4, 191-243.

Newhouse, W.H., and Glass, J.P. 1936. Some physical properties of certain iron oxides. *Econ. Geol.* 31, 699-711.

Nicholls, G.D. 1955. The mineralogy of rock magnetism. *Adv. Phys.* 4, 113-190.

Nishikawa, S. 1915. The structure of some crystals of the spinel group. *Proc. Math. Phys. Soc. Toyko* 8, 199-209.

Nishikawa, S., and Matukawa, K. 1928. Hemihedry of zinc blende and X-ray reflexion. *Proc. Imp. Acad. Tokyo* 4, 96-97.

Nowick, A.S. 1968. Paraelastic effects of 'off-centre' ions. *Comm. Solid State Phys.* 1, 49-51.

Nowick, A.S., and Heller, W.R. 1965. Dielectric and anelastic relaxation of crystals containing point defects. *Adv. Phys.* 14, 101-166.

O'Donovan, J.B., and O'Reilly, W. 1977. Range of non-stoichiometry and characteristic properties of the products of laboratory maghemitization. *Earth Planet. Sci. Lett.* 34, 291-299.

Ohnishi, H., and Teranishi, T. 1961. Crystal distortion in copper ferrite-chromite series. *J. Phys. Soc. Japan* 16, 35-43.

O'Horo, M.P., Frisillo, A.L., and White, W.B. 1973. Lattice vibrations of  $MgAl_2O_4$  spinel. *J. Phys. Chem. Solids* 34, 23-28.

O'Neill, H.S.C., Navrotsky, A. 1983. Simple spinels: crystallographic parameters, cation radii, lattice energies and cation distribution. *Am. Miner.* 68, 181-194.

O'Reilly, W. 1976. Magnetic minerals in the crust of the Earth. *Rep. Prog. Phys.* 39, 857-908.

O'Reilly, W. 1983. The identification of titanomaghemites: model mechanisms for the maghemitization and inversion processes and their magnetic consequences. *Phys. Earth Planet. Int.* 31, 65-76.

O'Reilly, W. 1984. *Rock and Mineral Magnetism*. Blackie, Glasgow.

O'Reilly, W., and Banerjee, S.K. 1965. Cation distribution in titanomagnetites  $(1-x)Fe_3O_4-x.Fe_2TiO_4$ . *Phys. Lett.* 17, 237-238.

O'Reilly, W., and Banerjee, S.K. 1966. Oxidation of titanomagnetites and self-reversal. *Nature* 211, 26-28.

O'Reilly, W., and Banerjee, S.K. 1967. The mechanism of oxidation in titanomagnetites : a magnetic study. *Min. Mag.* 36, 29-37.

O'Reilly, W., and Readman, P.W. 1971. The preparation and unmixing of cation-deficient titanomagnetites. *Z. Geophys.* 37, 321-327.

Özdemir, Ö., and O'Reilly, W. 1981. Laboratory synthesis of aluminium substituted titanomaghemites and their characteristic properties. *J. Geophys.* 49, 93-100.

Parker, R., and Tinsley, C.J. 1976. Electrical conduction in magnetite. *Phys. Stat. Solidi* 33, 189-194.

Peters, J., and Standley, K.J. 1958. The dielectric behaviour of magnesium manganese ferrite. *Proc. Phys. Soc.* 71, 131-133.

Polder, D. 1950. Ferrite materials. *Proc. IEEE.* 97, 246-256.

Preudhomme, J., and Tarte, P. 1971. Infrared studies of spinels III. The normal II-III spinels. *Spectrochim. Acta* A27, 1817-1835.

Price, G.D., Price, S.L., and Burdett, J.K. 1982. The factors influencing cation site preferences in spinels - a Mendelyevian approach. *Phys. Chem. Min.* 8, 69-76.

Racah, P.M., Bouchard, R.J., and Wold, A. 1966. Crystallographic study of chromium spinels. *J. Appl. Phys.* 37, 1436-1437.

Readman, P.W., and O'Reilly, W. 1970. The synthesis and inversion of non-stoichiometric titanomagnetites. *Phys. Earth Planet. Int.* 4, 121-128.

Readman, P.W., and O'Reilly, W. 1971. Oxidation processes in titanomagnetites. *Z. Geophys.* 37, 329-338.

Readman, P.W., and O'Reilly, W. 1972. Magnetic properties of oxidized (cation-deficient) titanomagnetites  $(\text{Fe, Ti, } \square)_3\text{O}_4$ . *J. Geomag. Geoelect.* 24, 69-90.

Renninger, M. 1937. 'Umweganregung', eine bisher unbeachtete wechselwirkungserscheinung bei raumgitterinterferenzen. Z. Phys. 106, 141-176.

Romeijn, F.C. 1953. Physical and crystallographical properties of some spinels. Philips Res. Rep. 8, 304-342.

Rooksby, H.P. 1961. In: The X-Ray Identification and Crystal Structures of Clay Minerals (ed. G. Brown). Jarrold and Sons, Norwich.

Rumble, D. 1976. Reviews in Mineralogy Volume 3: Oxide Minerals. Mineralogical Society of America.

Rouse, K.D., Thomas, M.W., and Willis, B.T.M. 1976. Space group of the spinel structure: a neutron diffraction study of  $MgAl_2O_4$ . J. Phys. C9, L231-L233.

Sack, H.S., and Moriarty, M.C. 1965. Low-temperature dielectric phenomena in doped ionic crystals. Solid State Comm. 3, 93-95.

Sakamoto, N., Ince, P.I., and O'Reilly, W. 1968. The effect of wet-grinding on the oxidation of titanomagnetites. Geophys. J. R. Astron. Soc. 15, 509-515.

Samuelson, E.J. 1974. Note on the space group of magnetite. J. Phys. C7, L115-L117.

Samuelson, E.J., and Steinsvoll, O. 1975. On the space group of spinel. J. Phys. C8, L427-L429.

Sasajima, S. 1961.  $\gamma$ -titanohematites in nature and the role they play in rock magnetism. J. Geomag. Geoelect. 12, 190-215.

Sawatsky, G.A., Coey, J.M.D., and Morrish, A.H. 1969. Mössbauer study of electron hopping in the octahedral sites of  $Fe_3O_4$ . J. Appl. Phys. 40, 1402-1403.

Sawatsky, G.A., van der Woude, F., and Morrish, A.H. 1969. Mössbauer study of several ferrimagnetic spinels. Phys. Rev. 187, 747-757.

Schrader, R., and Büttner, G. Untersuchungen über  $\gamma$ -eisen(III)-oxid. Z. Anorg. Allg. Chem. 320, 205-219.

Schult, A. 1968. Self-reversal of magnetization and chemical composition of titanomagnetites in basalts. Earth Planet. Sci. Lett. 4, 57-63.

Shannon, R.D. 1976. Revised effective ionic radii and systematic studies of interatomic distances in halides and chalcogenides. *Acta Cryst.* A32, 751-767.

Shirane, G., Chikazumi, S., Akimitsu, J., Chiba, K., Matsui, M., and Fujii, Y. 1975. Neutron scattering from the low-temperature phase of magnetite. *J. Phys. Soc. Japan* 39, 949-957.

Shirane, G., Cox, D.E., Takei, W.J., and Ruby, S.L. 1962. A study of the magnetic properties of the  $\text{FeTiO}_3$ - $\alpha$ - $\text{Fe}_2\text{O}_3$  system by neutron diffraction and the Mössbauer effect. *J. Phys. Soc. Japan* 17, 1598-1611.

Shull, C.G., Wollan, E.O., and Koehler, W.C. 1951. Neutron scattering and polarization by ferromagnetic materials. *Phys. Rev.* 84, 912-921.

Sievers, A.J., and Takeno, S. 1965. Isotope shift of a low-lying lattice resonant mode. *Phys. Rev.* 140, A1030-A1032.

Smit, J., and Wijn, H.P.J. 1959. *Ferrites*. Wiley, New York.

Smith, P.P.K. 1978. Note on the space group of spinel minerals. *Phil. Mag.* B38, 99-102.

Smith, P.P.K. 1979. The observation of enantiomorphous domains in a natural maghemite. *Contrib. Min. Petrol.* 69, 249-254.

Sosman, R.B., and Posnjak, E. 1925. Ferromagnetic ferric oxide, artificial and natural. *J. Washington Acad. Sci.* 15, 329-342.

Spencer, K.J., and Lindsley, D.H. 1981. A solution model for coexisting iron-titanium oxides. *Am. Miner.* 66, 1189-1201.

Srinivasan, R., and Srikrishnan, T. 1966. New statistical tests for distinguishing between centrosymmetric and non-centrosymmetric structures. *Acta Cryst.* 21, 648-652.

Srinivasan, R., and Vijayalakshmi, B.K. 1972. The use of X-ray anomalous scattering to resolve the space group ambiguity of dibenzyl disulphide. *Acta Cryst.* B38, 2615-2617.

Srivastava, V.C. 1969. Pressure dependence of ferromagnetic phase transitions of chromium chalcogenide spinels. *J. Appl. Phys.* 40, 1017-1019.

Stahl-Brada, R., and Low, W. 1959. Paramagnetic resonance spectra of chromium and manganese in the spinel structure. *Phys. Rev.* 116, 561-564.

Stephenson, A. 1969. The temperature dependent cation distribution in titanomagnetites. *Geophys. J. R. Astron. Soc.* 18, 199-210.

Stewart, J.M., Kruger, G.J., Amman, H.L., Dickinson, C., and Hall, S.R. 1974. X-Ray 74. University of Maryland, U.S.A.

Stout, G.H., and Jensen, L.H. 1968. X-ray Structure Determination: A Practical Guide. Collier-Macmillan, London.

Strickler, D.W., and Roy, R. 1961. Studies in the system  $\text{Li}_2\text{O}-\text{Al}_2\text{O}_3-\text{Fe}_2\text{O}_3-\text{H}_2\text{O}$ . *J. Amer. Ceram. Soc.* 44, 225-230.

Sweatman, T.R., and Long, J.V.P. 1969. Quantitative electron-probe microanalysis of rock-forming minerals. *J. Petrol.* 10, 332-379.

Syono, Y. 1965. Magnetocrystalline anisotropy and magnetostriction of  $\text{Fe}_3\text{O}_4-\text{Fe}_2\text{TiO}_4$  series - with special application to rock magnetism. *Jap. J. Geophys.* 4, 71-143.

Takei, H., and Chiba, S. 1966. Vacancy ordering in epitaxially-grown single crystals of  $\gamma\text{-Fe}_2\text{O}_3$ . *J. Phys. Soc. Japan* 21, 1255-1263.

Tanaka, M., Tokoro, T., and Aiyama, Y. 1966. Jahn-Teller effects on Mössbauer spectra of  $^{57}\text{Fe}$  in  $\text{FeCr}_2\text{O}_4$  and  $\text{FeV}_2\text{O}_4$ . *J. Phys. Soc. Japan* 21, 262-267.

Tarte, P., and Preudhomme, J. 1963. Infrared spectrum and cation distribution in spinels. *Acta Cryst.* 16, 227.

Thewlis, J. 1931. The structure of ferromagnetic ferric oxide. *Phil. Mag.* 12, 1089-1106.

Thompson, P., and Grimes, N.W. 1977. Multiple diffraction in spinel and the space group ambiguity. *J. Appl. Cryst.* 10, 369-371.

Tokonami, M. 1965. Atomic scattering factor for  $\text{O}^{2-}$ . *Acta Cryst.* 19, 486.

Tokonami, M., and Horiuchi, H. 1980. On the space group of spinel,  $\text{MgAl}_2\text{O}_4$ . *Acta Cryst.* A36, 122-126.

Tomas, P.A., Laruelle, P., Dormann, J.L., and Nogues, M. 1983. Affinement de la structure des formes ordonnée et désordonnée de l'octaoxopentaferate de lithium,  $\text{LiFe}_5\text{O}_8$ . Acta Cryst. C39, 1615-1617.

Ueda, R., and Hasegawa, K. 1962. Vacancy distribution in  $\gamma\text{-Fe}_2\text{O}_3$ . J. Phys. Soc. Japan Suppl. B11, 391-394.

van den Berg, K.G., Lodder, J.C., and Mensinga, T.C. 1976. Magnetic anisotropy and domain structure of manganese ferrite grown epitaxially on MgO. Thin Solid Films 34, 243-247.

van der Biest, O., and Thomas, G. 1975. Identification of enantiomorphism in crystals by electron microscopy. Acta Cryst. A31, 70-76.

van Oosterhout, G.W., and Rooijmans, C.J.W. 1958. A new superstructure in gamma-ferric oxide. Nature 181, 44.

van Uitert, L.G. 1956. Dielectric properties of and conductivity in ferrites. Proc. IRE. 44, 1294-1303.

Verhooijen, J. 1962. Oxidation of iron-titanium oxides in igneous rocks. J. Geol. 70, 168-181.

Verwey, E.J.W. 1935a. The crystal structure of  $\gamma\text{-Fe}_2\text{O}_3$  and  $\gamma\text{-Al}_2\text{O}_3$ . Z. Krist. 91, 65-69.

Verwey, E.J.W. 1935b. Incomplete atomic arrangement in crystals. J. Chem. Phys. 3, 592-593.

Verwey, E.J.W., and deBoer, J.H. 1936. Cation arrangement in a few oxides with crystal structures of the spinel type. Rec. Trav. Chem. Pays-Bas, 4th Ser. 55, 531-540.

Verwey, E.J.W., deBoer, J.H., and van Santen, F. 1948. Cation arrangement in spinels. J. Chem. Phys. 16, 1091-1092.

Verwey, E.J.W., Haayman, P.W., and Romeijn, F.C. 1947. Physical properties and cation arrangement of oxides with spinel structures II. Electric conductivity. J. Chem. Phys. 15, 181-187.

Verwey, E.J.W., and Heilmann, E.L. 1947. Physical properties and cation arrangement of oxides with spinel structures I. Cation arrangement in spinels. J. Chem. Phys. 15, 174-180.

- Vieland, L.J. 1975. On the cubic-rhombohedral transformation in magnetite. *Acta Cryst.* A31, 753-755.
- Wagner, P.A. 1927. Changes in oxidation of iron in magnetite. *Econ. Geol.* 22, 845-846.
- Walters, D.S., and Wirtz, G.P. 1972. Electron diffraction superlattice lines in magnesium ferrite. *J. Amer. Ceram. Soc.* 55, 59.
- Weber, von Kurt. 1969. Eine neue absorptionsfaktortafel für kugelförmige proben. *Acta Cryst.* B25, 1174-1178.
- Weber, H.P., and Hafner, S.S. 1971. Vacancy distribution in non-stoichiometric magnetites. *Z. Krist.* 133, 327-340.
- Welo, L.A., and Baudisch, O. 1925. The two-stage transformation of magnetite into haematite. *Phil. Mag.* 50, 399-408.
- White, W.B., and Keramidas, V.G. 1972. Application of infrared and Raman spectroscopy to the characterization of order-disorder in high temperature oxides. *Nat. Bur. Stand. Spec. Pub.* 364, 113-126.
- Wilson, A.J.C. 1949. Possible X-ray determination of a centre of symmetry. *Research* 2, 246.
- Wilson, A.J.C. 1951. Variance of X-ray intensities. *Research* 4, 141-142.
- Wilson, W.D., Hatcher, R.D., Dienes, G.J., and Smoluchowski, R. 1967. Off-centre  $\text{Li}^+$  in KCl. *Phys. Rev.* 161, 888-896.
- Wohlfarth, E.P. 1982. *Ferromagnetic Materials: A Handbook on the Properties of Magnetically Ordered Substances.* North-Holland, New York.
- Wold, A., Arnott, R.J., Whipple, E., and Goodenough, J.B. 1963. Crystallographic transitions in several chromium spinel systems. *J. Appl. Phys.* 34, 1085-1086.
- Woolfson, M.M. 1970. *An Introduction to X-Ray Crystallography.* Cambridge University Press, Cambridge.
- Zachariasen, W.H. 1967. A general theory of X-ray diffraction in crystals. *Acta Cryst.* 23, 558-564.

Zeller, C., and Babkine, J. 1965. Mise en évidence d'une loi reliant le paramètre cristalline au chimisme des titanomagnétites. C. R. Acad. Sci. (Paris) 250, 1375-1378.

Zeller, C., Hubsch, J., and Bolfa, J. 1967a. Relations entre les propriétés magnétiques et la structure d'une titanomagnétite au cours son oxidation. C. R. Acad. Sci. (Paris) B265, 1034-1036.

Zeller, C., Hubsch, J., Reithler, J.C., and Bolfa, J. 1967b. Determination de la structure spinelle à partir de l'aimantation absolue, des solutions solides  $x\text{Me}_2\text{TiO}_4 \cdot (1-x)\text{MeFe}_2\text{O}_4$ . C. R. Acad. Sci. (Paris) B265, 1335-1338.

### ACKNOWLEDGEMENTS

I am indebted to my two supervisors Dr. D.J. Vaughan and Dr. N.W. Grimes for their useful advice and encouragement throughout this project. In addition the technical staff of the Department of Geological Sciences have been very supportive, in particular Ms. S.V. Knox and Mr. K.N. Murthy.

I would like to express my gratitude to Dr. G. Longworth of A.E.R.E. Harwell for carrying out the low-temperature Mössbauer work.

Dr. C. Schwalbe, Dr. P.L. Lowe and Mr. P. Bryant of the Pharmacy Department provided many useful suggestions during my use of the Cad-4 diffractometer and I am grateful.

Many thanks to the staff of the Computer Centre, in particular Mr. D.J. Stops and Mr. R. Parsons, for their invaluable help with many of the computer related problems, in particular those associated with the link to Manchester University.

I would like to express my appreciation to Dr. G.D. Price of University College London and to the British Museum (Natural History) for the provision of crystal specimens.

Finally, I would like to thank Professor D.D. Hawkes in whose department much of this work was performed and the Natural Environment Research Council for providing financial support.